UNIVERSITY OF GHANA

THE LITHOLOGY AND SOIL GEOCHEMISTRY OF NTUMKUMSO AND ITS SURROUNDING AREAS IN THE ASHANTI REGION OF GHANA

BY

BLESTMOND BRAKO AFRIFA

(10395581)

THIS THESIS IS SUBMITTED TO THE UNIVERSITY OF GHANA, LEGON IN PARTIAL FULFILLMENT OF THE REQUIREMENT FOR THE AWARD OF M.PHIL GEOLOGY DEGREE

JULY, 2014

DECLARATION

This is to certify that this thesis is the result of research undertaken by Blestmond Brako Afrifa towards the award of the MPhil Geology in the Department of Earth Science, University of Ghana.

.

…… ……...

BRAKO AFRIFA BLESTMOND DATE

(STUDENT)

…… ……...

PROF. F.K. NYAME DATE

(SUPERVISOR)

…… ……

MR. RICHARD AFENU DATE

(SUPERVISOR)

ABSTRACT

Rocks and soil covering approximately 81km^2 in the Ntunkumso area in the Ashanti Region of Ghana were investigated in the present study. Petrographic studies of eighteen (18) rock samples collected suggest that the rocks are predominantly biotite schist, diorite, granodiorite, and granite. The biotite schist outcrops between Ntunkumso and Boiya and is made up of biotite, quartz, feldspar, iron oxides and opaque minerals. Diorite was encountered at Abesewase and Ofoase and is mineralogically composed of hornblende, plagioclase, microcline, biotite, quartz, iron oxides and opaque minerals. Granodiorite outcrops between Kokodie and Odoyefe. Major minerals in the rock are plagioclase, microcline, muscovite, quartz, garnet and opaque minerals. Granite in the study area outcrops at Apemso and Nkyerepoaso and consists of plagioclase, microcline, quartz, biotite, muscovite and opaque minerals.

Whole rock geochemical analysis of thirteen (13) representative rock samples using ICP-MS indicates that, SiO_2 concentration in the biotite schist ranges from 71.14 to 73.17 wt%, Al_2O_3 also varies from 14.66 to 15.39 wt%, Fe_2O_3 4.45 to 5.40 wt% MgO 2.57 to 3.56 wt% .The contents of some minor elements are as follows; Cu 1.20 to 21.50 ppm, Ni 86.90 to 102.50 ppm. SiO_2 in diorite varies from 59.87 to 61.64 wt%, Fe_2O_3 4.89 to 9.47 wt%, K_2O 0 .53 to 1.49 wt%, TiO_2 0.47 to 1.17 wt% and MgO 3.37 to 11.92 wt%. Cu and Ni concerntration range from 11.20 to 60.70 ppm, Ni 44.40 to 300.00 ppm. In granodiorite, SiO_2 content ranges from 68.80 to 76.41wt%, Al_2O_3 13.77 to 14.97 wt%, Fe_2O_3 4.89 to 9.47 wt%, K_2O 0 .53 to 1.49 wt%, TiO_2 0.47 to 1.17 wt%, MgO 3.37 to 11.92 wt%. The contents of some minor elements are as follows; Cr 16.00 to 148.00 ppm, Sr 381.00 to 686.00 ppm. SiO_2 content in granite varies from 69.38 to 83.93 wt%, Al_2O_3 11.19 to 13.60 wt%, K_2O 2.72 to 3.26 wt%, MgO 0.02 to 0.32 wt%. The contents of some minor elements are as follows: Cu 0.90 to 4.50 ppm,

Ba 10.00 to 240.00 ppm, Ni 0.90 to 4.90 ppm. XRF analysis of the thirty one soil samples (primary data) collected indicates that SiO_2 concentrations in the soils range from 40.48 wt% to 81.01 wt%, Al_2O_3 12.70 to 38.77 wt%, Fe_2O_3 1.16 to 12.23 wt%, MgO 0.95 to 3.56 wt%, K_2O 0.47 to 4.8 wt%. The trace element compositions are as follows, Cu 1.50 to 37.40 ppm, Ba 71.0 to 426.00 ppm, Ni 8.20 to 84.20 ppm, Rb 18.0 to 271.8 ppm. Soil sample data (secondary data) from the Ntunkumso area previously collected by the Geological Survey Department, Ghana, was also used for the present study. Multivariate statistical analysis was performed on the soil (primary and secondary data) and rock geochemical data. Comparing the mineralogical and geochemical compositions of the rock with the geochemistry of the soils, it has been established that soils overlying the biotite schist are representative of the biotite schist but have undergone moderate weathering due to the high concentrations of As, Ga, Zr, Cr and Sn in the soils than in the rock. The high concentrations of Zn, Ni and Cu in the biotite schist may also suggest hydrothermal alteration and leaching from the soil. CaO, MgO, Cr, Ni, Cu and Ba are highly concentrated in the diorite than in the soils overlying the diorite. This association may imply leaching of these elements from the soil. Also the diorite may have been affected by hydrothermal alteration. The granodiorite has experienced hydrothermal alteration. MgO and Fe_2O_3 show high concentration in the soils overlying the granodiorite than in the granodiorite implying probable transportation of mafic signatures to the area. The high concentration of Cu, Cr, Ni, Zr, MgO and Fe_2O_3 in the soil overlying the granite implies that the soil may not be in-situ because it has experienced some mafic contribution. The mineralogical potential of the area is not economically significant.

DEDICATION

I dedicate this piece of work to my Dad and Mum and all my lovely siblings.

I say thank you.

ACKNOWLEDGEMENT

First and foremost, I give thanks to the almighty GOD for guiding and giving me the gift of life and strength throughout my project period.

My personal gratitude and appreciation goes to my parents Mr. and Mrs. Brako Afrifa for their infallible financial support, moral training and parental instinct which have made me who I am now. Special thanks go to my supervisors, Prof. F.K. Nyame and Mr. Richard Afenu for their continual guidance, encouragement and advice.

Again, I thank all the lecturers in my department for impartation of knowledge, advice and encouragement.

Finally, to all my course mates and Christian brothers; I say thank you.

TABLE OF CONTENTS

Contents **Page**

LIST OF TABLES

LIST OF FIGURES

CHAPTER ONE

INTRODUCTION

1.1 Background of study

About two thirds of the land/ surface aea of Ghana is dominated by Paleoproterozoic Birimian rocks which consist of five evenly spaced volcanic belts trending northeast-southwest except for the N-S Lawra belt and the intervening sedimentary basins (Leube et al., 1990).

The study area is located in the Kumasi basin and is made up of biotite schist, diorite, granodiorite and granites (Moon and Mason, 1967)

The concentrations of elements in the soils help to understand the geochemistry of the underlying rock. According to Kalepertzis et al., (2012), similar dispersion patterns exhibited by a group of elements may imply that they are influenced by a common process. Geostatistical methods are used to analyze the behavior ofthese elements as well as their spatial distributions which are visually determined on the spatial distribution map.

In spite of the fact that soils are representative of the underlying geology, conditions like chemical weathering, topography, climate and anthropogenic activities can influence the concentrations of elements in soils.

Studying the geochemical associations between rock types and the soils present in the same area aids understanding the possible geochemical relationship between the lithologies and the soils present. This is because the geological importance of elements within an associated element group provides information about the soil forming processes and the underlying geology.

1.2 Problem statement

The Birimian of Ghana, which is made up mostly of metavolcanics (basalt, andesite and dacite), metasediments (greywackes, phyllite) and associated granitic rocks and other intrusives, outcrops extensively throughout the northern and southern parts of the country. According to workers such as Junner et al (1935), Kesse (1985), and Hirdes et al, (1992), the metavolcanics consist mainly of basalts while the metasediments are predominantly phyllite and greywackes. The intruded granitoids are described as dominated by the Cape Coast type (G1), Dixcove type (G2) and the Bongo type (G3) granites. The Birimian rocks often weather to give various types of soils in the surficial environment (Kesse, 1985; Dickson and Benneh, 1995).

Even though these rock types have been known to be associated with distinctive soils, (Kesse, 1985; Dickson and Benneh,1995), few studies if any have been done to investigate the nature and geochemical characteristics that may exist between the surficial soils and related underlying lithology or rock types in Birimian terrains. Because of possible physico-chemical and other changes that could potentially occur as rocks are transformed into soils in the weathering environment, it is often important that such changes are studied to provide information on the constituents in the underlying lithology as well as element abundances in the overlying soils.

In addition, because soils are more readily accessible than underlying rocks, such studies will provide important information on element distributions, abundancs enrichments or depletions, and indications of mineralization in rocks lying beneath the soils.This study was therefore undertaken to investigate the possible link between lithology and overlying soils in the Ntunkumso area of the Kumasi basin.

1.3 Objective of the study

The main objective of this study was to carry out rock and soil geochemical investigation to establish possible link between the rock types and soils in the study area.

1.4 Study area

The study area is approximately 81 km^2 and is located in the Sekyere East and Ejisu Juaben Districts of the Ashanti Region of Ghana. It is located about 189 km north-west of Accra and 27km from Kumasi, the Ashanti regional capital. It also lies between longitudes 1°19'57''- 1°24'54'' W and Latitudes 6°45'15''- 6° 50'12'' N on Field Sheet 0602B1. The study area can be accessed by the 38 km Kumasi – Efiduasi road.

The area is generally undulating and the underlying geology is made up of the Birimian sedimentary rocks, hornblende biotite- diorite hybrid enclosed by the batholithic granite and the post-Tarkwaian gabbro and dolerite dykes (Moon and Mason, 1967).

The study area lies within the semi-deciduous forest zone and is well drained by many streams and rivers, notably the Oyon, Anabkro, Ntunkum, Aprapon, Adansu, Danyame and Nkadan (Moon and Mason, 1967).

The major economic activities in the study area are farming, small-scale processing of agricultural produce and trades like hair dressing, tailoring and carpentry.

CHAPTER TWO

LITERATURE REVIEW

2.1 Geology of Ghana

Ghana falls mostly within the south eastern corner of the West African Craton which stabilized in the early Proterozoic (2000 Ma) during the Eburnean Orogeny. This orogeny also stabilized the Zaire Craton and affected vast parts of Western Africa and neighbouring regions in South America that were conterminous with the Eburnean tectonothermal province. The Birimian strata were deformed and metamorphosed during the ~2.2 Ga Eburnean Orogeny (Nyame, 1998) and other references therein. This orogeny is characterized by isoclinal folding as well as intrusion of pre-, syn-, and post-tectonic granites (Eisenlohr and Hirdes, 1992).

Reviews of the geology of Ghana by Kesse (1985), Wright (1985) and Leube *et al.* (1990) provide useful summaries. These reviews are particularly relevant because of the attention paid to mineral resource potential. Kesse (1985) presents a good treatise on specific mineral and rock resources available in Ghana; Wright (1985) relates the geology of Ghana to the regional geology of West Africa and Leube et al., (1990) present a significantly different stratigraphic interpretation for the Birimian System in Ghana, stressing lateral lithologic continuity and facies changes within the group. Unlike many previous workers, Leube et al., (1990) believe that some of the granitoids possess significant potential for gold mineralization.

2.1.1 The Birimian of Ghana

Birimian evolution possibly accompanying breakup of Archaean cratonic nuclei, commenced around 2350-2300 Ma with plutonic activity and the deposition in volcano-sedimentary basins including banded iron formations (BIFs).

The Birimian consists of metamorphosed volcanic and sedimentary rocks which form five subparallel belts of volcanic rock separated by broad “basins” of sedimentary rocks. Up to the early 1980's, except for Matthews and Milnes (1979) and Breakey and Breakey (1977), authors on the Birimian adopted a chronostratigraphic nomenclature. They divided the rocks into an older “Lower Birimian”, consisting of predominantly metasedimentary rocks, and a younger “Upper Birimian”, comprising chiefly metavolcanic rocks (Junner 1935, 1940; Bates, 1955). These ideas were based largely on mapping by the GSD in southern Ghana and are widely supported in Ghana.

The rock types present in the Lower Birimian sedimentary belt are greywackes with turbidite features, phyllites, slates, schists, weakly metamorphosed tuffs and sandstones. Some of the phyllites contain pyrite and finely divided carbonaceous matter present in most of them. Silicification is common in the phyllites, particularly towards the boundary with the Upper Birimian.

The Upper Birimian volcanic succession consists of lava flows and dyke rocks of basaltic and andesitic composition. Most of these rocks have now been metamorphosed to hornblende actinolite-schists, calcareous chlorite schists and amphibolites (the greenstones). Pillow structures indicating subaqueous eruption of the original basaltic lavas are commonly observed. Available major and trace element chemical data show that these Birimian metabasalts are tholeiitic.

However, felsic volcanic rocks also occur in this succession as well as in the predominantly sedimentary sections. The felsic units include dacitic pyroclastic rocks, minor andesitic and rhyolite flows, and undifferentiated volcanogenic sediments. Minor intrusions of mafic and ultramafic rocks cut the volcanics in some places. Mn-rich horizons also occur at stratigraphically lower level in the Upper Birimian and have been found in the uppermost Lower Birimian as well.

In 1964-66, the Soviet Geological Team (SGT) mapped the Bole and Lawra Belts. The SGT classified the Birimian into three sub series: Lower (sediments), Middle (pyroclastics) and Upper (lavas). The GSD developed a classification which incorporated and modified the SGT classification (Asihene and Barning 1975). In the slate 1970's the GSD developed an accepted stratigraphic nomenclature for the Birimian (Kesse, 1985). Currently the upper Birimian rocks are called Birimian metavolcanics rocks likewise; the lower Birimian rocks are also called Birmian metasediments rocks.

In Ghana, granitoids are found within the birimian rocks which form a substantial part of the Man Shield (Leube et al., 1990) which occupies the southernmost part of the West Africa craton. The granitoids occurs as intrusive bodies which occurred about 2.1Ga ago during the Eburnean Orogeny. Nyarko et al., (2012) proposed that over the years, it has been established that Eburnean granitoids can be group into:

(1) Sedimentary-basin granitoids (previously called the Cape Coast type, G1)

(2) Sedimentary-basin granitoids of the Winneba type, and,

(3) Volcanic-belt granitoids (previously called the Dixcove type, G2)

2.1.2 Sedimentary-Basin granitoids (previously called the Cape Coast type, G1)

The Cape Coast granites occur only within the Birimian sedimentary basins. Some of them are two mica granites. This group also includes gneisses, and these are especially well developed in the metasedimentary belts. They are typically biotite-bearing. It has been suggested that the Cape Coast granitoids, which appear migmatitic in some localities, might represent an older continental basement on which the Birimian supracrustals were deposited. However, there is no geochronologic support for this theory. Contacts between these granitoids and the metasediments are irregular; rafts of metasediments and relict structures from metasediments rise into the granitoids, and tendrils of granite vein the metasediments (Taylor et al., 1992). Based on the degree of foliation, early workers assumed that the Cape Coast granitoids intruded during regional deformation and that Dixcove granites were emplaced after deformation. (Junner, 1940; Kesse, 1985). However, later work by Hirdes et al. (1992) demonstrated, in contrast to long held views that Dixcove granitoids formed at about 2,175 Ma and are about 60 and 90 Ma older than the Cape Coast granitoids. Taylor et al. (1988, 1992) suggest that the Cape Coast and Dixcove granitoids are coeval.

2.1.3 Volcanic-Belt granitoids (previously called the Dixcove type, G2)

Dixcove-type granitoids are metaluminous and typically dioritic to granodioritic in composition.They intrude Birimian volcanic rocks. They are typically hornblende-bearing and are commonly associated with gold mineralisation where they occur as small plutons within the volcanic belts.

The granitoids are massive in outcrop, do not have a compositional banding or foliation, and are thus generally considered post-deformation. However, Dixcove-type

granitoids have never been shown to intrude or crosscut Cape Coast granitoids, and some workers (eg. Murray, 1960) have recognized Dixcove granitoid clasts in Cape Coast granitoids. The presence or absence of a foliation is not a sufficient criterion to establish timing relationships in granitoids (Paterson et al., 1989). In particular, amphibole bearing granitoids have been demonstrated to be less likely to develop a foliation during deformation than biotite-rich granitoids (Vernon and Flood, 1988).

2.1.4 Sedimentary-basin granitoids of the Winneba type

The Winneba granitoids occur at a single locality near the town of Winneba. It is the only rock suite so far encountered in Ghana which shows evidence for an Archean sialic precursor (Sm/Nd model age of about 2.6 Ga (Taylor et al., 1988, 1992).

2.1.5 Tarkwaian

A distinctive sequence of clastic sedimentary rocks occurs in elongate troughs developed on top of the Birimian System. These rocks host important paleo placer gold deposits and are known as the Tarkwa System. Most workers agree that the Tarkwaian sediments were deposited in intermontanegrabens formed by preferential rifting along the axes of the volcanic belts and that there is no evidence that the depositional basins were ever linked.

Kesse (1985) and Leube and Hirdes (1986) summarised the literature on the Tarkwaian up through the mid-1980's. More recent data is presented in Eisenlohr and Hirdes, (1992), and Oberthur (1994) for the Ashanti Belt and by Zitzman et al. (1993 a, b) for the Bui Belt. The rocks of the Tarkwaian System represent erosional products of the

Birimian and are dominated by coarse clastic sediments. They are widespread in the Ashanti and Bui volcanic belts and, to a lesser extent, in all of the other belts.

In the Ashanti Belt, the Tarkwa is made up of four units. The lowest unit, the Kawere Group consists of immature, polymictic, matrix supported and large pebble conglomerate dominated by mafic (Birimian) pebble lithologies. The Kawere is overlain by and is in marked contrast with, the Banket Series which consists of mature, clean, quartzite, grit, breccia and conglomerate composed in part of well sorted quartz pebble conglomerate beds known as “reefs” that host the gold mineralization. The Banket is overlain by the Tarkwa Phyllite which consists of a transition sequence from sandstone to chloritic and sericitic phyllite. The uppermost Tarkwa unit is the Huni Sandstone; sandstone and quartzite with interbeds of phyllite.

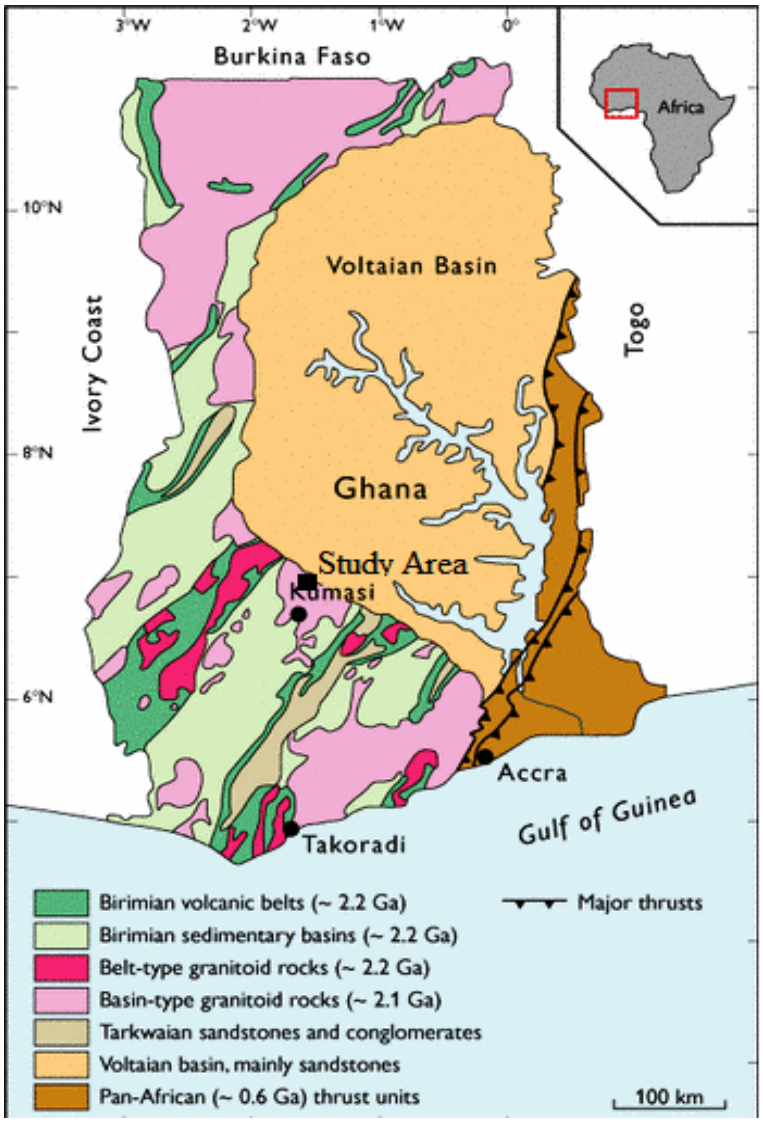

Figure 2.1: Map of Ghana showing the various lithologies and the study area, modified after Kesse (1985)

2.2 The local geology of the study area

The general geology of the study area is composed of Birimian metasedimentary rocks, Eburnean intrusive rocks, hornblende-biotite diorite hybrid rocks enclosed bybatholitic granites and Post-Tarkwaian gabbro and dolerite dykes. (Moon and Mason, 1967)

2.2.1 Birimian Metasedimentary rocks

The Precambrian rocks of the area are Birimian and to a small extent of the Tarkwaian System. Birimian Metasedimentary rocks are made up of phyllites, staurolites, garnet

and biotite schist, hornfels and granulites. Both Birimian and Tarkwaian sediments have been isoclinally folded and intruding granitiods referred to as the "Cape Coast" or "basin" type, some of which are two mica granites (Boamah, 1993) and other references therein. These rocks also present a northeast-southwest strike with steep dips predominantly to the north-west. The sediments of the Lower Birimian were invaded and altered by the Kumasi batholitic granite which, together with the intimately associated granitised sediments, forms approximately half of the basement outcrop. (Moon and Mason, 1967).

2.2.2 The hornblende - biotite diorite hybrid

The two narrow parallel belts in (Fig.2.1) are approximately 1.5 miles long, which vary in composition from epidiorite to hornblende-biotite diorite trend north-north- south, and south- south-east through Abetrim and Ofoase. The hybrids appear to be rimmed by hornfel sediments and schist which probably represent rock which have been indurated by the intrusion of basic sill. The basic sill has been partially assimilated and altered to their present hybrid composition. The schist and hornfels are penetrated by the granitic veins and locally migmatites have been developed. (Moon and Mason, 1967)

2.2.3 The Post -Tarkwaian gabbro and dolerite dyke

The post Tarkwaian gabbro and dolerite dyke are typically fresh rocks with little or no alteration except as a result of weathering processes. (Moon and Mason,1967). Unfortunately, these rocks were not encountered in the field probably due to weathering.

2.2.4 Eburnean intrusive rocks

The Eburnean intrusive rocks are composed of muscovite-biotite-adamelites and granodiorites of the Kumasi batholith. About two thirds of the study area is dominated by the Eburnean Intrusive rocks. The intrusive rocks encountered in the study area are the granodiorites and granites. These intrusive rocks are intermediate to felsic in composition. There are also the presencesof quartz and pegmatite veins in these rocks. The textural composition ranges from medium to coarse grained under the hand lens. These granites and granodiorite are mainly composed of biotite, muscovite, quartz and plagioclase. Structures present in these rocks are faults, fractures, joints and foliations.

2.3 Surface weathering and processes

An understanding of the geochemical environment is essential for the efficient application of geochemical surveys, whether at regional or local scale.

Levinson (1980) stated that geochemical exploration methods are largely based on a systematic study of dispersion of chemical elements in natural materials surrounding or associated with ore bodies. Dispersion is a process of distribution or re-distribution of elements by physical, chemical and biological activities (Rose et al., 1991). Physical processes include all those that cause rock disintegration without chemical or mineralogical changes. This disintegration increases the reactive surface area and thus facilitates the decomposition of rocks by chemical reaction with the abundant water, oxygen, and carbon dioxide of the surface environment. Biological activity contributes either directly or indirectly to both physical and chemical weathering. These processes usually take place side by side, though their importance varies according to environmental conditions. Thus, in extremes of arid deserts and arctic conditions, and

in many areas of mountainous relief, physical disintegration is usually the dominant mechanism of rock decay. Under most other climates, chemical attack is by far the dominant factor in controlling the nature of the weathering products at all depths within the zone of weathering. By contrast, the principal domain of biological activity is restricted to the near-surface zone of soil formation (Rose et al., 1991). The application of geochemistry to mineral exploration has progressed markedly since the 1950's.

Geochemical prospecting and geobotanical prospecting are based on the knowledge that an envelope of primary mineralization is likely to occur around a mineral deposit and a secondary dispersion pattern of chemical elements is often created during weathering and erosion of the deposit (Lawrance, 1995).

Geochemical methods are utilized to detect primary and secondary dispersion haloes, which invariably constitute a bigger target than the ore body itself. Geochemical environments related to dispersion have been subdivided by Levinson (1980) in:-

1. Primary environments - embraces those areas extending downward from the lower levels of circulating meteoric water to those of the deep-seated processes of igneous differentiation and metamorphism.

2. Secondary environment - comprises the surficial processes of weathering, soil formation and sedimentation at the surface of the earth.

CHAPTER THREE

METHODOLOGY

3.1Pre field work

3.1.1 Desk study

Previous geological, geophysical, geochemical literature together with the topographical map of the area and beyond were studied and reviewed.

3.2 Field work

3.2.1 Rock sampling

Suitable and representative fresh rock outcrops and exposures occurring in the area in-situ and loose specimen were sampled. Macro and micro features present were also carefully noted together with GPS locations of the outcrops and rocks sampled.

3.2.2 Soil sampling

A 1km x 1km grid of ninety (90) soil sample data from the Ntunkumso area, previously collected by the Geological Survey Department, Ghana, was used for the present study. These samples were labeled as secondary data. For the soil samples, two baselines were constructed, first, was a 4500m long 060^{O} NE-SW baseline running from Apemso to Ofoase, and secondly, a 3900m W-E baseline was also constructed from Ofoase to Nkyerepoaso. These baselines were constructed to cut across the various rock types in the study area such that the soil samples reflected the underlying geology. On reaching a sampling point with the aid of a GPS, the topsoil was removed using diggers (locally known as soso) to a depth of about 30cm. Below this depth, it was assumed that the soil was representative of the in-situ material in the locality. Each sample comprises material taken from 3 different sites with a separation distance of 10m and at a depth of

30cm to 40cm in a triangular unit-cell and then made into a composite. A pre-labeled sample bag indicating the sample number was filled with about 2 kg of soil material and then sealed. Some site descriptions of the samples are recorded on a log sheet and summarized as shown in the Appendix (Table 3.1).

Thirty one (31) representative soil samples were collected for the study. Thirteen (13) soil samples were collected from the first baseline and another thirteen (13) on the second baseline at irregular intervals. Five soil samples were randomly collected from the northern part of the study area to serve as a test sample for the data acquired from the Geological Survey Department, Ghana. These soil samples were generally, lateritic, loamy and clayey in nature.

3.3 Rock sample preparation

After the field work, the sample points for the various rock and soil samples were plotted on the geological map of the study area using MAPINFO software version 8, (Fig. 3.1).

The rock samples were transported to the Department of Earth Science, University of Ghana. Eighteen (18) of the rock samples were sliced for thin section analysis and thirteen (13) out of the eighteen (18) samples were also cut into blocks for geochemical analysis using the Inductively Coupled Mass Spectrometer (ICP-MS) analytical method at the Australian Laboratory Services(ALS),inCanada. Parameters analyzed were, the rare earth elements (REEs), major and minor trace elements.

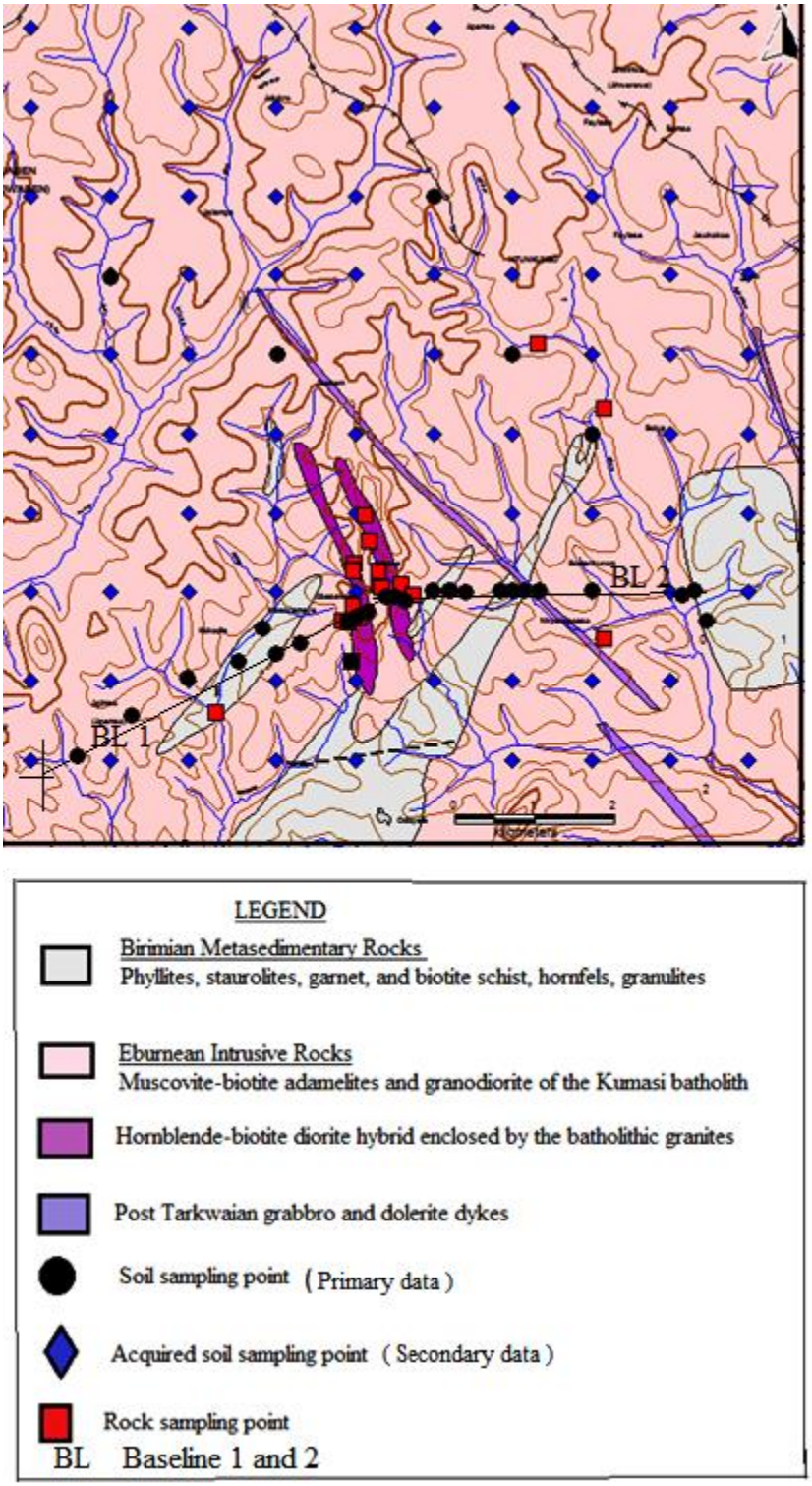

Figure 3.1: Geological map of the study area showing the individual sample points. Modified after Moon and Mason, (1967).

3.3.1 Thin section preparation

Eighteen (18) rocks samples were used to prepare thin sections. These rocks were first cleaned to prevent contamination. The individual rocks were critically examined for relevant areas or features where cross cutting was done to obtain representative thin slabs with flat surfaces. After that, the grinding machine and corundum dust were used to smoothen and flatten the surface of the sliced rock.The frosted side of the slide (glass) was then attached to the side of the chip that was grounded down to ensure constant thickness of epoxy spread across the section. The thickness and colour of the minerals, particularly of quartz were timely observed under the microscope at each stage of the grinding until the grains demonstrated a yellowish-grey interference colour when oriented parallel with the optical axis indicating the thickness was up to standard and therefore the grinding was stopped at this stage.

After mounting the rock chip on the glass slide, the slab was ground to the preferred thickness. A cover slip was then added to protect the section from damage and to increase the clarity observed in the microscope before the final polishing was done. These thin sections were studied using a polarized light microscope at the Department of Earth Science, University of Ghana.

3.3.2 Soil sample preparation and analysis

A total of one hundred and twenty one soil samples (ie. ninety for secondary data and thirty one for primary data) were prepared and analyzed at the Geological Survey Department (GSD) laboratory in Accra.The samples were sun-dried for 5-7 days (Fig. 3.2) and then sieved before they were made ready for X-ray fluorescence analysis.

During drying, the labeled bags were placed under the plastic bowls containing the soil samples to ensure easy identification. The coarser materials and any other materials are removed with a clean scoop leaving behind the finer materials, which were transferredinto thoroughly cleaned sieves with sizes -180µm and -125µm. The sieves containing the samples are placed on the electronic shakers and set to shake for 2 minutes. The powder obtained from -125 µm was poured into a Kraft paper which has been labeled to conform to the field identification.

The Kraft paper was sealed properly secure the samples. The sieve and the container were cleaned thoroughly to prevent contamination of the subsequent sample until all samples were sieved.

Figure 3.2: Photograph showing how the samples were sun dried.

For each analysis, 4.0g of sieved sample was well-mixed, homogenized with 0.9g of Hoechst Wax in a mill and pressed with 15 tons to a 32 mm pellet. Multi-element determinations from the prepared pellets were carried out using an energy-dispersive polarizing X-ray fluorescence spectrometer (SPECTRO X-LAB2000). Each sample was analyzed for major elements (SiO_2, Al_2O_3, Fe_2O_3, MgO, CaO, Na_2O, K_2O, TiO_2, P_2O_5, SO_3, and MnO), and trace elements (Cr, Zn, Cu, Pb, Co, V, As, Ni, Zn, Rb, Sr, Y, Zr, Nb, Ba, La, Ce, Pb, Th and U). Each reading was taking three (3) times to ensure accuracy.

3.4 Statistical data analyses

The major and minor elements for the rock samples dataset were in elemental form. Due to this, the major elements with concentrations in weight percentage (wt%) were converted into major oxides by using the formula below;

$$\text{Major Oxide Concentration} = \frac{\text{Molecular mass of major oxides}}{\text{Molecular mass of the metal}} \text{X} \text{Metal Concentration (wt \%)}$$

For the soil samples, U, Th, La, Cs, Te, Sb, In, Cd, Ag, Mo, Y, Se, Co, V, and Cl had more than 80% of their concentrations lessthan the detection limit and due to this they were deleted. Similarly, in the rock survey dataset, In, Re, S, Sb, Te, Cd, Ge, As, Ag had more than 60% of their concentration less than the detection limit and due to this they were also deleted. This is because a high number of elements with low detection limit in a dataset can greatly affect the correlation between variables by inducing spurious correlations (Swan and Sandilands, 1995).

After treating the data in Microsoft excel it was exported into the Statistical softwarePackage for the Social Sciences (SPSS) version 20, where summary statistics, p-p plots and histograms were constructed for every element in the dataset. The

summary statistics of the raw data was used to calculate the threshold values in Microsoft Excel. The mean + 1 standard deviation (SD) was used to calculate for the first threshold values after which the mean + 2SD was also used calculate for the second threshold value. Both threshold values were used to construct spatial distribution maps with the Sufer software version 20 for all the elements in order to study how they were distributed spatially.

3.5 Profiling

Concentration (Y axis) against distance (X axis) profiles were plotted for selected elements of the primary data in Microsoft Excel and the cross section of the geology of the study area projected under the profile to able to infer the associated geology.

3.6 Multivariate statistics

The Pearson's correlation coefficient was used to construct correlation matrix in SPSS for the datasets in order to assess the strength of the relationships between different elements. Scatter plots were also generated to show the inter-relationship between elements that were correlating well in the correlation matrix having values above 0.7.

Principal Component Analysis (PCA) was employed based on the high concentrations of some elements obtained in certain sampling sites and the strong correlation between the elements indicated by the Pearson's correlation matrix. Varimax orthogonal rotation with Kaiser Normalization was applied to the PCA in order to minimize the effects of non-normal data (Gong et al., 2010).The effects of high concentrations, and components were extracted based on Kaiser's default Eigenvalue of 1 by Field (2009). Component loadings in the PCA were also used to construct spatial distribution maps to aid the interpretation of the soil geochemistry.

The hierarchical cluster analysis was also done in SPSS to classify elements into homogeneous groups. Clustering, groups the observations into a number of clusters where the members of the first cluster are similar as possible while dissimilarity across clusters is minimized (Templ et al., 2008).The log transformed data and the Z- score were employed for the hierarchical cluster analysis.

CHAPTER FOUR

RESULTS

4.1 Petrography

This section is made up both field observation and thin section analysis of the rocks encountered in the study area.

The field observation in hand specimen entailed rock characteristics such as, grain sizes, mineral composition as well as the texture.

In the thin section examination, the representative rock samples were studied for their petrographical properties to derive information on the grain size, texture and mineralogical composition as well as structures and deformations. Modal estimation was done by the visual counting of the individual mineral grains present. The major rock types encountered in the study are biotite schist, diorite, granodiorite and granites.

4.1.1 Biotite schist

Biotite schist outcrops between Ntumkumso and Boiyaare medium to fine grained, dark grey or black (Fig 4.1a) with characteristic schistose foliation and contain quartz veins and veinlets (Fig 4.1b). The minerals present are pyrite, biotite, plagioclase and quartz. They are slightly-strongly foliated with joints and fractures. The foliations generally strike in the NE direction and dip in the SW. Thin section description shows stronglepido-blastictexturewith abundant lineated biotite, muscovites,quartz and feldsparminerals, with sutured penetrative contacts, all oriented in a preferred direction clearlyexhibitingaschistosetexture (schistose foliation), (Fig 4.2).

Figure 4.1a: Field photograph of biotite schist which outcrops between Ntumkumso and Boiya

Figure 4.1b: Hand sample of biotite schist

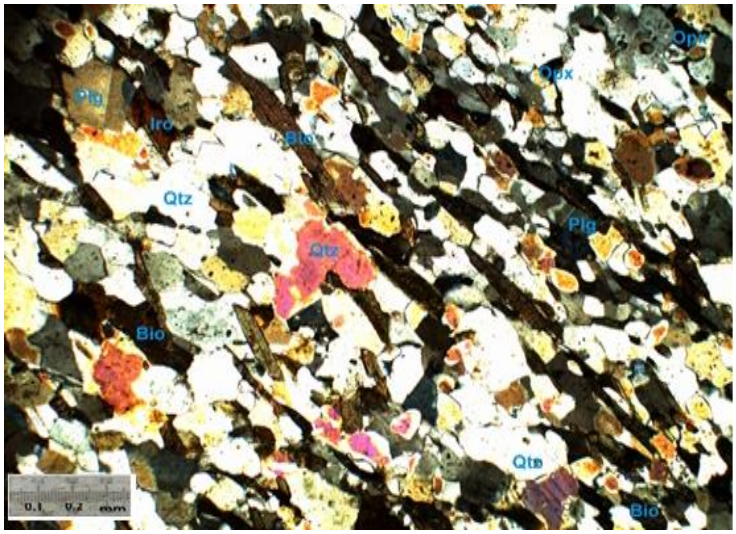

Figure 4.2: Photomicrograph of biotiteschistBio=biotite, Plg=plagioclase feldspar, Opx=opaquemineral, Qtz = quartz, Iro = iron oxide

Biotite minerals aresubhedral, elongated to acicular. They form thread-likelineated crystals parallel / sub-parallel to each other andoriented in a preferred direction. Theymostlyform penetrativeand sutured contacts with feldspar and quartz. Some show evidenceof alteration to chlorite (with green absorption colours and high interference

colours). They sometimes occur as rims surrounding feldspar and quartz minerals, and at other times occur as inclusions in them implying that biotite was part of the early crystallizing phases with feldspars crystallizing later.

Quartz minerals are anhedral with angular and irregular shapes nearly elongated with in auniform preferred orientation (Fig 4.2) bearing fractures and showing undulatory extinction (indicative of deformation) and distinctive yellow and blue interferencecolours (perhaps, the results of deformation or thickness of the thin section) and mostly associated with feldspar. They defer in sizes with some forming very fine grains perhaps due to the annealing responsible for the schistosity.

Feldspars are subordinate and are generally plagioclase with very few microclines. They are anhedral with large irregular shapes but uniformly oriented in preferred direction, mostly showing albite twinning. In thin section, plagioclase show poikiloblastic texture (Fig 4.2) owningto the inclusions of broken biotite.Some feldspars have been partially altered to sericite, indicating deuteric alteration, but their pseudomorphs are however retained

Opaque minerals are euhedral and irregular in shape and mostly occur at the boundary between plagioclase and biotite. They are perhaps ore minerals. Sericites occuras alteration of feldspars but the pseudomorphs of the feldspars are retained. Iron oxides are probably the weathered products of biotite

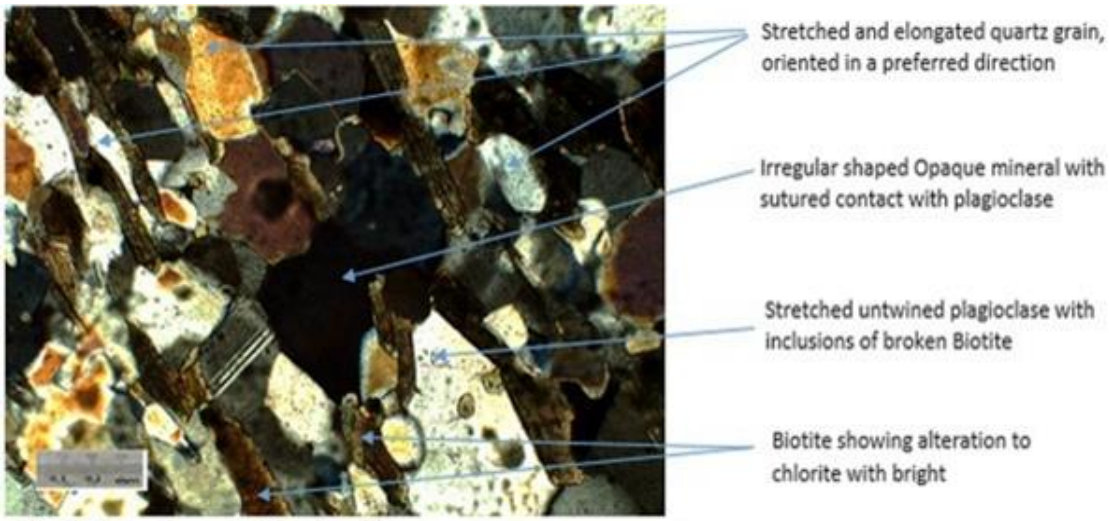

Fig 4. 3 Photomicrograph of Biotite schist

Table 4.1 Estimated modal compositions in biotite schist from two thin sections are presented below.

MINERAL	MODAL%
Quartz	**55 – 65**
Biotite	**22 -30**
Feldspar (plagioclase)	**10 – 15**
Opaque	**1 – 2**
Iron oxide	**1 – 2**

4.1.2 Diorite

Four outcrops of diorites were encountered in the study area specifically at Abesewase and Ofoase. They are dark coloured and medium to coarse grained in texture. Plagioclase, quartz, honblende and mica (biotite and muscovite) are the mineral constituents of the rock. They are generally competent, slightly weathered and contain some micro fractures and joints (Fig 4.4).

In thin section, it exhibits a hypidiomorphic (granular) texture with laths of clouded

plagioclase and hornblende. It also shows a porphyritic texture (Fig 4.5D) with phynocryst of feldspar in a phaneritic matrix of quartz, biotite and amphibole.

Plagioclase is the most dominant (Fig 4.5A) and occur as phenocryst and also show poikilitic/sieve texture (Fig 4.5D) owning to the inclusions of quartz, biotite and amphibole. They are mostly associated with amphibole and in most cases, amphibole forms rim around plagioclase. They exhibit polysynthetic twinning and also show yellowish interference colours because of their deformation. Some plagioglase show slight alteration to sericite (fine grained muscovite) but their relict polymorph twinning is preserved. The microcline shows cross hatched twinning anhedral to subhedral in shape. Under plane polar it is colourless.

Hornblende is euhedral, prisimatic with characteristic cross cutting cleavages at nearly 60^0 and 120^0 (Fig 4.5B). They are pale green in colour and exhibit a very feeble pleochroism from bottle green to greenish-yellow. Quartz minerals are irregular in shape and show yellowish interference colours (Fig 4.5C). Biotite is mottled shaped, with perfect cleavage.

Fig 4.4: Field photograph of Diorite which outcrops at Abesewase and Ofoase.

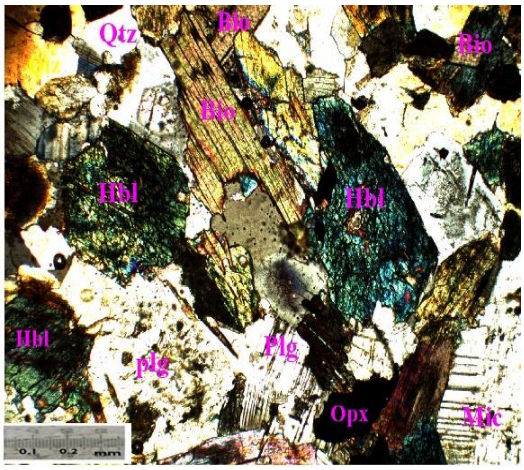

A

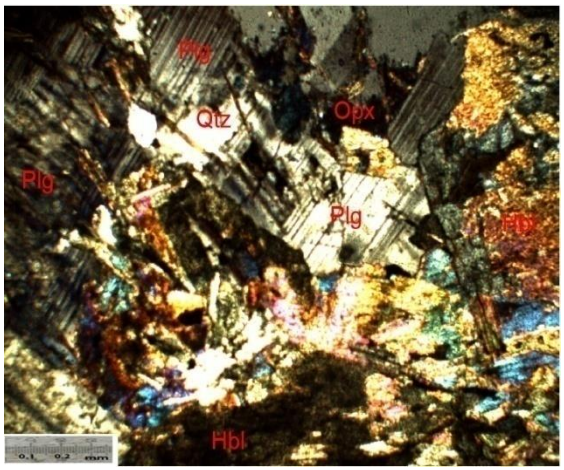

B

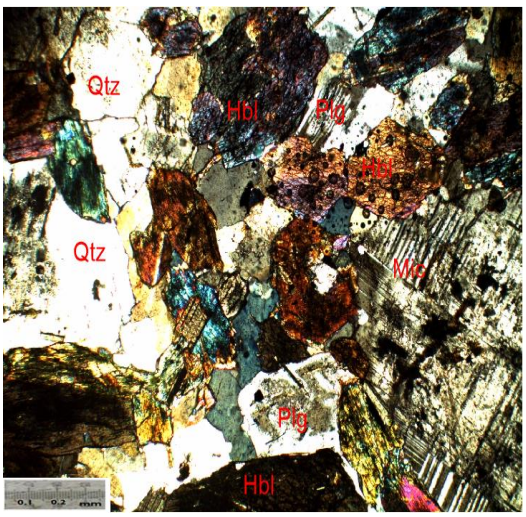

C

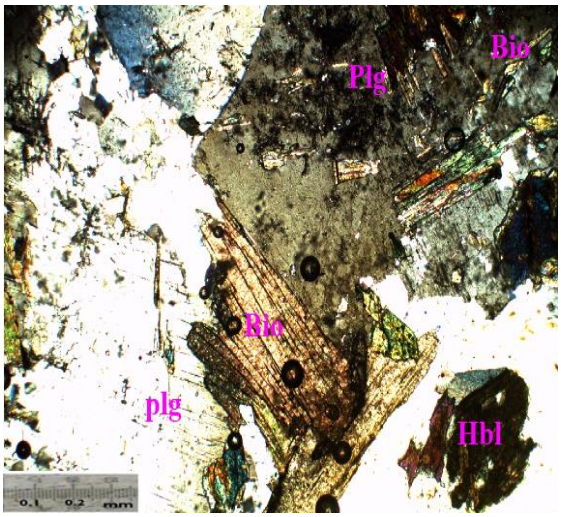

D

Fig 4.5 (A, B, C, D): Photomicrograph of diorite. Hbl=hornblende, Plg = plagioclase, Qtz = quartz.

Table 4.2: Estimated modal compositions in diorite from four thin sections are presented below.

MINERAL	MODAL%
Plagioclase	35-40
hornblende	25-30
Quartz	10 -15
Biotite	8- 10
Microcline	5 – 8
Iron oxide	1-2
Opaques	1-2

4.1.3 Granodiorite

The granodiorites outcrop between Kokodie and Odoyefe (Fig 4.6A and 4.6B). These granodiorites (Fig 4.6A) are light to dark grey in colour, coarse grained and composed of plagioclase, quartz, muscovite and biotite. Again, they are slightly weathered and contain fractures and joints. They generally, strike NE and dip in the SW direction.

In thin section, it shows granular texture composed of quartz, feldspar (plagioclase), muscovite and garnet. Minerals are generally stretched and oriented in a preferred direction (Fig 4.6C) showing that the rock is foliated. It is principally composed of polysynthetically twinned plagioclase, though some are untwinned and sometimes occur as inclusions in quartz. Quartz is also abundant but potash feldspars are very subordinate. Quartz occurs as lenticular plates, grains and invariably shows undulose extinction.

Plagioclase forms more than two-thirds of the total feldspars in all thin sections. In some sections, only plagioclase occurs with very few or no potash feldspar. Such rocks are herein referred to as granodiorites (Fig 4.6 D and E) and (Fig 4.6 C and F). Potash Feldspars are mostly microcline with distinctive tartan twinning. Muscovites mostly occur at quartz-palgioclase boundary. Garnet is euhedral with well-preserved hexagonal shape (Fig 4.6C) and characteristic isotropic nature. With its isotropic character, it is clearlyobserved becauseof its high relief and hexagonal form though same have distorted shapes. Muscovites are anhedral, tabular and sparsely distributed but always maintain their preferred orientation. They are generally lineated and oriented in a preferred direction with some occurring as inclusions within the feldspar mineral.

Fig 4.6A: Field photograph of granodiorite which outcrops at Kokodie and Odoyefe

Fig 4.6B: Field photograph of granodiorite which outcrops at Kokodie and Odoyefe

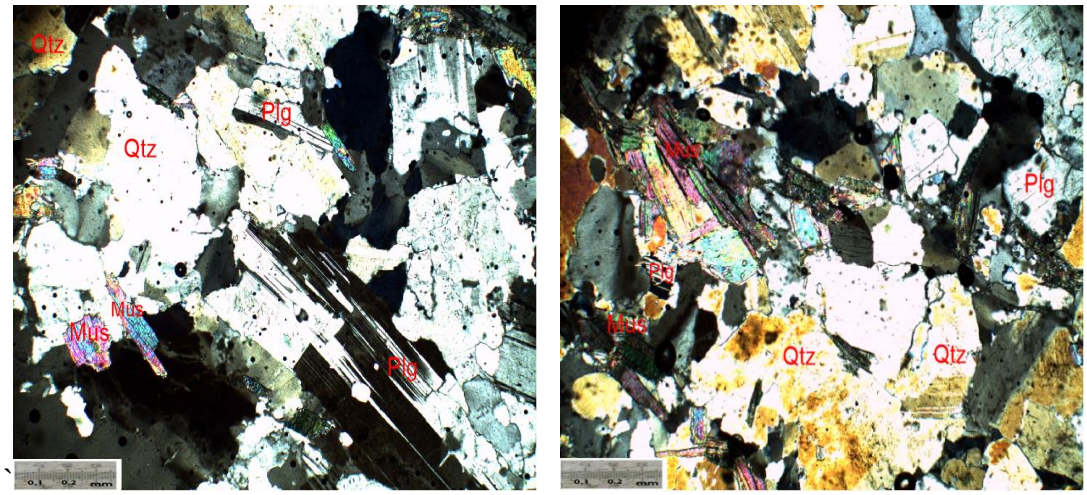

C D

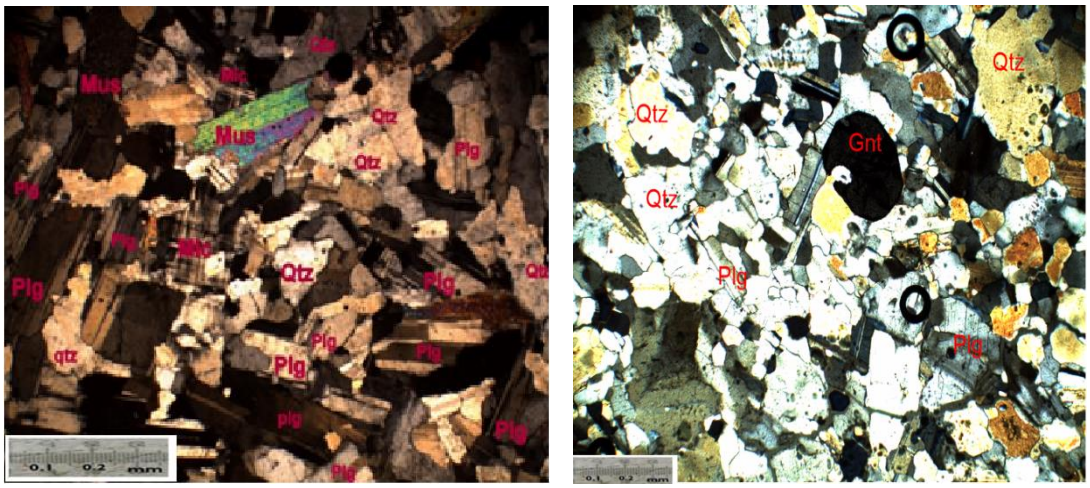

E F

Fig 4.6 (C, D, E, F): Photomicrograph of granodiorites. Mus = Muscovite, Plg=Plagioclase, Qtz=Quartz, Gnt=Garnet

Table.4.3 Estimated modal compositions in Granodiorite from three thin sections are presented below.

MINERAL	MODAL%
Plagioclase	5-55
Quartz	30-35
Muscovite	8-10
Microcline	0-10
Garnet	<1
Opaques	<1

4.1.4 Granites

The granites in the study area outcrop at Apemso and Nkyerepoaso. Some of them are pinkish whilst others are grey in colour. They are medium to coarse grained in texture when observed with hand lens. The minerals present are potash feldspars, plagioclase, muscovite and quartz and mostly dominated by muscovite. These granites have quartz vein in them and appear weathered (Fig 4.7a and 4.7b) with fractures and joints. They generally strike in the northeast direction and dip SW.

In thin section, they are coarse grained and composed of broad plates of plagioclase and microcline exhibiting feeble cross-hatching (Fig 4.8C and D). Flakes of biotite occur marginal to microcline and are pleochroic from brown to greenish-yellow (Fig 4.8C and D). Plagioclase is very subordinate with characteristic polysynthetic twinning. Quartz minerals are irregular in shape sometimes showing yellowish and bluish interference colours with inclusions of feldspars and biotites. Opaque minerals are also irregular forming sutured boundaries with other minerals. Biotite show slight

evidenceof alteration to chlorite (with green absorption colours and high interference colours

Fig 4.7a: Field photograph of granite which outcrops at Nkverepoaso

Fig 4.7b: Field photograph of weathered granite which outcrops atApemso

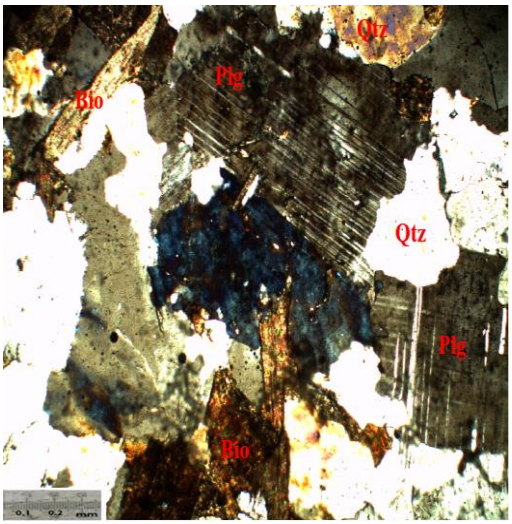

C (X40)

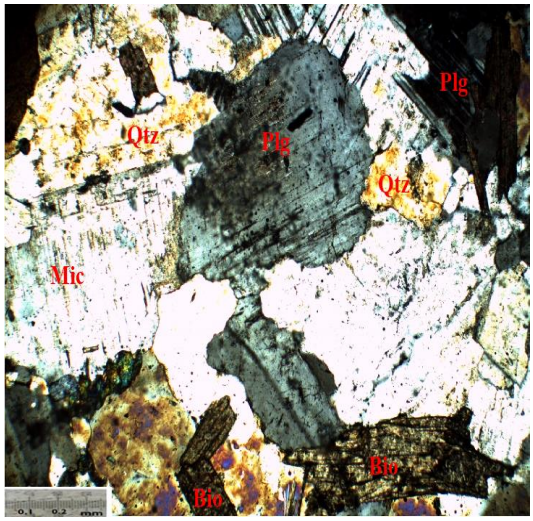

D (X 40)

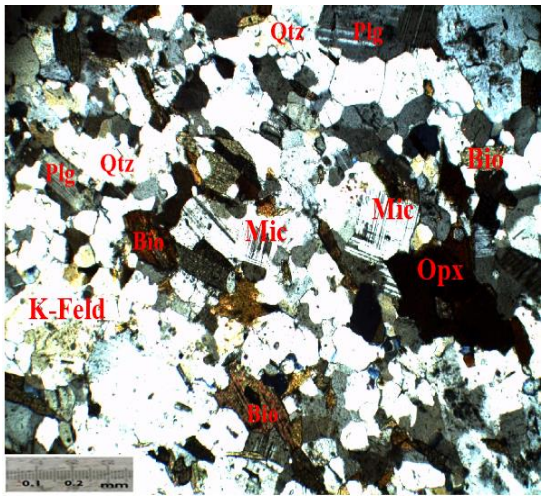

E (X10)

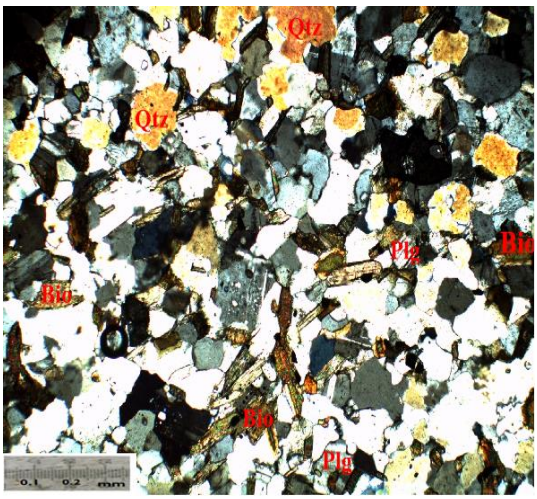

F (X10)

Fig 4.8: Photomicrograph of granite. Mic=microcline, K-feld= potash feldspar, Plg=plagioclase, Qtz=quartz

Table.4.4 Estimated modal compositions in granite from two thin sections are presented below.

MINERAL	MODAL%
Quartz	50-60
Potash feldspar (mostly Microcline)	20-25
Biotite	8-12
Plagioclase	8-10
Muscovite	< 1
Opaques	<1

4.1.5 Pegmatite

They intrude the granitoids that outcrop at Boiya, and Ofoase. In hand specimen, the pegmatite are coarse grained and contain biotite, muscovite, feldspar and quartz and are dark pink in colour.

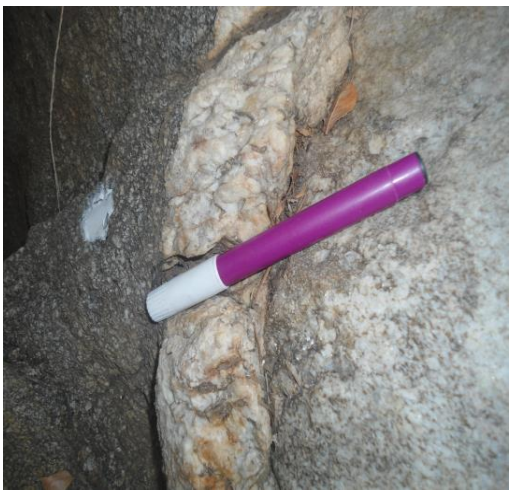

Figure 4.9a: Field photograph of pegmatiteIntruding granitoids at Boiya

Figure 4.9b: Hand sample of pegmatite

4.2 Whole rock geochemistry

Summary statistics for the individual rock samples are represented in Tables 4.5 to 4.8. This, and P-P plots were constructed to study how the elements were distributed. Observation from the p-p plots indicates that the distribution of elements deviates from the linearity such that the circles in the p-p plots mostly move away from the line of best fit. This implied that the data was skewed (Fig 4.10a), hence, the needs to log transform the dataset to base 10. After the log transformation, summary statistics of the entire elements in the dataset were again calculated in SPSS and p-p plots were plotted to study distributions of the individual elements after transforming the dataset.

Fig 4.10b, displays p-p plot for Sn after transformation. From this figure, it can be observed that the distribution of Sn is closer to linear than the raw data.

Table 4.9 displays comparison between the skewness values of the logarithmic transformed dataset and the raw dataset. From this table, it can be observed that some of the elements that were positively skewed became negatively skewed when transformed and vice versa. Arsenic (3.61) maintained its high skewness value even after it was transformed. TiO_2, Ba, Ce, La, Li, Mn, Sr, Zn, Eu, Nb, and Pr became more skewed after they were transformed. Example is TiO_2 with a skewness value of 0.48wt% and when transformed TiO_2 is -1.15 wt%. This signifies that the transformation of these elements was not necessary.

Table 4.5. Summary statistics for whole rock composition of biotite schist (oxides in weight percent (wt %) and elements in part(s) per million (ppm))

	N	Mean	Std. Dev	Variance	Minimum	Maximum
SiO2	2	**72.16**	1.44	2.06	**71.14**	**73.17**
TiO2	2	**0.50**	0.10	0.01	**0.43**	**0.57**
Al2O3	2	**15.03**	0.52	0.27	**14.66**	**15.40**
Fe2O3	2	**4.93**	0.68	0.46	**4.45**	**5.40**
MgO	2	**3.04**	0.67	0.45	**2.57**	**3.52**
CaO	2	**3.18**	0.64	0.41	**2.73**	**3.64**
Na2O	2	**4.07**	0.32	0.11	**3.84**	**4.30**
K2O	2	**1.99**	0.20	0.04	**1.84**	**2.13**
SO3	2	**0.09**	0.12	0.02	**0.00**	**0.18**
Ag	2	**0.06**	0.02	0.00	**0.04**	**0.07**
As	2	**0.30**	0.00	0.00	**0.30**	**0.30**
Ba	2	**685.00**	275.77	76050.00	**490.00**	**880.00**
Be	2	**6.58**	7.74	59.84	**1.11**	**12.05**
Bi	2	**0.07**	0.00	0.00	**0.07**	**0.07**
Cd	2	**0.05**	0.04	0.00	**0.02**	**0.07**
Ce	2	**26.85**	3.89	15.13	**24.10**	**29.60**
Co	2	**17.60**	0.28	0.08	**17.40**	**17.80**
Cr	2	**156.50**	36.06	1300.50	**131.00**	**182.00**
Cs	2	**37.80**	25.74	662.48	**19.60**	**56.00**
Cu	2	**11.35**	14.35	206.05	**1.20**	**21.50**
Ga	2	**21.45**	0.64	0.41	**21.00**	**21.90**
Ge	2	**0.16**	0.00	0.00	**0.16**	**0.16**
Hf	2	**2.30**	0.85	0.72	**1.70**	**2.90**
In	2	**0.03**	0.01	0.00	**0.03**	**0.04**
La	2	**12.30**	2.26	5.12	**10.70**	**13.90**
Li	2	**439.00**	171.12	29282.00	**318.00**	**560.00**
Mn	2	**483.00**	76.37	5832.00	**429.00**	**537.00**
Mo	2	**0.53**	0.04	0.00	**0.50**	**0.55**
Nb	2	**5.25**	1.91	3.65	**3.90**	**6.60**
Ni	2	**94.70**	11.03	121.68	**86.90**	**102.50**
P	2	**685.00**	77.78	6050.00	**630.00**	**740.00**
Pb	2	**9.50**	2.69	7.22	**7.60**	**11.40**
Rb	2	**115.85**	73.04	5335.45	**64.20**	**167.50**
Sc	2	**12.65**	1.77	3.13	**11.40**	**13.90**
Sn	2	**7.45**	8.84	78.13	**1.20**	**13.70**
Sr	2	**546.00**	127.28	16200.00	**456.00**	**636.00**
Ta	2	**0.50**	0.36	0.13	**0.24**	**0.75**
Th	2	**2.10**	0.28	0.08	**1.90**	**2.30**
Tl	2	**0.67**	0.39	0.15	**0.39**	**0.94**
U	2	**1.10**	0.00	0.00	**1.10**	**1.10**
V	2	**78.00**	11.31	128.00	**70.00**	**86.00**
W	2	**0.10**	0.00	0.00	**0.10**	**0.10**
Y	2	**10.20**	2.83	8.00	**8.20**	**12.20**
Zn	2	**77.00**	8.49	72.00	**71.00**	**83.00**
Zr	2	**84.40**	36.91	1362.42	**58.30**	**110.50**
Dy	2	**1.80**	0.46	0.21	**1.47**	**2.12**
Er	2	**1.10**	0.35	0.13	**0.85**	**1.35**
Eu	2	**1.02**	0.02	0.00	**1.00**	**1.03**
Gd	2	**2.37**	0.28	0.08	**2.17**	**2.56**
Ho	2	**0.40**	0.12	0.01	**0.31**	**0.48**
Lu	2	**0.16**	0.04	0.00	**0.13**	**0.19**
Nd	2	**12.75**	0.78	0.61	**12.20**	**13.30**
Pr	2	**3.31**	0.38	0.14	**3.04**	**3.57**
Sm	2	**2.39**	0.09	0.01	**2.33**	**2.45**
Tb	2	**0.37**	0.07	0.01	**0.32**	**0.42**
Tm	2	**0.15**	0.05	0.00	**0.11**	**0.18**
Yb	2	**0.99**	0.29	0.08	**0.78**	**1.19**

Table 4.6. Summary statistics for whole rock composition of diorites (oxides in weight percent (wt %) and elements in part(s) per million (ppm))

	N	Mean	Std. Dev	Variance	Skewness	Kurtosis	Minimum	Maximum
SiO2	4	**60.67**	0.89	0.80	0.18	-4.88	**59.87**	**61.64**
TiO2	4	**0.84**	0.29	0.08	-0.44	1.02	**0.47**	**1.17**
Al2O3	4	**14.36**	1.63	2.65	-1.64	2.64	**12.00**	**15.57**
Fe2O3	4	**7.44**	1.94	3.77	-0.72	0.48	**4.89**	**9.47**
MgO	4	**6.71**	3.76	14.12	1.21	1.21	**3.37**	**11.92**
CaO	4	**6.87**	1.68	2.82	-0.51	-0.55	**4.74**	**8.65**
Na2O	4	**3.24**	0.68	0.47	1.33	2.47	**2.60**	**4.21**
K2O	4	**1.11**	0.44	0.19	-0.89	-0.67	**0.53**	**1.49**
SO3	4	**0.28**	0.18	0.03	-1.34	2.54	**0.03**	**0.45**
Ag	4	**0.09**	0.02	0.00	-1.66	2.62	**0.06**	**0.10**
As	4	**0.30**	0.00	0.00			**0.30**	**0.30**
Ba	4	**322.50**	141.27	19958.33	-0.92	1.96	**130.00**	**470.00**
Be	4	**0.96**	0.13	0.02	0.41	-1.97	**0.83**	**1.12**
Bi	4	**0.08**	0.04	0.00	0.36	0.26	**0.04**	**0.13**
Cd	4	**0.09**	0.02	0.00	-1.78	3.14	**0.05**	**0.10**
Ce	4	**32.35**	11.73	137.54	1.97	3.91	**25.40**	**49.90**
Co	4	**29.35**	15.11	228.40	0.94	0.65	**14.60**	**49.70**
Cr	4	**214.25**	130.46	17018.92	1.61	2.53	**116.00**	**403.00**
Cs	4	**13.75**	10.50	110.28	1.20	1.16	**4.39**	**28.30**
Cu	4	**34.55**	20.55	422.47	0.38	0.80	**11.20**	**60.70**
Ga	4	**20.10**	2.13	4.52	-1.67	3.05	**17.00**	**21.80**
Ge	4	**0.22**	0.04	0.00	-1.76	3.23	**0.16**	**0.25**
Hf	4	**1.78**	0.10	0.01	0.86	-1.29	**1.70**	**1.90**
In	4	**0.07**	0.03	0.00	-0.63	1.07	**0.03**	**0.10**
La	4	**11.78**	4.50	20.28	1.95	3.82	**9.10**	**18.50**
Li	4	**340.88**	140.99	19878.06	-0.53	1.66	**156.50**	**500.00**
Mn	4	**657.50**	120.91	14619.00	0.61	1.17	**525.00**	**816.00**
Mo	4	**0.33**	0.08	0.01	0.00	0.79	**0.23**	**0.42**
Nb	4	**3.90**	1.45	2.09	-0.61	1.50	**2.00**	**5.50**
Ni	4	**130.63**	115.90	13432.60	1.71	2.98	**44.40**	**300.00**
P	4	**655.00**	426.97	182300.00	0.94	0.62	**240.00**	**1230.00**
Pb	4	**5.43**	1.86	3.47	-0.16	-4.66	**3.40**	**7.20**
Rb	4	**38.68**	16.00	255.87	1.32	2.43	**23.70**	**61.30**
Sc	4	**24.68**	10.68	114.08	0.27	-2.14	**13.30**	**37.40**
Sn	4	**1.55**	0.72	0.52	0.38	-3.68	**0.90**	**2.40**
Sr	4	**565.50**	130.22	16957.67	-1.34	2.42	**381.00**	**686.00**
Ta	4	**0.23**	0.13	0.02	0.00	-0.36	**0.08**	**0.38**
Th	4	**1.40**	0.68	0.46	-0.28	-2.73	**0.60**	**2.10**
Tl	4	**0.28**	0.14	0.02	1.66	2.69	**0.18**	**0.48**
U	4	**0.75**	0.27	0.07	0.86	-0.29	**0.50**	**1.10**
V	4	**159.25**	64.68	4183.58	-0.02	-1.29	**84.00**	**234.00**
W	4	**0.20**	0.08	0.01	0.00	1.50	**0.10**	**0.30**
Y	4	**19.93**	7.12	50.71	-1.36	1.47	**9.90**	**25.70**
Zn	4	**76.25**	7.23	52.25	-1.34	2.54	**66.00**	**83.00**
Zr	4	**45.93**	2.76	7.61	0.82	0.76	**43.10**	**49.60**
Dy	4	**3.75**	1.36	1.84	-1.56	2.81	**1.79**	**4.89**
Er	4	**2.26**	0.79	0.63	-1.57	2.43	**1.12**	**2.88**
Eu	4	**1.67**	0.42	0.18	-1.96	3.87	**1.04**	**1.92**
Gd	4	**4.86**	1.64	2.68	-1.72	3.18	**2.46**	**6.13**
Ho	4	**0.83**	0.30	0.09	-1.49	2.56	**0.40**	**1.08**
Lu	4	**0.28**	0.09	0.01	-0.88	-0.41	**0.16**	**0.36**
Nd	4	**21.88**	7.32	53.51	-0.02	1.44	**12.90**	**30.80**
Pr	4	**4.87**	1.71	2.92	1.16	2.27	**3.18**	**7.25**
Sm	4	**4.78**	1.57	2.47	-1.58	2.43	**2.51**	**5.98**
Tb	4	**0.76**	0.26	0.07	-1.60	2.88	**0.38**	**0.97**
Tm	4	**0.29**	0.10	0.01	-1.41	1.50	**0.15**	**0.36**
Yb	4	**1.83**	0.61	0.37	-1.16	0.35	**1.00**	**2.32**

Table 4.7. Summary statistics for whole rock composition of granodiorite (oxides in weight percent (wt %) and elements in part(s) per million (ppm))

	N	Mean	Std. Dev	Skewness	Minimum	Maximum
SiO2	3	**71.94**	3.98	1.34	**68.80**	**76.41**
TiO2	3	**0.42**	0.19	-1.36	**0.21**	**0.57**
Al2O3	3	**14.17**	0.66	1.73	**13.77**	**14.93**
Fe2O3	3	**3.82**	2.18	-1.53	**1.33**	**5.42**
MgO	3	**1.86**	1.66	1.12	**0.46**	**3.70**
CaO	3	**2.58**	1.56	0.18	**1.05**	**4.17**
Na2O	3	**3.61**	0.06	0.94	**3.56**	**3.68**
K2O	3	**2.55**	1.64	1.20	**1.21**	**4.37**
SO3	3	**0.07**	0.06	-1.73	**0.00**	**0.10**
Ag	3	**0.06**	0.02	-0.94	**0.04**	**0.07**
As	3	**0.37**	0.12	1.73	**0.30**	**0.50**
Ba	3	**506.67**	110.15	-1.67	**380.00**	**580.00**
Be	3	**2.21**	1.65	-1.66	**0.31**	**3.31**
Bi	3	**0.15**	0.16	1.73	**0.06**	**0.33**
Cd	3	**0.06**	0.02	0.00	**0.04**	**0.08**
Ce	3	**24.40**	13.22	0.91	**12.80**	**38.80**
Co	3	**11.30**	7.82	-0.88	**2.80**	**18.20**
Cr	3	**84.00**	66.09	-0.27	**16.00**	**148.00**
Cs	3	**23.93**	16.60	1.49	**11.55**	**42.80**
Cu	3	**12.60**	9.69	-1.60	**1.50**	**19.40**
Ga	3	**22.40**	7.49	0.53	**15.40**	**30.30**
Ge	3	**0.14**	0.01	0.00	**0.13**	**0.15**
Hf	3	**2.13**	0.96	-0.76	**1.10**	**3.00**
In	3	**0.03**	0.01	1.46	**0.03**	**0.04**
La	3	**11.03**	6.35	0.17	**4.80**	**17.50**
Li	3	**538.33**	235.07	1.20	**345.00**	**800.00**
Mn	3	**331.00**	214.67	-1.14	**93.00**	**510.00**
Mo	3	**0.51**	0.03	0.94	**0.48**	**0.54**
Nb	3	**3.73**	0.25	0.59	**3.50**	**4.00**
Ni	3	**36.83**	34.37	0.51	**4.60**	**73.00**
P	3	**586.67**	334.71	-1.35	**210.00**	**850.00**
Pb	3	**11.20**	7.55	1.70	**6.40**	**19.90**
Rb	3	**133.60**	91.48	1.70	**74.80**	**239.00**
Sc	3	**10.17**	5.99	-1.63	**3.30**	**14.30**
Sn	3	**3.20**	1.74	-1.63	**1.20**	**4.40**
Sr	3	**427.33**	199.75	-1.71	**197.00**	**553.00**
Ta	3	**0.25**	0.09	-1.71	**0.15**	**0.31**
Th	3	**3.00**	3.64	1.73	**0.80**	**7.20**
Tl	3	**0.76**	0.41	-0.50	**0.33**	**1.15**
U	3	**1.97**	2.72	1.72	**0.30**	**5.10**
V	3	**62.00**	40.71	-1.73	**15.00**	**86.00**
W	3	**0.17**	0.12	1.73	**0.10**	**0.30**
Y	3	**5.83**	1.27	0.80	**4.70**	**7.20**
Zn	3	**59.33**	15.95	1.13	**46.00**	**77.00**
Zr	3	**78.57**	31.77	-0.90	**44.00**	**106.50**
Dy	3	**1.15**	0.23	-1.04	**0.90**	**1.35**
Er	3	**0.66**	0.27	-0.71	**0.37**	**0.90**
Eu	3	**0.87**	0.23	0.00	**0.64**	**1.10**
Gd	3	**1.95**	0.44	0.38	**1.53**	**2.40**
Ho	3	**0.24**	0.08	-0.59	**0.16**	**0.31**
Lu	3	**0.12**	0.05	-1.65	**0.06**	**0.15**
Nd	3	**10.80**	5.91	1.24	**6.00**	**17.40**
Pr	3	**2.90**	1.70	1.05	**1.46**	**4.77**
Sm	3	**2.06**	0.99	1.45	**1.31**	**3.19**
Tb	3	**0.27**	0.01	0.00	**0.26**	**0.28**
Tm	3	**0.09**	0.04	-1.15	**0.05**	**0.12**
Yb	3	**0.67**	0.32	-1.69	**0.30**	**0.88**

Table 4.8. Summary statistics for whole rock composition of granite (oxides in weight percent (wt %) and elements in part(s) per million (ppm))

	N	Mean	Std. Deviation	Variance	Skewness	Kurtosis	Minimum	Maximum
SiO_2	4	**74.03**	6.80	46.22	1.68	2.74	**69.38**	**83.93**
TiO_2	4	**0.04**	0.07	0.01	2.00	4.00	**0.01**	**0.14**
Al_2O_3	4	**12.32**	1.05	1.11	0.33	-1.40	**11.19**	**13.60**
Fe_2O_3	4	**0.68**	0.37	0.14	1.65	2.63	**0.42**	**1.22**
MgO	4	**0.10**	0.14	0.02	1.98	3.94	**0.02**	**0.32**
CaO	4	**0.43**	0.22	0.05	1.87	3.52	**0.29**	**0.76**
Na_2O	4	**4.42**	1.48	2.19	-1.93	3.75	**2.21**	**5.35**
K_2O	4	**3.02**	0.23	0.06	-0.56	-0.57	**2.72**	**3.26**
SO_3	4	**0.00**	0.00	0.00			**0.00**	**0.00**
Ag	4	**0.02**	0.01	0.00	-2.00	4.00	**0.01**	**0.02**
As	4	**0.30**	0.00	0.00			**0.30**	**0.30**
Ba	4	**72.50**	112.06	12558.33	1.96	3.85	**10.00**	**240.00**
Be	4	**6.66**	1.56	2.45	0.96	2.02	**5.04**	**8.80**
Bi	4	**1.11**	0.80	0.63	0.16	0.99	**0.17**	**2.10**
Cd	4	**0.04**	0.01	0.00	2.00	4.00	**0.03**	**0.05**
Ce	4	**8.74**	11.91	141.83	2.00	3.99	**2.59**	**26.60**
Co	4	**0.73**	0.92	0.85	1.94	3.78	**0.20**	**2.10**
Cr	4	**8.50**	5.80	33.67	0.74	-1.05	**3.00**	**16.00**
Cs	4	**11.96**	2.46	6.05	-1.79	3.43	**8.33**	**13.80**
Cu	4	**2.40**	1.72	2.95	0.53	-2.90	**0.90**	**4.50**
Ga	4	**29.53**	7.74	59.94	1.36	2.30	**22.50**	**40.50**
Ge	4	**0.07**	0.02	0.00	1.54	2.89	**0.05**	**0.09**
Hf	4	**2.03**	0.57	0.32	-0.13	-4.12	**1.40**	**2.60**
In	4	**0.01**	0.01	0.00	2.00	4.00	**0.01**	**0.03**
La	4	**4.00**	5.34	28.48	1.99	3.97	**1.20**	**12.00**
Li	4	**134.60**	90.10	8117.81	1.23	1.42	**53.40**	**260.00**
Mn	4	**205.25**	131.27	17230.92	0.28	-4.08	**83.00**	**355.00**
Mo	4	**0.44**	0.21	0.04	0.46	-3.23	**0.25**	**0.69**
Nb	4	**8.10**	2.50	6.23	0.68	1.29	**5.40**	**11.40**
Ni	4	**2.08**	1.90	3.59	1.93	3.76	**0.90**	**4.90**
P	4	**425.00**	350.00	122500.00	1.77	3.35	**160.00**	**940.00**
Pb	4	**16.53**	6.07	36.78	-1.36	1.31	**8.00**	**21.20**
Rb	4	**320.00**	59.03	3484.00	0.21	-3.75	**261.00**	**387.00**
Sc	4	**1.05**	1.37	1.87	1.99	3.98	**0.30**	**3.10**
Sn	4	**12.58**	7.86	61.76	1.66	2.71	**6.80**	**24.00**
Sr	4	**45.65**	53.37	2848.08	1.63	2.54	**7.80**	**123.00**
Ta	4	**1.43**	0.47	0.22	1.55	2.34	**1.06**	**2.10**
Th	4	**1.93**	2.46	6.03	1.97	3.91	**0.50**	**5.60**
Tl	4	**1.58**	0.47	0.22	0.02	-3.13	**1.07**	**2.10**
U	4	**4.60**	2.88	8.31	1.93	3.76	**2.90**	**8.90**
V	4	**4.50**	7.00	49.00	2.00	4.00	**1.00**	**15.00**
W	4	**0.30**	0.20	0.04	2.00	4.00	**0.20**	**0.60**
Y	4	**3.05**	1.63	2.66	1.59	2.30	**1.90**	**5.40**
Zn	4	**32.50**	18.50	342.33	1.89	3.66	**20.00**	**60.00**
Zr	4	**44.78**	24.79	614.71	1.31	1.02	**26.10**	**79.40**
Dy	4	**0.40**	0.28	0.08	1.87	3.52	**0.22**	**0.81**
Er	4	**0.23**	0.12	0.01	1.41	1.50	**0.14**	**0.40**
Eu	4	**0.13**	0.16	0.02	1.95	3.83	**0.04**	**0.36**
Gd	4	**0.54**	0.65	0.42	2.00	3.99	**0.20**	**1.51**
Ho	4	**0.08**	0.05	0.00	1.65	2.70	**0.04**	**0.15**
Lu	4	**0.04**	0.02	0.00	0.37	-3.90	**0.03**	**0.06**
Nd	4	**3.63**	5.32	28.30	1.99	3.98	**0.80**	**11.60**
Pr	4	**1.03**	1.45	2.10	2.00	4.00	**0.28**	**3.20**
Sm	4	**0.69**	0.93	0.86	1.99	3.98	**0.19**	**2.08**
Tb	4	**0.09**	0.08	0.01	1.93	3.77	**0.04**	**0.20**
Tm	4	**0.04**	0.01	0.00	0.00	-1.20	**0.02**	**0.05**
Yb	4	**0.28**	0.08	0.01	-0.10	-5.27	**0.19**	**0.35**

4.2.1 Summary statistics for the rock dataset

Table 4.5 displays the summary statistics of the two (2) biotite schist analyzed. The highest concentration in terms of the major oxides is exhibited by SiO_2 which ranges from 71.14 to 73.17 wt% with a mean of 72.16 wt%. Al_2O_3 also varies from 14.66 to 15.39 wt% with a mean of 15.03wt%, Fe_2O_3 (4.45 to 5.40) wt%, MgO (2.57 to 3.52) wt% .TiO_2 (0.43 to 0.56) wt% and CaO (2.73 to 3.64) wt%. The contents of some minor elements are as follows; Cu (1.20 to 21.50) ppm, Ni (86.90 to 102.50) ppm, Ga (21.00 to 221.90) ppm, Rb (64.20 to 167.50ppm), and Sr (456.00 to 636.00) ppm.

The summary statistics for the four (4) samples of diorites are displayed in Table 4.6.The highest concentration in terms of the major oxides is exhibited by SiO_2 which ranges from 59.87 to 61.64 wt% with a mean of 60.67wt%. Fe_2O_3 (4.89 to 9.47) wt%, K_2O (0 .53 to 1.49) wt%, TiO_2 (0.47 to 1.17) wt%, MgO (3.37 to 11.92) wt%, CaO (4.74 to 8.65) wt% and Na_2O (2.60 to 4.21) wt%.

Some minor elements concentrations in the diorites are as follows; Cu (11.20 to 60.70) ppm, Ni (44.00 to 300.00) ppm, Rb (23.70 to 61.30) ppm, Sr (381.00 to 686.00) ppm.

Table 4.7 displays the summary statistics of three granodiorite samples that were analyzed. The major elements content are as follows; SiO_2 (68.80 to 76.41) wt% with a mean of 71.94wt% which is greater than the average estimated SiO_2 concentrations of granodiorites in the earth's crust, that is 67.17wt% (Mielke, 1979). Al_2O_3 is from 13.74 to 14.93 wt%, Fe_2O_3 (1.33 to 5.42) wt%, MgO (0.46 to 3.69) wt%, TiO_2 (0.21 to 0.57) wt%, CaO (1.05 to 4.17) wt% and Na_2O (3.56 to 3.68) wt%.

The minor elements content are as follows; Cu (1.50 to 19.40) ppm, Ba (380.00 to 580.00) ppm, Ni (4.60 to 73.00) ppm, Rb (74.80 to 239.00) ppm, Sr (197.00 to 553.00) ppm.

Table 4.8 displays the summary statistics of the four granite samples that were analyzed. The concentration of SiO_2 ranges from 69.38 to 83.93 wt%, with a mean of 74.03wt%. Al_2O_3 (11.19 to 13.60) wt% with a mean of 12.32 wt% which is slightly less than the average abundance of granite in the earth's continental crust (13.60 wt%) (Mielke, 1979), K_2O (2.72 to 3.26) wt%, MgO (0.02 to 0.32) wt%, TiO_2 (0.01 to 0.14) wt%, CaO (0.29 to 0.76) wt%, and Na_2O (2.21 to 5.35) wt%.

The contents of some minor elements are as follows: Cu (0.90 to 4.50) ppm, Ba (10.00 to 240.00) ppm, Ni (0.90 to 4.90) ppm, Rb (261.00 to 387.00) ppm and Sr (7.80to123.00) ppm.

Because of the scantiness of the data for the individual rock samples, the rest of the statistical analysis were done with all the individual dataset combined to obtain a general idea about the possible element associations in the study area.

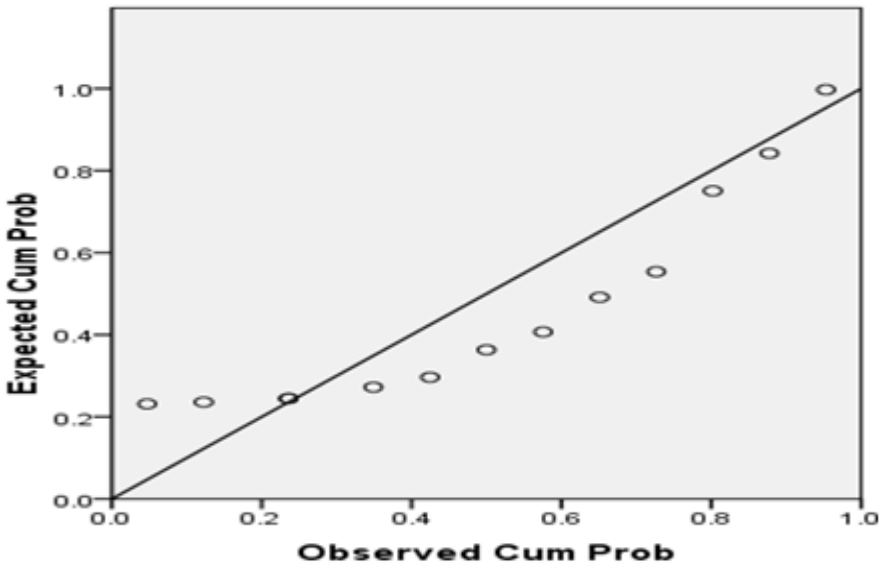

Fig.4.10a Probabilty-Probability plot for Tin

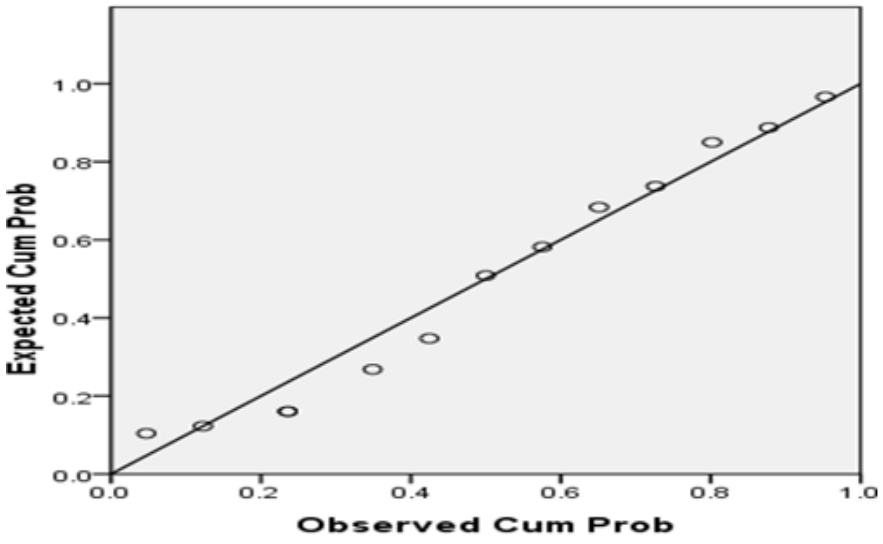

Fig 4.10b: Probabilty-Probability plot for Log_{10} Tin

Table 4.9 Comparing the difference in skewness for the rock dataset (oxides in weight percent (wt %) and elements in part(s) per million (ppm))

Elements	Raw	Transformed	Elements	Raw	Transformed
Al2O3	-0.52	-0.65	**Mo**	0.04	-0.42
CaO	0.63	-0.50	**Nb**	1.22	0.05
Fe2O3	0.20	-0.66	**Ni**	2.19	-0.49
K2O	0.48	-0.73	**P**	0.46	-0.34
MgO	1.61	-0.82	**Pb**	0.75	0.12
Na2O	0.10	-0.41	**Rb**	0.60	-0.12
SO3	1.20	-0.97	**Sc**	0.98	-0.88
TiO2	0.48	-1.15	**Sn**	1.73	0.23
SiO2	0.35	0.11	**Sr**	-0.38	-1.29
Ag	0.15	-0.68	**Ta**	1.33	0.12
As	3.61	3.61	**Th**	1.92	0.77
Ba	0.38	-1.23	**Tl**	0.77	-0.16
Be	1.08	-0.17	**U**	1.84	0.35
Bi	2.02	0.97	**V**	0.89	-0.93
Cd	0.33	-0.26	**W**	2.08	0.66
Ce	0.08	-1.13	**Y**	1.06	-0.04
Co	1.18	-0.86	**Zn**	-0.73	-1.11
Cr	1.40	-0.62	**Zr**	0.87	0.18
Cs	1.69	0.31	**Dy**	1.01	-0.36
Cu	1.44	-0.17	**Er**	0.97	-0.21
Ga	1.48	0.73	**Eu**	0.20	-1.12
Ge	0.14	-0.60	**Gd**	0.78	-0.89
Hf	0.40	-0.15	**Ho**	1.00	-0.34
In	1.05	-0.61	**Lu**	0.78	-0.29
La	-0.08	-1.07	**Nd**	0.47	-1.06
Li	0.67	-0.81	**Pr**	0.32	-1.05
Mn	-0.09	-0.99	**Sm**	0.62	-0.92
Tm	0.97	-0.13	**Tb**	0.92	-0.61
Yb	0.88	-0.11			

4.2.2 Correlation matrix for the rock data

The transformed data was used to produce the correlation matrix (Appendix C; Table 4). The inter-relationship between the forty-four (44) elements displays a wide range of correlations between negative and positive. About 60% of the inter- relationships were strongly correlating. The major oxides that strongly correlated are CaO, Fe_2O_3, MgO, SO_3 and TiO_2 (ie. 0.99-0.90). Also, Na_2O and Al_2O_3 are moderately correlated and SiO_2 is weakly correlated. SiO_2 correlates negatively with almost all the elements with the exception of Be, Bi, Hf, P, Pb, Sn and W all of which are very weakly and positively correlated. The inter-relationship of TiO_2 with these selected trace elements are however moderate to strong (between 0.74 and 0.99). Also the inter relationship of Fe_2O_3 with the trace elements is also moderate to strong (0.73-0.99).

It is evident that almost all the rare earth elements (REEs) show strong and positive correlation throughout the matrix. The weakest correlation among the rare earth elements exist between Tm-Pr (0.73) and the strongest correlation the whole dataset exist between Ho-Dy (0.99).

In this matrix, values above 0.90 implied strong correlations while values ranging from 0.75 to 0.89 implied moderate correlations and from 0.70 to 0.75indicated weakly correlation.

Considering the trace elements; Sr, Ba, Ce, Be, Cr, Ni, In, Rb, Sc and V correlated strongly. But Pb, Sn, Ta, Ti, U, Y, Cd, Ga, Ge, La, Li, Mn and Nb were moderately correlated. Again, very weak correlations exist between; As, Ag, Cs, Hf, Mo, Nb, P, Th, W, Zn and Zr. The inter relationship between these major oxides; Al_2O_3, CaO, Fe_2O_3, K_2O, MgO, Na_2O, SO_3 ,TiO_2 and minor oxides; Ba, Bi, Ce, Cr, Cu, In, Li, Mn, Ni, Pb, Rb, Sc, Sr, Ta, Ti, U, V,Y and Zn ranges from moderate to strong.

Scatter plots were plotted for these elements to have a visual observation of the various correlations between the elements selected ; Sc-MgO (0.99), Ni-Cr (0.97), Sc-CaO (0.97), Ni-Fe_2O_3(0.98), Mn-CaO (0.75), Cr- Fe_2O_3 (0.94), Cu-MgO (0.95), Cu-Fe_2O_3 (0.88),TiO_2-MgO (0.98), MgO-Fe_2O_3 (0.99), MgO-Al_2O_3 (0.71), MgO - CaO (0.99), K_2O-CaO (-0.79), Fe_2O_3-CaO (0.99), Pb- CaO (-0.87), Pb- Fe_2O_3 (-0.87), Pb-Cu (-0.95), SC-TiO_2 (0.99), Y - Bi (-0.77), La-Ce (0.99), Sn –Rb (0.85), Ni- Cr (0.97), Sc-Cr (0.92) , V-Cr (0.92), Pb-Cu (-0.93), Sc-Cu (0.87), La-Ge (0.87) , Zn-In (0.95), Y-Ni (0.88), Ta - Nb (0.93), Eu-CaO (0.94), Nd- Fe_2O_3 (0.83), Tb-TiO_2 (0.99).

From the scatter plots, it is evident that the Ho-Dy (0.99) has almost all the circles falling on line of fit; this signifies that the correlation between Ho-Dy (0.99) is the strongest amongst all the other correlations.

Also scatter plots with line of fit moving from right to left like K_2O- CaO (-0.93) indicate negative correlation. Whilst scatter plots with line of fit moving from left to right like MgO-Fe_2O_3 (0.99) implies positive correlation.

During the data exploration process it was found that all rare earth elements (REE) correlated strongly; which translated itself into issues of multicollinearity in the correlation matrix (too much correlation) overshadowing (hiding) other relevant correlations.

4.2.3 Results of the principal component analysis (PCA)

The principal component analysis was used in this study to describe the variation of a set of multivariate data in terms of a set of uncorrelated variables, each of which is a particular linear combination of the original variables. The new variables are derived in decreasing order of importance so that, for example, the first principal component accounts for most of the variation in the original data. The numerical output from a

standard PCA includes correlation between the variables, eigenvalues of the principal components, loadings of variables to each principal component, and principal component scores for each sample. The eigenvalues indicate the number of significant principal components, the first component has the largest eigenvalue, and the following components will have progressively smaller eigenvalues as their significance also decreases. The loadings indicate which variables have positive or negative correlation with the individual principal components. Another very helpful application of PCA, which does not involve any need for interpretation of the components, are low-dimensional plots of the data, which can be an aid in identifying outlying observations, clusters of similar observations, and so on (Everitt & Dunn 1991).

The Verimax rotation with Kaiser Normalization was employed in this study in order to minimize the effect of the non-normal data specifically, the effects of high concentration, and components were extracted based on Kaisers default Eigenvalues of 1.

Appendix Tables 4.2.1 shows the five factors extracted from the rock samples dataset by the PCA. These five factors accounted for 91.44% of the total variance, the first factor accounted for 64.98% of the total variance and is dominated by Al_2O_3, Na_2O, Fe_2O_3, MgO, TiO_2, Ba, Bi, Cd, Cr,Ge,In, La, Li, Ni, Pb, Sr, V, Zn, Ce,Co , Sc,Sr,Th,Dy,Eu, Gd, Nd, Pr and Tb, while the second factor explained 13.06% of the total variance and made up of negative loadings of K_2O, SiO_2, Ag, Cd, Be, Ga, Nb, Rb ,Sn, Tl and positive loadings of Ag, Er, Lu, Tm, Mn, CaO and Yb. The third factor also explained 5.97% of the total variance. The main contributors of this factors are Hf, and a negatively loaded As. Again, 3.86% of the total variance is explained by the fourth factor and the main contributors of this factor are SO_3 and W. Lastly, 3.55% of the total variance is explained by the fifth factor which is made up of only Cs. Although five

factors were extracted, the first three account for the bulk (approximately 80%) of the variance in the dataset.

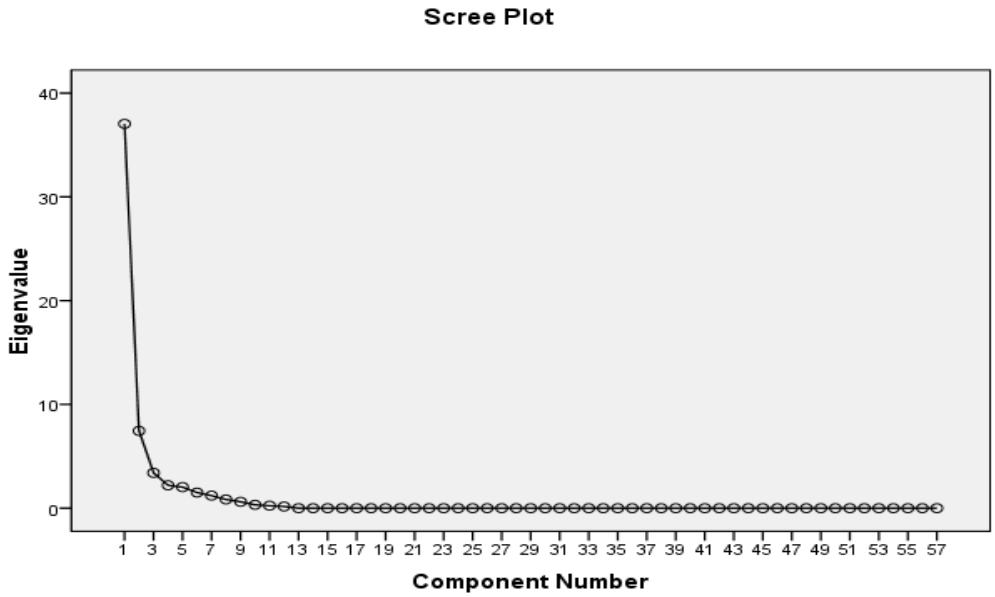

Fig 4.11: Scree plot for rock dataset. Components to the right of component 5 (beloweigenvalue of 1.0) do not account for a significant portion of variance in the dataset.

Table 4.10. Loadings for the rotated component matrix for the rock data

	Component				
	1	2	3	4	5
Al2O3	**0.754**	0.209	0.204	-0.311	0.165
CaO	0.663	**0.726**	-0.05	0.024	0.14
Fe2O3	0.69	0.676	-0.128	-0.006	0.208
K2O	-0.234	**-0.816**	0.379	-0.273	-0.122
MgO	**0.755**	0.621	-0.023	0.001	0.177
Na2O	**-0.742**	-0.062	0.055	-0.567	0.066
SO3	0.032	0.17	0.159	**0.768**	0.23
TiO2	**0.858**	0.496	-0.064	-0.022	0.096
SiO2	0.035	**-0.831**	-0.173	-0.185	0.194
Ag	0.389	**0.876**	-0.03	-0.116	0.081
As	0.134	-0.022	**-0.834**	-0.277	-0.035
Ba	0.919	0.156	-0.03	-0.262	0.091
Be	-0.301	**-0.714**	0.427	0.107	0.31
Bi	**-0.795**	-0.436	0.115	0.257	-0.169
Cd	0.281	0.668	0.341	0.169	-0.332
Ce	**0.951**	0.227	0.024	0.048	-0.077
Co	**0.757**	0.602	-0.112	-0.004	0.201
Cr	0.639	0.674	-0.041	-0.033	0.329
Cs	0.254	-0.081	-0.028	0.024	**0.881**
Cu	0.452	**0.718**	-0.245	0.211	-0.027
Ga	-0.01	**-0.774**	0.477	0.226	-0.232
Ge	**0.73**	0.65	-0.021	0.104	0.084
Hf	0.256	-0.257	**0.834**	-0.042	-0.099
In	**0.801**	0.547	0.037	0.218	0.022
La	**0.959**	0.138	-0.018	0.002	-0.083
Li	**0.807**	0.188	-0.089	-0.048	0.394
Mn	0.145	**0.837**	-0.006	-0.056	0.35

	Component				
	1	2	3	4	5
Mo	0.327	-0.42	0.324	-0.422	0.254
Nb	-0.189	**-0.757**	0.156	0.126	0.092
Ni	0.655	0.661	-0.08	0.014	0.329
P	0.655	-0.105	0.529	-0.064	0.076
Pb	-0.56	-0.636	0.228	-0.274	-0.129
Rb	-0.455	**-0.847**	0.163	-0.033	0.071
Sc	**0.779**	0.594	-0.119	0.016	0.148
Sn	-0.239	**-0.82**	0.229	0.252	0.34
Sr	**0.834**	0.44	-0.166	-0.131	0.124
Ta	-0.39	**-0.779**	0.251	0.084	0.093
Th	**0.708**	-0.472	0.342	-0.09	-0.345
Tl	-0.504	**-0.759**	0.297	-0.093	0.149
U	-0.468	-0.623	0.51	0.081	-0.262
V	**0.791**	0.579	-0.112	0.000	0.152
W	0.058	-0.428	0.212	**0.742**	-0.414
Y	0.658	0.68	0.132	0.229	0.072
Zn	**0.868**	0.387	0.116	0.056	0.214
Zr	0.691	-0.183	0.435	-0.315	0.03
Dy	**0.722**	0.658	0.05	0.169	0.064
Er	0.65	**0.719**	0.055	0.142	0.123
Eu	**0.834**	0.522	-0.077	0.003	0.071
Gd	**0.847**	0.498	0.015	0.143	-0.034
Ho	0.697	0.683	0.056	0.142	0.092
Lu	0.626	**0.733**	0.014	0.067	0.157
Nd	**0.902**	0.356	0.037	0.138	-0.077
Pr	**0.925**	0.297	0.035	0.116	-0.086
Sm	**0.874**	0.417	0.043	0.179	-0.083
Tb	**0.788**	0.585	0.041	0.157	0.01
Tm	0.589	**0.762**	0.069	0.126	0.125
Yb	0.549	**0.776**	0.011	0.105	0.172

4.2.4 Hierarchical cluster analysis

The Ward's Method was employed for the hierarchical cluster analysis. Basically, it looks at cluster analysis as an analysis of variance problem, instead of using distance metrics or measures of association.

This method involves an agglomerative clustering algorithm. It will start out at the leaves and work its way to the trunk. It looks for groups of leaves that it forms into branches, the branches into limbs and eventually into the trunk.

The Squared Euclidean distance was the interval used to measure dissimilarities in the variables. Also the Z-score was used as the standardized transformed value whilst the orientation of the data was done vertically. A phenon line was manually constructed across the dendrogram to distinguish the various clusters of interest. The cluster membership employed was the single solution and the number of clusters selected was three (3). The three distinct clusters were identified by the help of the phenon line. This was used to group the various rock types. The second hierarchical cluster analysis was conducted for the variables (elements) of this dataset.

4.2.5 Hierarchical cluster analysis for cases for the rock data grouping of rocks

The hierarchical cluster analysis displays the groupings (cases) of the various rock types in the study area (Fig 4.12). Here, thirteen rocks were fed into SPSS but only seven of them were analyzed successfully. Rocks that loaded in the first cluster were R8, R9 and R12. The second cluster is also made up of R 11 and R15. Lastly, R16 and R 17 made up the third cluster.

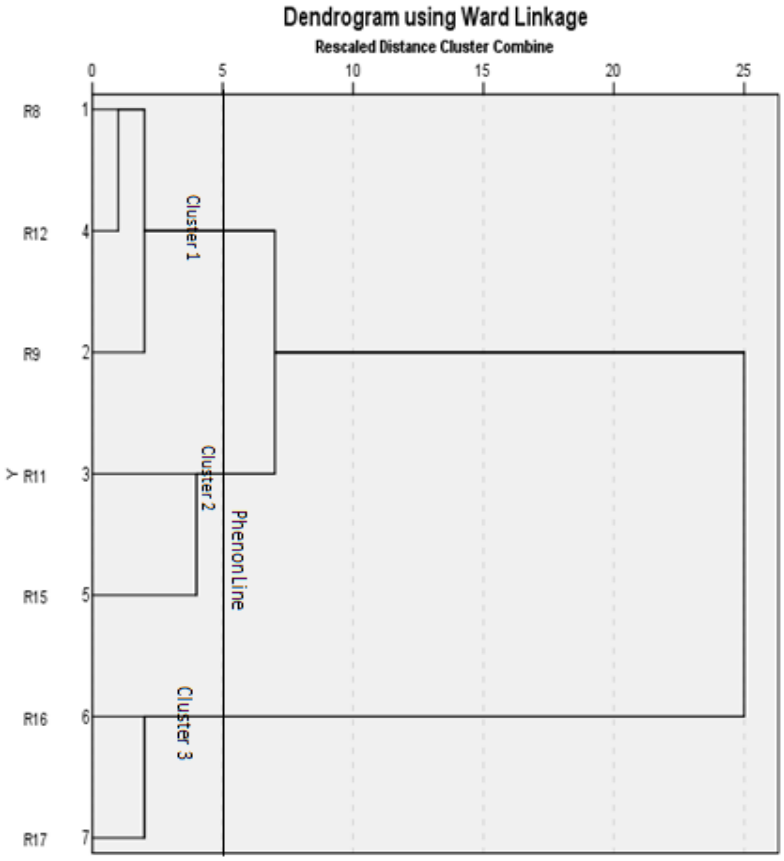

Figure 4.12: Hierarchical cluster analysis for cases for the rock data

4.2.6 Hierarchical cluster analysis for the variables of the rock data

The cluster membership employed was the single solution and the number of clusters as set at three appendix c Fig (4.13). The first cluster is made up of Al_2O_3, K_2O, Na_2O, Ba, Be, Ce, Ga, Hf, La, Nb, P, Pb, Sr, Ta, Th, U, and Zr. The second cluster is also made up of CaO, Fe_2O_3,MgO, SO_3,TiO_2, Ag, Bi, Cd, Co, Cr, Cu, Ge,In, Mn, Ni,Sc, V, W, Y, Zn, Dy, Er, Eu, Gd, Ho, Lu, Nd, Pr , Sm ,Tb, Tm, Yb and the last cluster is made up of SiO_2, As, Cs, Li, Mo, Rb, Sn, Tl respectfully.

GEOCHEMISTRY OF THE SECONDARY DATA

4.3 Summary statisticsfor thesecondary data

Summary statistics were calculated for every element in the three datasets (Table 4.11).The summary statistics covered the mean, median, standard deviation, and the percentile for each element. This, together with probability-probability (P-P plot) was constructed to study how the elements were distributed, whether normally distributed or skewed.

It was observed from the P-P plots that most of the elemental distributions were skewed thus, non –linear. (Fig 4.14a) shows that, the distribution of K_2O in the test sample dataset on the p-p plots is non- linear. Therefore they were logged transformed to the base ten in Microsoft excel and then exported back into SPSS. Summary statistics was again conducted with the log transformed datasets.

The summary statistics for the logged transformed dataset had skewness values that were very close to zero. Fig 4.14b displays that the P-P plot for the distribution of K_2O after logged transformation is very close to normal than for the raw data.

Table 4.11. Summary statistics of the secondary data

	N	Mean	Median	Std.Dev	Variance	Kurtosis	Mini	Maxi	Percentiles		
									25	50	75
Na2O	89	0.86	0.88	0.25	0.06	-0.09	0.26	1.50	0.69	0.88	1.04
MgO	90	1.34	1.28	0.45	0.20	28.82	0.81	4.50	1.13	1.28	1.41
Al2O3	90	25.86	25.25	8.46	71.57	-0.26	5.28	40.22	21.22	25.25	32.22
SiO2	90	58.57	56.58	8.76	76.71	1.48	44.98	88.27	52.20	56.58	63.12
P2O5	90	0.06	0.06	0.03	0.00	3.59	0.02	0.17	0.04	0.06	0.08
SO3	90	0.07	0.07	0.02	0.00	-0.24	0.04	0.11	0.06	0.07	0.08
K2O	90	1.29	0.95	1.09	1.18	8.01	0.27	6.18	0.64	0.95	1.55
CaO	90	0.16	0.12	0.18	0.03	22.27	0.02	1.29	0.07	0.12	0.20
TiO2	90	0.71	0.68	0.25	0.06	-0.80	0.19	1.27	0.51	0.68	0.89
MnO	90	0.03	0.02	0.03	0.00	6.75	0.00	0.17	0.01	0.02	0.04
Fe2O3	90	3.29	2.81	2.15	4.61	1.30	0.22	10.72	1.91	2.81	4.37
Cr	89	191.37	152.00	146.49	21458.85	0.41	11.50	584.00	66.15	152.00	293.00
Ni	90	15.91	12.65	15.80	249.60	37.59	2.20	135.70	8.00	12.65	18.60
Cu	57	8.09	6.70	7.09	50.33	7.14	0.50	40.50	3.20	6.70	10.55
Zn	90	23.21	22.00	10.98	120.59	2.77	2.30	67.90	15.85	22.00	28.75
Ga	90	18.40	18.40	6.87	47.14	-0.74	3.20	29.50	13.40	18.40	24.25
Ge	87	1.58	1.50	0.44	0.19	-0.64	0.70	2.60	1.20	1.50	1.90
As	90	4.94	4.40	2.33	5.41	0.60	0.40	11.50	3.50	4.40	6.18
Br	66	3.60	3.65	1.64	2.68	0.00	0.40	7.40	2.38	3.65	4.53
Rb	90	62.17	44.15	54.50	2969.76	5.38	6.10	300.80	26.90	44.15	71.48
Sr	90	27.10	22.35	17.20	295.98	8.99	8.10	111.80	17.40	22.35	32.23
Zr	90	544.95	524.00	171.34	29358.17	2.36	189.80	1181.00	422.50	524.00	624.00
Nb	87	21.22	19.20	10.39	107.88	0.72	5.60	54.90	13.40	19.20	28.20
Sn	74	6.06	5.20	3.22	10.35	-0.31	0.70	13.80	3.68	5.20	8.03
I	64	18.98	17.00	8.87	78.65	0.07	5.50	44.00	12.05	17.00	26.08
Ba	90	181.59	137.05	129.10	16666.06	6.89	49.50	769.00	91.25	137.05	259.55
Ce	66	60.64	58.00	21.27	452.45	2.46	27.00	142.00	43.00	58.00	72.25

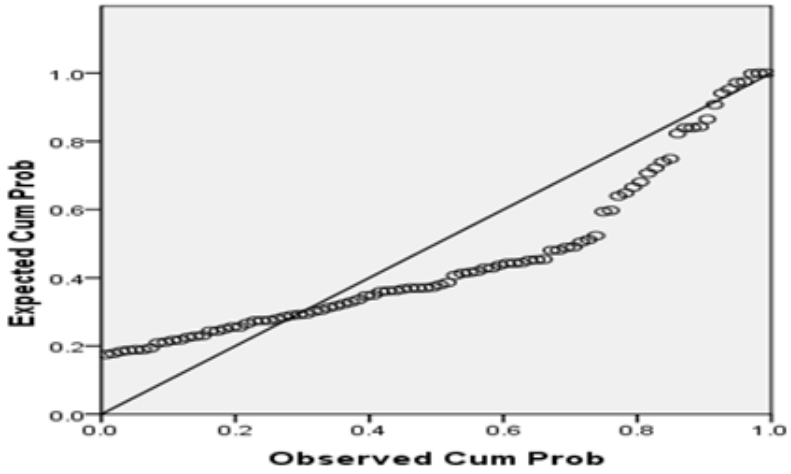

Fig. 4.14a: Probabilty-Probability plot for the distribution of K_2O

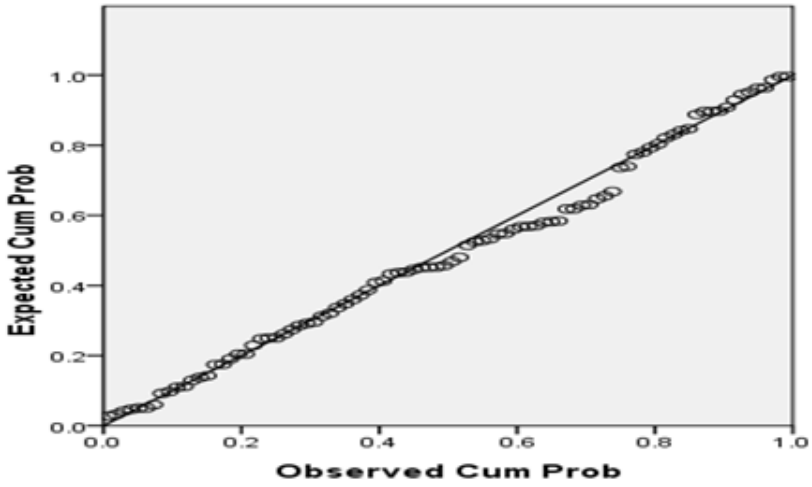

Fig. 4.14b: Probabilty-Probability plot for the distribution of $\log_{10} K_2O$

Table 4.12. Threshold values for the secondary data

	Mean	mean+1SD	mean+2SD	STD
Na2O	0.86	1.11	1.35	0.25
MgO	1.34	1.78	2.23	0.45
Al2O3	25.86	34.32	42.78	8.46
SiO2	58.57	67.32	76.08	8.76
P2O5	0.06	0.09	0.11	0.03
SO3	0.07	0.09	0.10	0.02
K2O	1.29	2.38	3.47	1.09
CaO	0.16	0.34	0.52	0.18
TiO2	0.71	0.96	1.21	0.25
MnO	0.03	0.06	0.09	0.03
Fe2O3	3.29	5.43	7.58	2.15
Cr	191.37	337.86	484.35	146.49
Ni	15.91	31.71	47.51	15.80
Cu	8.09	15.19	22.28	7.09
Zn	23.21	34.19	45.18	10.98
Ga	18.40	25.27	32.14	6.87
Ge	1.58	2.02	2.46	0.44
As	4.94	7.26	9.59	2.33
Br	3.60	5.24	6.87	1.64
Rb	62.17	116.67	171.16	54.50
Sr	27.10	44.30	61.50	17.20
Zr	544.95	716.29	887.63	171.34
Nb	21.22	31.61	42.00	10.39
Sn	6.06	9.28	12.49	3.22
I	18.98	27.85	36.72	8.87
Ba	181.59	310.69	439.79	129.10
Ce	60.64	81.91	103.18	21.27

4.3.1 Spatial distributions of the elements

Threshold value signifies the concentration of an element above which a sample is considered anomalous. Rose et al., (1979) defined anomaly as a deviation from the norm. In order to generate element distribution maps for the area, the threshold values were statistically determined for each distribution. The threshold values were calculated in Microsoft excel for every element using mean +1SD and also mean + 2SD. Table 4.12 displays the threshold (mean +1SD) and (mean +2SD) values that were used to create spatial distribution maps for elements of interest.

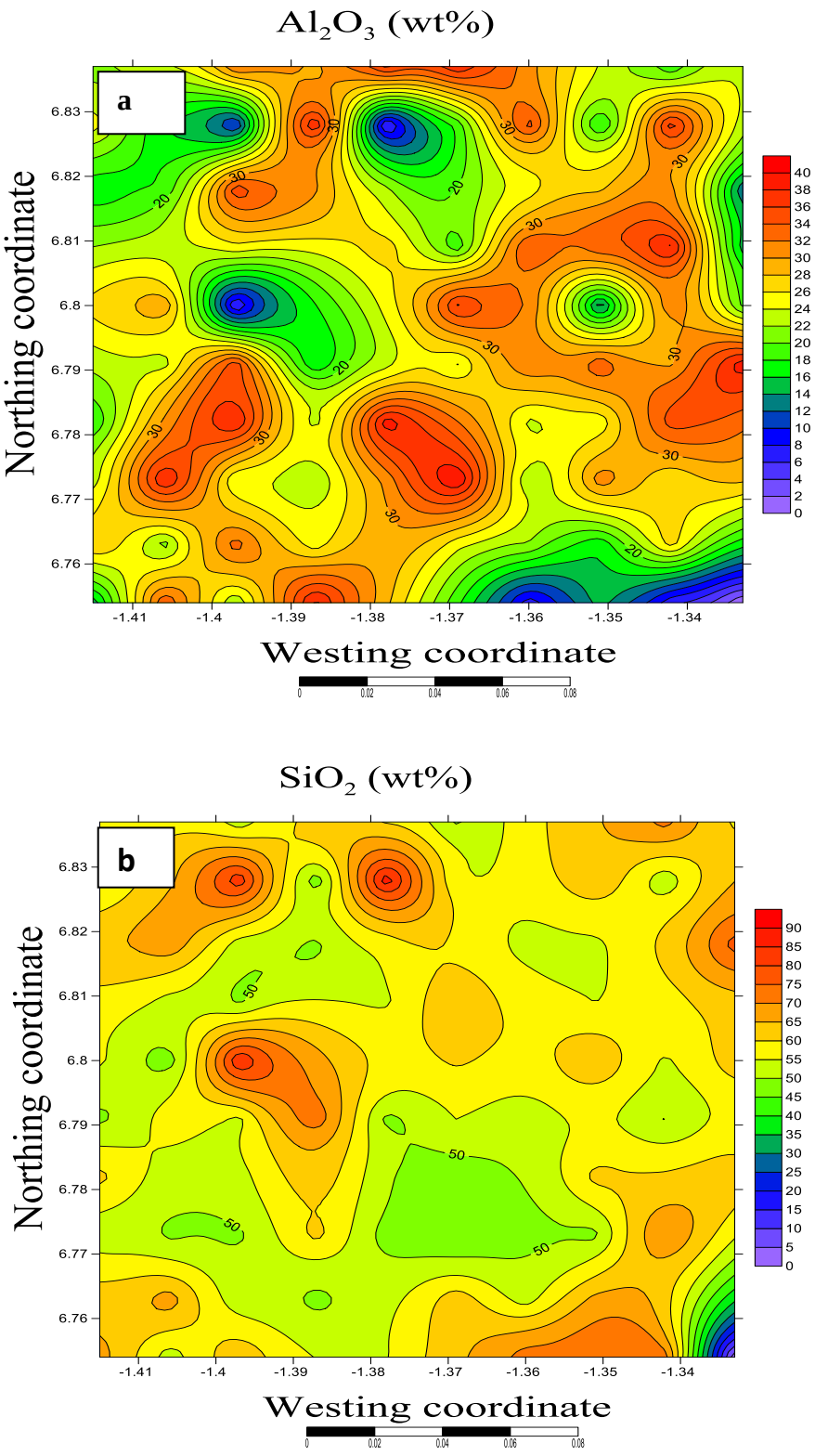

Fig 4.15 a and b show the element distribution map of Al_2O_3 and SiO_2 for the test data

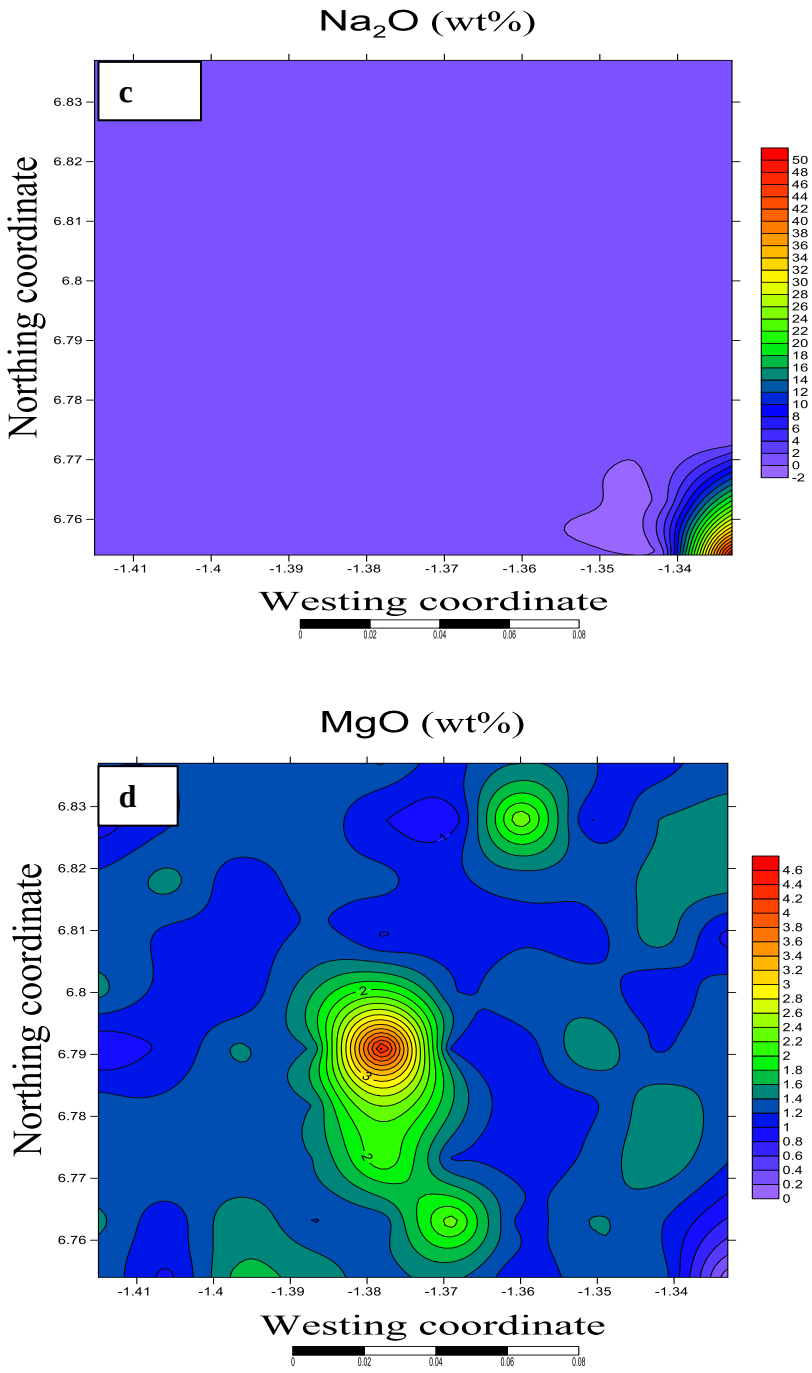

Fig 4.15 c and d show the element distribution map of Na_2O and MgO for the test data

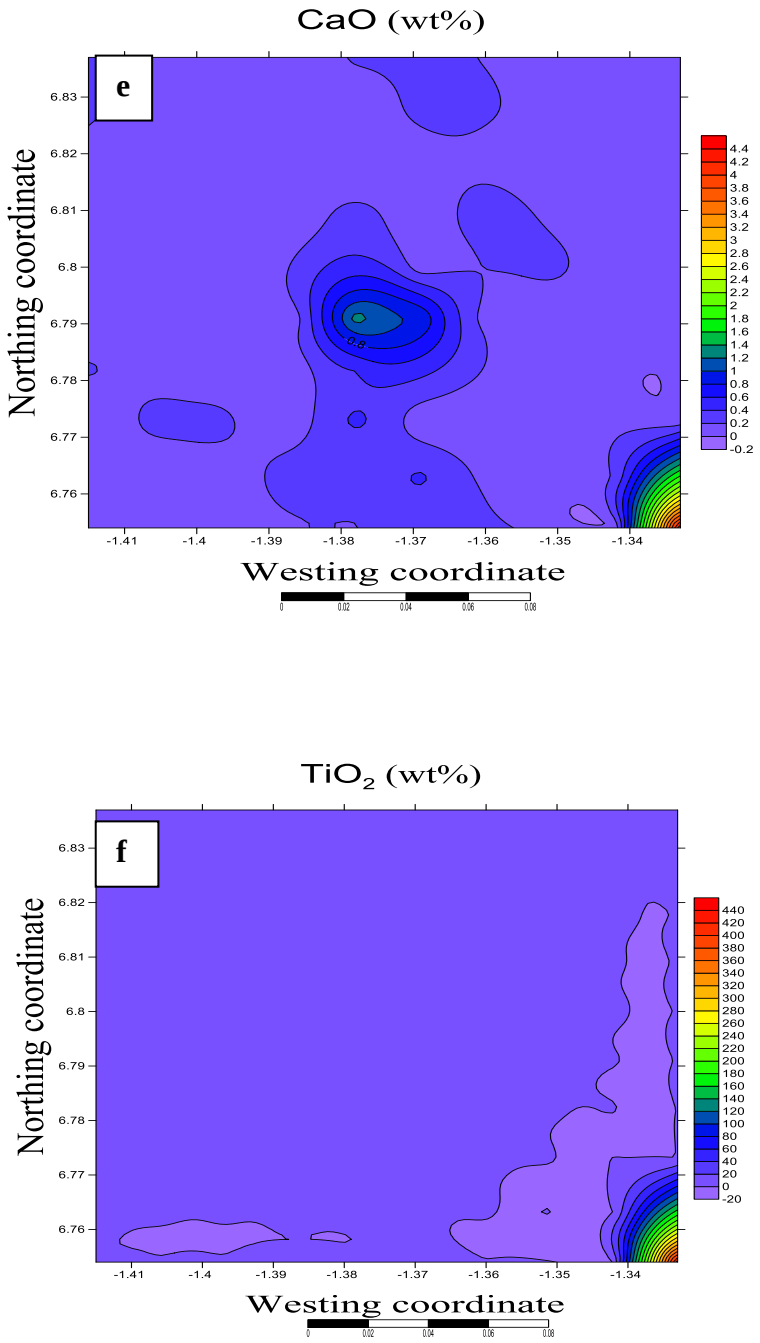

Fig 4.15 e and f show the element distribution map of CaO and TiO_2 for the test data

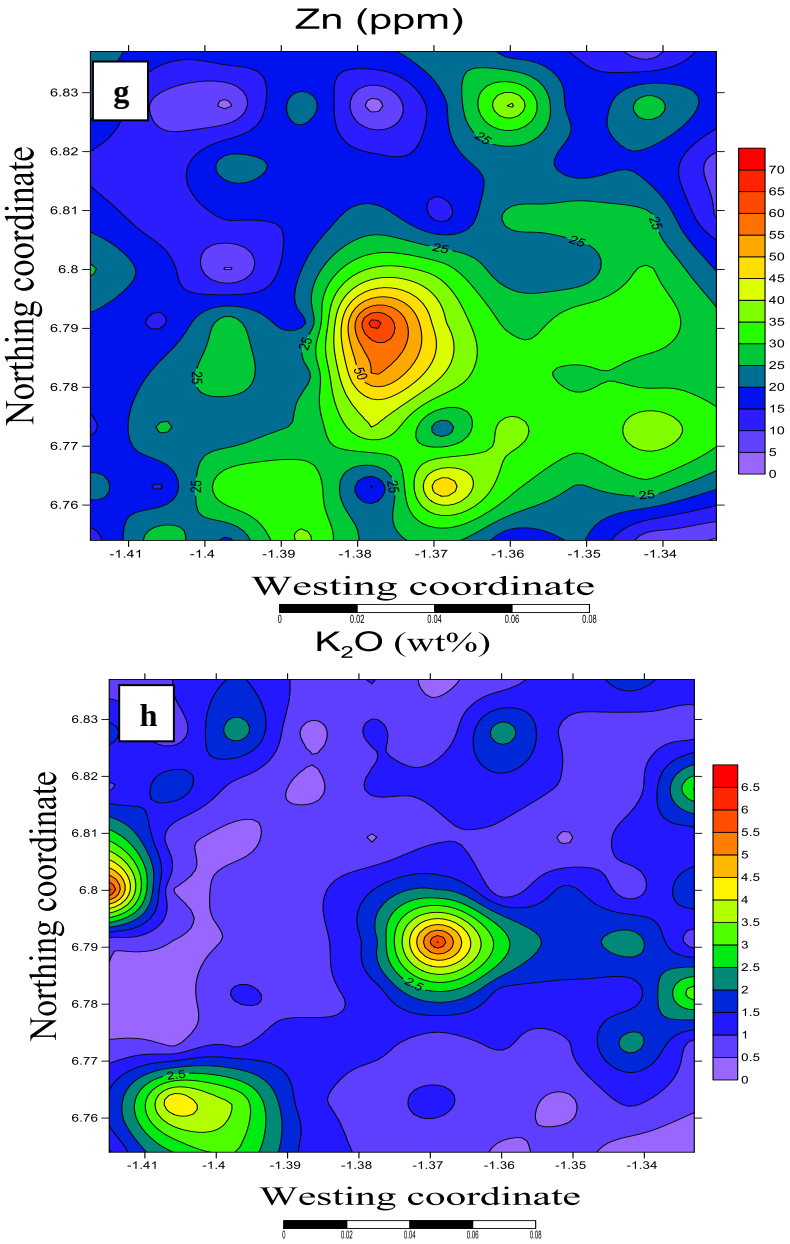

Fig 4.15 g and h show the element distribution map of Zn and K_2O for the test data

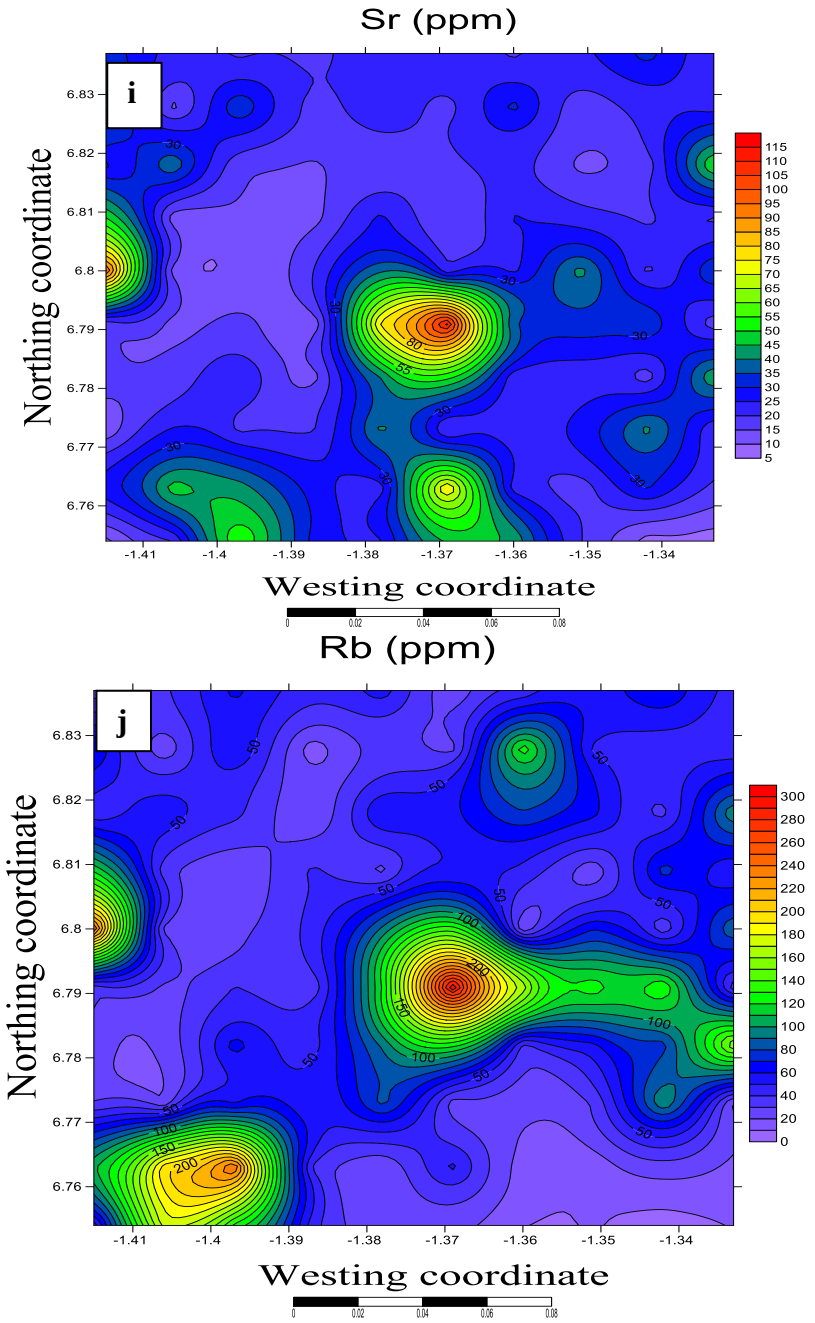

Fig 4.15 i and j show the element distribution map of Sr and Rb for the test data

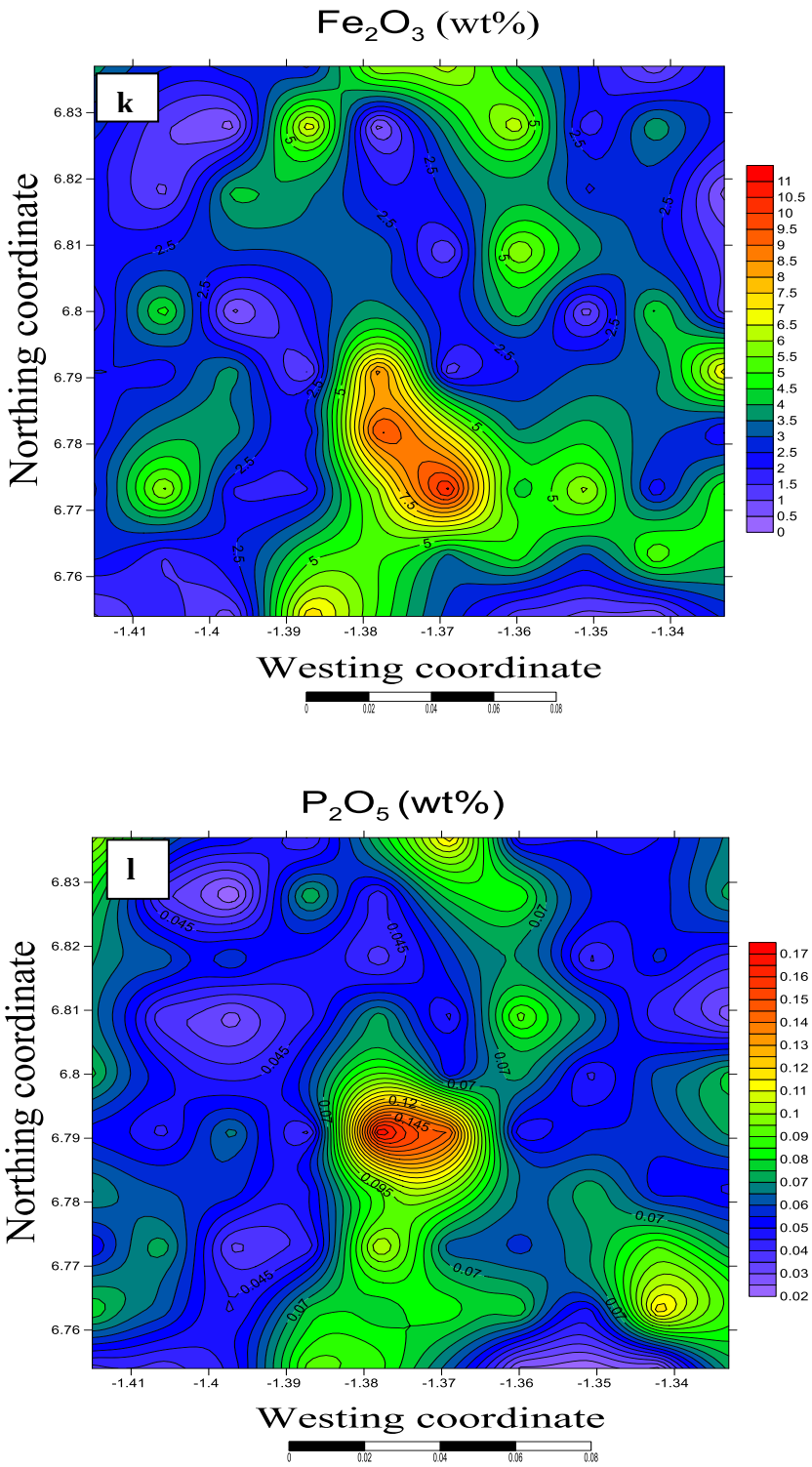

Fig 4.15 k and l show the element distribution map of Fe_2O_3 and P_2O_5 for test data

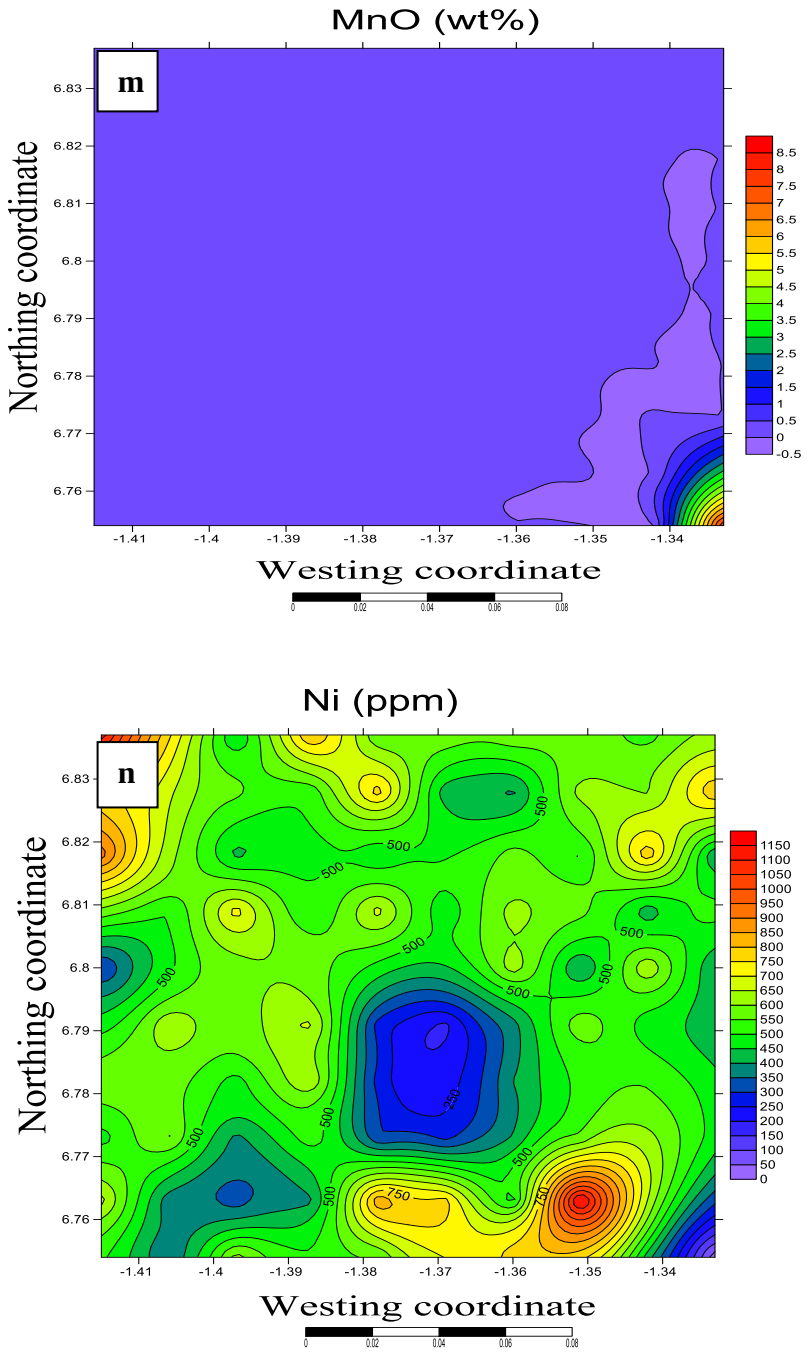

Fig 4.15 m and n show the element distribution map of MnO and Ni for the test data

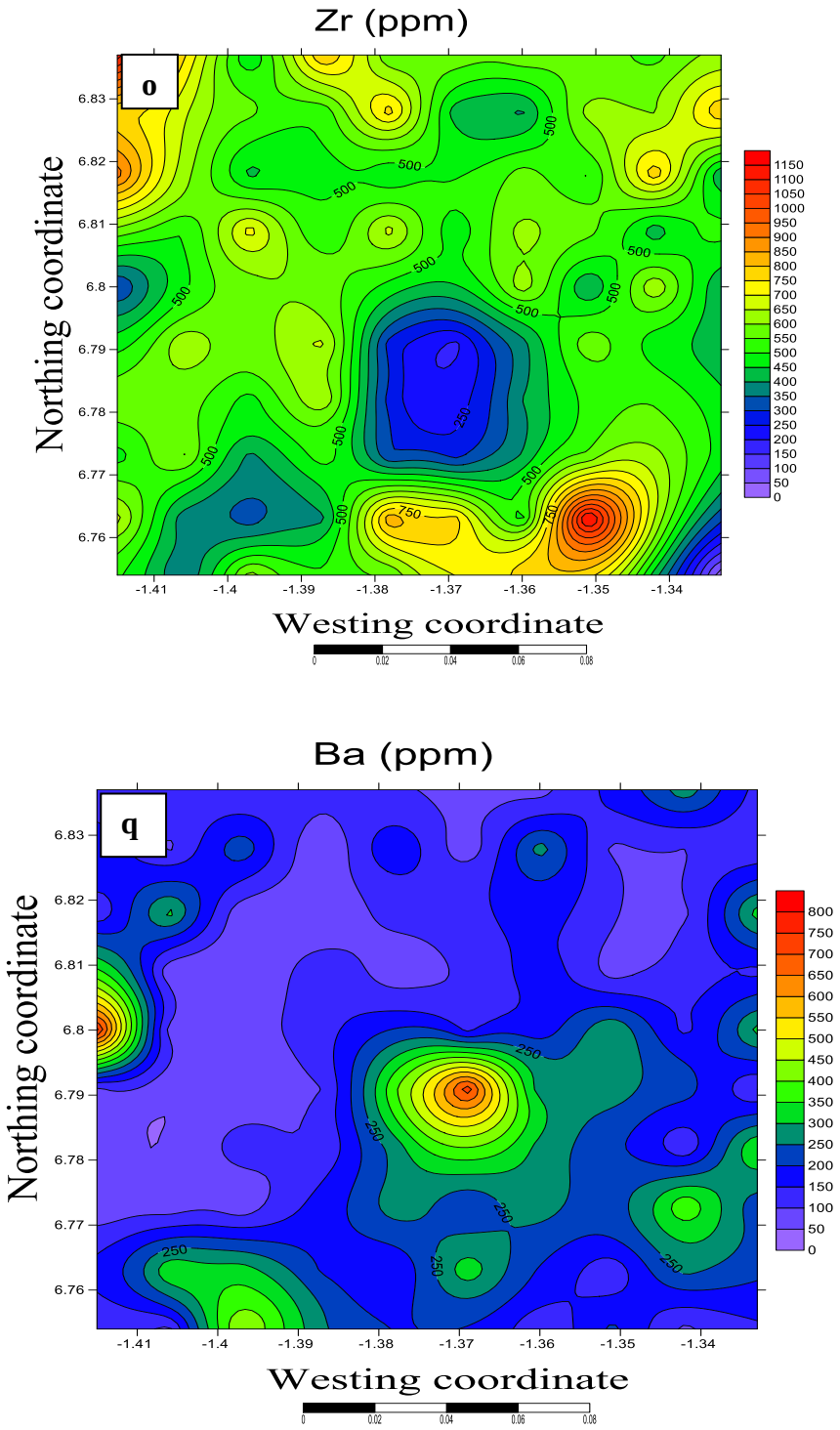

Fig 4.15 o and p show the element distribution map of Zr and Ba for the test data

Description of the spatial distribution maps for the test sample dataset (secondary data)

4.3.1.1 Silica (SiO_2) wt%

SiO_2 ranges from 44.98 wt% to 88.27 wt% with a mean concentration of 58.57 wt% which is less than the estimated average abundance of Silica in the continental crust (60.33 wt %). The mean is also less than the SiO_2 abundance in granite 74.23 wt% and granodiorite 67.17wt% (Taylor, 1964).

Fig. 4.15b and appendix B fig 4.16 S, show the element distribution map and histogram for SiO_2 respectively. The histogram is unimodally distributed and positively skewed. The threshold value for SiO_2 was estimated at 76.08 wt%. Four samples had values greater than the threshold, that is, 4.4% of the total population.

The element distribution map for SiO_2 displays high concentrations at the north western and central portions of the study area which are underlain by the Eburnean Intrusive rocks. Generally, all the rock types are showing moderate to high SiO_2 concentration in the study area.

4.3.1.2 Aluminium (Al_2O_3) wt%

Al_2O_3 forms part of the Group III of the periodic table alongside B, Ga, In and Ti. Al_2O_3 concentrations ranges from 5.28 to 40.22 wt% with a mean of 25.86 wt% which is above the estimated average abundance of Al_2O_3 in the continental crust (15.55 wt%). The mean is also greater than the Al_2O_3 in granite 13.6 wt % and granodiorite (15.5 wt%) (Taylor, 1964).

Fig. 4.15a and appendix B fig 4.16 R, show element distribution map and histogram for Al_2O_3 respectively. The log transformed histogram displays unimodal and

negatively skewed distribution. The threshold value for Al_2O_3 was estimated at 34.32 wt% and sixteen (16) samples had values greater than the threshold value, representing 17.7% of the total population. Al_2O_3 concentration is generally high throughout the study area with few areas in the Eburnean granitoids recording low concentrations. It is evident that all the rock types in the study area exhibit high association with Al_2O_3.

4.3.1.3 Iron oxide (Fe_2O_3) wt%

Fe_2O_3 concentrations ranges from 0.22 wt% to 10.72 wt% with a mean concentration of 3.29wt% which is less than the estimated average abundance of Fe_2O_3 in the continental crust 5.6 wt % and also higher in granite that is 2.7 wt% (Taylor, 1964).

Fig. 4.15k and appendix B fig 4.16 A2, show the element distribution map and the histogram for Fe_2O_3 respectively. The log transformed Fe_2O_3 histogram show a bimodal and negatively skewed distribution. The threshold value for Fe_2O_3 estimated at 7.58wt% and Three samples had values greater than the threshold value, representing 3.3% of the total sample.

Form the spatial distribution map, Fe_2O_3 concentration is generally low throughout the study area. High concentrations are displayed at the central portion of the study area precisely in Ofoase where all the rock types cluster.

4.3.1.4 Potassium oxide (K_2O) wt%

Potassium is in the Group 1 together with H, Li, Na, K, Rb, Cs, Fr, K_2O concentration ranges from 0.27 wt% to 6.18 wt% with a mean of 1.29 wt% which is greater than the estimated average abundance of potassium in the continental crust, 1.1 wt%. The mean is also less than the estimated abundance of K_2O in granite, which is 5.06 wt%.

Fig. 4.15h and appendix B fig 4.16 Y, show element distribution map and histogram for K_2O respectively. The histogram is unimodal and also positively skewed. The threshold value is 3.47 wt%. Three sample values were greater than the threshold value, representing 3.33% of the total population. The element distribution map reveals high concentrations at the central and south western portions which are underlain by Eburnean Intrusive rocks.

4.3.1.5 Magnesium oxide (MgO) wt%

Mg is in the same period with Ca, Sr and Br. The concentration ranges from 0.81wt% to 4.50 wt% with a mean of 1.34 wt % which is less than the average cluster abundance (2.3%). The mean is less than the estimated abundance in granites (0.16 wt %) and also in granitoid 0.10 wt%; (Levinson, 1974).

Fig. 4.15(b) and appendix B fig 4.16 (U), show element distribution map and histogram for MgO respectively. The histogram is uniformly skewed and also unimodal. The threshold value was 2.23 (mean +2S.D). There are 4 samples that have values greater than the threshold value. The element distribution map reveals moderate concentrations at the lower and central portions of the study area which are underlain by the Birimian metasedimentary rocks and hornblende respectively.

4.3.1.6 Manganese oxide (MnO) wt%

Mn is in Group VII of the Periodic Table. The concentration ranges from 0.00 to 0.17wt% with a mean of 0.03wt% which is below the estimated average abundance of MnO in the earth crust (0.09 to 1.00 wt%). Threshold value was estimated at 0.09 wt% and four samples had values greater than the threshold value.

Fig. 4.15m and appendix B fig 4.16 (A4), show element distribution map and histogram for MnO respectively. The log transformed histogram displays unimodal and negatively skewed distribution. MnO concentration in the south-eastern portions of the study area is higher. This area is underlain by the Eburnean Intrusive rocks. The concentration is generally low throughout the study area as indicated by the special distribution map.

4.3.1.7 Titanium oxide (TiO_2) wt%

TiO_2 alongside Zr, Hf and Th are located in Group IV of the periodic table.TiO_2 concentrations ranges from 0.19 to 1.27wt% with a mean concentration of 0.76wt% which is slightly below the estimated average abundance concentration of TiO_2 (0.93wt %) (Taylor 1964; Mielke, 1979).

Fig. 4.15f and appendix B fig 4.16 W, show element distribution map and histogram TiO_2 respectively. The histogram shows that TiO_2 is negatively skewed and unimodally distributed. The threshold was estimated at 1.21wt% with two samples having values greater than the threshold. The element distribution map reveals low concentrations of TiO_2 at the South-eastern portions of the study area which is underlain by Eburnean Intrusive rocks. The concentration is generally low throughout the study area as indicated by the special distribution map.

4.3.1.8 Sodium oxide (Na_2O) wt%

Na together with K, Rb, Cs and Fr make up Group 1 of the Periodic table. The concentration of Na_2O ranges from 0.26 to 1.50 wt% with a mean concentration of 0.86 wt% which is less than the estimated average abundance of Na_2O continental crust (2.84 wt %) (Taylor 1964; Mielke,1979).

Fig. 4.15c and appendix B fig 4.16 T, show element distribution map and histogram of Na_2O respectively. The log transformed histogram is negatively skewed and unimodally distributed. The threshold was estimated at 1.35 wt% (mean + 2 SD) with three samples having values greater than the threshold. The element distribution map reveals low concentrations of Na_2O at the South-eastern portion of the study area which is underlain by Eburnean Intrusive rocks. The concentration is generally low throughout the study area.

4.3.1.9 Nickel (Ni) ppm

Nickel is a transitional element .Nickel concentration ranges from 2.20ppm to 135ppm with a mean of 15.91ppm which is greater than the estimated average abundance of Ni in the continental crust (75 ppm) (Taylor 1964; Mielke, 1979). The mean is also less than the estimated abundance in soils 30ppm.

Fig. 4.15n and appendix B fig 4.16 (A5), show element distribution map and histogram for Ni respectively. The histogram is bimodal and uniformly skewed. The threshold value is 47.51ppm. Three sample values are greater than the threshold value, representing 3.33% of the total population. Nickel concentrations are generally scattered throughout the study area. The concentration ranges from moderate to high in the upper and lower extremities (that is the North-western and the south-eastern portion). The north-western portion is generally underlain by Eburnean Intrusive rocks.

Ni concentration in Ofoase area generally very low, this area is predominantly underlain by the Birimian metasedimentary rocks, the hornblende biotite- diorite and the Post Tarkwaian dyke.

4.3.1.10 Rubidium (Rb) ppm

Rb is in Group 1 with H, Li, Na, K, Rb, Cs, and Fr. Concentrations of Rb ranges from 6.10 to 300.80 ppm with a mean of 62.17ppm which is less than the estimated average abundance of Rb in the continental (90ppm) (Taylor 1964; Mielke, 1979). The mean is also lower than the estimated in granites, which is 276ppm.

Fig. 4.15j and appendix B fig 4.16 (A1), show element distribution map and histogram for Rb respectively. The log transformed histogram displayed a unimodal and negatively skewed distribution. The threshold value is 171.16 ppm and five samples were above the threshold value, which represents 5.55% of the total population. Generally, it can be seen that the central and south-western parts of the study area which are underlain by Eburnean Intrusive rocks show moderate to high concentration of Rb.

4.3.1.11 Zinc (Zn) ppm

Zn is a transitional element and is in the same group with Cd and Hg. The maximum concentration value of Zn is 67. 90 ppm and the minimum concentration value is 2.30ppm with a mean value of 23.21ppm which is below the estimated abundance in the continental crust (70ppm) (Taylor 1964; Mielke, 1979). The mean is also less than the estimated abundance in soils, which is 50ppm.

Fig. 4.15g and appendix B fig 4.16 X, show element distribution map and histogram of Zn respectively. The log transformed histogram displayed a unimodal and negatively skewed distribution. The estimated threshold value was 45.18ppm and three samples had values greater than the threshold which represents 3.33% of the total population. Generally, it can be seen that higher concentrations of Zn are displayed ranging from

low to high. High concentrations are probably associated with the Birimian Metasedimentary rocks, the hornblende biotite- diorite and the Post Tarkwaian dyke. Areas underlain by the Eburnean Intrusive rocks generally show low concentrations.

4.3.1.12 Strontium (Sr) ppm

Histogram of log transformed Sr displayed a unimodal and positively skewed distribution. Sr ranges from 8.10ppm to 111.80ppm with a mean concentration of 27.10ppm which is far less than the estimated concentration in the continental crust (i.e. 370ppm) (Taylor 1964; Mielke, 1979). A threshold value for Sr was estimated at 61.50ppm (mean +2SD) and four samples had values greater than the threshold representing 4.44% of the entire samples.

Fig. 4.15i and appendix B fig 4.16 Z, show element distribution map and histogram for Sr respectively. The element distribution map reveals higher concentrations at the central and the western flanks which are underlain by Eburnean Intrusive Rocks. There are also moderate concentrations at the southern parts of the study area which are also underlain by the Birimian metasedimentary rocks (biotite schist).

4.3.1.13 Calcium oxide (CaO) wt%

CaO is in group II of the periodic table together with Mg, Sr and Ba. The concentration of CaO ranges from 0.02wt% to 1.29wt% with a mean of 0.16wt% which is less than the estimated continental crust value (4.15wt% to 5.8wt %) and also below the estimated values for granites (0.7wt %). (Taylor 1964; Mielke, 1979);

Fig. 4.15e and appendix fig 4.16 V, show element distribution map and histogram of CaO respectively. The log transformed histogram displays a negatively skewed and also a unimodal distribution. The threshold value was estimated at 0.52 wt% (mean +2SD) with three samples having values greater than the threshold. From the spatial distribution map, CaO displayed very low concentrations throughout the study area.

4.3.1.14 Barium (Ba) ppm

Fig. 4.15q and appendix fig 4.16 (A7), show element distribution map and histogram for Ba respectively Histogram for log transformed Ba displayed a positively skewed and a unimodal distribution. Ba concentrations range from 49.50 ppm to 769.00 ppm with a mean concentration of 181.59 ppm which is less than the estimated Ba concentration in the continental crust 425 ppm (Taylor 1964; Mielke, 1979); as well as less than the average estimated values in granite and granidiorite 600 ppm and 500 ppm respectively. Threshold value was chosen at 439.79 ppm and six samples had values greater than the threshold representing 19.35% of the total samples.

The spatial distribution map showed that Ba concentration in the study area is concentrated at the center of the study area. Generally, the central portion of the study area displayed medium to high concentration of Ba which is underlain by the Eburnean Intrusive rocks. Ba concentration is low throughout the study area.

4.4 Correlation matrix

Table 4.13 shows that, the inter- relationship between the twenty-seven elements indicated a wide range of correlation ranging from negative to positive. Emphasis was made on values greater or equal to 0.7 and the negatives (in bold). Twenty two correlations were established with the strongest correlation existing between Ga and Al_2O_3 with 0.96 and the rest ranging from 0.70 to 0.89. Also a strong correlation exists between Rb–K_2O (0.88), Ni-Fe_2O_3 (0.89) and Al_2O_3-Na_2O (0.81). Moderate correlations also exist between Ba-K_2O (0.81), Fe_2O_3-SiO_2 (0.81), Fe_2O_3-Al_2O_3 (0.80), Ba-Sr (0.79). Lastly weak correlation exist between Ga-Na_2O (0.766) ,SiO_2 -Al_2O_3 (-0.75), Zn-Al_2O_3 (0.72) ,Ga – SiO_2 (-0.77), CaO-P_2O_5 (0.71), MnO-P_2O_5 (0.71), MnO-CaO (0.76), Ni –TiO_2(0.72), Ni-MnO (0.72), Zn-MnO (0.72), Zn-Fe_2O_3 (0.75) , Ga-Fe_2O_3 (0.76) , Zn-Ni (0.71) and Sn-Ga (0.71). Generally, the major oxides Al_2O_3, Na_2O, Fe_2O_3, SiO_2, CaO, MnO, P2O5 and TiO_2 were found to correlate moderately with these minor elements Ga, Zn, Ba, Rb, Ni, and Zn.

The inter-relationship between these major elements were negative; SiO_2-Al_2O_3, Fe_2O_3-Al_2O_3, Fe_2O_3-SiO_2, Fe_2O_3-Al_2O_3, Fe_2O_3-SiO_2 and Ga-SiO_2. It can be noted that SiO_2 correlated negatively with all the elements except Sr and Zr.

Table 4.13. Correlation matrix for thesecondary data

	Na2O	MgO	Al2O3	SiO2	P2O5	SO3	K2O	CaO	TiO2	MnO	Fe2O3	Cr	Ni
Na2O	1.000												
MgO	0.340	1.000											
Al2O3	**0.814**	0.205	1.000										
SiO2	-0.576	-0.034	**-0.747**	1.000									
P2O5	0.363	0.314	0.479	-0.398	1.000								
SO3	0.302	0.079	0.331	-0.485	0.592	1.000							
K2O	0.168	0.211	0.031	0.175	0.127	0.040	1.000						
CaO	0.293	0.349	0.286	-0.325	**0.708**	0.588	0.095	1.000					
TiO2	0.231	0.186	0.399	-0.326	0.352	0.142	-0.648	0.216	1.000				
MnO	0.262	0.310	0.480	-0.525	**0.707**	0.569	-0.005	**0.763**	0.408	1.000			
Fe2O3	0.601	0.220	**0.805**	**-0.805**	0.606	0.435	-0.278	0.437	0.677	0.673	1.000		
Cr	0.073	0.231	0.077	-0.288	0.169	0.317	-0.232	0.181	0.267	0.299	0.344	1.000	
Ni	0.505	0.428	0.656	-0.698	0.609	0.475	-0.322	0.516	**0.724**	**0.719**	**0.888**	0.416	1.000
Cu	0.295	0.366	0.312	-0.221	0.695	0.437	0.160	0.600	0.382	0.656	0.639	0.126	0.677
Zn	0.618	0.405	**0.723**	-0.638	0.587	0.460	0.134	0.581	0.350	**0.715**	**0.745**	0.174	**0.707**
Ga	**0.766**	0.146	**0.956**	**-0.765**	0.447	0.304	0.067	0.272	0.314	0.473	**0.757**	0.019	0.610
Ge	0.291	0.239	0.364	-0.261	0.213	-0.054	0.005	0.149	0.233	0.246	0.340	-0.005	0.301
As	0.369	-0.078	0.540	-0.668	0.461	0.600	-0.252	0.417	0.418	0.574	0.635	0.160	0.572
Br	0.263	0.208	0.477	-0.281	0.261	0.103	-0.164	0.337	0.287	0.333	0.391	0.072	0.449
Rb	0.311	0.274	0.270	-0.034	0.193	0.038	**0.882**	0.135	-0.544	0.113	-0.105	-0.270	-0.129
Sr	0.314	0.369	0.098	0.008	0.450	0.326	0.671	0.594	-0.217	0.338	0.001	-0.146	0.055
Zr	-0.245	-0.180	-0.219	0.392	-0.170	-0.172	-0.453	-0.125	0.489	-0.109	-0.125	-0.001	-0.066
Nb	0.314	-0.114	0.499	-0.327	0.271	0.095	-0.450	0.096	0.608	0.250	0.464	-0.052	0.437
Sn	0.387	0.331	0.666	-0.434	0.259	0.075	0.187	0.174	-0.019	0.342	0.442	0.063	0.385
I	0.537	0.193	0.647	-0.485	0.303	0.084	-0.303	0.229	0.453	0.243	0.662	0.009	0.594
Ba	0.134	0.364	-0.029	0.152	0.315	0.201	**0.806**	0.272	-0.350	0.149	-0.127	-0.064	-0.106

Table 4.14. Continuation of the correlation matrix for the secondary data

	Cu	Zn	Ga	Ge	As	Br	Rb	Sr	Zr	Nb	Sn	I	Ba	Ce
Cu	1.00													
Zn	0.65	1.00												
Ga	0.14	0.67	1.00											
Ge	0.11	0.37	0.33	1.00										
As	0.04	0.54	0.58	0.18	1.00									
Br	0.34	0.19	0.43	0.26	0.21	1.00								
Rb	0.02	0.26	0.36	0.11	-0.10	-0.07	1.00							
Sr	0.60	0.37	0.12	0.16	0.03	0.11	0.58	1.00						
Zr	-0.21	-0.30	-0.25	-0.12	-0.05	0.08	-0.49	-0.27	1.00					
Nb	-0.16	0.21	0.54	0.23	0.41	0.31	-0.18	-0.21	0.42	1.00				
Sn	0.17	0.53	**0.71**	0.28	0.19	0.37	0.45	0.19	-0.36	0.17	1.00			
I	0.48	0.39	0.59	0.30	0.18	0.48	-0.14	0.18	-0.22	0.35	0.26	1.00		
Ba	0.54	0.27	-0.09	0.08	-0.20	-0.11	0.57	**0.80**	-0.37	-0.51	0.06	-0.08	1.00	

4.4.1 Scatter plots

Elements that correlated well on the correlation matrix were used to plot scatter plots in SPSS in order to graphically assess the correlation between them. A total of 22 scatter plots were plotted. It is evident that the strongest correlation exists between Ga and Al_2O_3 with 0.956. This is because; this inter-relationship has the line of fit passing through most of the circles. Also scatter plot for Fe_2O_3-Al_2O_3 (0.805) is an example of moderate correlation. The scatter plot for Zn-Ni (0.707) is an example of weak correlation here the line of fit passed through a few number of circles. Scatter plot SiO_2-Al_2O_3 (-0.75) plotted negatively (i.e. from right to left).

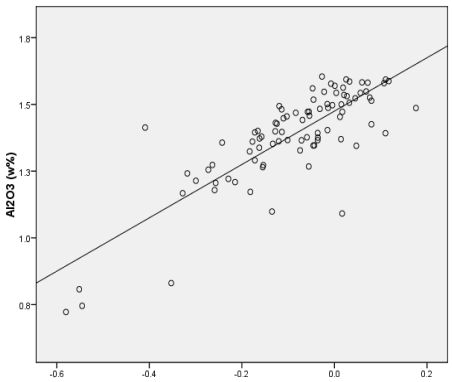

A: Al_2O_3-Na_2O

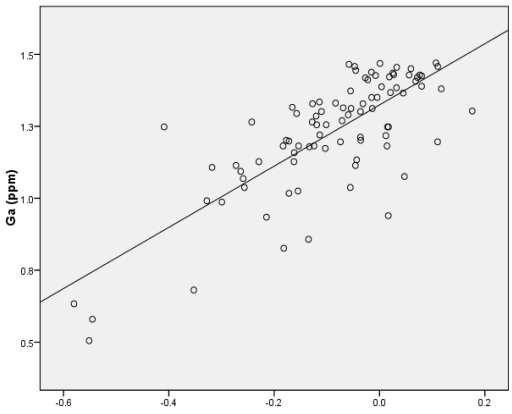

B: Ga-Na_2O

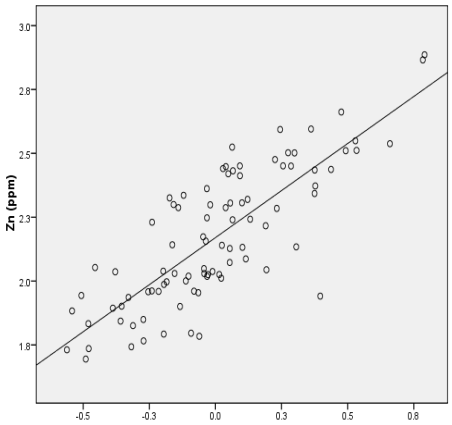

C. Zn-Ni

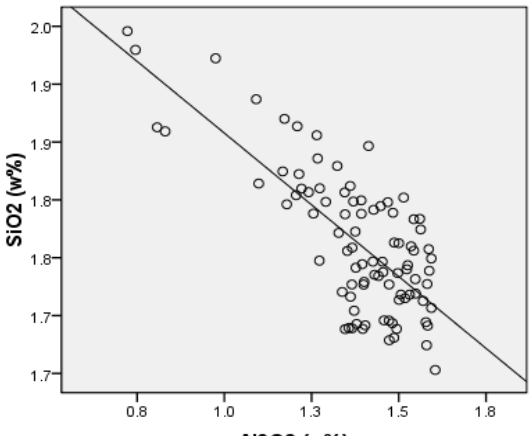

D: SiO_2-Al_2O_3

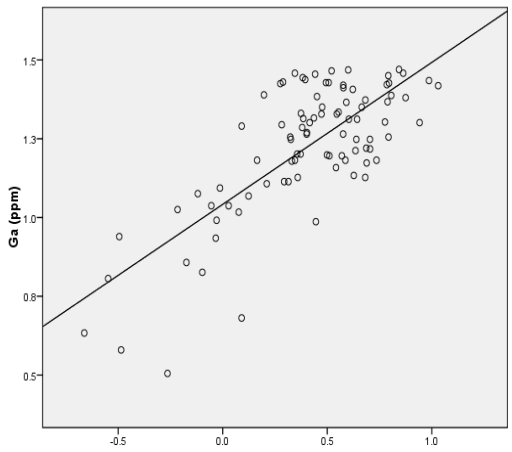

E: Ga-Fe_2O_3

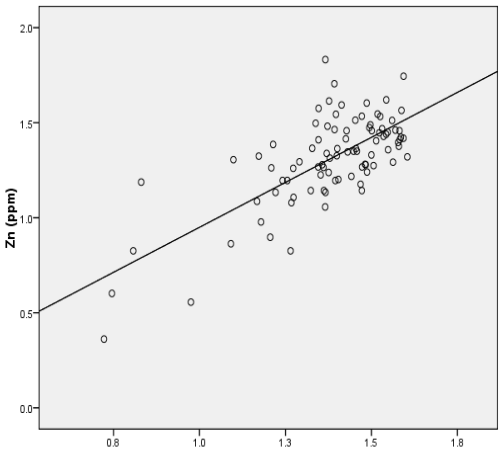

F: Al_2O_3-Zn

4.4.2 Results of the PCA

This analysis extracted four factors explaining 77.430 % of the total variability. The variances explained by each of the factors extracted are indicated in (Appendix A: Table 7) and the rotated component matrix (Table 4.15).

The first factor accounted for 34.07% of the total variance and is dominated by P_2O_5, MnO, CaO, Cu, Zn, and Sr. Also Ni (0.68) loaded weakly in component one. While the second factor explained 21.437 % of the total variance and is associated with Al_2O_3, Fe_2O_3, Na_2O, Ga, I and a minor inclusion of -SiO_2 (- 0.58). The negative loading of silica implies that, as SiO_2 increases Al_2O_3, Fe_2O_3, Na_2O, Ga, and iodine will also decrease and vice versa. The third component had K_2O, Rb,-As and a weak loading of Ba explaining 11.397% and the fourth component had Cr, -Zr and -Nb which explains 10.527% of the total variance.

Although four factors were extracted, the first three account for the bulk (approximately 67%) of the variance in the dataset.

4.4.3 Scree plot

The scree plot (Fig 4.17) shows the Eigenvalues sorted from large to small as a function of the principal component number. The first four component numbers were selected. This was because eigenvalues are selected from the highest values to where the elbow begins. These selected eigenvalues corresponds to Loading of the verimax rotated matrix for the four factor model shown. Evidently, the first four factors are more correlated than the rest.

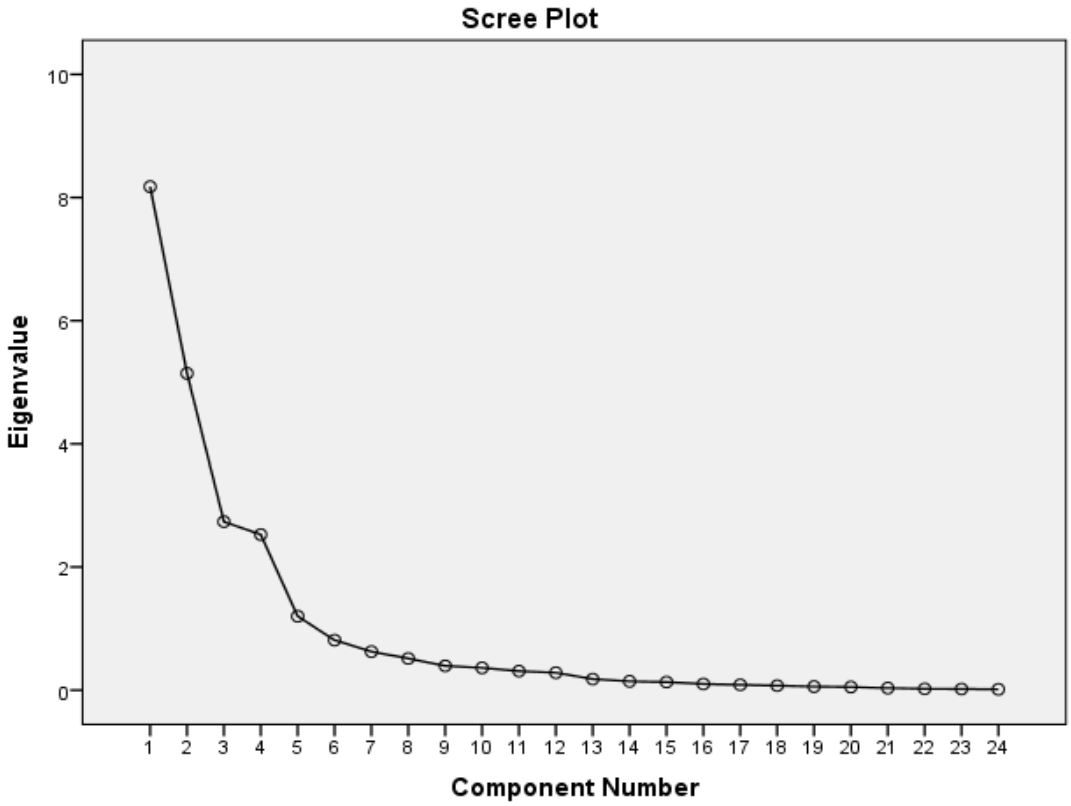

Figure 4.17: Scree plot for the secondary data. Components to the right of component 5 (below eigenvalue of 1.0) do not account for a significant portion of variance in the dataset.

Table 4.15.Rotated component matrix for the secondary data

	Component			
	1	2	3	4
Na2O	-.023	**.825**	-.120	.049
MgO	.458	.295	.518	.140
Al2O3	.084	**.914**	-.021	-.102
SiO2	-.027	-.586	.341	-.591
P2O5	**.911**	.090	.072	-.027
SO3	.484	-.174	-.267	.621
K2O	.211	-.231	**.846**	.199
CaO	**.851**	-.025	.020	.125
TiO2	.562	.374	-.367	-.441
MnO	**.870**	-.049	.154	.115
Fe2O3	.496	**.723**	-.074	.250
Cr	.139	-.025	-.046	**.814**
Ni	.690	.524	.001	.204
Cu	**.839**	.294	-.034	.129
Zn	**.700**	.400	.388	.130
Ga	.032	**.919**	-.069	-.125
As	.110	.082	**-.704**	.161
Rb	.165	-.040	**.878**	-.008
Sr	**.859**	.047	.378	.011
Zr	-.032	-.440	-.285	**-.731**
Nb	-.096	.230	-.504	**-.721**
Sn	.110	.617	.453	.002
I	.386	**.726**	-.415	-.016
Ba	.551	-.098	.634	.247

4.4.4. Description of the spatial distribution maps for the loadings of the PCA component analysisfor the secondary data.

4.4.4.1 Principal component one: Log_{10} (P_2O_5, MnO, CaO, Cu, Zn, Sr)

Generally, concentrations of log_{10} (P_2O_5, MnO, CaO, Cu, Zn, Sr) are high at the central portion of the study area precisely in the Ofoase area. This high concentration may probably be coming from the Birimian Metasedimentary rocks, the hornblende biotite-diorite and the Post Tarkwaian dyke. Low concentrations of these elements are displayed in the western parts of the study area which is underlain by the Eburnean intrusive rocks.

4.4.4.2 Principal component two: Log10 (Al_2O_3, Fe_2O_3, Na_2O, Ga, I, - SiO_2)

Log_{10} (Al_2O_3, Fe_2O_3, Na_2O, Ga, I, - SiO_2) shows high scattered concentrations across the study area. The areas with high concentrations are underlain by the Eburnean Intrusive rocks. Also portions displaying low to moderate concentrations are probably associated with the Birimian Metasedimentary rocks and Post Tarkwaian dyke.

4.4.4.3 Principal component three: Log 10 (K_2O, Rb,-As)

From the element distribution map, these elements: log_{10} (K_2O, Rb,-As) show high concentration in the south eastern portion of the study area predominantly dominated by the Birimian Metasedimentary rocks (biotite schist). Similar observation is displayed in the north eastern part of the study area which is underlain by the Ebunearn intrusive rocks.

4.4.4.4 Principal component four: Log_{10} (Cr, -Zr, -Nb)

Log_{10} (Cr, -Zr, -Nb) show high from the middle to southern part of the study area. The Ofoase area displayed high concentration of these elements. The Apemso Eburnean intrusives displays low concentration of these elements. Generally, high concentration

is seen in areas underlain by the Birimian Metasedimentary rocks, the hornblende biotite-diorite and the Post Tarkwaian dyke. Low to moderate concentration is observed in areas underlain by the Eburnean intrusive rocks.

Element distribution maps for the principal component loadings of the PCA

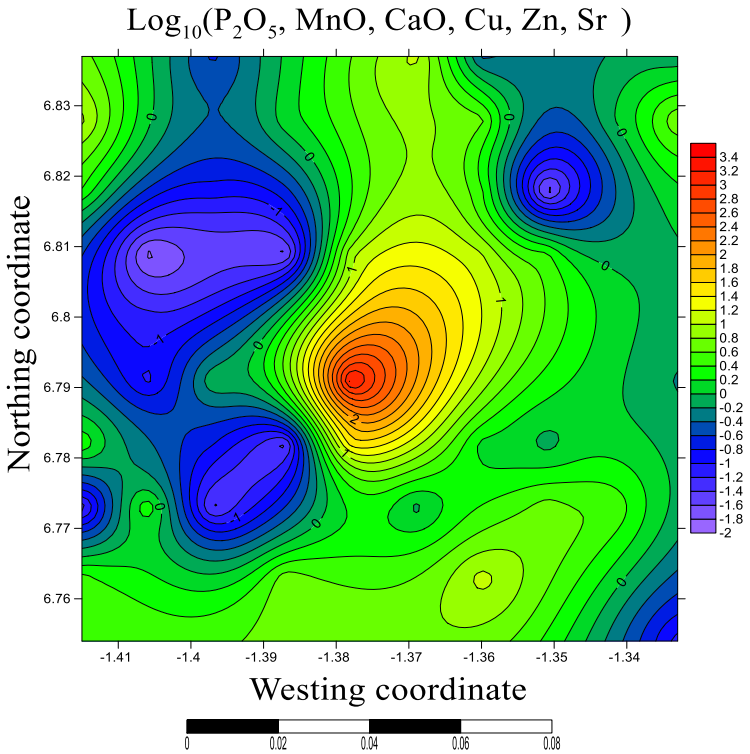

Fig 4.18a Spatial distribution maps for $\log_{10}$ (P_2O_5, MnO, CaO, Cu, Zn, Sr)

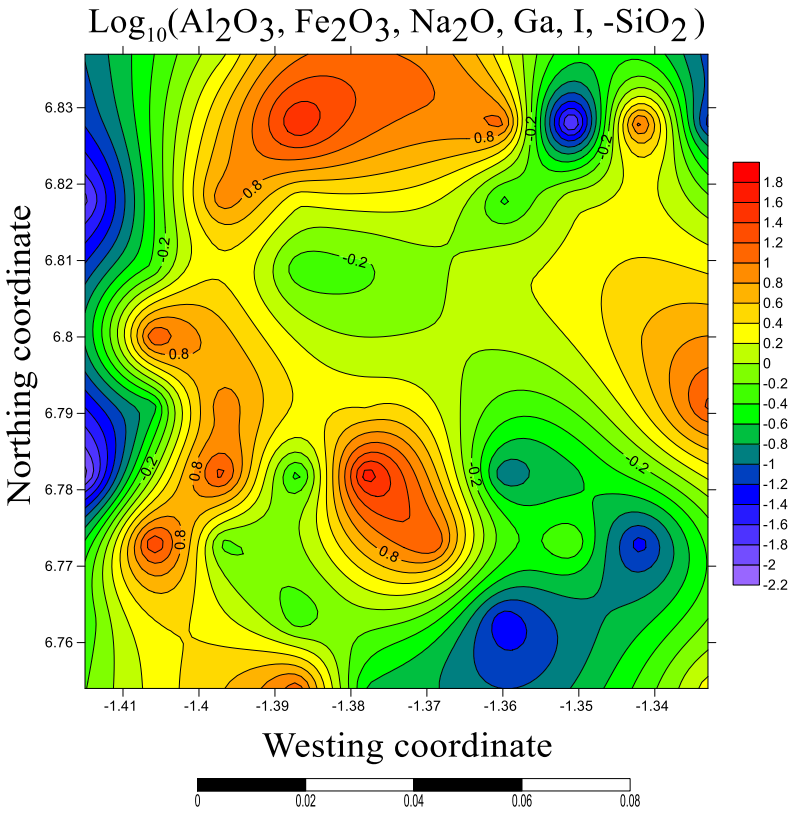

Fig 4.18b Element distribution maps for Log_{10} (Al_2O_3, Fe_2O_3, Na_2O, Ga, I, - SiO_2)

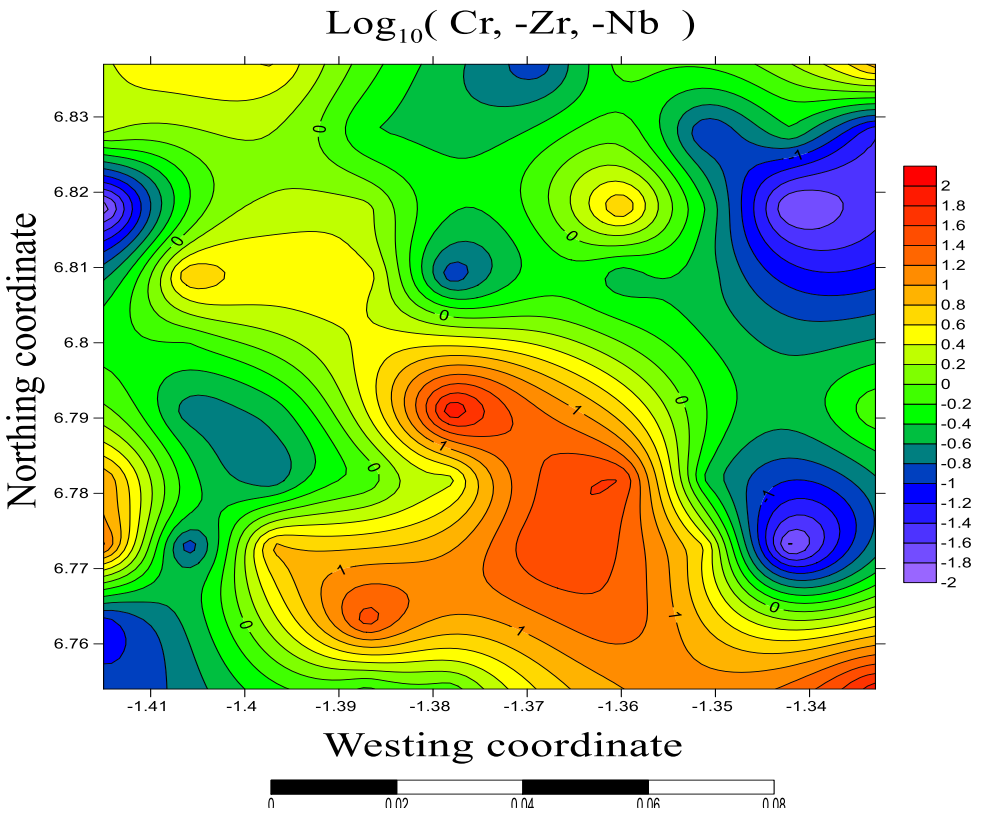

Fig 4.18c: element distribution maps for Log_{10} (Cr, -Zr, -Nb)

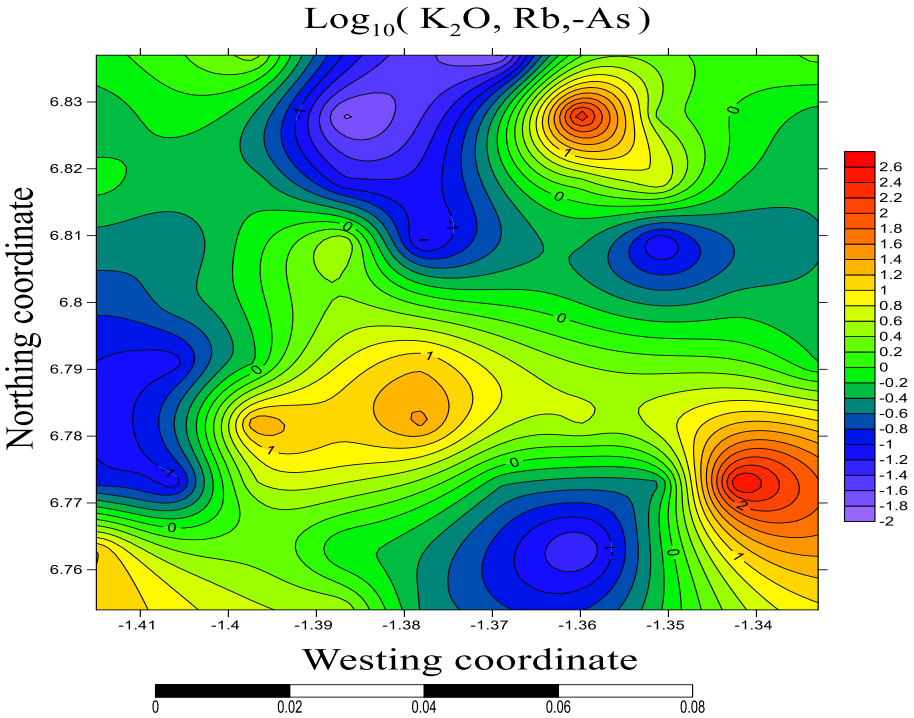

Fig 4.18d: Element distribution maps for Log_{10} (K_2O, Rb,-As)

4.4.4.5Hierarchical cluster analysis for thesecondarydata

The hierarchical cluster analysis for the secondary data is displayed in Fig 4.19. The first cluster was made up of Na_2O, Al_2O_3, TiO_2, Ga, Ge, Br, Sn, I, and Ce. The second cluster is made up of MgO, P_2O_5, SO_3, K_2O, CaO, MnO, Fe_2O_3, Cr, Ni, Cu, Zn, As, Rb, Sr, and Ba. The last cluster was also made up of SiO_2, Zr and Nb.

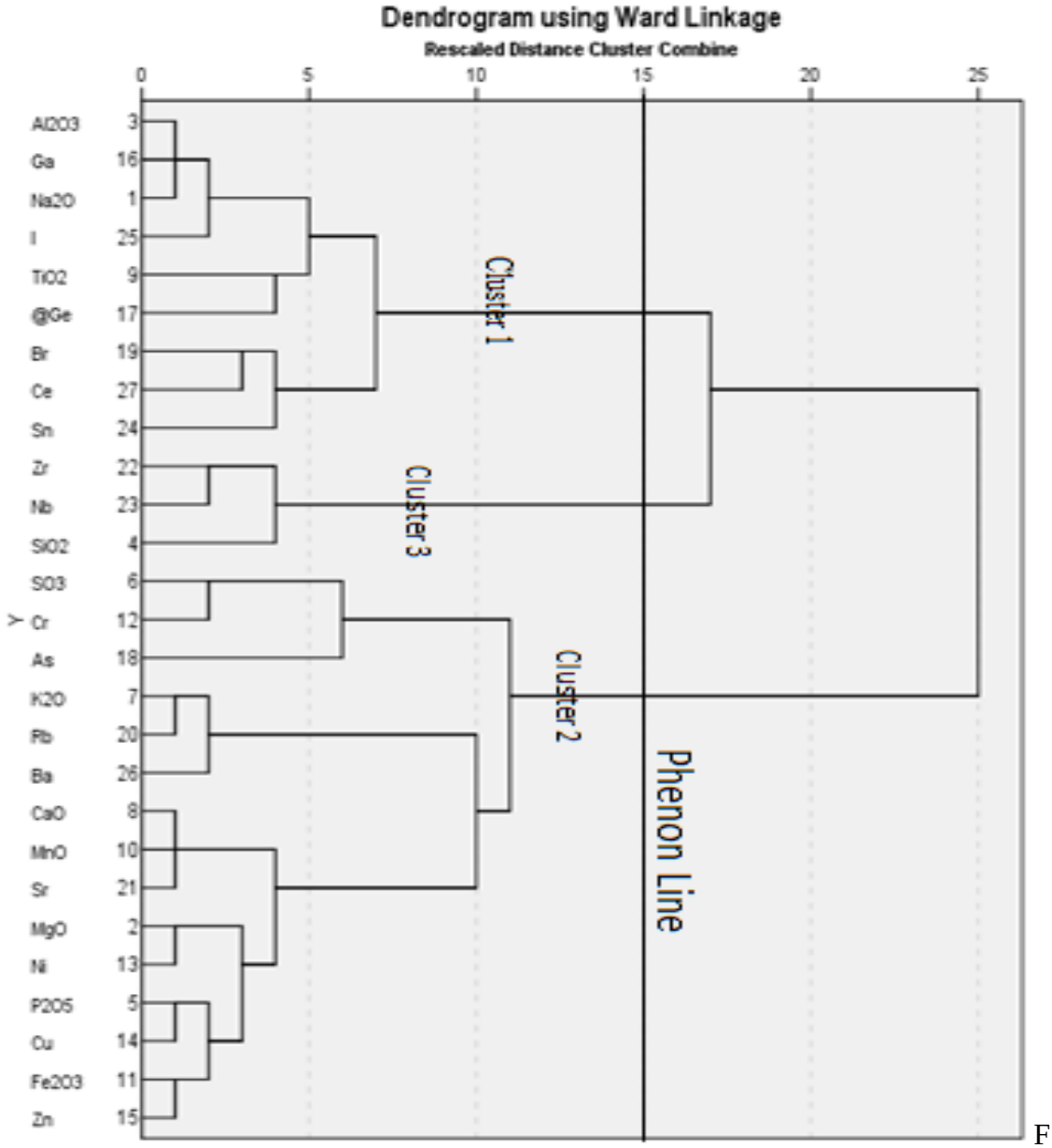

Figure 4.19: Dendrogram displaying multi-elemental cluster for thesecondary data.

GEOCHEMISTRY OF THE PRIMARY DATA

4.5 Summary statistics

The summary statistics for each element are displayed in table 4.16 and the measured parameters are the mean, median, standard deviation, variance and the percentiles. This, together with P-P plots were constructed to study how the elements were distributed, whether normally distributed or skewed.

Most of the p-p plots were skewed thus, non–linear. Example is the (Fig 4.20a) which shows the distributions of CaO in the dataset. It can be noted that the distribution of most of the elements are non-linear thus the need to log transform the data to base ten (10). Fig 4.20b also displays p-p plot for the distribution of CaO after log transformation. It is evident that the log transformed dataset is closer to normal compared to the raw dataset

Appendix A: table 5 displays a comparison between the skewness values of the dataset before and after log transformation. It can be noted that most of the elements had their skewness values close to zero when they were log transformed than when were not. Considering CaO which had a skewness value of 2.57 and when it was log transformed assumed a value of 0.34 making it more normal than it was before transformation.

Also elements like Na_2O, P_2O_5, Ba, Ni, and zinc had their distributions in the raw data more normalized than when transformed. For this reason, transforming such elements was not necessary. Example is Cu which had a skewness value of 0.32 but when transformed it deviated largely from normal (-1.13).

Table 4.16: Summary statistics for detailed survey dataset

	N	Mean	Median	SD	Kurtosis	Mini	Maxi	Percentiles		
								25	50	75
Na2O	30	1.03	1.03	0.29	-0.07	0.41	1.59	0.86	1.03	1.25
MgO	31	1.66	1.53	0.61	3.38	0.95	3.56	1.34	1.53	1.71
Al2O3	31	29.23	33.34	7.95	-1.22	12.70	38.77	21.80	33.34	36.22
SiO2	31	55.17	54.33	7.29	4.39	40.48	81.01	50.65	54.33	58.63
P2O5	31	0.08	0.08	0.03	0.10	0.02	0.16	0.05	0.08	0.11
SO3	31	0.07	0.07	0.02	3.75	0.05	0.13	0.06	0.07	0.07
K2O	31	1.31	1.19	0.90	7.80	0.47	4.81	0.78	1.19	1.41
CaO	31	0.24	0.15	0.28	7.41	0.02	1.33	0.07	0.15	0.26
TiO2	31	0.87	0.97	0.30	-0.92	0.28	1.48	0.60	0.97	1.10
MnO	31	0.06	0.04	0.05	1.09	0.01	0.20	0.02	0.04	0.08
Fe2O3	31	5.36	5.87	3.07	-0.83	1.16	12.23	2.21	5.87	7.33
Cr	31	300	300	200	-4900	0.00	600	100	300	400
Ni	31	29.54	22.10	23.81	0.24	8.20	84.20	11.60	22.10	33.30
Cu	25	16.21	14.80	10.49	-0.73	1.50	37.40	7.65	14.80	25.05
Zn	31	35.60	37.50	12.69	-0.02	12.60	66.10	25.80	37.50	42.10
Ga	31	19.63	19.90	5.13	-0.83	9.60	29.40	14.70	19.90	23.80
Ge	30	1.64	1.60	0.46	-0.84	0.80	2.50	1.30	1.60	2.03
As	31	6.62	5.90	2.77	0.85	3.00	14.20	4.40	5.90	8.00
Br	26	4.82	4.35	3.04	0.97	0.60	12.50	2.60	4.35	5.35
Rb	31	70.33	43.90	62.38	3.20	18.80	271.80	31.30	43.90	87.80
Sr	31	32.21	29.30	15.45	0.82	13.80	74.10	19.70	29.30	36.60
Zr	31	526.44	519.00	168.20	2.91	217.20	1079.00	434.00	519.00	608.00
Nb	31	19.33	19.30	5.74	0.50	10.00	35.00	15.00	19.30	23.10
Sn	26	7.62	7.40	4.69	1.64	1.10	21.50	3.78	7.40	10.25
I	28	22.01	20.25	12.08	-1.03	4.50	46.00	11.13	20.25	32.00
Ba	31	246.52	257.10	109.96	-1.32	71.00	426.00	126.40	257.10	345.40
Ce	26	70.62	60.50	25.09	-0.46	39.00	124.00	51.75	60.50	92.00

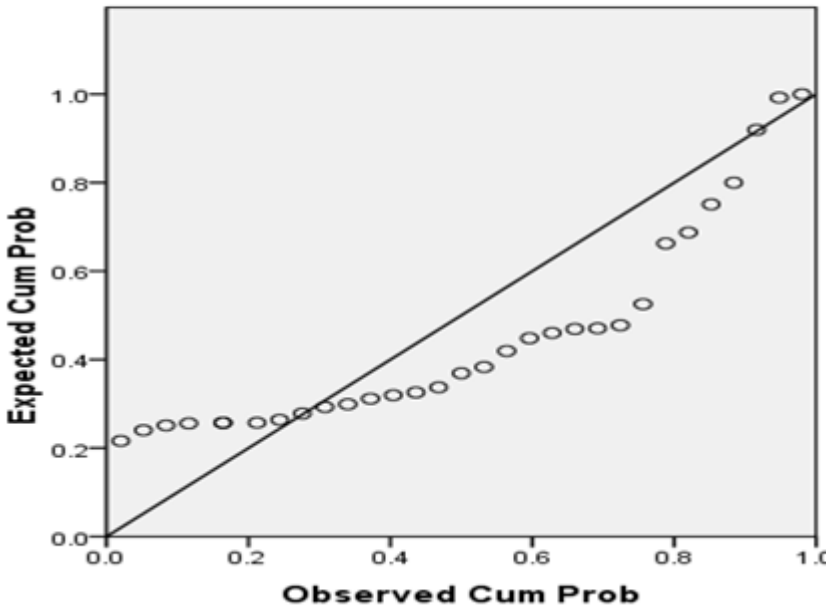

Figure.4.20a: Probabilty-Probability plot for CaO

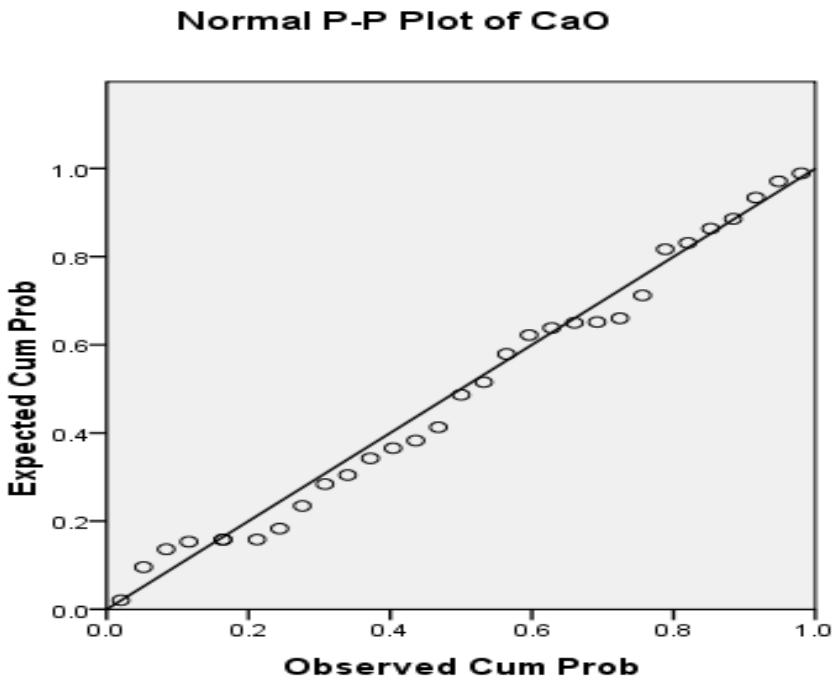

Figure.4.20b: Probabilty-Probability plot for Log_{10} CaO

4.5.1 Spatial distributions of elements

The threshold values were calculated in Microsoft Excel for every element using mean +1SD and also mean + 2SD (Table 4. 17). Profiles of selected elements were created in Microsoft Excel and used to study their distribution patterns.

Table 4.17: Threshold value for primary data

	Mean	Mean+1SD	mean+2SD	Mini	Maxi
Na_2O	1.03	1.32	1.61	0.41	1.59
MgO	1.66	2.28	2.89	0.95	3.56
Al_2O_3	29.23	37.17	45.12	12.70	38.77
SiO_2	55.17	62.46	69.74	40.48	81.01
P_2O_5	0.08	0.11	0.15	0.02	0.16
SO_3	0.07	0.09	0.11	0.05	0.13
K_2O	1.31	2.21	3.10	0.47	4.81
CaO	0.24	0.53	0.81	0.02	1.33
TiO_2	0.87	1.18	1.48	0.28	1.48
MnO	0.06	0.11	0.17	0.01	0.20
Fe_2O_3	5.36	8.43	11.50	1.16	12.23
Cr	0.03	0.05	0.06	0.00	0.06
Ni	29.54	53.35	77.16	8.20	84.20
Cu	16.21	26.70	37.19	1.50	37.40
Zn	35.60	48.29	60.97	12.60	66.10
Ga	19.63	24.76	29.89	9.60	29.40
Ge	1.64	2.10	2.56	0.80	2.50
As	6.62	9.40	12.17	3.00	14.20
Br	4.82	7.86	10.89	0.60	12.50
Rb	70.33	132.71	195.09	18.80	271.80
Sr	32.21	47.66	63.10	13.80	74.10
Zr	526.44	694.64	862.84	217.20	1079.00
Nb	19.33	25.07	30.81	10.00	35.00
Sn	7.62	12.31	17.01	1.10	21.50
I	22.01	34.10	46.18	4.50	46.00
Ba	246.52	356.48	466.44	71.00	426.00
Ce	70.62	95.70	120.79	39.00	124.00

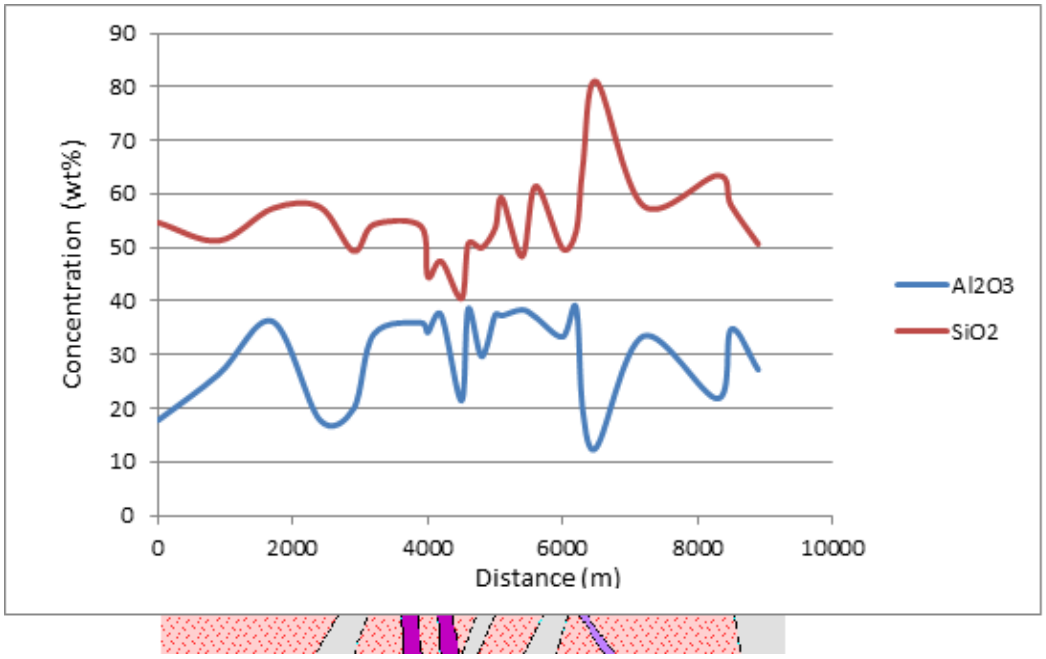

Sketch of the geology of the study area

Figure 4.21a: Profiles of Al_2O_3 and SiO_2

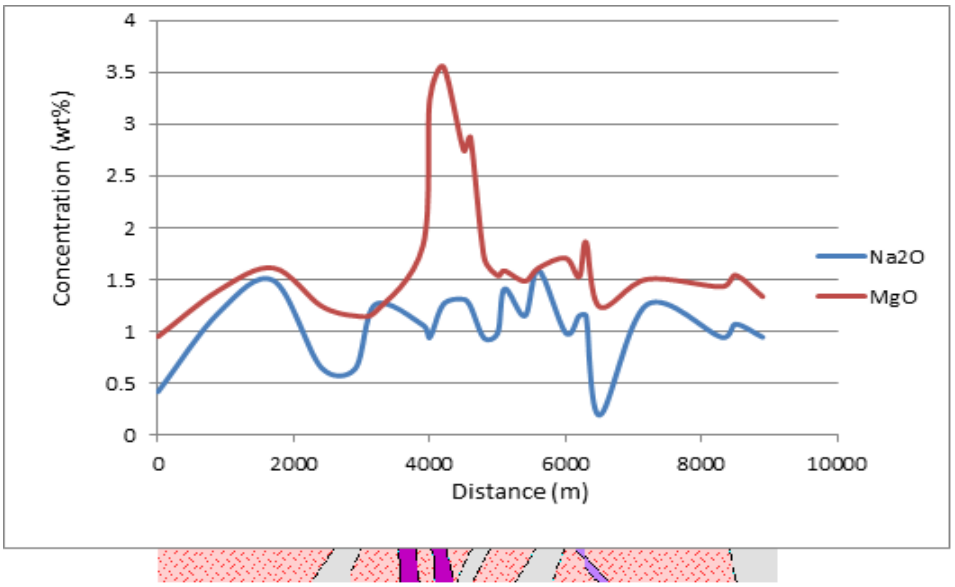

Sketch of the geology of the study area

Figure 4.21b:Profiles of MgO and Na_2O

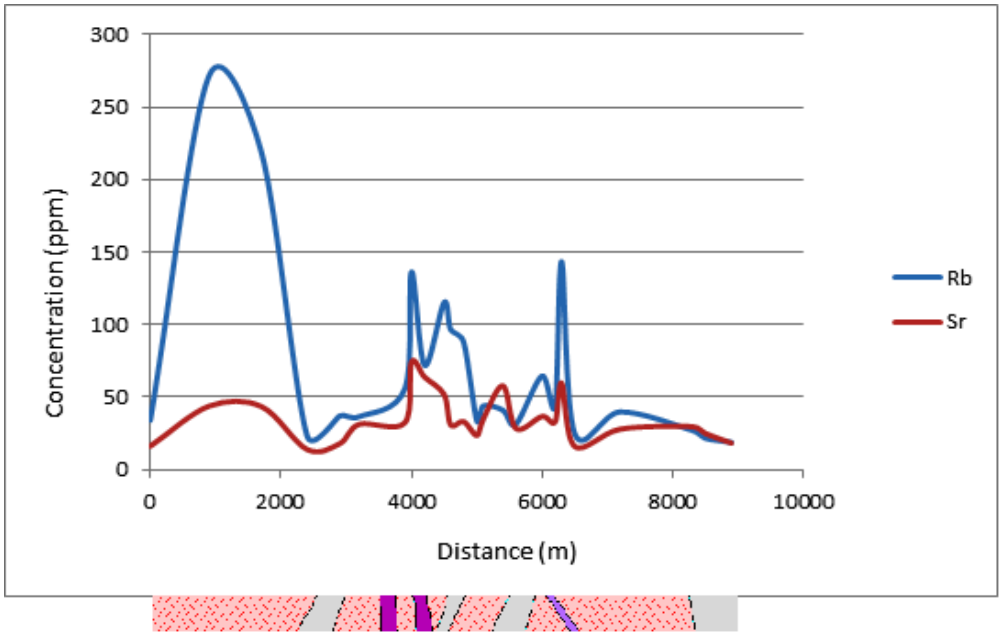

Sketch of the geology of the study area

Figure 4.21c: Profiles of Rb and Sr

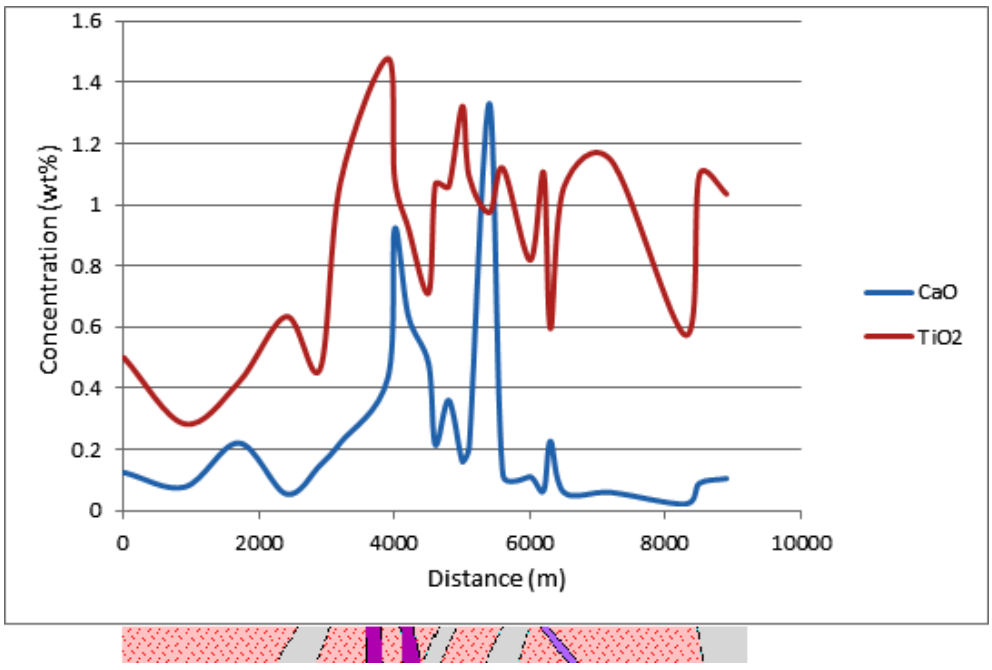

Sketch of the geology of the study area

Figure 4.21d: Profiles of CaO and TiO_2

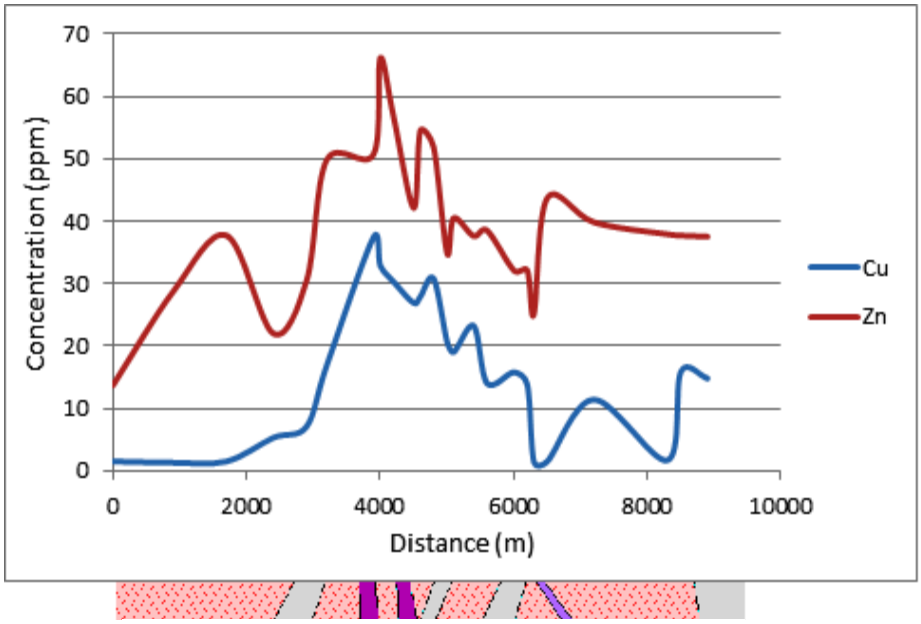

Sketch of the geology of the study area

Figure 4.21e: Profiles of Zn and Cu

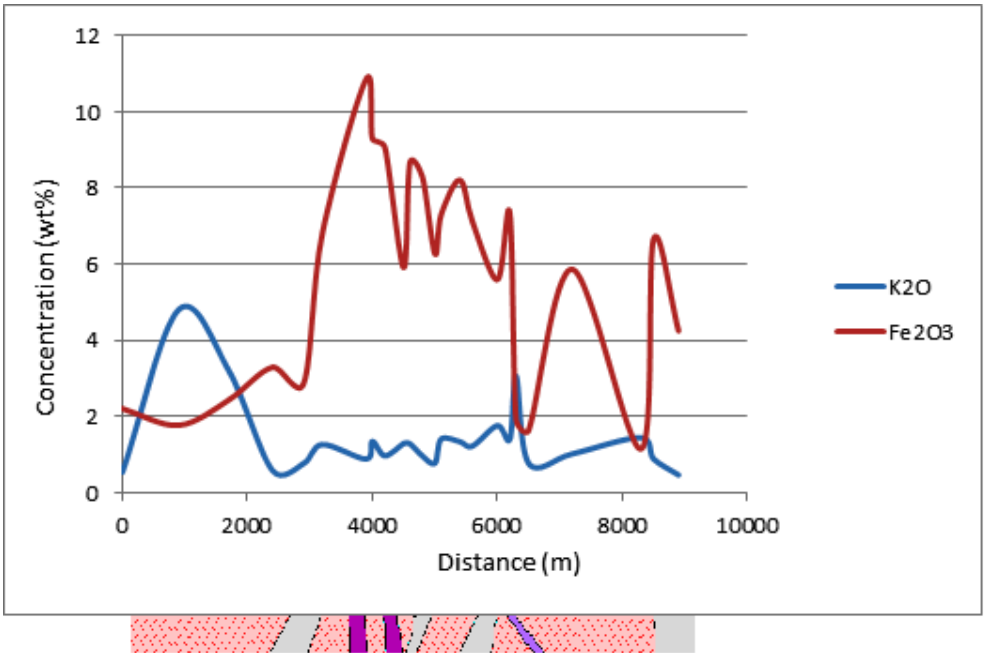

Sketch of the geology of the study area

Figure 4.21f: Profiles of K_2O and Fe_2O_3

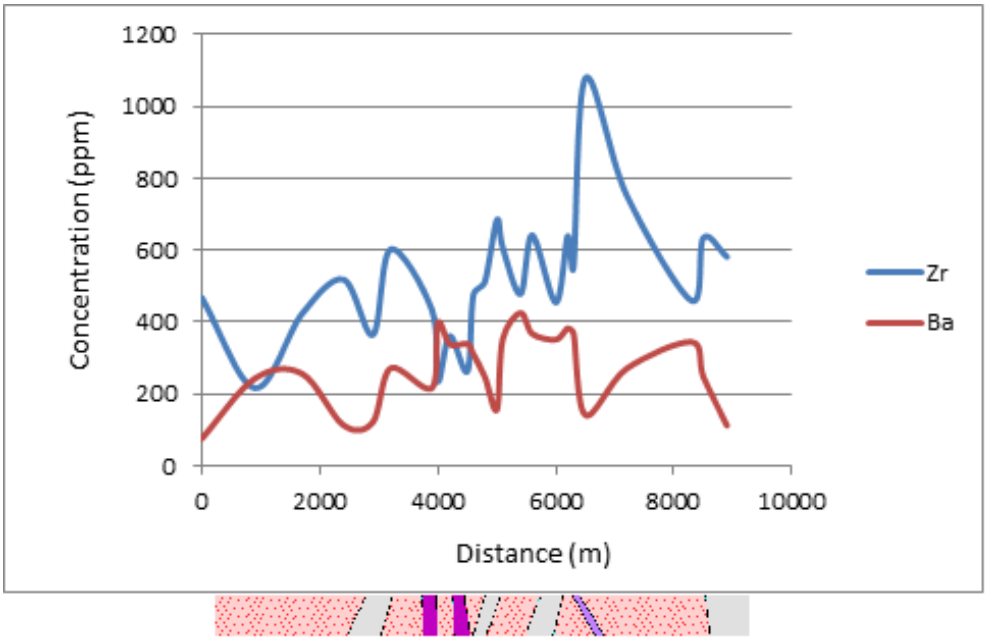

Sketch of the geology of the study area

Figure 4.21g: Profiles of Zr and Ba

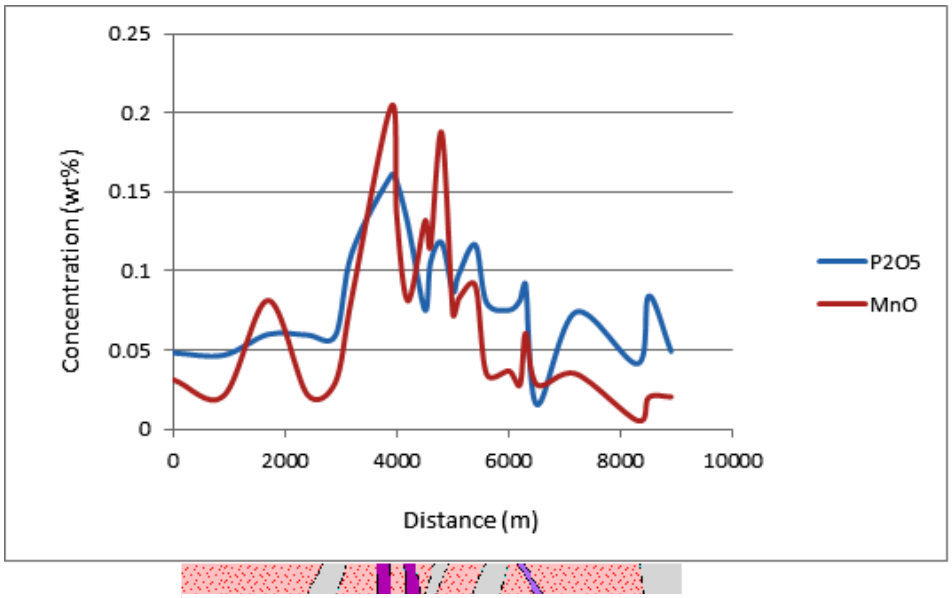

Sketch of the geology of the study

Figure 4.21h: Profiles of P_2O_5 and MnO

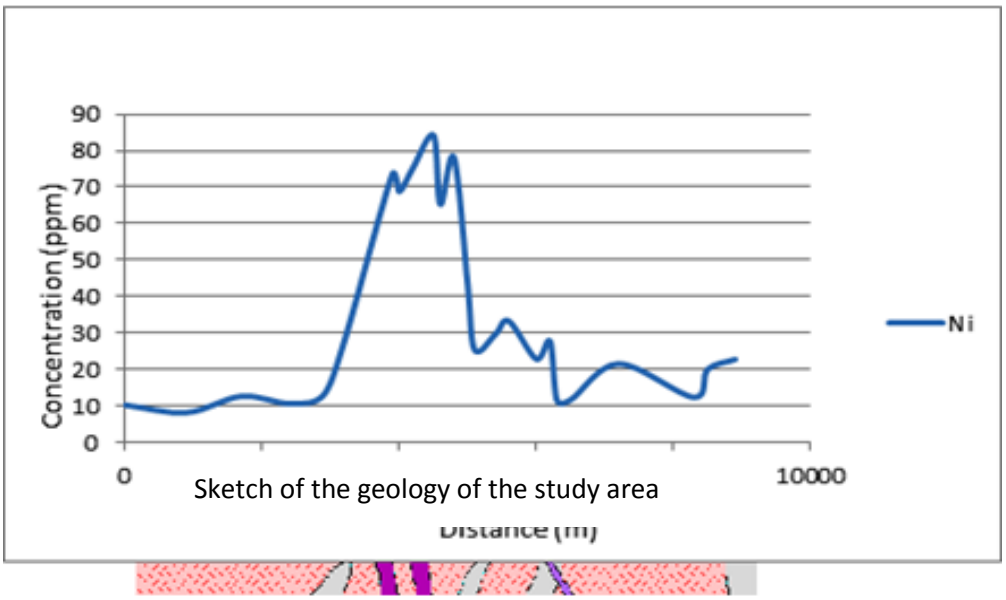

Figure 4.21i: Profiles of Ni

4.5.2 Element distribution in detailed soil samples

4.5.2.1 Silica (SiO_2)

SiO_2 ranges from 40.48wt% to 81.01wt% with a mean of 55.17wt% which is less than the estimated average abundance of silica in the continental crust (60.33 wt%) and also less than the SiO_2 abundance in granite (74.23wt%) and granodiorite (67.17wt%) Taylor, (1964). Histogram of log transformed SiO_2 displayed bimodal distribution. The threshold value for SiO_2 was estimated at 69.74wt% and only one sample had concentration greater than the threshold representing about 1% of the total samples.

The west to east profile of SiO_2 shows anomalous concentrations of SiO_2 in the eastern portions of the study area (Fig 4.21a). Generally, the Eburnean granitoids show a medium concentration of SiO_2. Low concentrations are also observed in areas underlain by the hornblende biotite-diorites and the Birimian metasedimentary rocks.

4.5.2.2 Aluminum oxides (Al_2O_3)

Al_2O_3 forms part of the Group III of the periodic table alongside, Cd and Hg (Goldschmidt, 1954). Al_2O_3 concentrations ranges from 12.70 to 38.77 wt% with a mean concentration of 29.23 wt% comparatively greater than the estimated average abundance of Al_2O_3 in the continental crust (15.55 wt%)and also greater than estimated concentration in granite (13.6wt%) and granodiorite (15.5wt%). Taylor, (1964).

Histogram of log-transformed Al_2O_3 displayed a negatively skewed, unimodal distribution. Threshold value was estimated at 37.17wt% (mean +1S.D) and seven (7) samples had concentrations higher than the threshold representing 22% of the entire samples. The west to east Al_2O_3 profile (Fig 4.21a). High concentrations are displayed by the Eburnean granitoids in the western part of the study area. Generally, low concentrations are displayed in areas underlain by the Birimian Metasedimentary rocks. The Hornblende Biotite diorites and the Post Tarkwaian gabbro- dolerite dykes in the study area both display moderate concentrations of Al_2O_3.

4.5.2.3 Iron oxide (Fe_2O_3)

Fe alongside Co and Ni belong to the Group VIII. Histogram of log Fe_2O_3 shows a unimodal distribution. Fe_2O_3 ranges from 1.16wt% to 12.23wt% with a mean concentration of 5.36wt% which is below the estimated abundance of Fe in the continental crust (5.6wt %) and also higher in granite (i.e. 2.7wt%) (Taylor, 1964). Threshold concentration was estimated at 11.50wt%. Only one sample had concentration above the threshold.

From the profile, Fe_2O_3 concentration is generally high in the Ofoase area especially in areas underlain by the Eburnean intrusives and low in the Birimian Metasedimentary rocks (Fig 4.21f), the hornblende biotite diorite and the Post Tarkwaian dyke.

4.5.2.4 Magnesium oxide (MgO)

Mg is in the same group with Ca, Sr and Ba. Histogram of log MgO shows a unimodal and positively skewed distribution. MgO concentration ranges from 0.95 to 3.56wt% with a mean of 1.66 wt% which is less than the average cluster abundance (2.3 wt%). But the mean concentration is above the estimated abundance in granites (0.16 wt%) and also in granitoids (1.0 wt%); (Levinson, 1974) and other references therein. The threshold value was estimated at 2.89 wt% and two samples had concentrations greater than the threshold value.

The profile of MgO displayed a high concentration in the Apemso area which is underlain by Eburnean intrusives (Fig 4.21b). Generally, hornblende biotite- diorite and the Birimian Metasedimentary rocks the in the study area display low concentrations of MgO. The lowest concentration is seen in the Post Tarkwaiah gabbro and dolerite dykes.

4.5.2.5Potassium oxide (K_2O)

Potassium alongside Na, Rb belongs to Group 1 of the periodic table (Goldschmidt 1954). The concentration of K_2O in the earth crust is estimated at 1.1 wt% which is less than the mean concentration of K_2O in the samples 1.31wt%.

K_2O concentration ranges from 0.47 to 4.81 wt% and from the histogram, it displays a unimodal distribution. Threshold value was estimated as 3.10 wt% (mean + 2SD) and 3

samples have values greater than the threshold representing 9.4% of the entire samples. The profile for the study area displayed K_2O the highest concentrations at the Apemso area (Fig 4.21f), predominantly underlain by Eburnean granitoids. K_2O distribution in the rest of the rock types is generally low.

4.5.2.6 Manganese oxides (MnO)

Mn is in Group VII of the periodic table. Histogram plot for log transformed MnO displayed a bimodal and negatively skewed distribution. MnO concentration ranges from 0.01 to 0.2 wt% with a mean of 0.06 wt% which is below the estimated average abundance of MnO (0.09 to 1.00 wt%) in the earth crust (Taylor, 1964).

Threshold value was estimated at 0.17 wt% (mean +2SD) and only two samples had values greater than the threshold representing 6.45 wt% of the entire samples.

The west to east profile of MnO displayed high concentration of in areas just below the central portion of the study area precisely in Ofoase (Fig 4.21h). This high concentration can be attributed to the Eburnean granitoids in the study area. Moderate concentration of MnO is generally observed throughout the Hornblende-biotite diorite hybrid, the Post Tarkwaian dyke and the Birimian Metasedimentary rocks.

4.5.2.7 Titanium oxide (TiO_2)

Ti alongside Zr, Hf and Th are located in group IV of the periodic table. Histogram of log transformed TiO_2 demonstrated a negatively skewed and a unimodally distributed concentration. TiO_2 ranged from 0.02 wt% to 1.48 wt% with a mean of 0.87 wt%

which is slightly below the estimated average abundance of TiO_2 (0.93wt %) in the crust (Taylor, 1964).

Threshold value was chosen at 1.18 wt% and five samples had values greater than the threshold value representing 16.13 wt% of the entire samples. The profile of TiO_2 showed high concentration in the central part of the study mostly in areas that are underlain by the Birimian Metasedimentary rocks (Fig 4.21d). The Eburnean intrusives rocks also show some intermediate association with the TiO_2.

4.5.2.8 Sodium oxide (Na_2O)

Sodium together with K, Rb, Cs and Fr make up Group 1 of the periodic table. Histogram plot for log transformed Na_2O showed unimodal and negatively skewed distribution. Na_2O ranges from 0.41 to 1.59 wt% with a mean concentration of 1.03 wt% which is less than the estimated distribution in the continental crust (2.84 wt%) (Taylor,1964). Threshold value was estimated at 1.32 wt% and four samples gave values higher than the threshold representing 12.9 wt% of the total samples.

In the west to east profile of Na_2O, concentration is mainly high in the Eburnean granitoids especially in Apemso and Ofoase area (Fig 4.21b). Na_2O concentration is low in the Post Tarkwaian dyke.

4.5.2.9 Calcium oxides (CaO)

Calcium is in group II of the periodic table together with Mg, Sr and Ba. Histogram plot of log transformed CaO showed a unimodal as well as positively skewed distribution. The concentration of CaO ranges from 0.02 to 1.33 wt% with a mean

concentration of 0.24wt% which is less than the estimated average continental crust value (4.15 – 5.8) wt% and also below the estimated value for granites (0.7 wt%).

Threshold value was estimated at 0.81 wt% and two samples had values great than the threshold representing 6.45 wt%. The profile of CaO showed low concentrations almost throughout the study area (Fig 4.21d). The hornblende biotite diorite showed slightly high concentration of CaO. Sample A16, which displays the highest concentration of CaO is located on the contact between the Eburnean intrusive rock and the Birimian Metasedimentary rocks.

4.5.2.10 Rubidium (Rb)

Rubidium alongside Mg, Ca, Sr and Ba lies in Group II of the periodic table (Goldschmidt, 1954). The concentration of Rb ranges from 18.0ppm to 271.8 ppm and with a mean concentration of 70.33ppm which is less than the estimated average continental crust value of 90 ppm.

Histogram of log transformed Rb provides a unimodal and positively skewed distribution. Threshold value for Rb is estimated at 195.09 ppm (mean +2SD) with six samples having values greater than the threshold value representing 19.35% of the total samples. From the profile, Rb displays anomalous concentration throughout the study area (Fig 4.21c). The highest concentration of Rb is recorded at the Apemso area, which is underlain by the Eburnean intrusive rocks. The Birimian Metasedimentary rocks generally show low concentration of Rubidium.

4.5.2.11 Zinc (Zn)

Zn together with Cd and Hg are located in Group II of the periodic table (Goldschmidt, 1954). Histogram plot for log transformed Zn displayed a negatively skewed and unimodal distribution. Zn in the study area ranges from 12.60 to 66.10ppm with a mean concentration of 35.60 ppm which is much below the estimated average abundance in the continental crust (70 ppm) by (Taylor ,1964) but close to the average abundance in granite which is 40ppm.

Threshold value for Zn was estimated at 48.29 ppm (mean +1SD) and six samples had values greater than threshold representing 19.35% of the total samples. The profile of Zn shows high concentrations in Ofoase area where the underlying rock is the hornblende biotite- diorite (Fig 4.21e). Zn is generally high in the eburnean intrusive rocks and low in the Birimian Metasediments.

4.5.2.12 Nickel (Ni)

Histogram for log transformed Ni was positively skewed and also unimodally distributed. Ni concentrations ranged from 8.20 ppm to 84.20ppm with a mean value of 29.54 ppm which is below the Ni concentration estimated to be in the continental crust 75 ppm (Taylor, 1964) but close to the estimated concentration in the granodiorite 20 ppm (Levinson, 1974) and reference therein.

Threshold value was estimated at 77.16 ppm with only two samples having values greater than the threshold representing 6.5% of the total sample. The profile for Ni displayed high concentrations only in Ofoase area which in underlain by the hornblende

biotite diorite. Ni shows moderate concentrations in the Birimian Metasedimentary and the Eburnean intrusive rocks.

4.5.2.13 Copper (Cu)

Copper, Ag and Au are all Group I elements of the periodic table. Histogram of log transformed Cu indicated a unimodal and negatively skewed distribution. Cu concentration ranged from 1.50 to 37.40 ppm with a mean value of 16.21ppm. The mean concentration is lower than the estimated abundance of Cu in the continental crust (55 ppm) but greater than the concentration of Cu in granite 10ppm (Taylor, 1964).

Threshold value was chosen at 26.70ppm (mean +SD) and six (6) samples had values greater than the threshold representing 19.4% of the total population.The profile of Cu displayed high concentration in the Ofoase area underlain by Hornblende biotite - diorite which occurs just in the central portion (Fig 4.21e). The Eburnean intrusives generally show low concentrations of Cu.

4.5.2.14Barium (Ba)

Histogram for log transformed Ba displayed a negatively skewed and a unimodal distribution. Ba ranges from 71ppm to 426.00ppm with a mean concentration of 246.52 ppm which is less than the estimated Ba concentration in the continental crust (425 - 600)ppm as well as less than the average estimated values in granite and granodiorite 600 ppm and 500 ppm respectively. Threshold value was chosen at 356.48 ppm. Six samples had values greater than the threshold value representing 19.35% of the total samples.

The profile showed that Ba concentration in the study area is almost uniformly distributed (Fig 4.21g). Generally, the central portion of the study area displayed medium to high concentration of Ba. The lowest concentration of Ba is observed in the Birimian Metasedimentary rocks.

4.5.2.15 Strontium (Sr)

Histogram of log transformed Sr displayed a unimodal and a positively skewed distribution. Sr ranges from 13.80 ppm to 74.10 ppm with a mean concentration of 22.21 ppm which is far less than the estimated concentration in the continental crust (i.e. 370 ppm). A threshold value for Sr was estimated at 63.10 ppm (mean +2SD) and two samples had values greater than the threshold representing 6.5% of the entire samples.

The west to east profile of Sr shows low concentration throughout the Eburnean intrusives (Fig 4.21c). The hornblende biotite-diorite showed some minor concentration of Sr. High concentration is generally displayed in the Ofoase community.

4.6 Correlation matrix

Visual examination of the correlation matrix shows that there are a number of significant correlations ranging from 0.70 to 1.00 (in bold). Table 4.18 shows the inter-relationship between twenty seven elements and also displays a wide range of inter-correlation from negative to positive. A total of thirty inter- correlations were established. The strongest correlation exists between Cu-Fe_2O_3 (0.92). From the table, strong positive correlations exist between Fe_2O_3-P_2O_5 (0.807), Ga-Al_2O_3 (0.84), Cu - P_2O_5 (0.838), MnO-CaO (0.846), Ni-Fe_2O_3 (0.823), Ga-Cu (0.80), Ba-Sr (0.829) and

Cu-Ni (0.863). Moderate correlation existed between Fe_2O_3-Al_2O_3 (0.761). Cu-Al_2O_3 (0.762).I- Al_2O_3 (0.778), As-SO_3 (0.77), Fe_2O_3-TiO_2 (0.772).I- Cu (0.779).I - Zn (0.787). Sr- Br (0.776).

Weak correlation existed between I-TiO_2 (0.720), Ni-MnO (0.745), Zn-Ni (0.751), I-Ni (0.751), Ni- MgO (0.746), Sr- MgO (0.731), P_2O_5- Al_2O_3 (0.731), Rb- K_2O(0.726), I- P_2O_5 (0.752), Ni -P_2O_5 (0.731), Br-CaO (0.705) and Zr -SiO_2 (0.709)

Generally, strong correlation exist between these minor elements; Cu, Ni, Ba, Sr and Ga , I and their inter-relationship with these major elements; Al_2O_3, Fe_2O_3, P_2O_5, MnO and CaO ranges from moderate to strong. The inter-relationship between Cu, Ni, Br, Sr, Ga, I and Fe_2O_3 ranges from weak to very strong (0.358-0.916). Despite the high concentration values depicted by SiO_2, it is evident that it correlates negatively with almost all the elements except Zr (0.709) which displayed moderate correlation and also with Nb (0.26) and Ce which displayed very weak correlation. The moderate loading of Zr probably implies that, it is resistance to weathering.

Also the inter-relationship between minor trace elements ranges from moderate to strong that is, from 0.731 to 0.863. Again the relationship between minor trace elements and SO_3 is very weak with the exception of Arsenic (As) which is moderately correlated (0.765), indicating low level of SO_3 concentration in the study area.

Table 4.18. Correlation matrix for the primary soil data

	Na_2O	MgO	Al_2O_3	SiO_2	P_2O_5	SO_3	K_2O	CaO	TiO_2	MnO	Fe_2O_3	Cr
Na2O	1.00											
MgO	0.43	1.00										
Al2O3	0.68	0.38	1.00									
SiO2	-0.10	-0.49	-0.37	1.00								
P2O5	0.48	0.58	**0.73**	-0.57	1.00							
SO3	0.13	0.10	0.39	-0.54	0.61	1.00						
K2O	0.41	0.28	0.13	-0.03	0.08	-0.08	1.00					
CaO	0.30	0.55	0.36	-0.62	0.65	0.65	0.11	1.00				
TiO2	0.36	0.30	0.52	0.00	0.50	0.30	-0.40	0.22	1.00			
MnO	0.42	0.55	0.40	-0.48	0.69	0.62	0.11	**0.84**	0.41	1.00		
Fe2O3	0.49	0.49	**0.76**	-0.48	**0.81**	0.56	-0.16	0.57	**0.77**	0.66	1.00	
Cr	-0.27	0.19	-0.25	-0.19	-0.15	-0.01	-0.04	0.02	0.06	-0.04	0.00	1.00
Ni	0.47	**0.75**	0.56	-0.58	**0.73**	0.51	-0.09	0.64	0.67	**0.75**	0.82	0.24
Cu	0.63	0.65	**0.76**	-0.58	**0.84**	0.50	0.31	0.55	0.67	0.67	**0.92**	-0.14
Zn	0.62	0.68	0.42	-0.28	0.48	0.34	0.20	0.44	0.53	0.58	0.55	0.27
Ga	0.53	0.43	**0.84**	-0.55	0.65	0.43	0.23	0.46	0.22	0.49	0.60	-0.23
Ge	0.27	0.40	0.24	-0.45	0.43	0.37	0.18	0.50	0.01	0.57	0.21	-0.25
As	-0.14	-0.19	0.11	-0.36	0.35	**0.77**	-0.12	0.39	0.06	0.43	0.32	-0.12
Br	0.57	0.51	0.57	-0.52	0.63	0.44	0.41	**0.71**	0.27	0.62	0.60	0.14
Rb	0.14	0.47	0.00	-0.34	0.19	0.06	**0.73**	0.37	-0.42	0.41	-0.12	-0.03
Sr	0.58	**0.73**	0.41	-0.45	0.57	0.32	0.68	0.64	0.06	0.53	0.36	0.06
Zr	0.02	-0.41	-0.04	**0.71**	-0.25	-0.22	-0.40	-0.45	0.50	-0.23	0.00	-0.19
Nb	0.25	-0.05	0.58	0.03	0.32	0.29	-0.21	-0.02	0.61	0.22	0.47	-0.19
Sn	0.22	0.39	0.16	-0.41	0.31	0.17	0.29	0.30	0.01	0.53	0.06	0.18
I	0.58	0.47	0.78	-0.29	**0.75**	0.53	-0.07	0.42	**0.72**	0.53	**0.79**	0.08
Ba	0.65	0.61	0.44	-0.20	0.48	0.19	0.64	0.33	0.28	0.35	0.44	0.14
Ce	0.54	0.24	0.66	0.01	0.49	0.14	-0.11	0.19	0.51	0.39	0.46	0.02

Table 4.19. Continuation of the correlation matrix for the primary soil data

	Ni	Cu	Zn	Ga	Ge	As	Br	Rb	Sr	Zr	Nb	Sn	I	Ba	Ce
Ni	1														
Cu	**.863**	1													
Zn	**.751**	.663	1												
Ga	.532	**.800**	.333	1											
Ge	.362	.343	.334	.365	1										
As	.203	.155	-.111	.218	.227	1									
Br	.647	.595	.590	.675	.233	-.017	1								
Rb	.117	.374	.183	.322	.486	.025	.320	1							
Sr	.512	.644	.580	.443	.431	-.007	**.776**	.605	1						
Zr	-.187	-.247	-.104	-.337	-.346	-.190	-.379	-.609	-.520	1					
Nb	.266	.368	.148	.443	.040	.087	.097	-.228	-.103	.463	1				
Sn	.381	.259	.391	.512	.487	-.040	.423	.662	.388	-.274	.167	1			
I	**.731**	**.779**	**.787**	.609	.205	.028	.578	-.153	.377	.159	.503	.237	1		
Ba	.494	.591	.664	.272	.150	-.081	.617	.321	**.829**	-.174	-.008	.173	.493	1	
Ce	.528	.507	.533	.536	.082	-.078	.377	-.119	.108	.212	.540	.177	.624	.115	1

4.6.1 Scatter plots for the profile

Elements that Correlated well on the correlation matrix were used to plot scatter plots in SPSS in order to graphically assess the correlation between the variables. A total of 22 scatter plots were plotted.

It is evident that the strongest correlation exists between Cu and Fe_2O_3 (0.92). This is because this inter-relationship has the line of fit passing through most of the circles. Also scatter plot for Fe_2O_3-Al_2O_3 (0.76) is an example of moderate correlation. Lastly,

the scatter plot for Zr –SiO_2 (0.71) is a display of weak correlation. Generally, most of the elements show non- linear distribution.

4.6.2 Principal component analysis (PCA)

Appendix A (Table 6) displays the total variance explained by the extracted components in the PCA. The rotated factor solutions are also presented in table 4.5. Varimax rotation was used for the rotation in this study.

Five factors accounted for 82.54% of the total variance. The first factor accounted for 43.33% of the total variance and is dominated by CaO, SO_3, P_2O_5 and a negative loading of SiO_2. There is also the weak associations of MnO (0.69), Fe_2O_3 (0.65) and Ni (-0.68). The second factor also accounted for 17.86% of the total variance and composed of positive loadings of Sr, Ba, Zn and Na_2O while the third factor is made up of Al_2O_3, Ga and Nb which explained 9.48% of the total variance. The fourth factor having TiO2 as the major dominating factor also shows some weak associations with K_2O (-0.67), Rb (-0.67) and Zr (0.68) which explained 6.47%, and the fifth factor also contributed 5.38% of the total variance and it is composed of a positively loaded Sn.

Although five factors were extracted, the first three accounts for the bulk (approximately 70%) of the total variance in the dataset.

4.6.3 Scree plot

The scree plot for the detailed soil samples (Fig 4.22). The first five component numbers were selected. This was because Eigenvalues were selected from the highest values to where the elbow began. These selected eigenvalues corresponds to loadings

of the verimax rotated matrix for the five factor model shown (Table 4.20). Evidently, the first five factors are more correlated than the rest.

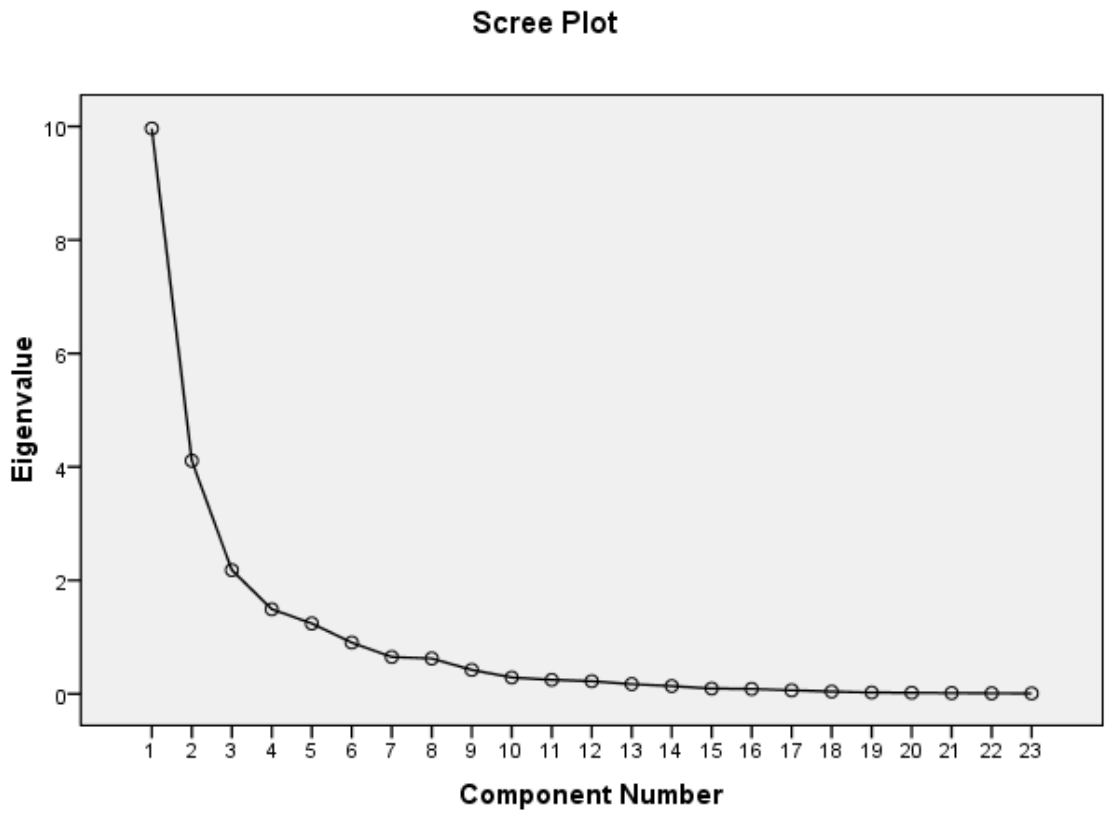

Figure 4.22: Scree Plot for the soil samples dataset. Components to the right of component 5 (below eigenvalue of 1.0) do not account for a significant portion of variance in the dataset

Table 4.20. Rotated components for the primary data

	Component				
	1	2	3	4	5
Na_2O	.021	**.727**	.421	.086	.078
MgO	.473	.653	-.003	.011	.306
Al_2O_3	.358	.346	**.813**	.057	-.138
SiO_2	**-.857**	-.038	-.074	.268	-.064
P_2O_5	**.718**	.341	.422	.083	-.015
SO_3	**.748**	-.021	.211	.117	.003
K_2O	-.160	.634	.071	-.679	.139
CaO	**.816**	.256	.007	-.020	.205
TiO_2	.232	.250	.368	**.819**	-.025
MnO	.685	.283	.169	.156	.430
Fe_2O_3	.652	.320	.455	.409	-.135
Ni	.680	.426	.223	.394	.253
Cu	.564	.432	.494	.028	.014
Zn	.320	**.703**	.089	.366	.332
Ga	.474	.181	**.756**	-.234	.136
Rb	.200	.305	-.045	-.675	.558
Sr	.408	**.783**	.054	-.319	.161
Zr	-.551	-.122	.200	.682	-.107
Nb	-.005	-.112	**.804**	.379	.102
Sn	.145	.125	.154	-.142	**.875**
I	.310	.467	.404	.523	.120
Ba	.157	**.936**	.083	-.047	-.053
Ce	.047	.107	.634	.348	.275

4.6.4 Hierarchical cluster analysis for the profile

The number of clusters was set at three and Na_2O, Al_2O_3, P_2O_5, TiO_2, Fe_2O_3, Ga, Nb, I and Ce made up the first cluster in this dataset. The second cluster also loaded MgO, K_2O, CaO, MnO, Cr, Ni, Cu, Zn, Cu, Br, Kb, Sr, Sn and Ba. The association of K_2O, Ba and Rb in the second cluster implies the presence of felsic source. Cluster three is also made up of SiO_2, SO_3, As and Zr.

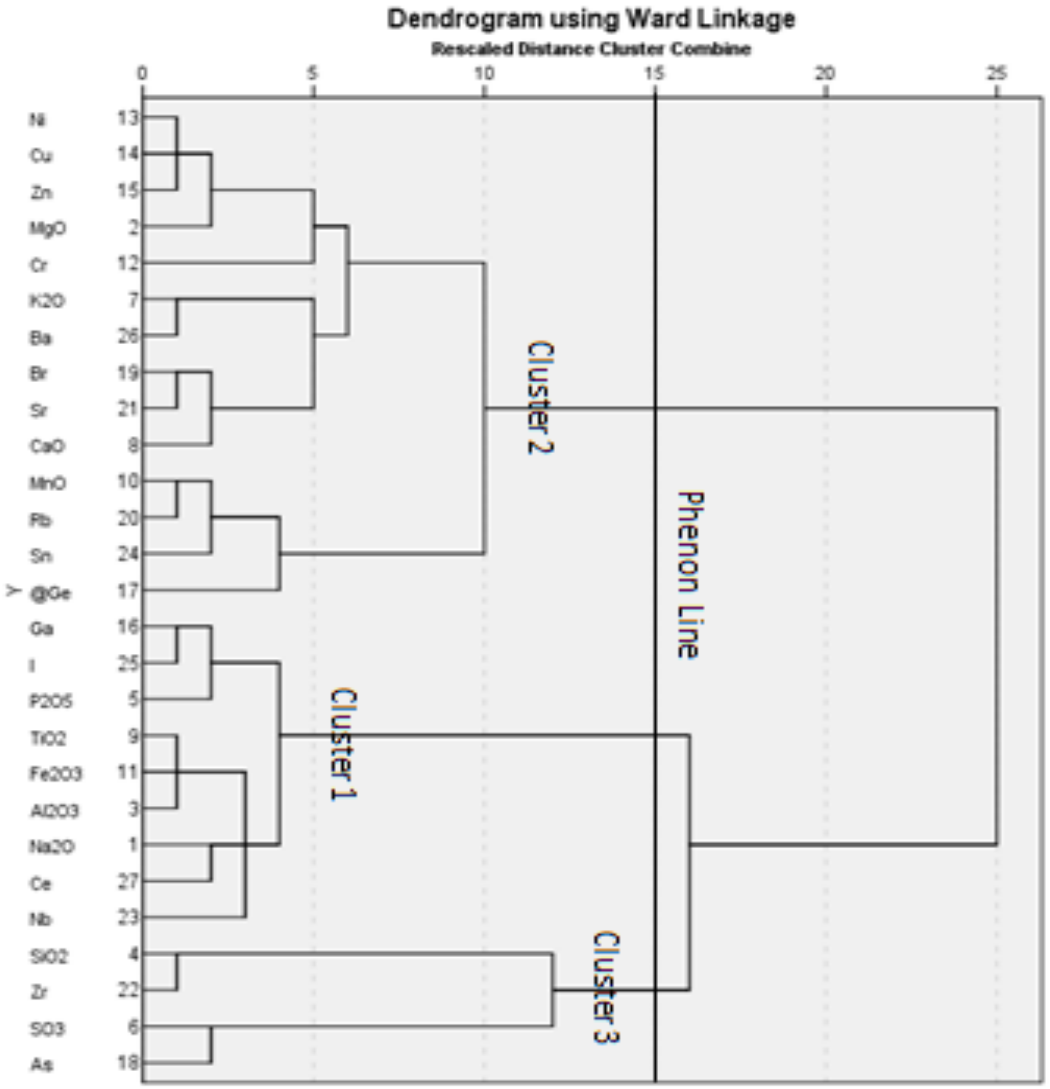

Figure 4.23: Dendrogram displaying clusters multi-element cluster for the primary data.

CHAPTER FIVE

DISCUSSION

5.1Petrography

Petrographic studies of eighteen rock samples collected suggest that the rocks are predominantly biotite schist, diorite, granodiorite, and granite. The biotite schist outcrops between Ntunkumso and Boiya and is made up of biotite, quartz, feldspar, iron oxides and opaque minerals. Diorite was encountered at Abesewase and Ofoase and is mineralogically composed of hornblende, plagioclase, microcline, biotite, quartz, iron oxides and opaque minerals. Granodiorite outcrops between Kokodie and Odoyefe and the major minerals in the rock are plagioclase, microcline, muscovite, quartz, garnet and opaque minerals. Granite in the study area outcrops at Apemso and Nkyerepoaso and consists of plagioclase, microcline, quartz, biotite, muscovite and opaque minerals.

5.2 Comparison of dispersion patterns

Table 5.1 displays a summary of the results of the multivariate statistics for all the datasets employed in this study. The principal component factor one of the secondary data is the same as PCA factor one for the primary dataset.Both provided dispersion pattern related to mafic to intermediate influence and also obtained a correlation implying a plutonic source, which is confirmed by the coarse grained texture of the rocks in the study area.

The hierarchical cluster loading one for both datasets displayed a felsic dispersion pattern. PCA factor 2 for the detailed soil samples displayed a dispersion pattern that is influenced by felsic rocks. Whilst the PCA factor 2 for the reconnaissance soil sampling dataset displayed mafic dispersion pattern.

The hierarchical cluster analysis for both dataset displays an intermediate dispersion pattern of both mafic and felsic rocks.

PCA factor 3 for both dataset displays a dispersion pattern that is felsic in composition. The cluster analysis loading 3 for the datasets implies the influence of hydrothermal alteration.

Also the results of the third loading for both dataset in the hierarchical cluster analysis is almost the same and displays a dispersion pattern of elements SiO_2, Zr , $\pm$ Nb, SO_3 and As. PCA factor 4 for the reconnaissance soil sample dataset displayed Cr, Zr and Nb and PCA factors 4 and 5 produced TiO_2, Zr, I, Rb and Sn respectively.

Table 5.1. Comparing the geochemistry of the three datasets

Component 1	**Elements**	**Implication**
Secondary data	P_2O_5, MnO, CaO ,Cu, Zn, Sr, Ni	Mafic composition and a hydrothermal source
Primary data	CaO, SO_3, P_2O_5, MnO, Fe_2O_3, Ni, -SiO_2	Mafic to intermediate source
Rock	Ba, Bi, Fe_2O_3, MgO, TiO_2, Al_2O_3, Na_2O,Cd,Cr,Ge, In, La, Li, Ni, Pb, Sr, V, Zn, Ce, Co , Sc, Sr, Th, Dy, Eu, Gd, Nd, Pr ,Tb	Intermediate composition and Hydrothermal alteration (plutonic)
Cluster 1		
Secondary data	Na_2O , Al_2O_3, TiO_2, Ga, Ge , Br, Sn, I, Ce	felsic
Primary data	Na_2O , Al_2O_3 , P_2O_5, TiO_2 , Fe_2O_3 , Ga , Nb , I, Ce	felsic
Rock	Al_2O_3, K_2O, Na_2O, Ba, Be, Ce, Ga, Hf, La, Nb, P, Pb, Sr, Ta, Th, U, Zr	felsic
Component 2		
Secondary data	Al_2O_3, Fe_2O_3, Ga, I, Na_2O, SiO_2	Mafic
Primary data	Sr, Ba, Zn ,Na_2O	mafic
Rock	Negative (K_2O, SiO_2, Ag, Cd, Be, Ga, Nb, Rb,Sn, Tl) positive (Ag, Er, Lu, Tm, Mn, CaO and Yb).	felsic
Cluster 2		
Secondary data	MgO, P_2O_5, SO_3, K_2O, CaO, MnO, Fe_2O_3, Cr, Ni, Cu, Zn, As, Rb, Sr, Ba.	Intermediate composition
Primary data	MgO, K_2O, CaO, MnO, Cr, Ni, Cu, Zn , Ge, Br, Rb, Sr, Sn, Ba	Intermediate composition and Hydrothermal alteration (plutonic)
Rock	CaO, Fe_2O_3,MgO, SO_3,TiO_2, Ag, Bi, Cd, Co, Cr, Cu, Ge, In, Mn, Ni, Sc, V, W, Y, Zn, Dy, Er, Eu, Gd, Ho, Lu, Nd, Pr , Sm ,Tb, Tm, and Yb	Intermediate composition and Hydrothermal alteration (plutonic)
Component 3		
Secondary data	K_2O, Rb, Ba	felsic
Primary data	Al_2O_3, Ga , Nb, Ce	Hydrothermal alteration (plutonic)
Rock	Hf, As	Hydrothermal alteration
Cluster 3		
Secondary data	SiO_2, Zr and Nb	
Primary data	SiO_2,SO_3,As, Zr.	Hydrothermal alteration (plutonic)
Rock	SiO_2, As, Cs, Li, Mo, Rb, Sn, Tl	Hydrothermal alteration (plutonic)
Component 4		
Secondary data	TiO_2, Zr	Hydrothermal alteration
Primary data	Cr, Zr, Nb	Hydrothermal alteration
Rock	SO_3,W	

5.2.1 Comparison of the dispersion pattern between the primary soil data and rock dataset.

Three clusters were considered for both datasets (Table 5.1). The PC factor one for the soil survey displayed a loading that implies a mafic index whilst the PC factor one for the rock dataset suggests an intermediate. These associations can probably be attributed to the presence of the biotite schist, diorite, granodiorite and the granite.

The second PC factor for both datasets (Table 5.1) displayed a mafic composition. Also, PC factor three of the soil dataset (Table 5.1) indicate hydrothermal alteration whilst component 3 of the rock dataset displayed(As and Hf) hydrothermal alteration. The fourth and fifth components were negligible such that they contributed very little to the total variance giving 3.8% and 3.5% respectively.

Considering the hierarchical cluster analysis for both dataset, cluster one for soil survey implied a felsic composition whilst the cluster one of the rock survey also produced an intermediate composition. This can also be linked to the cases of the rock cluster which displayed R8, R12 and R9. From the petrogaphy and geochemistry, R8 and R12 are biotite schists and R9 is also a diorite which is intermediate composition. The second cluster also displayed an intermediate composition for both datasets. The cases cluster two of the rocks produced R11 and R18 which are both granodiorites.

The third cluster for the soil survey indicated a plutonic source probably due to the coarse grained texture of the rocks. There is also the presence of hydrothermal alteration. The third rock cluster produced R16 and R17 which are both diorites implying a felsic composition.

5.3 Concentrations of soils and their underlying rock types (Appendix A: table1-4)

5.3.1 Biotite schist

Some major element concentrations in these soils are as follows; SiO_2 (47.45 to 57.77) wt%, TiO_2 (0.92 to 1.14) wt%, Al_2O_3 (29.69 to 38.57) wt%, Fe_2O_3 (5.87 to 9.06)wt%, MgO (1.50 to 3.56) wt%, CaO (0.06 to 0.64) wt%, Na_2O (0.93 to 1.26) wt%, and K_2O (0.97-1.29) wt%. The contents of some minor elements are; Cr (111.00 to 469.00) ppm, Ni (21.60 to 78.10) ppm, Cu (11.40 to 30.80) ppm, As (3.00 to 12.50) ppm, and I (18.50 to 46.00) ppm. (Appendix A: table 1)

SiO_2 concentration in the biotite schist ranges from 71.14 to 73.17 wt%, Al_2O_3 also varies from 14.66 to 15.39 wt%, Fe_2O_3 (4.45 to 5.40) wt%, MgO (2.57 to 3.56) wt%, TiO_2 (0.43 to 0.57) wt% and CaO (2.73 to 3.64) wt%. The contents of some minor elements are as follows; Cu (1.20 to 21.50) ppm, Ni (86.90 to 102.50) ppm, Ga (21.00 to 221.90) ppm, Rb (182.00 to 131.00) ppm, As (0.30 to 0.30) ppm and Sr (456.00 to 636.00) ppm.

5.3.2 Diorites

In soils overlying the diorite, some major elements concentrations are: SiO_2 (44.54 to 53.67) wt%, TiO_2 (0.92 to 1.32) wt%, Al_2O_3 (29.69 to 38.57) wt%, Fe_2O_3 (6.28 to 9.30) wt%, MgO (1.54 to 3.56) wt%, CaO (0.16 to 0.92) wt%, Na_2O (0.93 to 1.26) wt%, and K_2O (0.78 to 1.29) wt%.The contents of some minor elements are; Cr (301.00 to 630.00) ppm, Ni (11.70 to 75.20) ppm, Cu (1.50 to 37.40) ppm,As (3.00 to 14.20) ppm, and I (22.70 to 42.50) ppm.(Appendix A: table 2)

SiO_2 in diorite varies from ranges from 59.87 to 61.64 wt%, Fe_2O_3 (4.89 to 9.47) wt%, Al_2O_3 (12.00 to 15.57) wt%, K_2O (0 .53 to 1.49) wt%, TiO_2 (0.47 to 1.17) wt%, MgO

(3.37 to 11.92)wt%, CaO (4.743 to 8.65) wt% and Na_2O (2.60 to 4.21) wt%. Some minor elements concentrations are as follows; Cu (11.20 to 60.70) ppm, Ni (44.40 to 300.00) ppm, Sr (381.00 to 686.00) ppm. Cr (116.00to 403.00)ppm and As (0.30 to 0.30) ppm.

5.3.3 Granodiorite

The soils overlying the granodiorite are made up of SiO_2ranging from (44.54 to 81.01) wt%, TiO_2 (0.92 to 1.48) wt%, Al_2O_3 (12.70 to 37.39) wt%, Fe_2O_3 (1.64 to 10.86)wt%, MgO (1.19 to 3.56) wt%, CaO (0.06 to 0.92) wt%, Na_2O (0.94 to 1.26) wt%, and K_2O (0.78 to 1.35) wt%. The contents of some minor elements are; Cr (233.00 to 469.00) ppm, Ni (43.20 to 78.10) ppm, Cu (20.70 to 32.90) ppm, As (3.00 to 12.50) ppm, and I (26.30 to 46.00) ppm.(Appendix A: table 3)

In granodiorite, SiO_2 content ranges from 68.80 to 76.41wt%, Al_2O_3 (13.77 to 14.97) wt%, Fe_2O_3 (4.89 to 9.47) wt%, K_2O (0 .53 to 1.49) wt%, TiO_2 (0.47 to 1.17) wt%, MgO (3.37 to 11.92) wt%, CaO (4.74 to 8.65) wt% and Na_2O (2.61 to 4.21) wt%. Some minor elements Cr (16.00to 148.00) ppm, Sr (381.00 to 686.00) ppm, Ni (4.60 to 73.00) ppm, Cu (1.50 to 19.40) ppm and As (0.30 to 0.50) ppm

5.4 Granite (RI, R2, R5, R10)

SiO_2concentration in soils overlying the granite varies from (44.54 to 60.36) wt%, TiO_2 (0.46 to 1.10) wt%, Al_2O_3 (17.80 to 35.01) wt%, Fe_2O_3 (1.78 to 12.23) wt%, MgO (1.15 to 3.24) wt%, CaO (0.04to 0.92) wt%, Na_2O (0.41 to 1.00) wt%, and K_2O (0.59 to 1.35) wt%.The contents of some minor elements are; Cr (79.50 to 468.00) ppm, Ni

(9.40to 68.80) ppm, Cu (1.50 to 32.90) ppm, As (4.40to 11.10) ppm, and I (7.00 to 40.10) ppm. (Appendix A: table 4)

SiO_2 content in granite varies from 69.380 to 83.930 wt%, Al_2O_3 (11.186 to 13.604) wt% K_2O (2.72 to 3.26) wt%, MgO (0.02 to 0.32) wt%, TiO_2 (0.07 to 0.14) wt%, CaO (0.29 to 0.76) wt%, and Na_2O (2.21 to 5.35) wt%. The contents of some minor elements are as follows: Cu (0.90 to 4.500) ppm, Ba (10.00 to 240.00) ppm, Ni (0.90 to 4.90) ppm, Cr (3.00 to 16.00) ppm, As (0.30 to 0.30) ppm and Sr (7.80 to 123.00) ppm.

5.5 The associations between the rock types and their respective soils

5.5.1 Biotite schist

High Al_2O_3 concentration in the soils that overlie biotite schist may be attributed to significant weathering. There are high concentrations of As, Ga, Zr, Cr and Sn in the soil than in the rock. This may suggest that the soil may have been transported from other sources due to the undulating nature of the topography. The high concentrations of Zn, Ni and Cu in the rock may also suggest hydrothermal alteration and leaching from the soil.

CaO, MgO, SO_3, K_2O, Na_2O and SiO_2 exhibit higher concentrations in the rock than in the soils. These high concentrations may be attributed to the presence of rock forming minerals such as plagioclase feldspar and biotite. TiO_2, Al_2O_3 and Fe_2O_3 were also highly concentrated in the soil than in the rock and this can be attributed to the presence of accessory minerals such as sphene, apatite, and pyrite.

5.5.2 Diorite

SiO_2 is slightly high in the soil compared to the rock. However, Fe_2O_3 concentration is almost similar in both media. High Al_2O_3 concentration in the soil may be due to weathering.

CaO, MgO, Cr, Ni, Cu and Ba are highly concentrated in the rock than in the soil. This association may imply leaching of these elements from the soil. The presence of K_2O and Al_2O_3 may be attributed to the presence of plagioclase and also CaO and Na_2O may be due to the mica minerals (e.g. biotite). Fe_2O_3 and MgO may also be as a result of some amphiboles (e.g. hornblende) mineral presence. The presence of TiO_2 may be attributed to the minor contributions of accessory minerals such as ilmenite and some opaque minerals such as titanomagnetite.

5.5.3 Granodiorite

In the granodiorite, SiO_2, Na_2O, K_2O and CaO are highly concentrated in the rock than in the soil. Due to this, concentrations of MgO, Fe_2O_3 are expected to be lower in the soil. However, MgO and Fe_2O_3 show high concentration in the soil implying probable transportation of mafic signatures or the existence of mafic bodies within the study area. From the field observations, some granodiorites are close to mafic rocks. These mafic rocks may have contributed to the high concentrations of MgO and Fe_2O_3 in the soil. The presence of K_2O may be attributed to the presence of potassium feldspar and also the CaO is due to the existence of calcic plagioclase.

The minor elements with high concentrations in the soil are Cr, V, Cu, Ga, Ge, As, Zr, Nb, Sn, Zn, Ba, Ce, Ni, and Co. This association can be attributed to the presence of garnet, sphene, pyrite and probably some degree of hydrothermal alteration or transportation from other sources.

5.5.4 Granite

The granite is felsic in composition and high concentrations of SiO_2, Na_2O and K_2O confirm it. This high concentration may be attributed to the presence of feldspars (plagioclase, microcline and albite) in the granite. However, Al_2O_3, Fe_2O_3, CaO and MgO also show high concentrations in the soils than in the rock. This can be attributed to the presence of mafic signatures either close to the granite or transported from other areas.

Secondly, Cu, Cr, Ni, Zr and As are highly concentrated in the soil than in the rock. This implies that the soil may not be in-situ as confirmed by the cluster three (Table 5.1) for the soil sample dataset. Also, high Rb concentration in the rock signifies the occurrence of hydrothermal alteration. Pathfinder elements such as As, Fe_2O_3 and Cu may suggest the presence of gold but since they are highly concentrated in the soil than in the rock, the gold content may not be economically significant.

Field observation proofs that, there are some mafic rocks close to the felsic ones which may have contributed to the variation in concentrations of the soils.

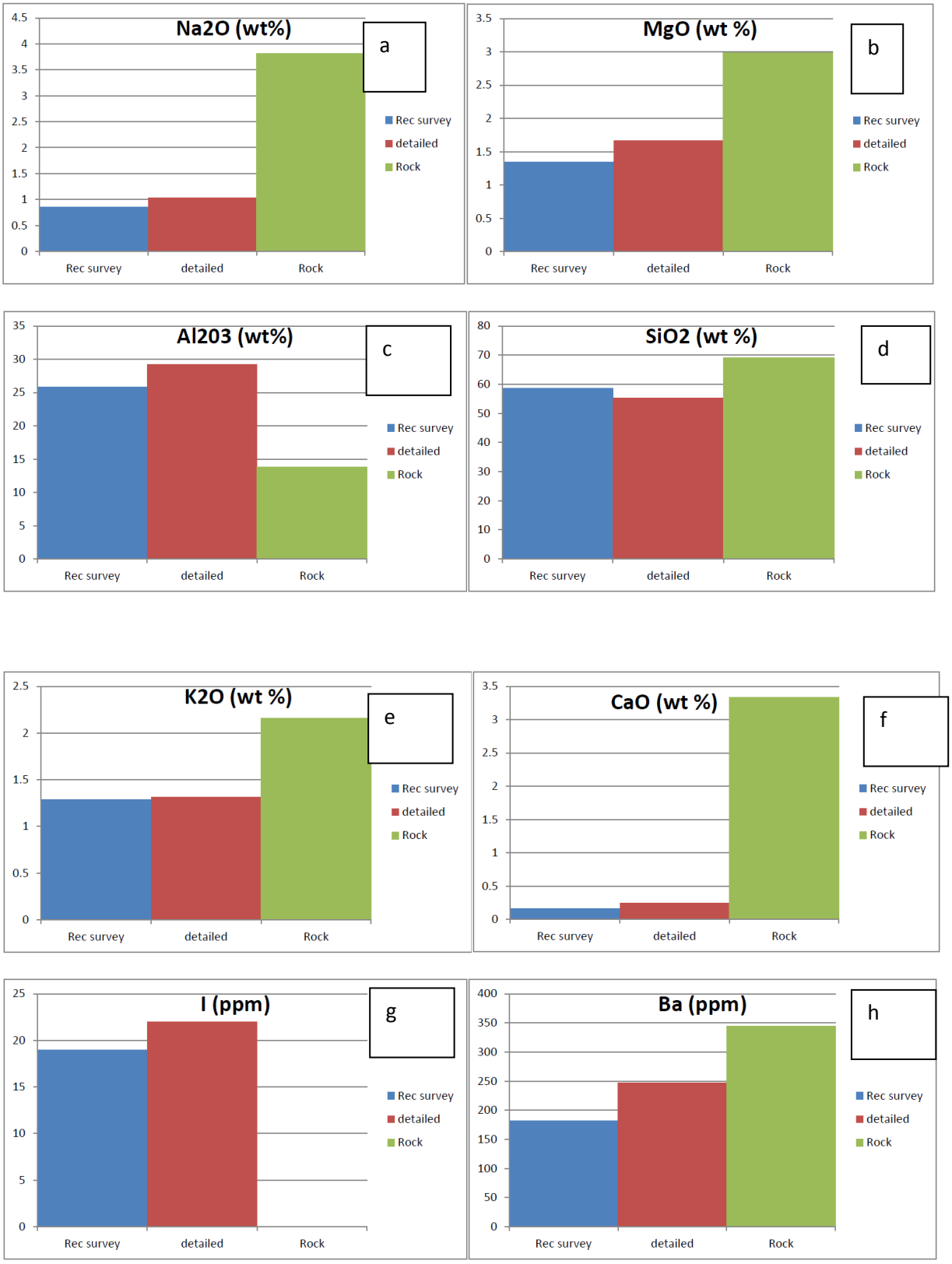

Fig 5.1: Comparison between the individual elements in all the three datasets

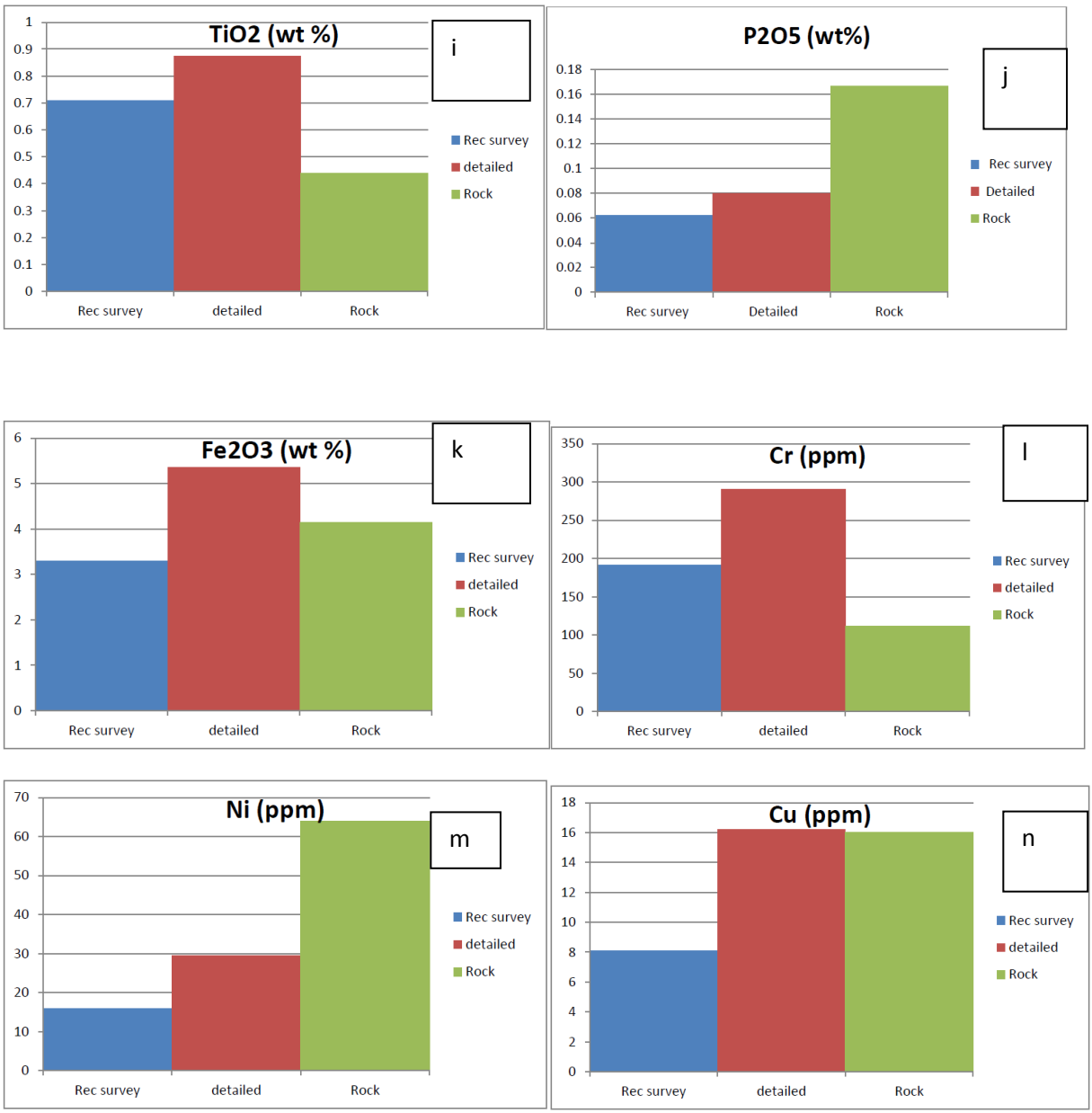

Fig 5.2: Comparison between the individual elements in all the three datasets

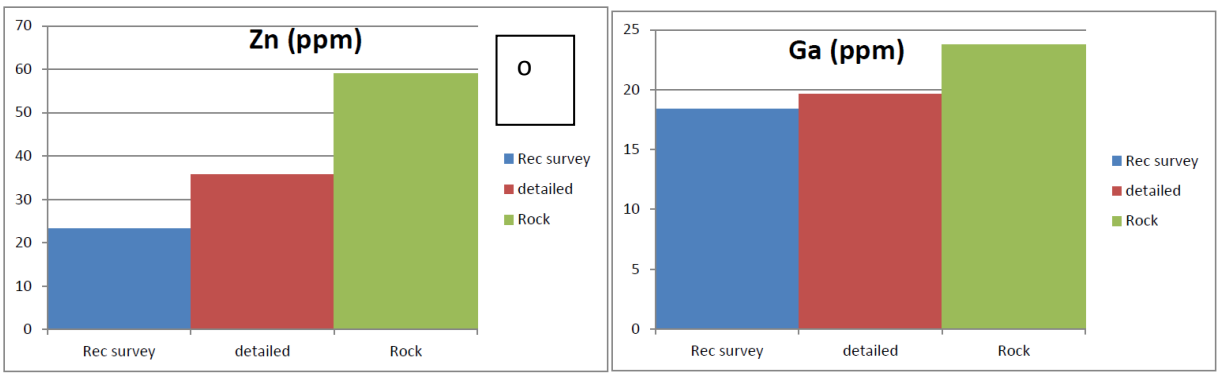

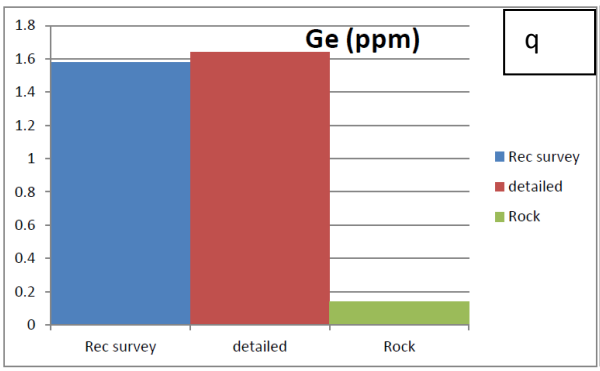

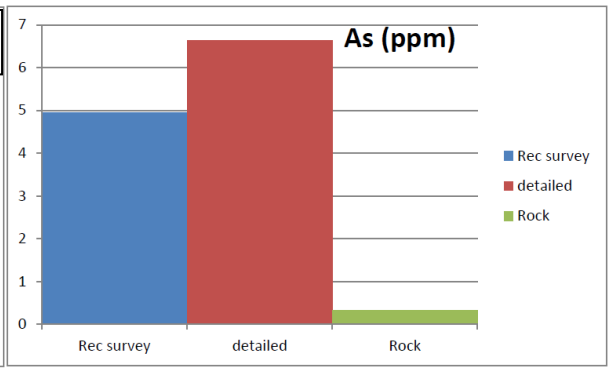

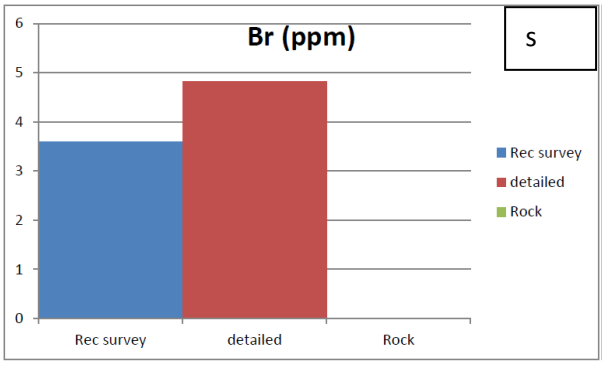

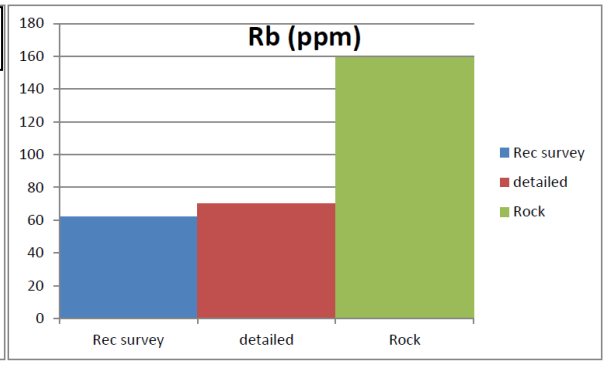

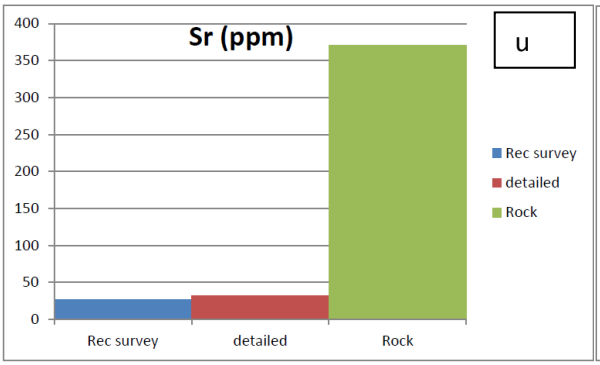

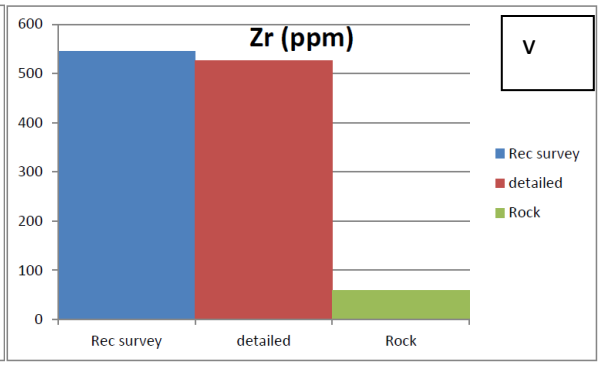

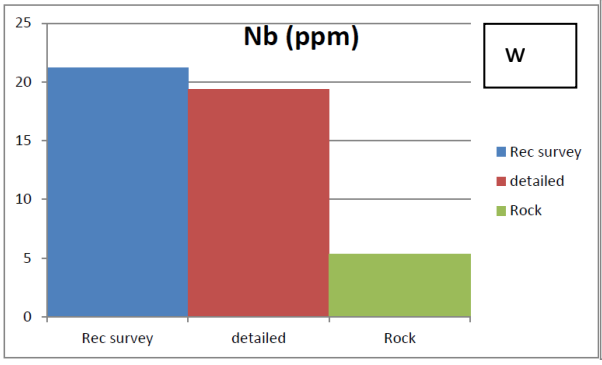

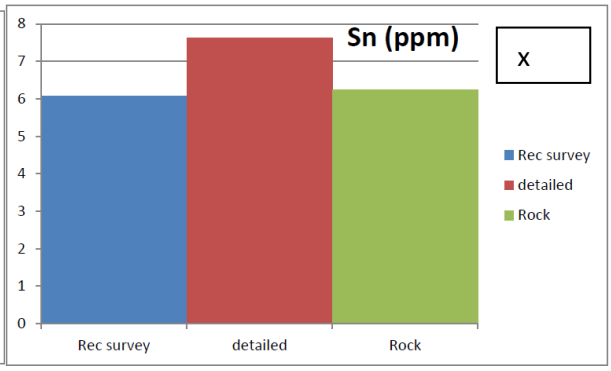

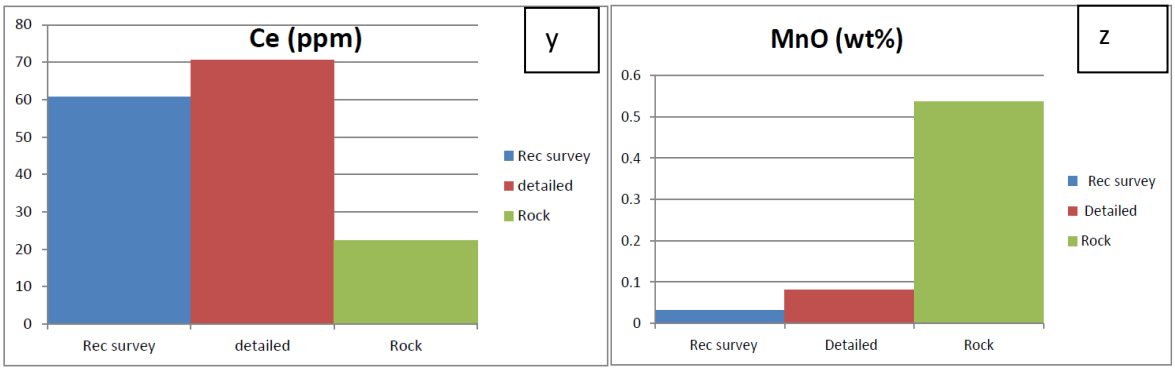

Figure 5.1 a-z: Comparison between the individual elements in all the three datasets.

CHAPTER SIX

CONCLUSION AND RECOMMENDATIONS

6.1 Conclusion

These conclusions is based on what has been discussed in chapter five with respect to the petrography of rocks, whole rock and soil geochemistry. From this research, there is a linkage between the rock types and their respective soil samples, the following conclusions can be drawn from the discussion;

The biotite schist, diorite and their respective soils in the study area show some disparities in their concentrations. Both soils indicated high Al_2O_3 concentrations than in the rocks which may be attributed tosignificant weathering that has masked the ideal characteristics the soil. However, high concentrations of As, Ga, Zr, Cr, Sn, in the soil and also high Zn, Ni and Cu in the rock indicates hydrothermal source. Soils overlying the diorite have undergone some amount of leaching resulting in the low concentrations of CaO, MgO, Cr, Ni, Cu and Ba in the soil compared to the rock.

The unexpected high contents of MgO and Fe_2O_3 in the soils overlying the granodioriteindicate the existence of mafic bodies within the study area or the transportation of mafic to this area. High concentrations of certain minor elements in the soils such as;Cr, V, Cu, Ga, Ge, As, Zr, Nb, Sn, Zn, Ba, Ce, Ni, and Co can be attributed to the presence of garnet, sphene, pyrite and probably, some degree of hydrothermal alteration or transportation from other sources and significant weathering. The granitic soils in the study area have also experienced some amount of mafic contributions. The granite has also undergone hydrothermal alteration.

6.2 Recommendations

Deep sampling methods such as drilling programs to investigate the subsurface occurance of the various rock types may be helpful.

Secondly, detailed geological (and exploration) mapping should be carried out in the study area to comprehensively study the mineralization potential, since there are some abundant small scale mining sites in the study area.

REFERENCES

Abouchami, W., Boher M., Michard A. and Albarede F. (1990). A major 2.1 Ga events of magmatism in West Africa: an early stage of crustal accretion. Journal of Research, 95 (B11), 17605-17629.

Anan-Yorke, R. (1980).A new classification proposal for the Voltaian Basin sediments.Ghana: Geological Survey Ann. Rep.

Asiedu, D.K., Dampare, S.B., Sakyi, A.P., Banoeng-Yakubo, B., Osae, S., Nyarko B.J.B. and Manu J. (2003) Geochemistry of Paleoproterozoic metasedimentary rocks from the Birim diamondiferous field, southern Ghana: Implications for provenance and crustal evolution at the Archean-Proterozoic boundary.Geochemical Journal, 38: 215- 228.

Bailey, T.C. and Gatrell, A.C. (1995).Interactive spatial data analysis.Longman Scientific & Technical, Harlow, 413.

Bates, D.A. (1955). Geological map of Ghana: Ghana Geological Survey Department, scale 1:1,000,000. Reprinted by the Geological Survey Department in 1966.

Boher, M., Abouchami, W., Albarede, F. and Arndt, N. T. (1992).Crustal growth in West Africa at 2.1 Ga. Journal of Geophysical Research. 97(B1), 345-369.

Breakey, A., and Breakey, E. (1977). The geology of ¼° field sheets 0603A3 (117), Goaso S.W. and 0603A4 (118), Goaso S.E.: Ghana Geological Survey Department and Minerals Commission Archive Report No. 42, Accra, 86 pp.

Cahen, L., Snelling, N.J., Delhal, J. and Vail, J.R. (1984).The Geochronology and Evolution of Africa. New York: Oxford University Press.

Dickson, K.B. and Benneh, G. (1995).A New Geography of Ghana.Revised Edition.Longman, England, UK, 170 pp.

Eisenlohr, B.N. and Hirdes, W. (1992). The structural development of the early Proterozoic Birimian and Tarkwaian rocks of southwest Ghana. West Africa Journal of African Earth Sciences 14: 313-325.

Field, A. P. (2009). Discovering Statistics Using SPSS (And Sex And Drugs And Rock' N' Roll) (3rd Ed.).London: Sage.

Garrett, R.G. (1991). The management, analysis and display of exploration geochemical Exploration (2nd ed.). Academic Press, London.

Goldschmidt, V. M. (1954). Geochemistry.Oxford University Press-. 924.

Hirdes, W. and Nunoo, B. (1994). The proterozoic paleoplacers at Tarkwa Gold Mine, SW Ghana: sedimentology, mineralogy, and precise age dating of the main reef and west reef, and bearing of the investigations on source area aspects. Geologisches Jahrbuch D 100, 247–311.

Hirdes, W., Davis, D. W. and Eisenlohr, B. N. (1992). Reassessment of Proterozoic granitoid ages in Ghana on the basis of U/Pb zircon and monazite dating. Precambrian Res. 56, 89–96.

Hirdes, W.,and Davis, D.W. (1998). First U–Pb zircon age of extrusive volcanism in the Birimian Supergroup of Ghana West Africa. Journal of African Earth Sciences 27(2), 291–294.

Junner, N.R. (1935). Gold in the Gold Coast: Gold Coast Geological Survey Memoir No. 4, Accra, 67 pp.

Junner, N.R. (1940). Geology of the Gold Coast and Western Togoland. Gold Coast Geological Survey, Memoir No. 11: 40.

Kesse, G.O. (1985). The Mineral and Rock Resources of Ghana. A.A. Balkema. Precambrian Research 46, 139–165

Kesse, G.O. (1995). The mineral and rock resources of Ghana, Bal kema, Rotterdam, 610 pp.Lawrence, L.M. Supergene Ore Deposit Geochemistry. 17th International Geochemical Exploration Symposium, Short Course, Townsville, 64.

Lawrence, L.M. (1995) Supergene Ore Deposit Geochemistry. 17th International Geochemical Exploration Symposium, Short Course, Townsville, 64 pp.

Leube, A., and Hirdes, W. (1986). The Birimian Supergroup Of Ghana, Depositional Environment, Structural Development And Conceptual Model Of An Early Proterozoic Suite: BGR Archive Report No. 99529, Hannover, 259 p. (unpublished).

Leube, A., Hirdes, W., Mauer, R. and Kesse, G. O. (1990). The Early Proterozoic Birimian Supergroup of Ghana And Some Aspects Of Its Associated Gold Mineralization. Precambrian Res. 46, 139–165.

Levinson, A.A. (1980). Introduction to Exploration Geochemistry.2nd Ed.Applied publishing Ltd, Illinois, 924pp.

Loh, G., Hirdes, W., Anani, C., Davis, D.W. and Vetter, U. (1999). Explanatory Notes for the Geological Map of Southwest Ghana 1: 100,000. Geologisches Jahrbuch B 93, 150.

Matthews, R.N., and Milnes, P.T. (1979). The Geology of ¼° Field Sheets 121 (06031B3) and 123 (06031B1), Kukuom S.W. and N.W.: Ghana Geological

Survey Department and Minerals Commission Archive Report No. 76, Accra, 112 pp.

Mazzullo, S.J., Anderson-Underwood, K.E., Burke, C.D. and Bischoff, W.D. (1992). Holocene coral patch reef ecology and sedimentary architecture, northern Belize, Central America. Palaois, 7, 591–601 pp.

Mielke, J.E. (1979). Compostion of the Earth's Crust and distribution of the elements.13-37. In Review of research on modern problems in geochemistry Siegel, F.R. (Ed.). International Association for Geochemistry and Cosmo chemistry Earth Science Series No 16, Paris, UNESCO.

Moon, P.A. and Mason, D. (1967). Geological Survey, Bulletin No. 31

Murray, R.J. (1960). The Geology Of The "Zuarungu" 1/2° Field Sheet: Ghana Geological Survey Department Bulletin No.25, Accra, 118 pp.

Nude, P.M., Asigri, J.M., Yidana S.M., Arhin, E., Foli G., and Kutu, M.J. (2012).Identifying Pathfinder Elements for Gold in Multi-Element Soil Geochemical Data from the Wa-Lawra Belt, Northwest Ghana: A multivariate Statistical Approach.International Journal of Geosciences. 3, 62-70.

Nyame, F.K..(1998). Mineralogy, Geochemistry and Genesis of the Nsuta Manganese Deposit, Ghana.Unpublished Ph.D. thesis. Okayama University, Japan.

Nyarko, E.S., Osea, S., Dampare, S., Zakaria, N., Hanson, J., Osei J., Enti-Brown, S. and Tulasi D. (2012). Geochemical characteristics of the basin-type granitoids in the Winneba area of Ghana.Proceedings of the International Academy of Ecology and Environmental Studies. 2 (3): 177-192.

Oberthur, T., Vetter, U., Mumm, A.S., Weiser, T.,Amanor, J.A., Gyapong, W., Kumi, R. and Blenkinsop, T.G. (1994). The Ashanti gold deposit at Obuasi: Mineralogical, geochemical, stable isotope and fluid inclusion studies on the metallogenesis of the deposit. In Metallogenesis of Selected Gold Deposits in Africa (T. Oberthur, ed.). Geologisches Jahrbuch Reihe, 100, 31 - 131.

Oberthür, Thomas, (ed.), (1994). Metallogenesis of Selected Gold Deposits in Africa: Hannover, Geologisches Jahrbuch Reihe D, Heft 100, 679 pp.

Owusu, E.A., Dzigbodi-Adjimah K and Matheis, G. (2003).Integration of spatial and non-spatial information for the interpretation of soil geochemical patterns.Journal of science and technology, 23(2).

Paterson, S.R., Vernon, R.H., and Tobisch, O.T. (1989). A Review Of Criteria For The Identification Of Magmatic And Tectonic Foliation In Granitoids: Journal Of Structural Geology V. 11, P. 349-363.

Pigois, J.-P.,Groves, D.I., FIetcher, I.R., McNaughton N.J and Snee, L.W. (2003). Age constraints on Tarkwaian palaeoplacer and lode-gold formation in the Tarkwa-Damang district, SW Ghana. Mineralium Deposita, 38(6), 695-714

Reimann, C., Kashulina, G., de Caritat, P. and Niskavaara, H. (2001). Multi-element, multi-medium regional geochemistry in the European Arctic: element concentration, variation and correlation. Applied Geochemistry, 16: 759-780.

Reimann, C.and Filzmoser, P. (2000). Normal and lognormal data distribution in geochemistry: death of a myth. Consequences for the statistical treatment of geochemical and environmental data. Environmental Geology, 39: 1001-1014.

Rose, A.W., Hawkes, H.E., and Webb, J.S. (1991). Geochemistry in Mineral Exploration. 2 nd. Edition, Academic Press, London, 657 pp

Taylor, P.N., Moorbath, S., Leube, A. and Hirdes, W. (1992).Early Proterozoic crustal evolution in the Birimian of Ghana, Constraints from geochronology and isotope geochemistry.Precamb.Res., 56, 97-111pp.

Taylor, P.N., Moorbath, S., Leube, A., and Hirdes, W. (1988). Geochronology And Crustal Evolution Of Early Proterozoic Granite-Greenstone Terrains In Ghana, West Africa: *in* International Conference and Workshop on the Geology of Ghana with Special Emphasis on Gold: Programme and Abstracts, Accra, pp. 43-45.

Taylor, S.R. (1964). Abundance of Chemical Elements in the Continental Crust: A New Table. Geochim.Acta, 28, 1273 – 1285 pp.

Templ, M., Filzmoser, P., Reimann, C. (2008). Cluster Analysis Applied ToRegional Geochemical Data: Problems And Possibilities. ApplGeochem 23(8):2198–2213 pp.

Vernon, R. H. and Flood, R. H. (1988).Contrasting deformation of Sand 1-type granitoids in the Lachlan fold belt, Eastern Australia.Tectonophysics 147,127-143.

Wright, J. B. (1985). Geology and Mineral Deposits of West Africa: Allen and Unwin, London, 189 pp.

Zitzmann, A., Kiessling, R., and Loh, G. (1993). New results from the Birimian and Tarkwaian ofthe Bui-Belt area in West Ghana: *in* Peters, J.W., Kesse, G.O., and Acquqh, P.C. (eds.),Proceedings of the 9th International Geological Conference, Accra, 2nd to 7th November, 1993, Geological Society of Africa and Geological Society of Ghana publication, pp. 409-417.

Appendix A: Table 1. Summary statistics for soils overlying biotite schist

	N	Mean	Median	Std. Deviation	Skewness	Kurtosis	Minimum	Maximum
SiO2	4	51.47	50.33	4.42	1.39	2.52	47.45	57.77
TiO2	4	1.05	1.06	0.09	-0.90	1.93	0.92	1.14
Al2O3	4	34.79	35.44	4.03	-0.64	-1.79	29.69	38.57
Fe2O3	4	7.97	8.48	1.44	-1.72	3.09	5.87	9.06
MgO	4	2.41	2.29	0.97	0.37	-3.47	1.50	3.56
CaO	4	0.32	0.29	0.25	0.64	0.16	0.06	0.64
Na2O	4	1.17	1.25	0.16	-1.98	3.93	0.93	1.26
K2O	4	1.07	1.00	0.15	1.84	3.39	0.97	1.29
SO3	4	0.08	0.07	0.03	1.82	3.36	0.06	0.12
MnO	4	0.10	0.10	0.06	0.54	0.35	0.03	0.19
P2O5	4	0.11	0.11	0.02	-1.09	1.11	0.07	0.13
Cr	4	322.50	355.00	151.87	-1.17	1.98	111.00	469.00
Ni	4	60.05	70.25	26.21	-1.75	3.06	21.60	78.10
Cu	4	25.10	29.10	9.22	-1.89	3.60	11.40	30.80
Zn	4	50.70	53.15	7.54	-1.59	2.63	39.80	56.70
Ga	4	23.33	24.55	2.77	-1.93	3.76	19.20	25.00
Ge	4	2.03	2.15	0.43	-1.50	2.65	1.40	2.40
As	4	6.35	4.95	4.39	1.34	1.17	3.00	12.50
Rb	4	74.00	79.85	24.97	-1.11	0.74	39.80	96.50
Sr	4	38.88	31.90	16.75	1.91	3.70	27.90	63.80
Zr	4	525.75	494.00	164.59	1.08	1.91	362.00	753.00
Nb	4	21.90	23.55	6.44	-0.85	-1.32	13.50	27.00
Sn	4	10.98	8.05	7.08	1.89	3.62	6.30	21.50
Ba	4	292.30	291.60	41.09	0.07	-2.61	247.00	339.00
Ce	4	81.00	85.50	20.58	-1.05	0.63	53.00	100.00
Br	4	7.15	7.70	3.99	-0.30	-4.26	2.60	10.60
I	4	31.43	30.60	11.33	0.42	1.26	18.50	46.00

Appendix A: Table 2. Summary statistics for soils overlying diorite

	N Valid	Mean	Median	Std. Dev	Skewness	Kurtosis	Minimum	Maximum
SiO2	5	56.26	53.98	14.46	1.77	3.44	44.54	81.01
TiO2	5	1.12	1.07	0.21	1.66	3.51	0.92	1.48
Al2O3	5	30.82	34.18	10.23	-2.13	4.63	12.70	37.39
Fe2O3	5	7.53	9.06	3.60	-1.43	2.05	1.64	10.86
MgO	5	2.21	1.83	1.12	0.44	-2.89	1.19	3.56
CaO	5	0.46	0.43	0.34	0.35	-0.89	0.06	0.92
Na2O	4	1.13	1.16	0.16	-0.48	-3.32	0.94	1.26
K2O	5	1.05	0.97	0.25	0.31	-2.44	0.78	1.35
SO3	5	0.08	0.08	0.02	-0.18	-1.23	0.05	0.10
MnO	5	0.11	0.08	0.07	0.66	0.47	0.03	0.20
P2O5	5	0.11	0.13	0.06	-1.64	2.82	0.02	0.16
Cr	5	390.60	336.00	136.96	2.00	4.08	301.00	630.00
Ni	5	51.38	68.80	29.56	-0.74	-2.36	11.70	75.20
Cu	5	23.80	30.30	14.62	-1.05	0.00	1.50	37.40
Zn	5	53.40	50.70	8.46	0.76	0.58	43.70	66.10
Ga	5	21.08	23.70	6.82	-1.65	2.77	9.60	26.70
Ge	5	1.76	1.70	0.60	0.01	-1.48	1.00	2.50
As	5	6.38	5.80	4.60	1.72	3.19	3.00	14.20
Rb	5	65.06	55.80	43.78	1.36	1.95	24.70	136.40
Sr	5	43.50	32.40	24.39	0.37	-2.15	16.00	74.10
Zr	5	542.80	434.00	327.79	1.40	2.04	236.00	1079.00
Nb	5	17.58	17.40	2.84	-0.46	-0.10	13.50	20.90
Sn	4	9.73	9.30	1.74	1.12	0.55	8.20	12.10
Ba	5	273.82	272.40	100.19	-0.11	-0.99	142.30	398.00
Ce	4	93.50	100.00	25.62	-1.39	2.62	57.00	117.00
Br	4	7.90	7.75	4.23	0.10	-4.25	3.60	12.50
I	4	33.60	34.60	9.32	-0.33	-3.52	22.70	42.50

Appendix A: Table 3. Summary statistics for soils overlying granodiorite

	N Valid	Mean	Median	Std. Deviation	Skewness	Kurtosis	Minimum	Maximum
SiO2	5	49.26	49.96	3.45	-0.23	-0.13	44.54	53.67
TiO2	5	1.09	1.07	0.14	1.06	2.52	0.92	1.32
Al2O3	5	35.46	37.39	3.62	-1.31	1.01	29.69	38.57
Fe2O3	5	8.32	8.66	1.20	-1.70	3.07	6.28	9.30
MgO	5	2.58	2.87	0.91	-0.32	-2.79	1.54	3.56
CaO	5	0.46	0.36	0.32	0.81	-0.86	0.16	0.92
Na2O	5	1.07	0.98	0.16	0.56	-3.22	0.93	1.26
K2O	5	1.07	0.97	0.24	0.14	-2.10	0.78	1.35
SO3	5	0.08	0.07	0.03	1.37	1.58	0.06	0.12
MnO	5	0.12	0.12	0.05	0.83	0.16	0.07	0.19
P2O5	5	0.12	0.12	0.03	0.40	0.28	0.09	0.16
Cr	5	344.40	334.00	86.93	0.34	0.70	233.00	469.00
Ni	5	66.12	68.80	13.78	-1.52	2.53	43.20	78.10
Cu	5	28.52	30.30	4.72	-1.49	2.44	20.70	32.90
Zn	5	52.80	54.50	11.36	-0.94	2.06	34.90	66.10
Ga	5	24.86	24.80	1.18	0.90	1.65	23.50	26.70
Ge	5	2.12	2.20	0.43	-1.52	2.57	1.40	2.50
As	5	6.54	5.90	3.88	0.99	0.39	3.00	12.50
Rb	5	85.28	87.80	37.33	-0.03	0.95	33.80	136.40
Sr	5	45.04	33.00	22.41	0.61	-2.47	23.50	74.10
Zr	5	454.00	474.00	167.99	0.11	0.07	236.00	684.00
Nb	5	21.48	20.20	6.59	0.10	-2.02	13.50	29.30
Sn	5	11.38	8.70	5.99	1.71	2.79	7.20	21.50
Ba	5	290.48	312.00	92.53	-0.59	-0.05	156.40	398.00
Ce	5	90.40	92.00	24.85	0.00	0.35	57.00	124.00
Br	5	8.38	10.40	3.94	-0.50	-2.45	3.40	12.50
I	5	34.72	32.10	8.15	0.62	-1.45	26.30	46.00

Appendix A: Table 4. Summary statistics for soils overlying granite

	N	Mean	Median	Skewness	Kurtosis	Minimum	Maximum
SiO2	5	53.84	57.35	-0.75	-1.48	44.54	60.36
TiO2	5	0.79	0.66	0.27	-2.66	0.46	1.10
Al2O3	5	26.07	23.45	0.34	-2.97	17.80	35.01
Fe2O3	5	5.90	3.30	0.77	-1.95	1.78	12.23
MgO	5	1.71	1.45	2.11	4.55	1.15	3.24
CaO	5	0.27	0.15	2.09	4.47	0.04	0.92
Na2O	5	0.73	0.65	-0.10	-1.52	0.41	1.00
K2O	5	0.99	1.03	-0.23	-1.58	0.59	1.35
SO3	5	0.07	0.07	-0.09	1.97	0.06	0.09
MnO	5	0.05	0.03	2.02	4.28	0.01	0.13
P2O5	5	0.08	0.06	1.81	3.23	0.05	0.16
Cr	5	302.70	310.00	-0.75	0.55	79.50	468.00
Ni	5	24.82	13.10	2.03	4.18	9.40	68.80
Cu	5	11.98	7.10	1.65	2.82	1.50	32.90
Zn	5	32.52	25.50	1.95	3.96	18.50	66.10
Ga	5	18.16	17.60	1.30	2.32	12.80	26.70
Ge	5	1.56	1.60	0.58	-0.51	0.90	2.50
As	5	7.32	7.20	0.70	0.78	4.40	11.10
Rb	5	55.72	36.90	1.61	2.47	18.90	136.40
Sr	5	30.30	17.80	1.95	3.84	13.80	74.10
Zr	5	451.80	519.00	-0.90	-0.91	236.00	586.00
Nb	5	15.86	17.40	-0.60	-2.18	10.00	19.70
Sn	5	4.62	3.90	1.50	2.40	1.10	12.10
Ba	5	212.06	122.40	0.74	-2.45	99.90	398.00
Ce	5	45.40	45.00	-0.48	-0.61	24.00	62.00
Br	5	4.64	4.10	1.34	1.85	0.60	12.50
I	5	16.98	11.20	1.96	4.01	7.00	40.10

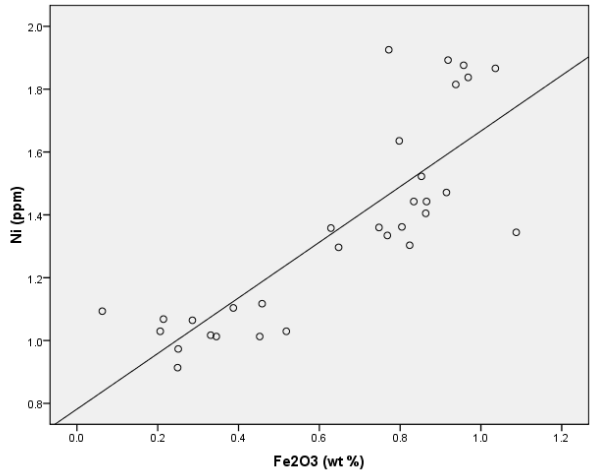

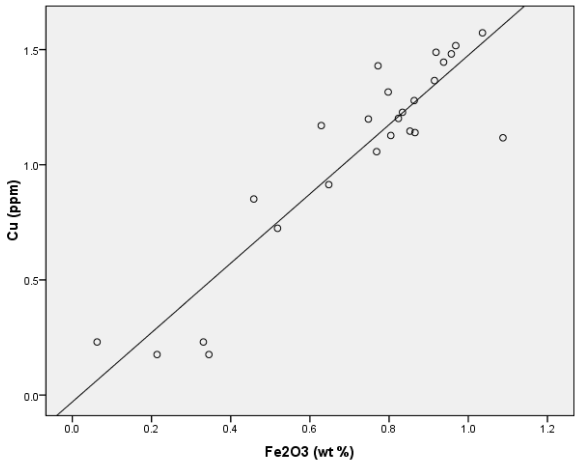

I. Ni - Fe2O3

J. Cu - Fe2O3

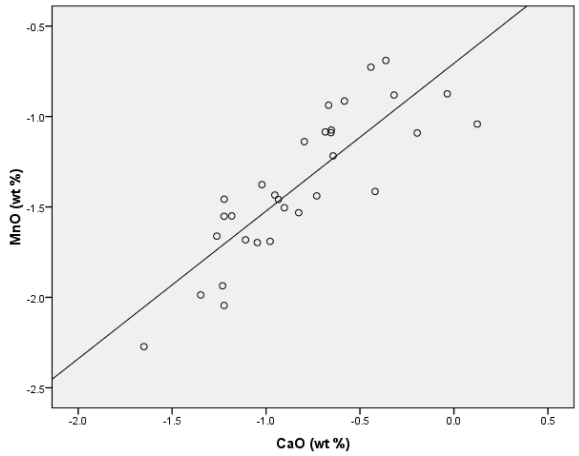

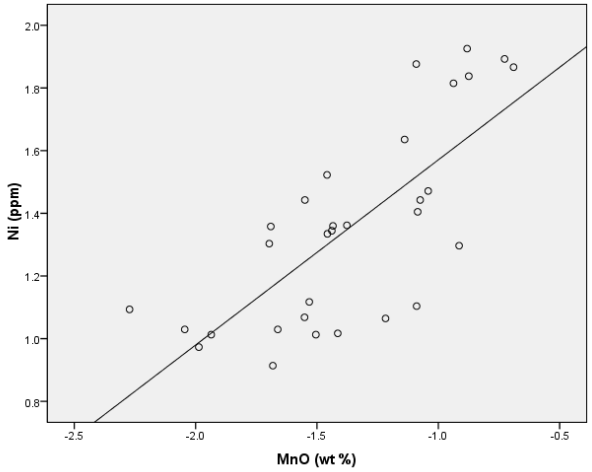

K: MnO-CaO

L: Ni-MnO

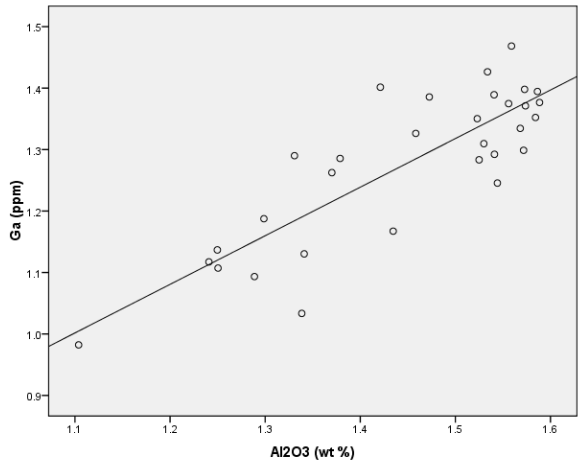

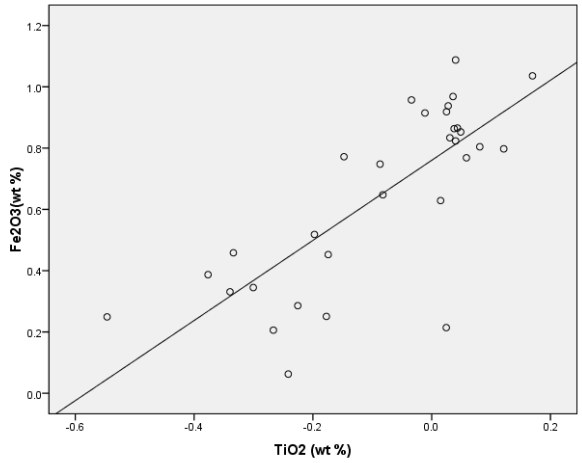

M. Ga- Al2O3

N. FeO3-TiO2

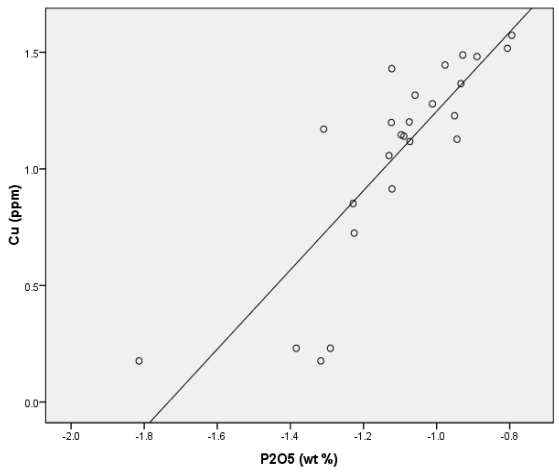

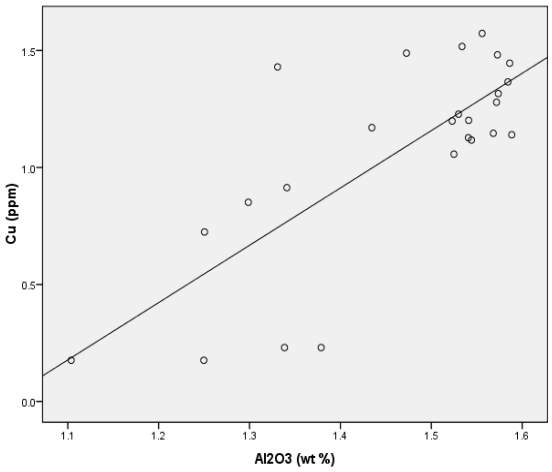

O: Cu-P2O5 P: Cu-Al2O3

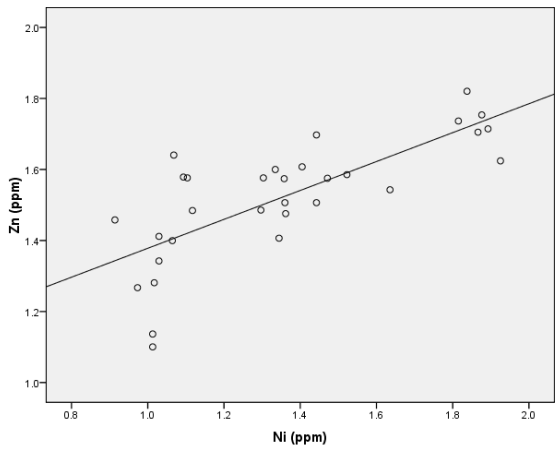

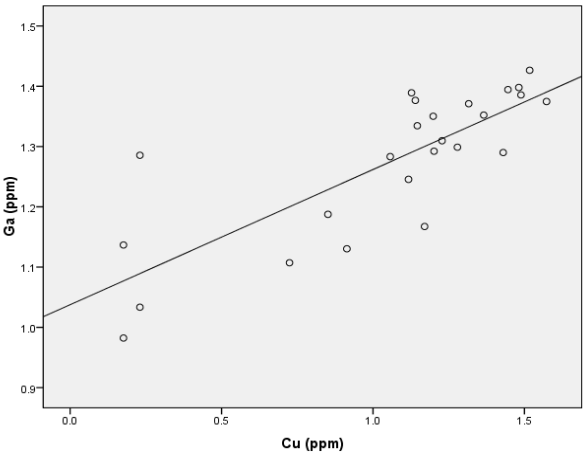

Q: Ba-Sr S: Ga-Cu

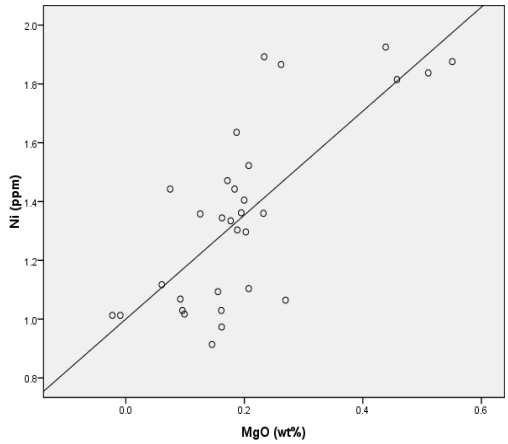

A. Ni-MgO

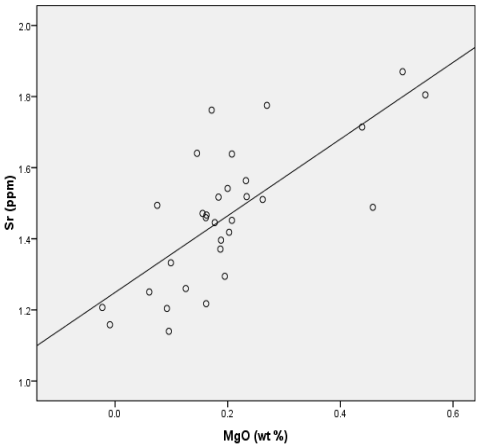

B. Sr- MgO

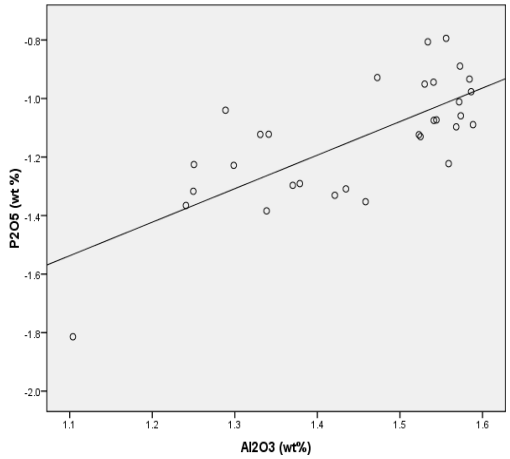

c. P2O5 - Al2O3

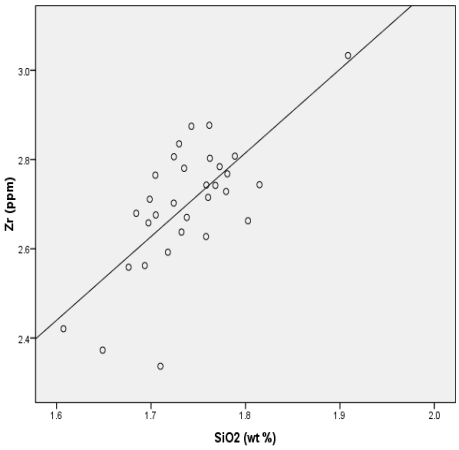

d. Zr-SiO2

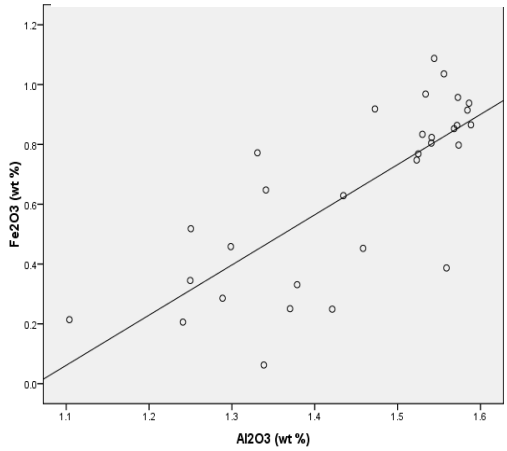

E: Fe2O3- Al2O3

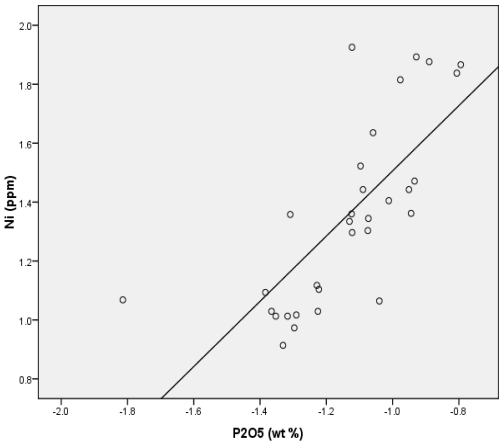

F: Ni –P2O5

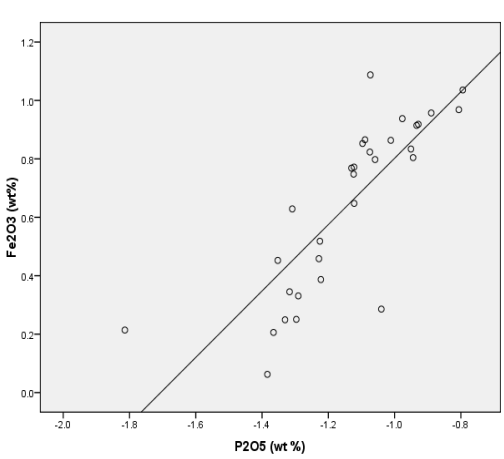

G: Fe2O3 –P2O5

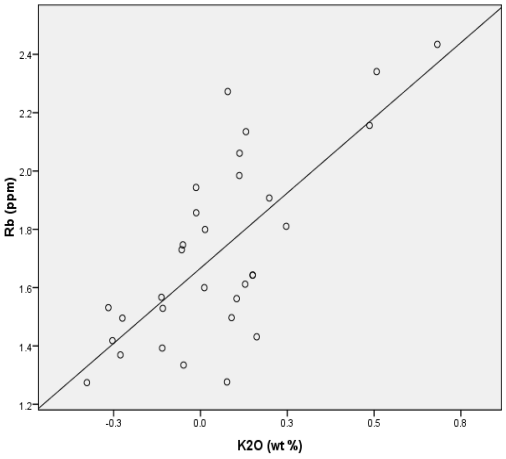

H: K2O-Rb

Appendix A: Figure 4.61. Scatter plots elements with correlations between 0.7 and 0.9

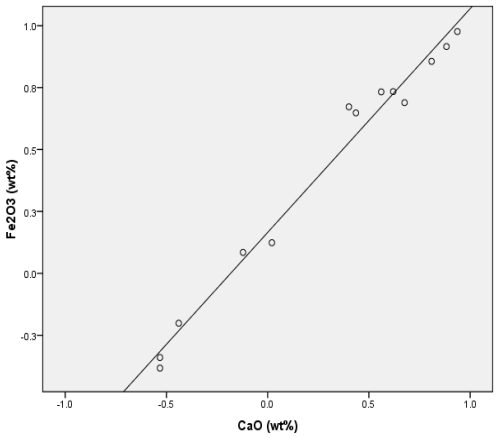

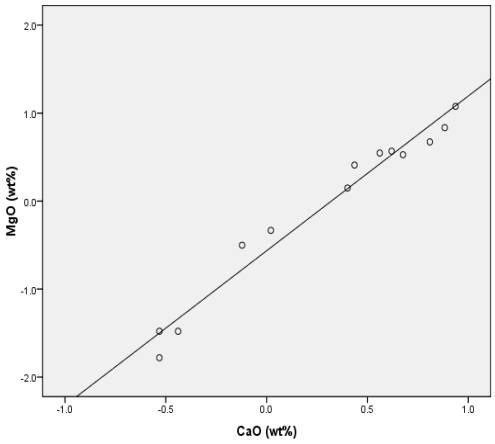

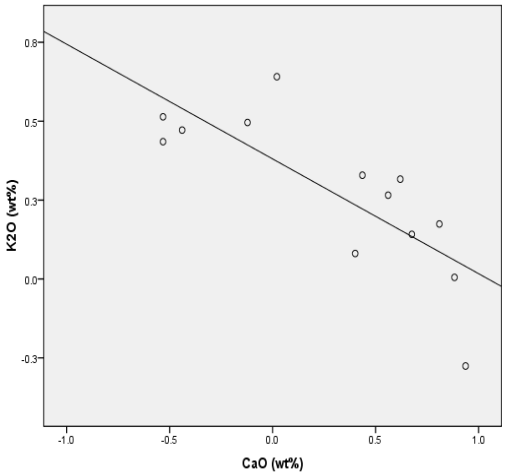

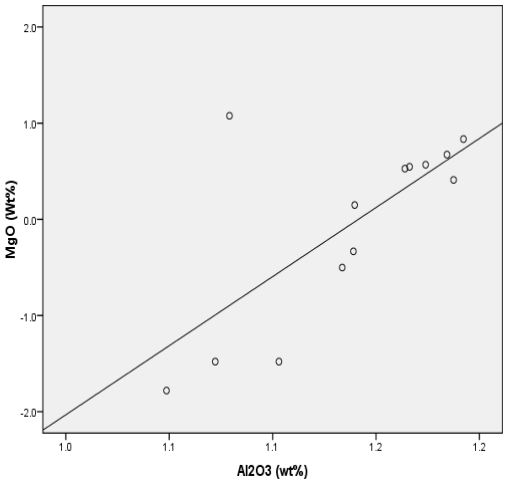

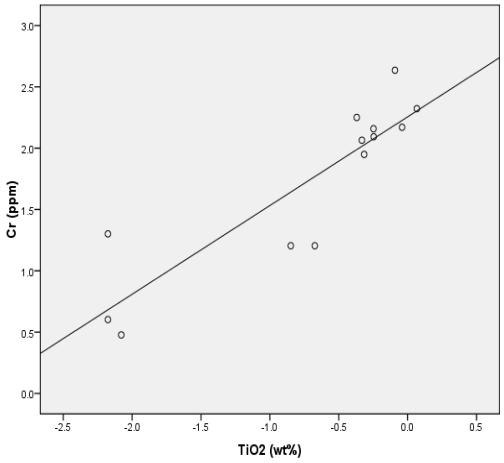

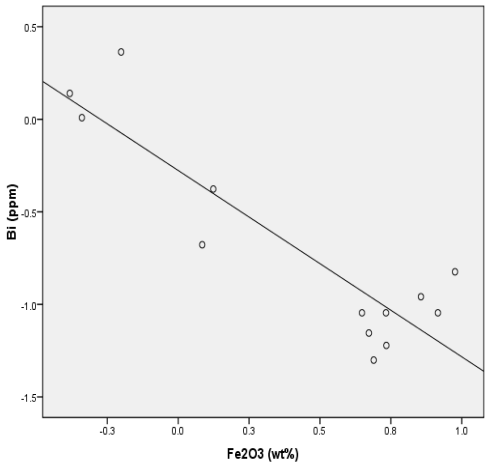

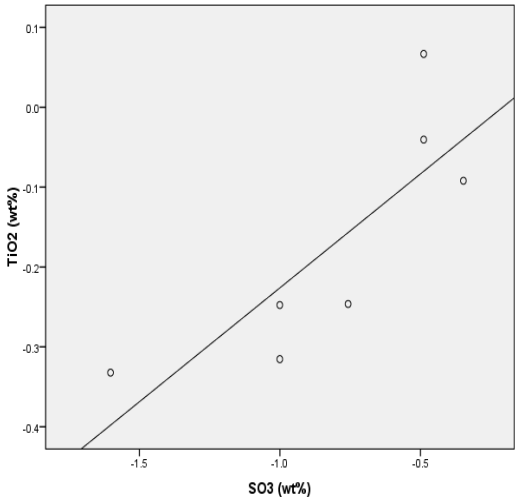

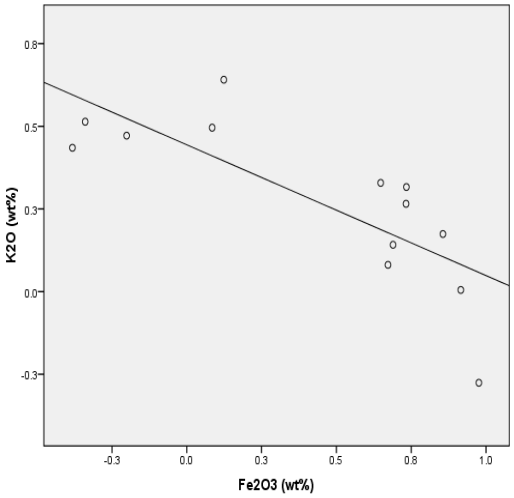

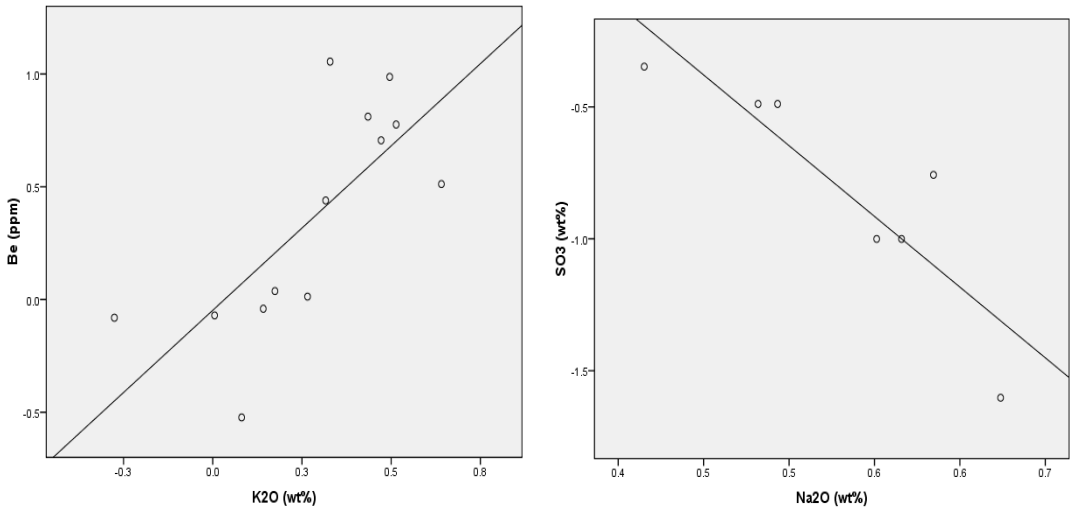

Appendix A: Figure 4.61. Scatter plots elements with correlations between 0.7 and 0.9

Appendix A : Table 5. Comparison of skewness for the detailed soil sample

	Transformed	Raw
Na2O	-1.198	-.351
MgO	1.155	1.928
Al2O3	-.819	-.458
SiO2	.504	1.256
P2O5	-.933	.587
SO3	1.106	1.816
K2O	.821	2.603
CaO	.338	2.569
TiO2	-.818	-.191
MnO	-.266	1.267
Fe2O3	-.408	.333
Cr	-.913	.331
Ni	.513	1.280
Cu	-1.132	.319
Zn	-.714	.304
Ga	-.729	-.285
Ge	-.552	-.031
As	.121	1.030
Br	-.839	1.190
Rb	.636	1.868
Sr	.248	1.144
Zr	-.634	.858
Nb	.081	.784
Sn	-.830	.990
I	-.504	.295
Ba	-.731	-.197
Ce	.408	.833

Appendix A :Table 6. The total variance for detailed soil samples

Component	Initial Eigenvalues			Extraction Sums of Squared Loadings			Rotation Sums of Squared Loadings		
	Total	% of Variance	Cumulative %	Total	% of Variance	Cumulative %	Total	% of Variance	Cumulative %
1	9.965	43.326	43.326	9.965	**43.326**	43.326	5.566	24.201	24.201
2	4.108	17.861	61.187	4.108	**17.861**	61.187	4.657	20.246	44.447
3	2.181	9.485	70.671	2.181	**9.485**	70.671	3.605	15.676	60.123
4	1.490	6.479	77.150	1.490	**6.479**	77.150	3.355	14.588	74.711
5	1.239	5.388	82.538	1.239	**5.388**	82.538	1.800	7.827	82.538
6	.904	3.929	86.468						
7	.650	2.825	89.292						
8	.622	2.706	91.999						
9	.421	1.831	93.830						
10	.287	1.249	95.079						
11	.246	1.071	96.150						
12	.224	.972	97.122						
13	.172	.746	97.868						
14	.138	.599	98.467						
15	.094	.407	98.874						
16	.086	.376	99.250						
17	.062	.270	99.520						
18	.040	.176	99.696						
19	.023	.098	99.794						
20	.019	.080	99.874						
21	.013	.057	99.932						
22	.010	.042	99.974						
23	.006	.026	100.000						

Appendix A: Table 7. Total variance explained by the components

Component	Initial Eigenvalues			Extraction Sums of Squared Loadings			Rotation Sums of Squared Loadings		
	Total	% of Variance	Cumulative %	Total	% of Variance	Cumulative %	Total	% of Variance	Cumulative %
1	8.177	34.070	34.070	8.177	**34.070**	34.070	6.312	26.298	26.298
2	5.145	21.437	55.507	5.145	**21.437**	55.507	5.245	21.856	48.154
3	2.735	11.397	66.903	2.735	**11.397**	66.903	4.038	16.827	64.981
4	2.527	10.527	77.430	2.527	**10.527**	77.430	2.988	12.450	77.430
5	1.200	5.000	82.430						
6	.813	3.386	85.817						
7	.626	2.608	88.424						
8	.514	2.142	90.566						
9	.395	1.647	92.213						
10	.363	1.511	93.724						
11	.310	1.293	95.017						
12	.284	1.184	96.201						
13	.180	.751	96.952						
14	.143	.598	97.549						
15	.132	.548	98.097						
16	.100	.418	98.516						
17	.086	.360	98.876						
18	.073	.302	99.178						
19	.058	.243	99.421						
20	.051	.212	99.633						
21	.034	.142	99.774						
22	.021	.089	99.863						
23	.020	.081	99.945						
24	.013	.055	100.000						

Extraction Method: Principal Component Analysis.

Appendix A

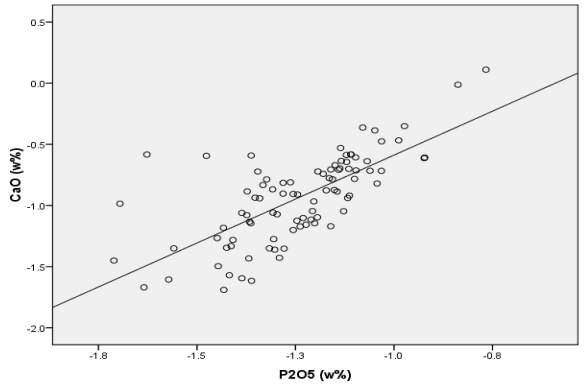

G: P2O5-CaO

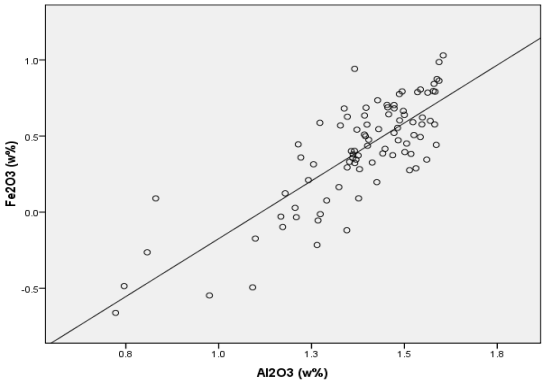

H: Al2O3-Fe2O3

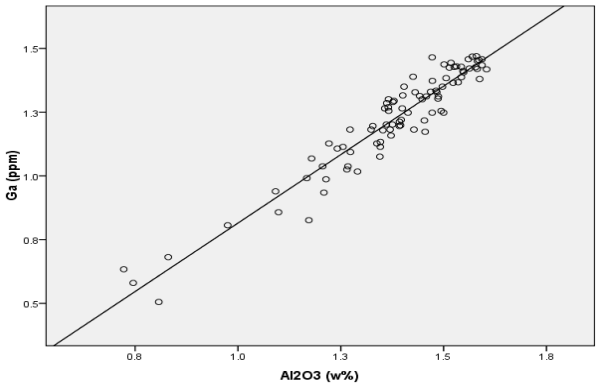

I: Al2O3-Ga

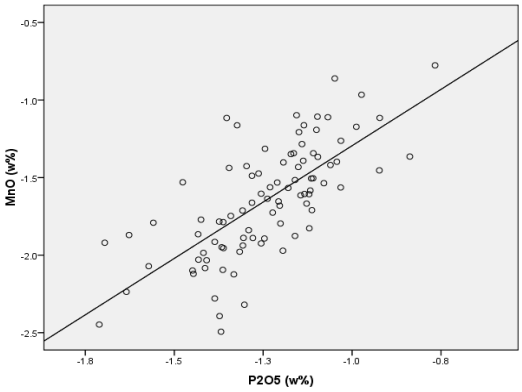

J: P2O5- MnO

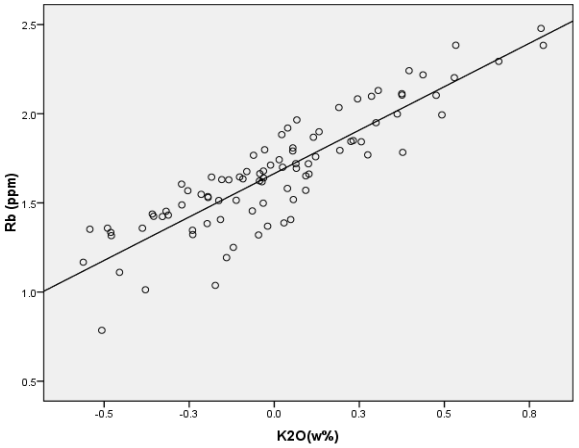

K: K2O-Rb

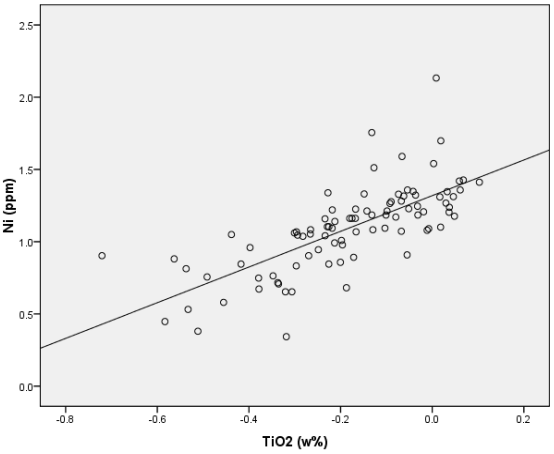

L: Ni -TiO2

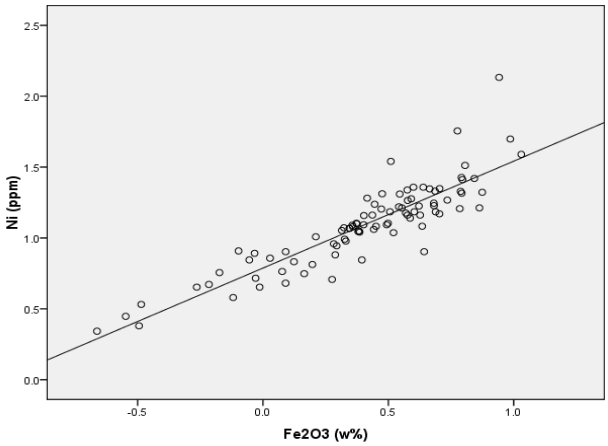

M: Fe2O3- Ni

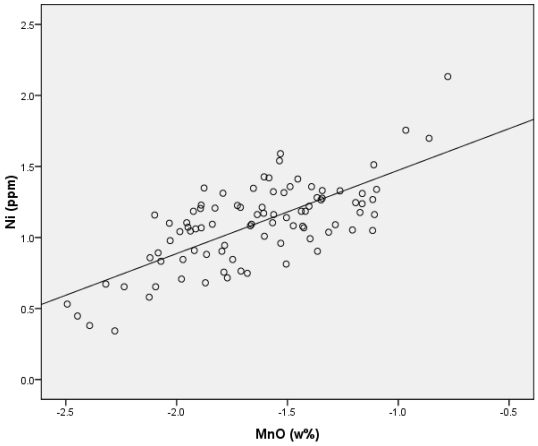

N: MnO -Ni

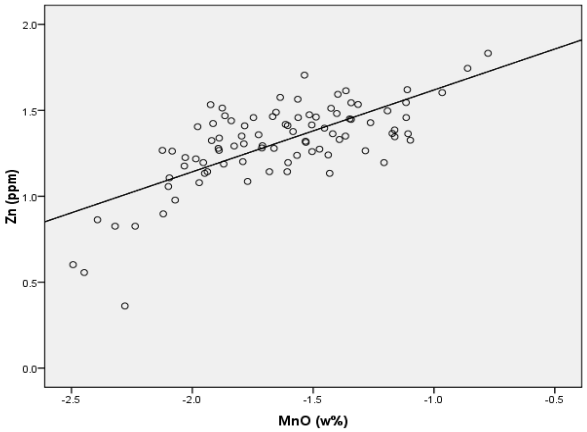

O: MnO-Zn

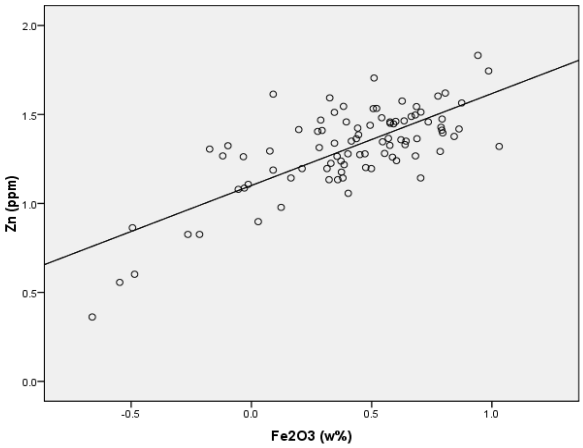

P: Fe2O3-Zn

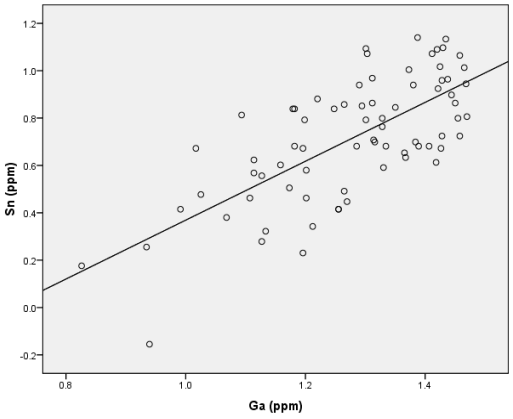

Q: Ga- Sn

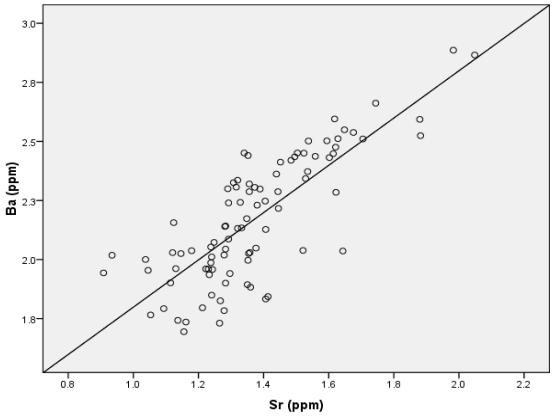

R: Sr-Ba

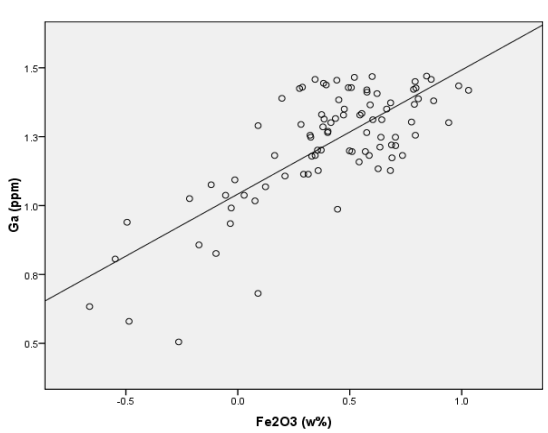

S: Fe2O3-Ga

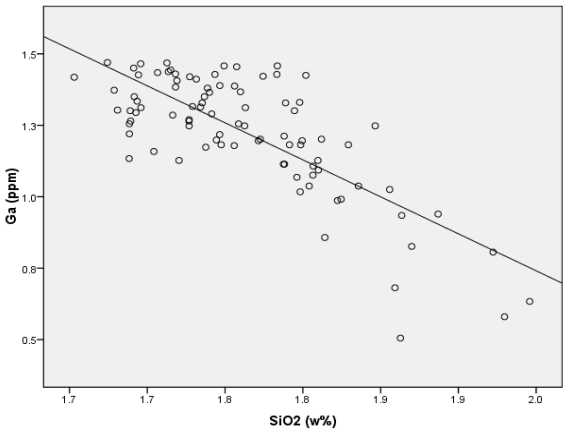

T: SiO2-Ga

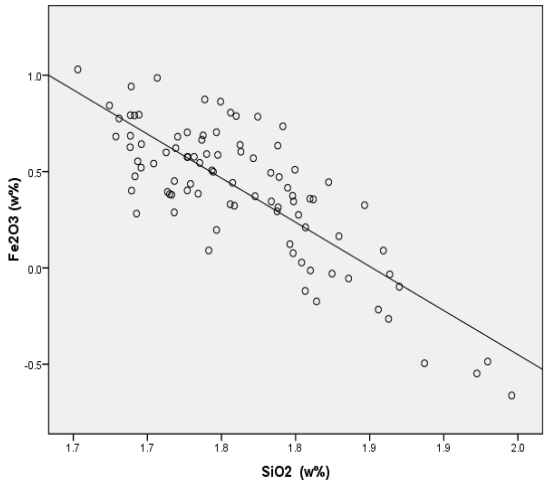

U: SiO2-Fe2O3

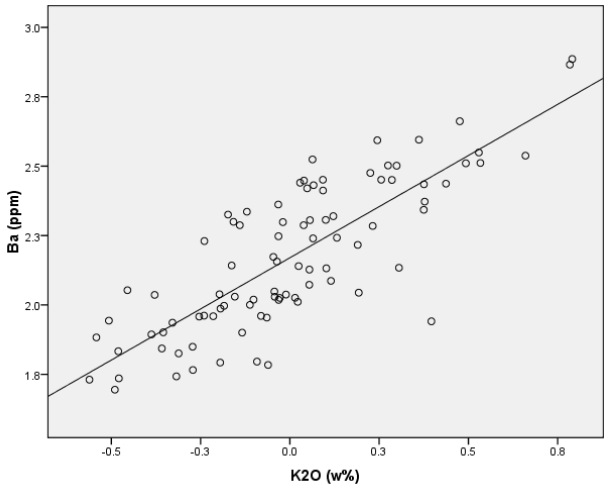

V: K2O- Ba

Appendix A: Figure 2. Scatter plots for the test data (secondary data)

Appendix B Histograms for the primary soil samples

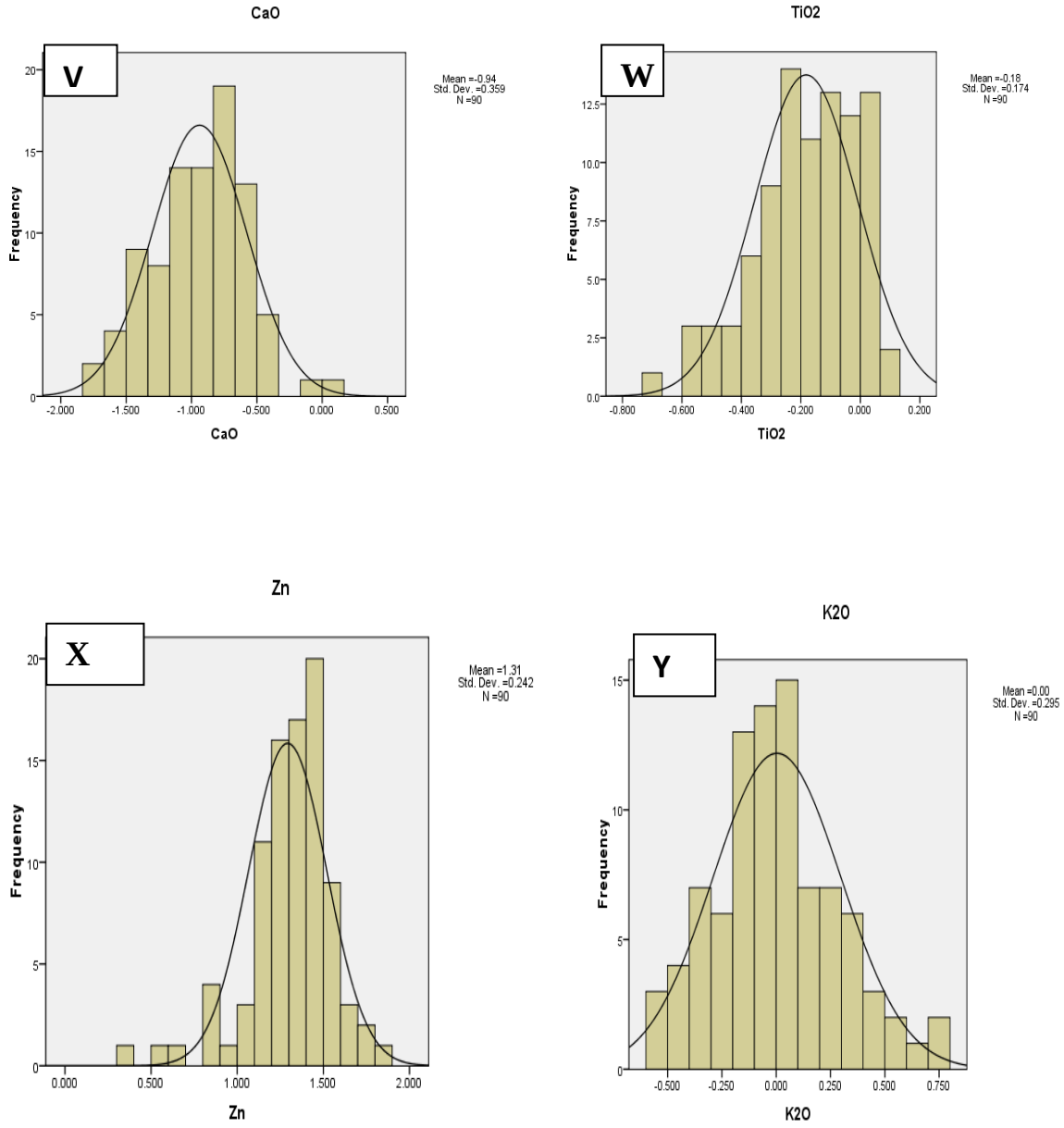

Fig 4.16 Histogram showing element distribution for V (CaO), W (TiO_2), X (Zn), Y (K_2O)

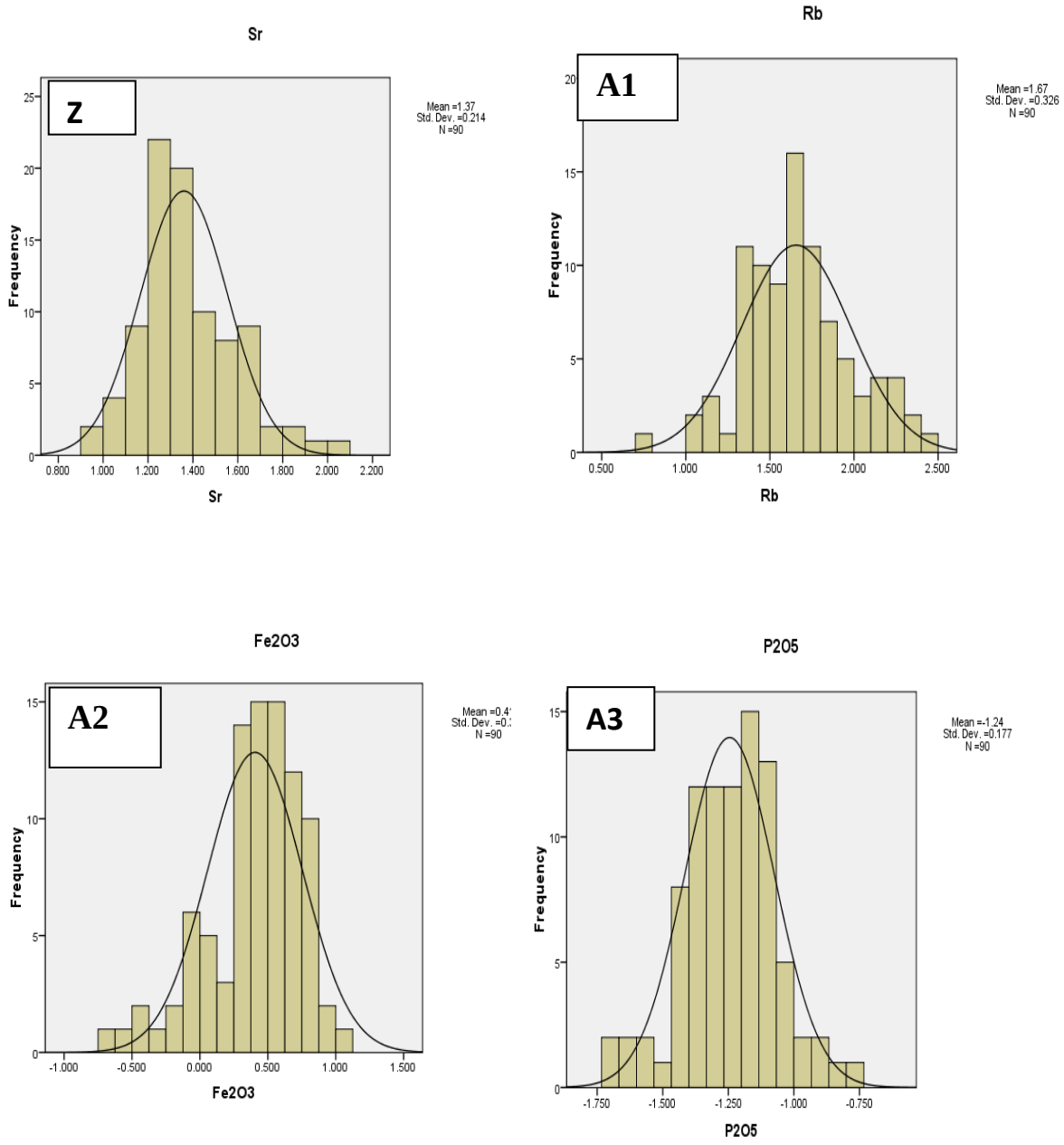

Fig 4.16 Histogram showing element distribution for Z (Sr), A1 (Rb), A2 (Fe_2O_3), A3 (P_2O_5)

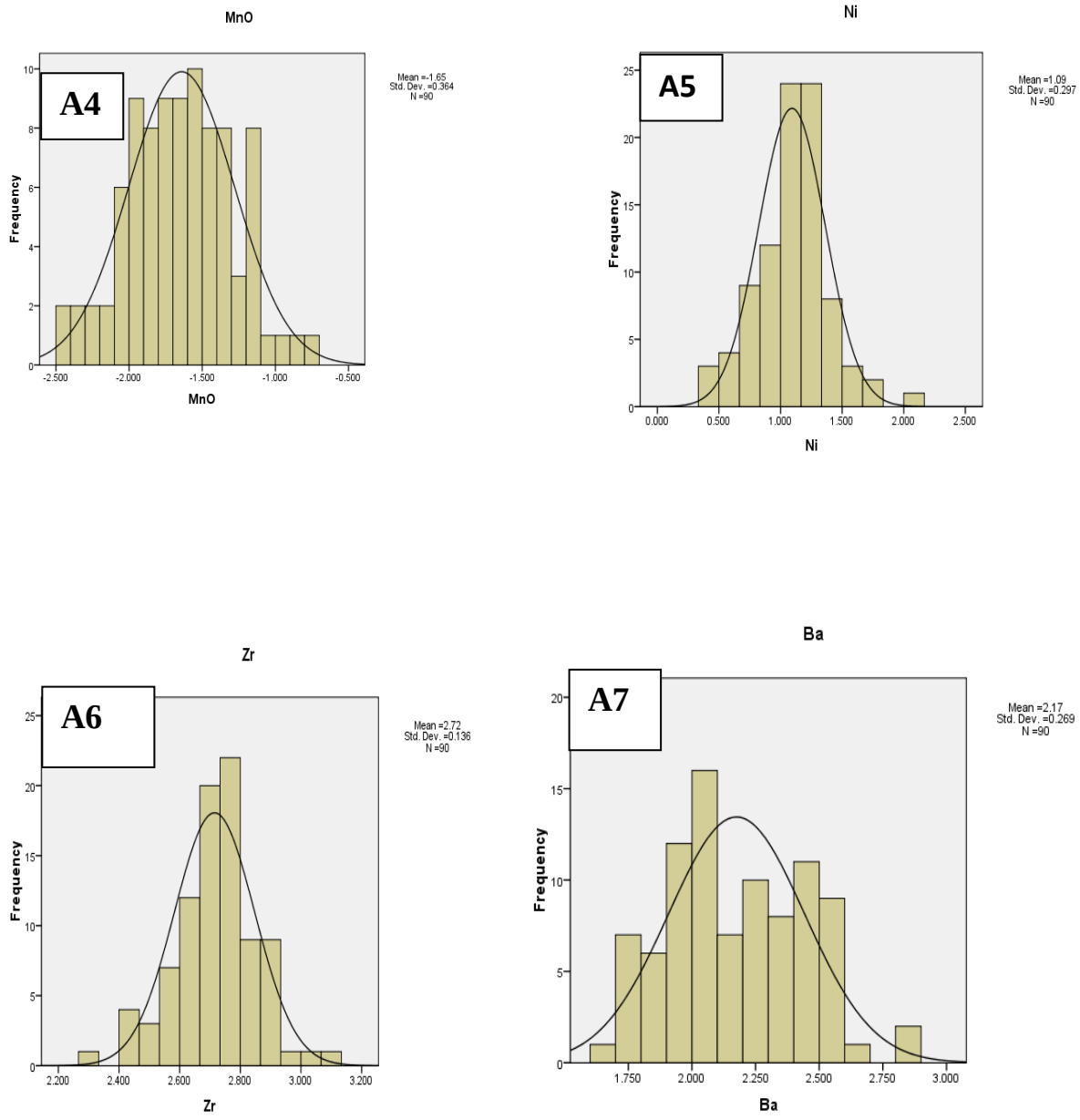

Fig 4.16 Histogram showing element distribution for A4 (MnO), A5 (Ni), A6 (Zr), A7 (Ba)

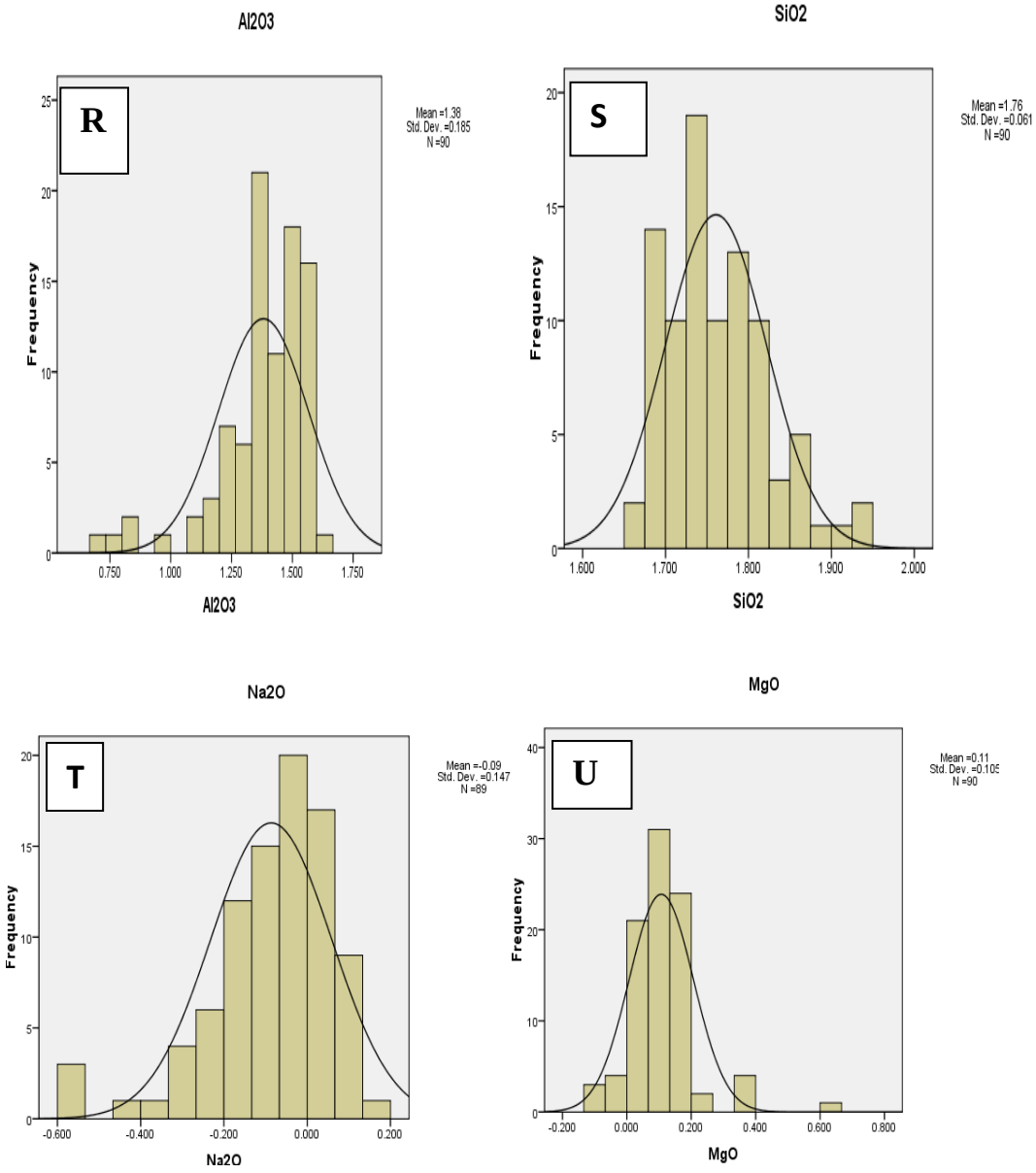

Table 4.8 Comparison between skewness of the raw and transformed values

	Transformed	Raw
Na2O	-1.188	-.144
MgO	1.933	4.533
Al2O3	-1.667	-.404
SiO2	.746	1.145
P2O5	-.222	1.364
SO3	-.079	.513
K2O	.398	2.551
CaO	.045	4.127
TiO2	-.691	.131
MnO	-.041	2.244
Fe2O3	-.938	1.049
Cr	-.624	1.029
Ni	.076	5.317
Cu	-.557	2.199
Zn	-1.291	1.071
Ga	-1.371	-.239
Ge	-.313	.259
As	-1.420	.658
Br	-1.230	.397
Rb	.185	2.183
Sr	.712	2.661
Zr	-.274	1.013
Nb	-.129	.946
Sn	-.638	.659
I	-.181	.766
Ba	.320	2.167
Ce	.145	1.201

Scatter plots for the rock dataset

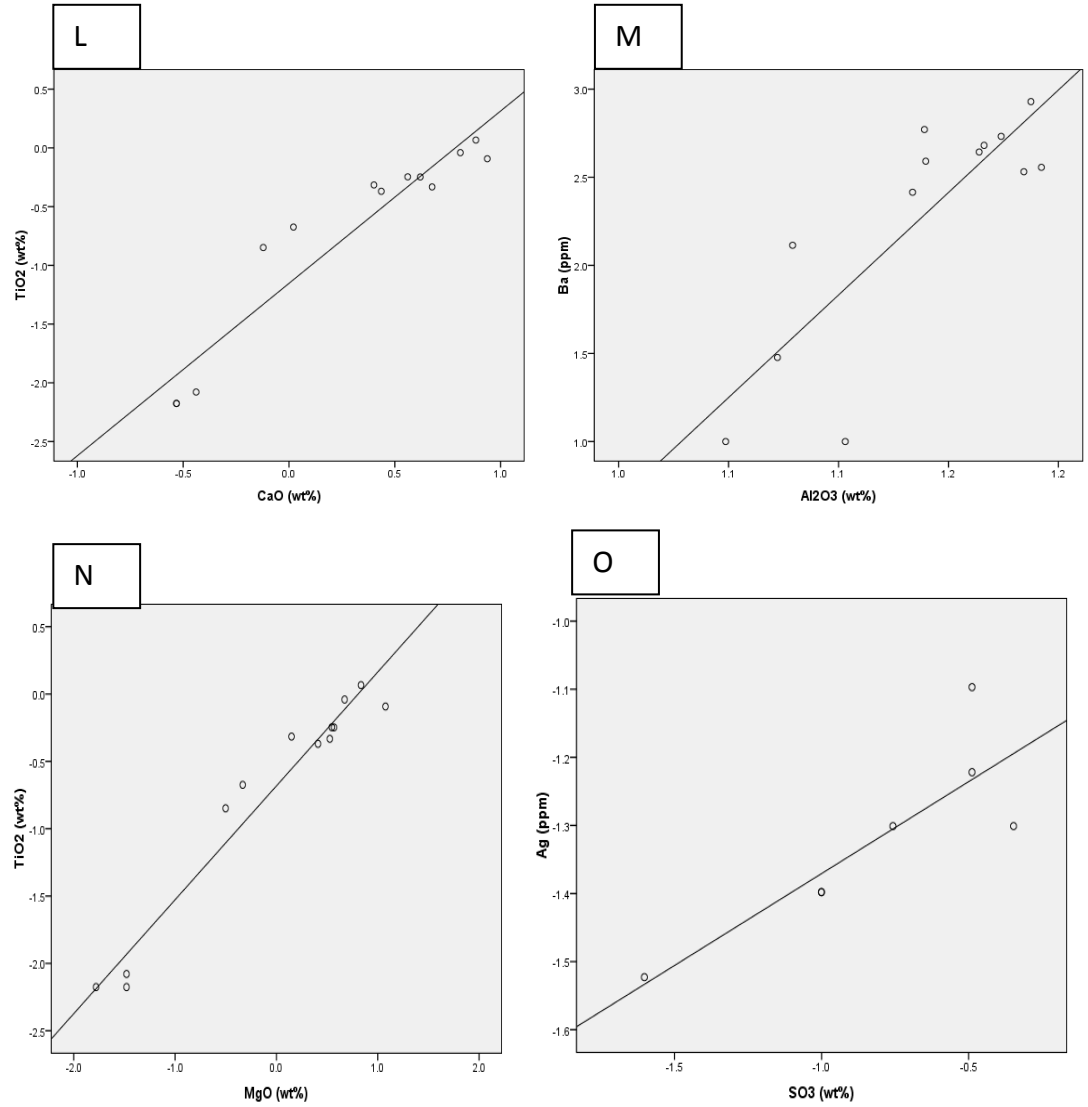

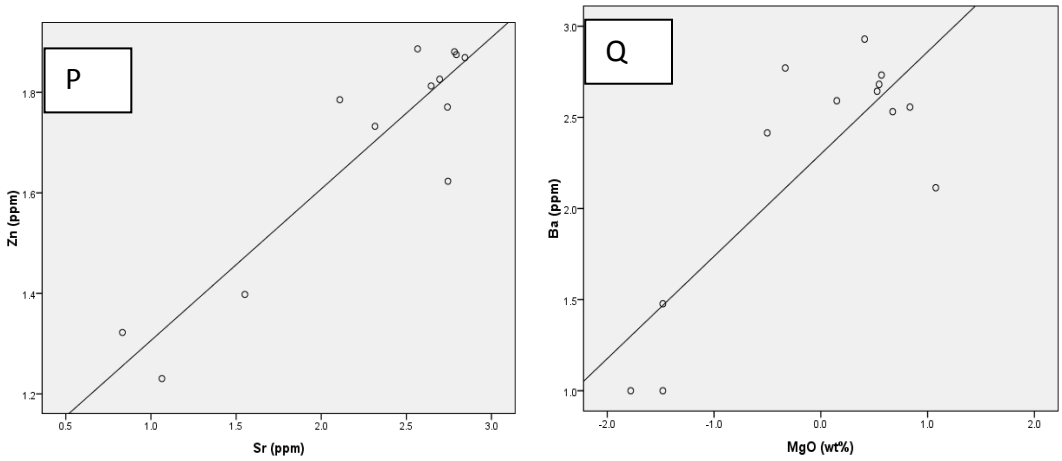

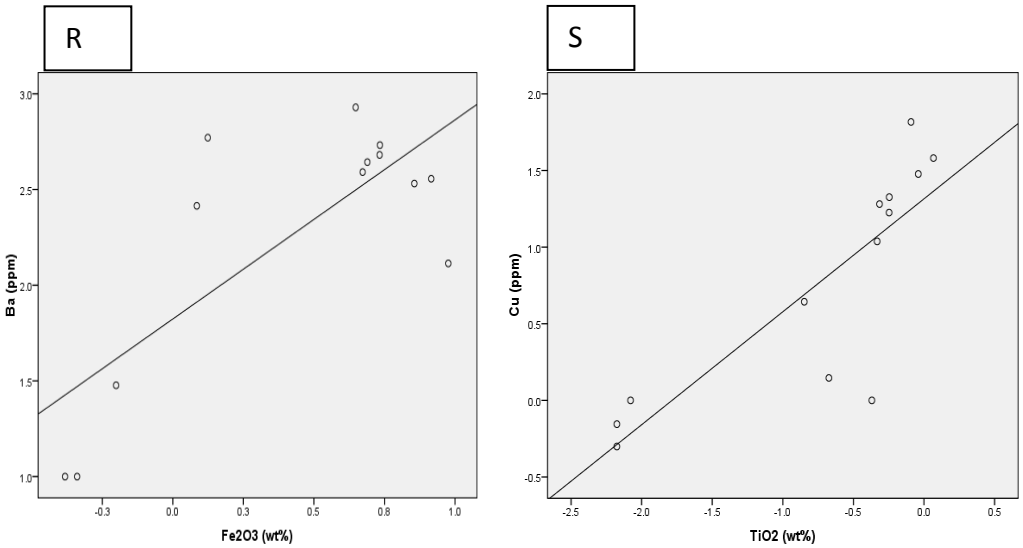

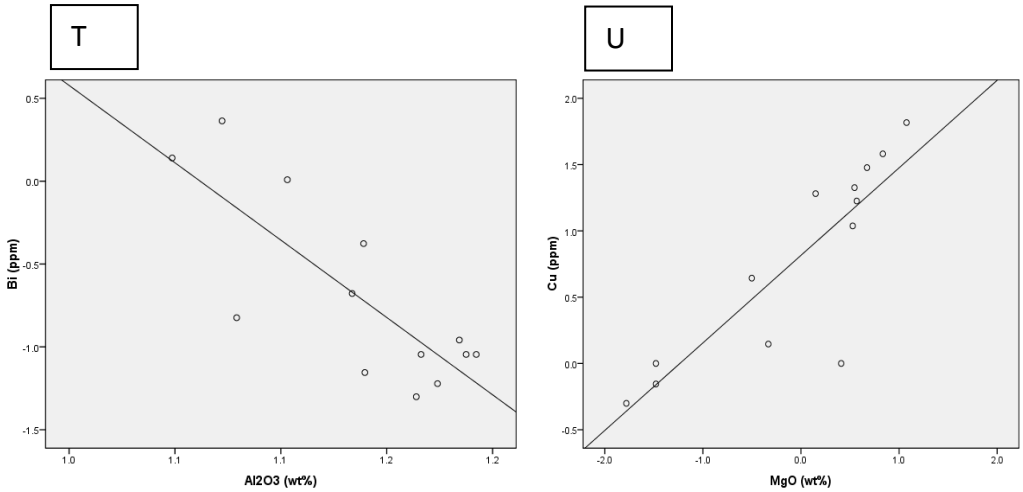

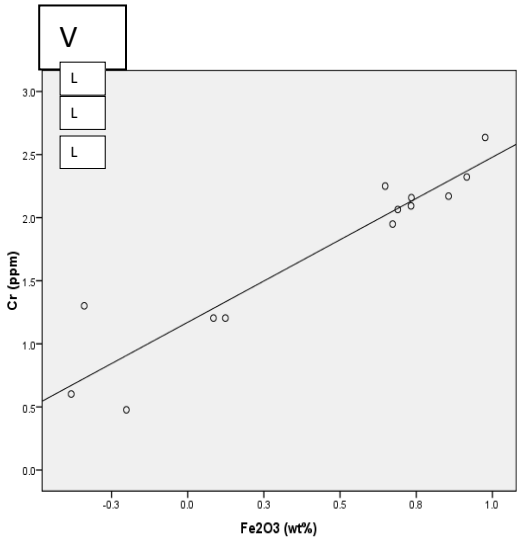

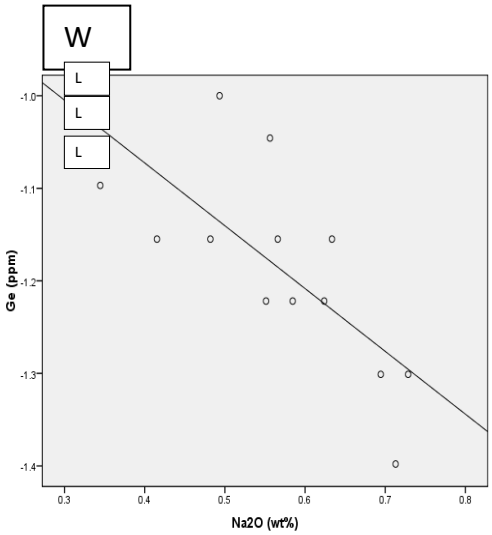

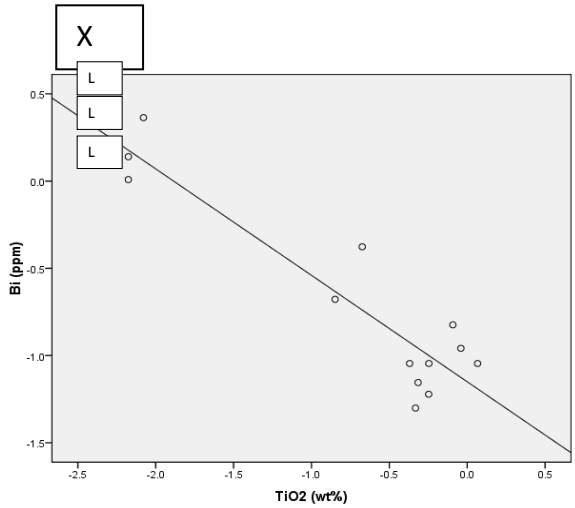

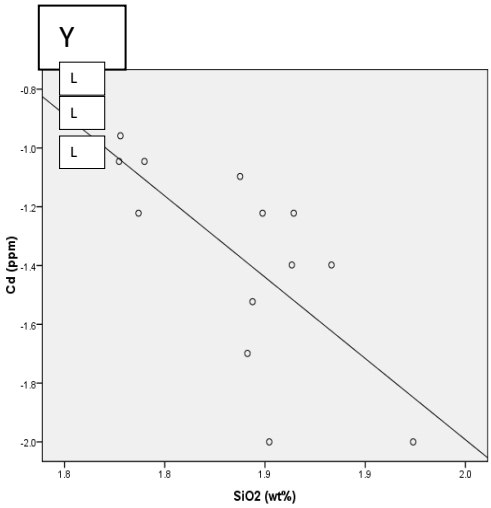

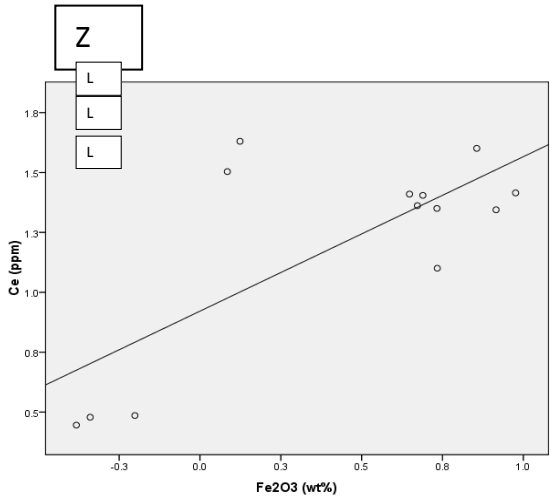

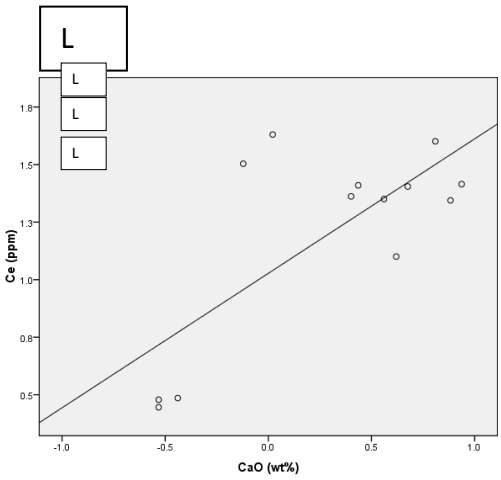

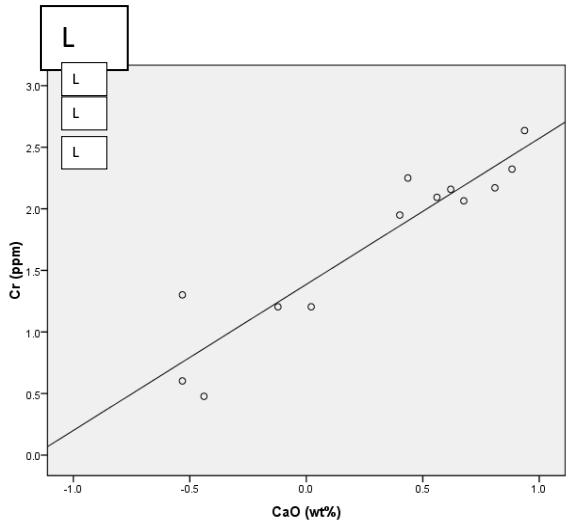

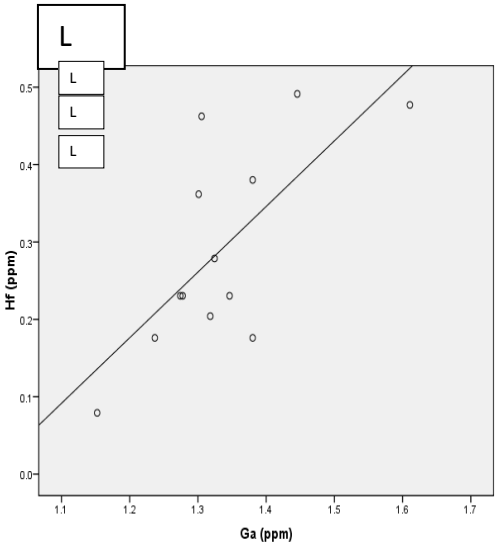

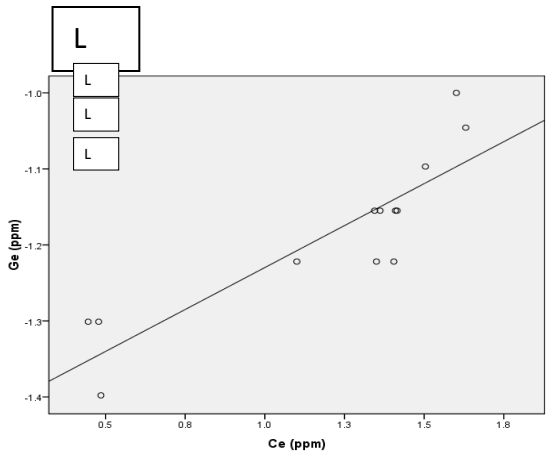

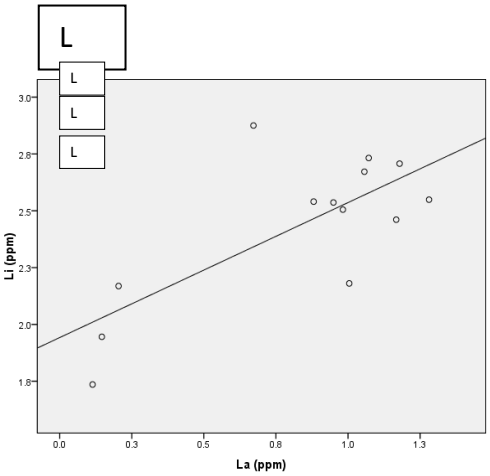

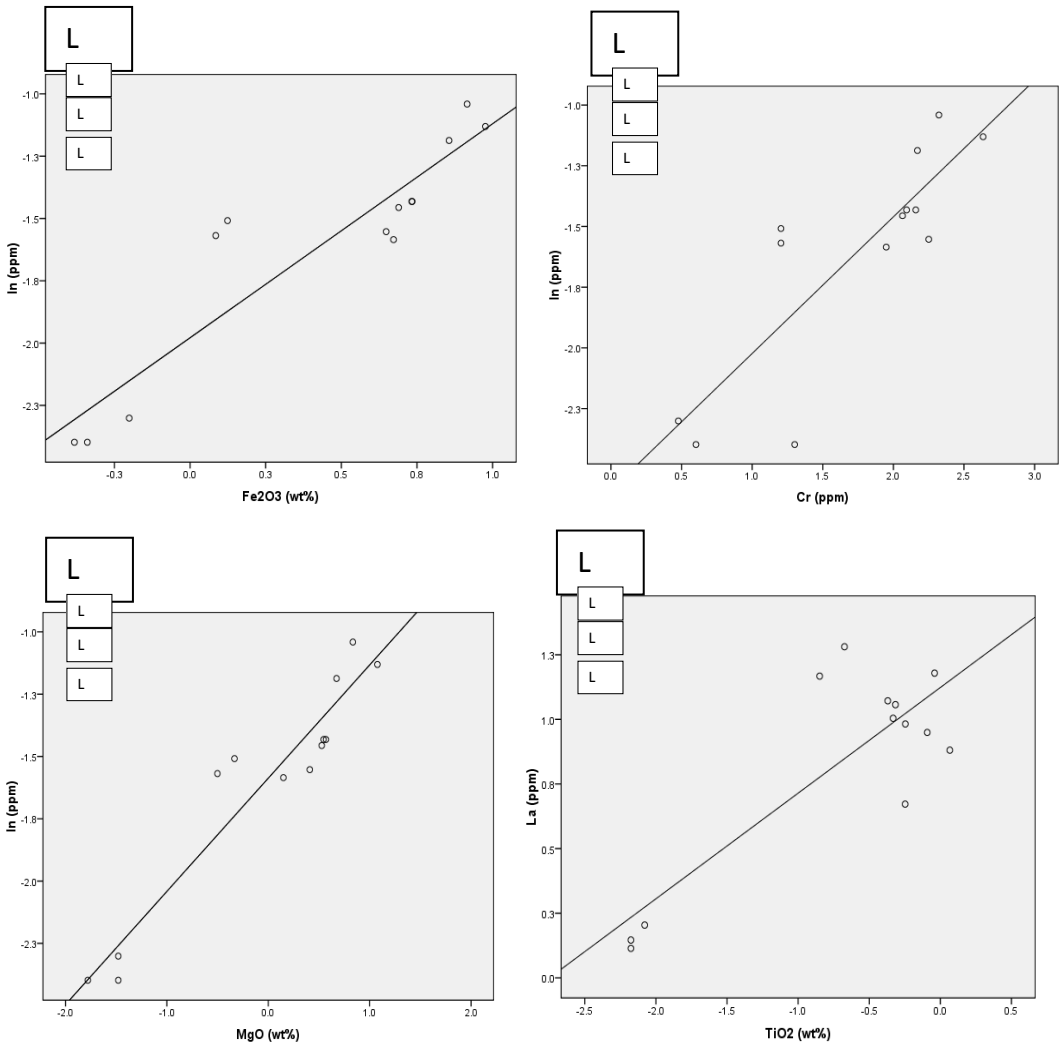

Table 4.5 Total variance explained

Component	Initial Eigenvalues			Extraction Sums of Squared Loadings			Rotation Sums of Squared Loadings		
	Total	% of Variance	Cumulative %	Total	% of Variance	Cumulative %	Total	% of Variance	Cumulative %
1	37.043	64.987	64.987	37.043	64.987	64.987	23.434	41.111	41.111
2	7.449	13.068	78.055	7.449	13.068	78.055	19.407	34.047	75.159
3	3.404	5.972	84.026	3.404	5.972	84.026	3.704	6.498	81.657
4	2.202	3.864	87.890	2.202	3.864	87.890	2.848	4.997	86.653
5	2.024	3.552	91.442	2.024	3.552	91.442	2.730	4.789	91.442
6	1.503	2.637	94.079						
7	1.205	2.114	96.193						
8	.837	1.469	97.661						
9	.615	1.079	98.741						
10	.321	.563	99.304						
11	.234	.411	99.715						
12	.162	.285	100.000						
13	.000	.000	100.000						

Table 3.1: Summary of the log sheet used for the soil sampling

Sample number;		
GPS readings - latitude/longitude;		
Sample description; (dry, humid or water saturated);		
Soil matrix;		
Soil colour;		
Lateritic gravel content, and		
General comment		

Table 5.2: Comparison between rock and soil samples in this study

	MINI (SOIL)	MAX (SOIL)	MINI (ROCK)	MAX (ROCK)
SEDEROPHILES				
Fe2O3	1.16	12.23	0.41	9.46
Ni	8.2	84.2	0.8	283
Ge	0.8	2.5	0.04	0.1
Sn	1.1	21.5	0.9	25.5
Ga	9.6	29.4	14.2	40.8
Cu	1.5	37.4	0.5	65.6
As	3	14.2	0.1	0.6
Co			0.1	51.8
CHALCOPHILES				
Ag			0.02	0.08
MgO	0.95	3.56	0.02	11.92
Ca	0.02	1.33	0.29	8.65
Sr	13.8	74.1	6.8	698
Ba	71	426	10	850
In			0	0.09
TI			0.17	2.09
Sn	1.1	21.5	0.9	25.5
Pb			3.7	21.8
Bi			0.05	2.31
S	0.05	0.13	0	0.45
Mo			0.22	1.2
LITHOPHILES				
Li			54.4	750
Na2O	0.41	1.59	2.21	5.35
K2O	0.47	4.81	0.53	4.37
Rb	18.8	271.8	18.1	374
Cs			4.19	53.7
Al2O3	12.7	38.77	11.19	15.57
Y	40.48		1.7	21.4
SiO2	0.28	81.01	59.89	83.93
TiO2	217.2	1.48	0.1	1.17
Zr		1079	23.1	99.7
Hf			1.2	3.1
Th			0.5	7.8
P2O5 and P	0.02	0.16	180	1260
V			0.9	234
Nb	10	35	1.6	11.5
Ta			0.08	2.31
Cr	0	0.06	3	432
U			0.3	9.2
Cl				
MnO	0.01	0.2	87	770
Zn	12.6	66.1	17	77
I	4.5	46		

Appendix c: Table 2. Raw data for rocks.

sample	LATITUDE(N)	LONGITUDE(W)	**SiO2**	**TiO2**	**Al2O3**	**Fe2O3**	**MgO**
RI	6.75938N	-1.39388	69.380	0.008	11.809	0.629	0.033
R2	6.77022N	-1.3775	69.790	0.007	11.186	0.415	0.017
R5	6.80125N	-1.35711	83.930	0.142	13.604	1.215	0.315
R8	6.77861N	-1.37666	73.170	0.567	14.663	5.404	3.515
R9	6.77625N	-1.37811	61.640	0.911	15.286	7.177	4.709
R10	6.77569N	-1.37828	73.010	0.007	12.679	0.458	0.033
R11	6.77569N	-1.37828	76.410	0.484	13.793	4.704	1.409
R12	6.77390N	-1.3754	61.220	0.465	14.587	4.890	3.366
R13	6.76779N	-1.34949	71.140	0.427	15.399	4.446	2.570
R14	6.79388N	-1.34963	68.800	0.212	13.774	1.330	0.464
R15	6.77276N	-1.37137	70.600	0.565	14.927	5.419	3.698
R16	6.76983N	-1.37947	59.870	0.809	11.998	9.465	11.922
R17	6.7697N	-1.3788	59.960	1.166	15.569	8.235	6.832

Appendix c: Table 2. Raw data for rocks (continued)

sample	LATITUDE(N)	LONGITUDE(W)	**CaO**	**Na2O**	**K2O**	**SO3**	Ag
RI	6.75938N	-1.39388	0.364	5.163	2.963	0.000	0.020
R2	6.77022N	-1.3775	0.294	4.947	2.722	0.000	0.020
R5	6.80125N	-1.35711	0.756	2.211	3.132	0.000	0.010
R8	6.77861N	-1.37666	3.638	3.842	1.843	0.175	0.070
R9	6.77625N	-1.37811	6.450	3.114	1.494	0.325	0.090
R10	6.77569N	-1.37828	0.294	5.352	3.264	0.000	0.020
R11	6.77569N	-1.37828	2.519	3.680	1.205	0.100	0.060
R12	6.77390N	-1.3754	4.743	4.206	1.385	0.025	0.060
R13	6.76779N	-1.34949	2.728	4.300	2.132	0.000	0.040
R14	6.79388N	-1.34963	1.049	3.599	4.373	0.000	0.040
R15	6.77276N	-1.37137	4.170	3.559	2.072	0.100	0.070
R16	6.76983N	-1.37947	8.647	2.602	0.530	0.449	0.100
R17	6.7697N	-1.3788	7.640	3.033	1.012	0.325	0.100

Appendix c: Table 2. Raw data for rocks (continued)

sample	LATITUDE(N)	LONGITUDE(W)	As	Ba	Be	Bi	Cd
RI	6.75938N	-1.39388	0.300	30.000	5.040	2.100	0.030
R2	6.77022N	-1.3775	0.300	10.000	6.390	1.220	0.030
R5	6.80125N	-1.35711	0.300	240.000	8.800	0.170	0.030
R8	6.77861N	-1.37666	0.300	490.000	1.110	0.070	0.070
R9	6.77625N	-1.37811	0.300	340.000	1.120	0.090	0.100
R10	6.77569N	-1.37828	0.300	10.000	6.410	0.960	0.050
R11	6.77569N	-1.37828	0.500	380.000	0.310	0.060	0.040
R12	6.77390N	-1.3754	0.300	470.000	1.010	0.040	0.050
R13	6.76779N	-1.34949	0.300	880.000	12.050	0.070	0.020
R14	6.79388N	-1.34963	0.300	560.000	3.310	0.330	0.080
R15	6.77276N	-1.37137	0.300	580.000	3.000	0.060	0.060
R16	6.76983N	-1.37947	0.300	130.000	0.830	0.130	0.090
R17	6.7697N	-1.3788	0.300	350.000	0.890	0.070	0.100

Appendix c: Table 2. Raw data for rocks (continued)

sample	LATITUDE(N)	LONGITUDE(W)	Ce	Co	Cr	Cs	Cu
RI	6.75938N	-1.39388	3.120	0.400	3.000	12.900	3.100
R2	6.77022N	-1.3775	2.590	0.200	5.000	8.330	1.100
R5	6.80125N	-1.35711	26.600	2.100	16.000	13.800	4.500
R8	6.77861N	-1.37666	24.100	17.800	131.000	19.600	21.500
R9	6.77625N	-1.37811	49.900	22.200	140.000	14.150	29.000
R10	6.77569N	-1.37828	2.650	0.200	10.000	12.800	0.900
R11	6.77569N	-1.37828	21.600	12.900	88.000	17.450	19.400
R12	6.77390N	-1.3754	25.400	14.600	116.000	4.390	11.200
R13	6.76779N	-1.34949	29.600	17.400	182.000	56.000	1.200
R14	6.79388N	-1.34963	38.800	2.800	16.000	11.550	1.500
R15	6.77276N	-1.37137	12.800	18.200	148.000	42.800	16.900
R16	6.76983N	-1.37947	27.300	49.700	403.000	28.300	60.700
R17	6.7697N	-1.3788	26.800	30.900	198.000	8.150	37.300

Appendix c: Table 2. Raw data for rocks (continued)

sample	LATITUDE(N)	LONGITUDE(W)	Ga	Ge	Hf	In	La
RI	6.75938N	-1.39388	26.500	0.060	1.400	0.006	1.600
R2	6.77022N	-1.3775	22.500	0.060	1.700	0.006	1.200
R5	6.80125N	-1.35711	40.500	0.090	2.600	0.027	12.000
R8	6.77861N	-1.37666	21.000	0.160	2.900	0.036	10.700
R9	6.77625N	-1.37811	21.000	0.240	1.900	0.065	18.500
R10	6.77569N	-1.37828	28.600	0.050	2.400	0.006	1.200
R11	6.77569N	-1.37828	15.400	0.140	1.100	0.026	10.800
R12	6.77390N	-1.3754	20.600	0.160	1.700	0.032	10.100
R13	6.76779N	-1.34949	21.900	0.160	1.700	0.028	13.900
R14	6.79388N	-1.34963	30.300	0.130	3.000	0.028	17.500
R15	6.77276N	-1.37137	21.500	0.150	2.300	0.036	4.800
R16	6.76983N	-1.37947	17.000	0.250	1.700	0.075	9.400
R17	6.7697N	-1.3788	21.800	0.230	1.800	0.096	9.100

Appendix c: Table 2. Raw data for rocks (continued)

sample	LATITUDE(N)	LONGITUDE(W)	Li	Mn	Mo	Nb	Ni
RI	6.75938N	-1.39388	135.500	83.000	0.250	8.200	1.400
R2	6.77022N	-1.3775	53.400	355.000	0.280	5.400	0.900
R5	6.80125N	-1.35711	260.000	108.000	0.530	11.400	4.900
R8	6.77861N	-1.37666	318.000	537.000	0.550	3.900	86.900
R9	6.77625N	-1.37811	500.000	665.000	0.420	5.500	70.100
R10	6.77569N	-1.37828	89.500	275.000	0.690	7.400	1.100
R11	6.77569N	-1.37828	470.000	390.000	0.480	3.500	32.900
R12	6.77390N	-1.3754	156.500	525.000	0.310	3.900	44.400
R13	6.76779N	-1.34949	560.000	429.000	0.500	6.600	102.500
R14	6.79388N	-1.34963	345.000	93.000	0.500	3.700	4.600
R15	6.77276N	-1.37137	800.000	510.000	0.540	4.000	73.000
R16	6.76983N	-1.37947	353.000	816.000	0.230	2.000	300.000
R17	6.7697N	-1.3788	354.000	624.000	0.340	4.200	108.000

Appendix c: Table 2. Raw data for rocks (continued)

sample	LATITUDE(N)	LONGITUDE(W)	P	Pb	Rb	Sc	Sn
RI	6.75938N	-1.39388	160.000	20.500	261.000	0.400	6.800
R2	6.77022N	-1.3775	320.000	21.200	351.000	0.300	8.100
R5	6.80125N	-1.35711	940.000	8.000	281.000	3.100	24.000
R8	6.77861N	-1.37666	630.000	7.600	64.200	13.900	1.200
R9	6.77625N	-1.37811	1230.000	6.800	61.300	19.000	2.400
R10	6.77569N	-1.37828	280.000	16.400	387.000	0.400	11.400
R11	6.77569N	-1.37828	210.000	6.400	74.800	14.300	1.200
R12	6.77390N	-1.3754	700.000	7.200	35.900	13.300	0.900
R13	6.76779N	-1.34949	740.000	11.400	167.500	11.400	13.700
R14	6.79388N	-1.34963	850.000	19.900	239.000	3.300	4.400
R15	6.77276N	-1.37137	700.000	7.300	87.000	12.900	4.000
R16	6.76983N	-1.37947	450.000	3.400	33.800	37.400	1.900
R17	6.7697N	-1.3788	240.000	4.300	23.700	29.000	1.000

Appendix c: Table 2. Raw data for rocks (continued)

sample	LATITUDE(N)	LONGITUDE(W)	V	W	Y	Zn	Zr
RI	6.75938N	-1.39388	1.000	0.200	1.900	26.000	26.100
R2	6.77022N	-1.3775	1.000	0.200	2.000	20.000	27.600
R5	6.80125N	-1.35711	15.000	0.600	5.400	60.000	79.400
R8	6.77861N	-1.37666	86.000	0.100	12.200	71.000	110.500
R9	6.77625N	-1.37811	134.000	0.200	24.200	78.000	44.800
R10	6.77569N	-1.37828	1.000	0.200	2.900	24.000	46.000
R11	6.77569N	-1.37828	86.000	0.100	5.600	46.000	44.000
R12	6.77390N	-1.3754	84.000	0.100	9.900	66.000	49.600
R13	6.76779N	-1.34949	70.000	0.100	8.200	83.000	58.300
R14	6.79388N	-1.34963	15.000	0.300	4.700	55.000	106.500
R15	6.77276N	-1.37137	85.000	0.100	7.200	77.000	85.200
R16	6.76983N	-1.37947	234.000	0.200	19.900	83.000	43.100
R17	6.7697N	-1.3788	185.000	0.300	25.700	78.000	46.200

Appendix c: Table 2. Raw data for rocks (continued)

sample	LATITUDE(N)	LONGITUDE(W)	Dy	Er	Eu	Gd	Ho
RI	6.75938N	-1.39388	0.250	0.150	0.040	0.200	0.050
R2	6.77022N	-1.3775	0.220	0.140	0.070	0.230	0.040
R5	6.80125N	-1.35711	0.810	0.400	0.360	1.510	0.150
R8	6.77861N	-1.37666	2.120	1.350	1.000	2.560	0.480
R9	6.77625N	-1.37811	4.290	2.690	1.840	5.550	0.950
R10	6.77569N	-1.37828	0.320	0.230	0.040	0.200	0.070
R11	6.77569N	-1.37828	1.210	0.700	1.100	1.910	0.250
R12	6.77390N	-1.3754	1.790	1.120	1.040	2.460	0.400
R13	6.76779N	-1.34949	1.470	0.850	1.030	2.170	0.310
R14	6.79388N	-1.34963	0.900	0.370	0.640	2.400	0.160
R15	6.77276N	-1.37137	1.350	0.900	0.870	1.530	0.310
R16	6.76983N	-1.37947	4.020	2.350	1.860	5.280	0.870
R17	6.7697N	-1.3788	4.890	2.880	1.920	6.130	1.080

Appendix c: Table 2. Raw data for rocks (continued)

sample	LATITUDE(N)	LONGITUDE(W)	Lu	Nd	Pr	Sm	Tb	Tm	Yb
RI	6.75938N	-1.39388	0.030	0.900	0.320	0.230	0.050	0.020	0.190
R2	6.77022N	-1.3775	0.030	1.200	0.310	0.260	0.040	0.030	0.220
R5	6.80125N	-1.35711	0.060	11.600	3.200	2.080	0.200	0.050	0.350
R8	6.77861N	-1.37666	0.190	12.200	3.040	2.450	0.420	0.180	1.190
R9	6.77625N	-1.37811	0.360	30.800	7.250	5.980	0.860	0.360	2.320
R10	6.77569N	-1.37828	0.050	0.800	0.280	0.190	0.060	0.040	0.340
R11	6.77569N	-1.37828	0.140	9.000	2.480	1.690	0.280	0.100	0.830
R12	6.77390N	-1.3754	0.160	12.900	3.180	2.510	0.380	0.150	1.000
R13	6.76779N	-1.34949	0.130	13.300	3.570	2.330	0.320	0.110	0.780
R14	6.79388N	-1.34963	0.060	17.400	4.770	3.190	0.270	0.050	0.300
R15	6.77276N	-1.37137	0.150	6.000	1.460	1.310	0.260	0.120	0.880
R16	6.76983N	-1.37947	0.260	21.500	4.500	4.950	0.810	0.290	1.760
R17	6.7697N	-1.3788	0.330	22.300	4.530	5.660	0.970	0.360	2.240

Appendix C: Table 3. Raw data for soil samples (detailed)

SAMPLE POINTS	LATITUDE (N)	LONGITUDE (W)	Na2O	MgO	Al2O3	SiO2	P2O5
A01	6.75438	-1.4097	0.417	0.949	17.77	54.68	0.0482
A02	6.7591	-1.4036	1.185	1.398	26.37	51.28	0.0467
A03	6.7633	-1.3971	1.49	1.612	36.22	57.31	0.0599
A04	6.7652	-1.3913	0.652	1.246	17.8	57.6	0.0595
A05	6.7661	-1.3871	0.636	1.15	19.89	49.36	0.0591
A06	6.7673	-1.3843	1.26	1.188	33.88	54.33	0.112
A07	6.7689	-1.3885	1	1.453	35.01	57.35	0.0845
A08	6.7697	-1.3788	1.06	1.828	35.97	53.98	0.1606
A09	6.7703	-1.3778	0.94	3.239	34.18	44.54	0.1562
A10	6.7708	-1.3766	1.26	3.555	37.39	47.45	0.129
A11	6.7726	-1.3735	1.31	2.745	21.42	40.48	0.0754
A12	6.7725	-1.3745	1.24	2.868	38.57	50.7	0.1055
A13	6.772	-1.3722	0.933	1.712	29.69	49.96	0.1179
A14	6.7733	-1.3692	0.982	1.538	37.47	53.67	0.0873
A15	6.7732	-1.3672	1.41	1.584	37.3	59.24	0.0974
A16	6.7732	-1.3671	1.15	1.484	38.39	48.34	0.1165
A17	6.7731	-1.3653	1.59	1.612	37	61.49	0.08
A18	6.7733	-1.3615	0.986	1.707	33.34	49.8	0.0752
A19	6.7733	-1.3612	1.15	1.526	38.77	52.99	0.0814
A20	6.7733	-1.36	1.152	1.86	19.44	65.29	0.0912
A21	6.7733	-1.3587	< 0.19	1.236	12.7	81.01	0.01534
A22	6.7733	-1.357	1.26	1.503	33.49	57.77	0.0741
A23	6.7732	-1.3509	0.942	1.43	21.8	63.48	0.0413
A24	6.7727	-1.3407	1.07	1.542	34.76	57.85	0.0842
A25	6.7732	-1.3393	0.943	1.335	27.2	50.65	0.0491
A26	6.7699	-1.3378	0.411	1.451	23.45	60.36	0.0505
A27	6.8	-1.36	0.872	0.979	28.73	60.18	0.0444
A28	6.8088	-1.406	1.25	1.566	34.73	55.3	0.1137
A29	6.8001	-1.3868	0.667	1.449	17.41	58.63	0.0431
A30	6.791	-1.351	0.839	1.256	23.92	52.22	0.0512
A31	6.818	-1.369	0.772	1.594	21.93	52.97	0.0755

Appendix C: Table 3. Raw data for soil samples (detailed) continued

SAMPLE POINTS	LATITUDE (N)	LONGITUDE (W)	SO3	K2O	CaO	TiO2	MnO
A01	6.75438	-1.4097	0.0723	0.543	0.1252	0.5007	0.0313
A02	6.7591	-1.4036	0.0628	4.811	0.0778	0.2841	0.0208
A03	6.7633	-1.3971	0.0744	3.216	0.2216	0.4202	0.0814
A04	6.7652	-1.3913	0.0718	0.588	0.0547	0.6347	0.0218
A05	6.7661	-1.3871	0.0709	0.772	0.1493	0.4636	0.0294
A06	6.7673	-1.3843	0.0815	1.271	0.2226	1.073	0.0842
A07	6.7689	-1.3885	0.0722	1.192	0.1861	1.097	0.0364
A08	6.7697	-1.3788	0.1028	0.89	0.434	1.478	0.2042
A09	6.7703	-1.3778	0.0874	1.352	0.9212	1.086	0.1335
A10	6.7708	-1.3766	0.0616	0.972	0.6375	0.9245	0.0811
A11	6.7726	-1.3735	0.0726	1.296	0.4801	0.7117	0.1314
A12	6.7725	-1.3745	0.0575	1.294	0.2152	1.066	0.1155
A13	6.772	-1.3722	0.1247	0.971	0.3614	1.059	0.1875
A14	6.7733	-1.3692	0.0717	0.779	0.1598	1.322	0.0726
A15	6.7732	-1.3672	0.0668	1.414	0.2067	1.091	0.0822
A16	6.7732	-1.3671	0.1215	1.345	1.331	0.9743	0.0908
A17	6.7731	-1.3653	0.0655	1.229	0.1163	1.119	0.0348
A18	6.7733	-1.3615	0.0736	1.766	0.1114	0.8186	0.0368
A19	6.7733	-1.3612	0.0661	1.413	0.0657	1.105	0.0282
A20	6.7733	-1.36	0.059	3.069	0.2275	0.595	0.0606
A21	6.7733	-1.3587	0.049	0.776	0.0598	1.058	0.0281
A22	6.7733	-1.357	0.0706	1.026	0.0599	1.144	0.0349
A23	6.7732	-1.3509	0.0533	1.452	0.0224	0.5735	0.00534
A24	6.7727	-1.3407	0.0663	0.894	0.0899	1.097	0.0201
A25	6.7732	-1.3393	0.0773	0.471	0.1051	1.035	0.0204
A26	6.7699	-1.3378	0.0552	1.031	0.0449	0.6648	0.01031
A27	6.8	-1.36	0.054	0.596	0.0587	0.6695	0.01159
A28	6.8088	-1.406	0.0715	0.558	0.0951	1.205	0.042
A29	6.8001	-1.3868	0.0585	1.578	0.0598	0.5413	0.00902
A30	6.791	-1.351	0.071	0.883	0.3808	0.4576	0.0385
A31	6.818	-1.369	0.0685	1.198	0.2613	0.8275	0.1218

Appendix C: Table 3. Raw data for soil samples (detailed) continued

SAMPLE POINTS	LATITUDE (N)	LONGITUDE (W)	Ga	Ge	As	Br	Rb
A01	6.75438	-1.4097	13.7	1	9.2	2.8	34
A02	6.7591	-1.4036	25.2	1.6	5.3	< 0.3	271.8
A03	6.7633	-1.3971	29.4	2.1	6.5	5.8	219.2
A04	6.7652	-1.3913	12.8	1.8	11.1	0.6	23.4
A05	6.7661	-1.3871	15.4	1.6	7.2	4.1	36.9
A06	6.7673	-1.3843	20.4	1.7	5.8	5.1	36.5
A07	6.7689	-1.3885	17.6	1	8	5.2	18.9
A08	6.7697	-1.3788	23.7	1.4	14.2	3.6	55.8
A09	6.7703	-1.3778	26.7	2.5	5.9	12.5	136.4
A10	6.7708	-1.3766	25	2.2	3	10.4	71.9
A11	6.7726	-1.3735	19.5	1.9	8.2	5.9	115.1
A12	6.7725	-1.3745	24.8	1.4	3.4	5	96.5
A13	6.772	-1.3722	24.3	2.4	12.5	10.6	87.8
A14	6.7733	-1.3692	23.5	2.1	7.9	3.4	33.8
A15	6.7732	-1.3672	19.9	2	5.4	4.7	44
A16	6.7732	-1.3671	22.5	1.7	11.1	10.4	40.9
A17	6.7731	-1.3653	21.6	1.2	7.2	4.6	31.4
A18	6.7733	-1.3615	22.4	1.3	7.1	5.2	64.6
A19	6.7733	-1.3612	23.8	1.6	5.5	3.9	43.9
A20	6.7733	-1.36	12.4	1.9	4.4	< 0.3	143.3
A21	6.7733	-1.3587	9.6	1	3	< 0.3	24.7
A22	6.7733	-1.357	19.2	2.1	6.5	2.6	39.8
A23	6.7732	-1.3509	10.8	1.4	3.4	< 0.3	27
A24	6.7727	-1.3407	19.6	0.8	4.2	2.6	21.6
A25	6.7732	-1.3393	14.7	1.5	4.2	2.3	18.8
A26	6.7699	-1.3378	18.3	< 0.8	4.4	0.8	63
A27	6.8	-1.36	21.2	1.3	5	3.6	31.3
A28	6.8088	-1.406	24.5	1.5	5.3	5	26.2
A29	6.8001	-1.3868	13.1	0.9	4.8	< 0.4	80.8
A30	6.791	-1.351	19.3	2	8.2	2.5	53.7
A31	6.818	-1.369	13.5	2.2	7.4	2.1	187.3

Appendix C: Table 3. Raw data for soil samples (detailed) continued

SAMPLE POINTS	LATITUDE (N)	LONGITUDE (W)	Sr	Zr	Nb	Sn	I	Ba	Ce
A01	6.75438	-1.4097	16.1	468	17.8	4.4	4.5	76.4	< 23
A02	6.7591	-1.4036	43.7	217.2	16	7.4	7.4	244.1	61
A03	6.7633	-1.3971	43.5	424	18.2	12	20.3	257.1	72
A04	6.7652	-1.3913	13.8	519	12.5	1.1	11.1	114	39
A05	6.7661	-1.3871	17.8	365	10	4.9	11.2	122.4	45
A06	6.7673	-1.3843	31.2	603	19.5	8.2	22.7	272.4	100
A07	6.7689	-1.3885	29.3	553	19.7	1.1	15.5	326	62
A08	6.7697	-1.3788	32.4	434	20.9	9.9	42.5	217.4	117
A09	6.7703	-1.3778	74.1	236	17.4	12.1	40.1	398	57
A10	6.7708	-1.3766	63.8	362	13.5	8.7	29.1	339	100
A11	6.7726	-1.3735	51.8	263.5	12.6	10.7	13.3	340	54
A12	6.7725	-1.3745	30.8	474	20.2	7.4	32.1	312	92
A13	6.772	-1.3722	33	514	27	21.5	46	247	79
A14	6.7733	-1.3692	23.5	684	29.3	7.2	26.3	156.4	124
A15	6.7732	-1.3672	34.8	608	28.3	3.4	35.6	353	118
A16	6.7732	-1.3671	57.8	478	19.4	2.5	34.4	426	55
A17	6.7731	-1.3653	28.3	642	15.5	3.4	20.2	368	83
A18	6.7733	-1.3615	36.6	455	23.1	12.2	18.7	352	< 24
A19	6.7733	-1.3612	32.9	640	21.6	8.1	31.7	383	55
A20	6.7733	-1.36	59.6	554	13.2	< 1.8	8.1	369	50
A21	6.7733	-1.3587	16	1079	16.6	< 2.2	< 5.6	142.3	< 23
A22	6.7733	-1.357	27.9	753	26.9	6.3	18.5	271.2	53
A23	6.7732	-1.3509	29.6	460	13.1	< 2.1	< 5.6	345.4	60
A24	6.7727	-1.3407	24.9	635	23.9	< 2.0	27.3	248.2	51
A25	6.7732	-1.3393	18.2	582	23.4	2.6	28	112.9	73
A26	6.7699	-1.3378	16.5	586	19.7	3.9	7	99.9	< 23
A27	6.8	-1.36	14.4	535	19.3	4.7	7.5	71	< 23
A28	6.8088	-1.406	19.7	749	35	10.1	34.8	126.4	92
A29	6.8001	-1.3868	28.8	552	13.6	< 1.8	< 5.6	275.3	52
A30	6.791	-1.351	21.5	391	15	9	14.7	78.9	51
A31	6.818	-1.369	26.2	504	17.1	15.3	7.8	197.5	41

Appendix C: Raw data for test samples

SAMPLE POINT	LATITUDE(N)	LONGITUDE (W)	Na2O	MgO	Al2O3	SiO2	P2O5	SO3	K2O	CaO
A1	6.837	-1.415	0.843	1.235	21.270	59.080	0.103	0.103	0.635	0.341
A2	6.828	-1.415	0.683	0.854	25.160	53.590	0.080	0.091	1.706	0.247
A3	6.818	-1.415	0.590	1.252	16.640	64.520	0.071	0.056	0.905	0.134
A5	6.8	-1.415	1.202	1.469	26.650	55.800	0.077	0.090	6.176	0.199
A6	6.791	-1.415	0.572	0.814	22.740	48.900	0.052	0.092	0.610	0.125
A7	6.782	-1.415	0.534	1.305	18.000	61.400	0.071	0.098	0.469	0.214
A8	6.773	-1.415	0.758	1.275	23.000	52.040	0.049	0.087	0.535	0.087
A9	6.763	-1.415	0.776	1.455	28.050	62.320	0.080	0.069	1.549	0.193
A10	6.754	-1.415	0.470	1.361	14.700	66.770	0.038	0.046	0.930	0.045
B2	6.828	-1.406	0.554	1.173	16.060	63.690	0.036	0.053	0.575	0.032
B3	6.818	-1.406	0.880	1.499	18.510	68.510	0.064	0.100	1.883	0.080
B4	6.809	-1.406	0.849	1.131	23.200	53.320	0.036	0.064	0.638	0.054
B5	6.8	-1.406	0.881	1.145	29.690	47.720	0.053	0.058	0.442	0.044
B6	6.791	-1.406	0.792	1.013	23.250	57.370	0.043	0.065	0.481	0.074
B8	6.773	-1.406	1.147	1.348	38.250	49.120	0.074	0.057	0.331	0.231
B9	6.763	-1.406	0.656	1.063	21.070	67.490	0.063	0.049	4.569	0.108
B10	6.754	-1.406	1.064	0.934	33.970	52.250	0.037	0.069	2.491	0.066
C1	6.837	-1.397	1.077	1.262	32.070	52.260	0.055	0.073	1.559	0.155
C2	6.828	-1.397	< 0.19	1.320	9.441	83.620	0.019	0.055	2.385	0.036
C3	6.818	-1.397	1.171	1.075	35.360	52.370	0.060	0.069	0.809	0.070
C4	6.809	-1.397	0.966	1.134	25.340	49.160	0.028	0.062	0.324	0.045
C5	6.8	-1.397	0.285	1.033	5.563	85.040	0.043	0.048	0.862	0.037
C6	6.791	-1.397	0.950	1.446	35.260	53.890	0.067	0.070	0.534	0.133
C7	6.782	-1.397	1.180	1.396	38.150	53.370	0.059	0.056	1.134	0.079
C8	6.773	-1.397	0.696	1.257	23.940	49.280	0.033	0.057	0.869	0.255
C9	6.763	-1.397	0.901	1.576	32.950	51.880	0.044	0.072	3.417	0.116
C10	6.754	-1.397	1.115	1.668	22.130	64.040	0.047	0.062	2.991	0.147
D1	6.837	-1.387	0.825	1.297	29.410	62.800	0.039	0.049	0.791	0.052
D2	6.828	-1.387	1.280	1.292	37.990	47.250	0.076	0.065	0.275	0.115
D3	6.818	-1.387	0.769	1.286	30.310	49.370	0.049	0.071	0.332	0.135
D4	6.809	-1.387	0.673	1.230	24.840	55.520	0.044	0.062	0.920	0.024

Appendix C: Raw data for test samples (continued)

SAMPLE POINT	LATITUDE(N)	LONGITUDE (W)	Na2O	MgO	Al2O3	SiO2	P2O5	SO3	K2O	CaO
D6	6.791	-1.387	0.610	1.426	16.180	73.040	0.039	0.057	0.773	0.047
D7	6.782	-1.387	1.033	1.406	23.430	62.890	0.050	0.055	0.907	0.053
D8	6.773	-1.387	0.900	1.397	22.180	61.310	0.042	0.036	1.161	0.083
D9	6.763	-1.387	0.770	1.180	24.930	48.810	0.078	0.083	1.093	0.261
D10	6.754	-1.387	1.310	1.578	38.680	54.790	0.093	0.065	1.238	0.192
E1	6.837	-1.378	1.044	1.419	36.530	59.490	0.076	0.052	1.034	0.227
E2	6.828	-1.378	0.263	1.004	5.276	88.270	0.041	0.042	1.138	0.025
E3	6.818	-1.378	0.736	1.291	22.510	57.000	0.037	0.054	1.133	0.020
E4	6.809	-1.378	0.746	0.976	26.960	54.360	0.073	0.071	0.438	0.295
E6	6.791	-1.378	0.920	4.501	23.230	48.870	0.171	0.108	1.757	1.289
E7	6.782	-1.378	1.060	2.439	39.210	50.890	0.089	0.066	1.165	0.411
E8	6.773	-1.378	1.500	2.176	30.640	47.960	0.106	0.093	1.095	0.445
E9	6.763	-1.378	1.040	1.275	29.660	53.320	0.076	0.108	0.899	0.259
E10	6.754	-1.378	0.789	1.292	28.510	54.650	0.087	0.069	0.956	0.192
F1	6.837	-1.369	0.983	1.118	37.810	49.470	0.119	0.070	0.287	0.244
F2	6.828	-1.369	0.702	0.837	18.730	55.910	0.078	0.110	0.488	0.261
F4	6.809	-1.369	0.545	1.073	18.770	64.560	0.043	0.052	0.975	0.072
F5	6.8	-1.369	0.897	1.217	36.320	60.760	0.051	0.056	2.021	0.085
F6	6.791	-1.369	0.872	1.155	23.810	55.130	0.145	0.101	6.083	0.971
F8	6.773	-1.369	0.940	1.171	40.220	44.980	0.062	0.083	0.695	0.077
F9	6.763	-1.369	1.289	2.337	24.670	63.030	0.083	0.096	1.157	0.433
G1	6.837	-1.36	0.969	1.393	30.700	57.950	0.045	0.065	0.735	0.190
G2	6.828	-1.36	1.009	2.419	34.930	57.030	0.086	0.056	2.374	0.230
G3	6.818	-1.36	0.745	1.279	25.080	53.310	0.070	0.085	1.354	0.164
G4	6.809	-1.36	1.049	1.180	34.300	57.530	0.093	0.076	0.929	0.335
G5	6.8	-1.36	1.035	1.406	31.620	57.880	0.073	0.073	0.576	0.201
G6	6.791	-1.36	0.965	1.062	31.700	51.710	0.046	0.068	2.736	0.115
G7	6.782	-1.36	0.689	1.100	23.560	50.610	0.064	0.076	1.237	0.190
G8	6.773	-1.36	0.905	1.098	22.200	48.790	0.058	0.081	1.068	0.067

Appendix C: Raw data for test samples (continued)

SAMPLE POINT	LATITUDE(N)	LONGITUDE (W)	Na2O	MgO	Al2O3	SiO2	P2O5	SO3	K2O	CaO
G9	6.763	-1.36	0.688	1.124	21.770	52.530	0.079	0.086	0.724	0.165
G10	6.754	-1.36	0.444	1.004	6.768	72.310	0.024	0.045	0.418	0.261
H2	6.828	-1.351	0.481	0.976	17.440	64.070	0.056	0.054	0.830	0.124
H3	6.818	-1.351	0.853	1.242	27.650	54.230	0.038	0.060	0.937	0.027
H4	6.809	-1.351	1.109	1.081	33.340	54.950	0.069	0.082	0.410	0.167
H5	6.8	-1.351	0.733	1.303	12.550	65.180	0.043	0.088	1.680	0.256
H6	6.791	-1.351	1.192	1.616	33.540	55.400	0.056	0.056	1.931	0.063
H7	6.782	-1.351	0.920	1.136	24.700	61.370	0.075	0.064	1.323	0.090
H8	6.773	-1.351	0.760	1.241	31.180	48.810	0.069	0.074	0.928	0.197
H9	6.763	-1.351	0.502	1.413	16.370	66.420	0.048	0.056	0.351	0.163
H10	6.754	-1.351	0.658	1.353	14.870	74.130	0.020	0.071	0.671	0.104
I1	6.837	-1.342	0.700	1.109	18.400	71.750	0.050	0.051	1.802	0.044
I2	6.828	-1.342	1.002	1.404	37.130	51.600	0.052	0.069	0.654	0.153
I3	6.818	-1.342	0.930	1.497	30.430	61.500	0.057	0.060	0.557	0.075
I4	6.809	-1.342	1.078	1.529	38.520	57.210	0.041	0.065	1.303	0.087
I5	6.8	-1.342	0.990	1.012	31.410	54.540	0.062	0.070	0.687	0.090
I6	6.791	-1.342	0.875	1.161	29.650	49.630	0.057	0.070	2.371	0.123
I7	6.782	-1.342	1.138	1.511	34.910	60.710	0.051	0.051	1.052	0.037
I8	6.773	-1.342	0.390	1.567	25.900	70.230	0.091	0.063	2.299	0.151
I9	6.763	-1.342	0.751	1.226	26.780	61.860	0.120	0.095	1.118	0.247
I10	6.754	-1.342	0.281	1.376	6.419	72.900	0.023	0.038	0.311	0.021
J1	6.837	-1.333	0.921	1.312	23.740	59.240	0.066	0.074	1.265	0.181
J2	6.828	-1.333	0.665	1.494	22.950	64.860	0.072	0.066	0.701	0.196
J3	6.818	-1.333	1.039	1.505	12.340	77.080	0.042	0.039	3.110	0.130
J4	6.809	-1.333	0.551	0.911	15.100	62.540	0.027	0.054	1.058	0.025
J5	6.8	-1.333	0.673	1.344	19.530	62.850	0.077	0.097	1.991	0.121
J6	6.791	-1.333	1.290	1.394	39.190	56.150	0.072	0.071	0.639	0.130
J7	6.782	-1.333	1.202	1.315	32.650	63.380	0.048	0.051	3.383	0.045
J8	6.773	-1.333	1.028	1.216	28.390	55.790	0.069	0.074	0.758	0.068
J10	6.754	-1.333	49.650	0.063	0.077	1.260	0.072	0.537	0.016	4.393

Appendix C: Raw data for test samples (continued)

SAMPLE POINT	LATITUDE(N)	LONGITUDE (W)	TiO2	MnO	Fe2O3	Cr	Ni	Cu	Zn
A1	6.837	-1.415	1.118	0.067	3.711	150.000	15.000	5.800	23.200
A2	6.828	-1.415	0.679	0.078	2.730	215.000	14.500	5.300	23.100
A3	6.818	-1.415	0.975	0.037	2.285	43.000	12.000	3.300	13.600
A5	6.8	-1.415	0.290	0.031	1.574	219.000	6.500	< 1.3	26.000
A6	6.791	-1.415	0.605	0.022	2.519	46.700	12.400	< 1.3	19.000
A7	6.782	-1.415	0.542	0.062	2.062	559.000	11.300	4.100	15.700
A8	6.773	-1.415	0.508	0.012	2.399	294.000	11.100	1.200	13.900
A9	6.763	-1.415	0.856	0.043	2.605	220.000	19.100	4.400	22.400
A10	6.754	-1.415	0.460	0.017	0.935	136.100	5.200	< 1.3	12.200
B2	6.828	-1.406	0.630	0.008	1.067	249.000	7.200	< 1.4	7.900
B3	6.818	-1.406	0.595	0.011	0.882	144.700	7.000	< 1.4	12.000
B4	6.809	-1.406	0.583	0.008	2.526	315.000	14.400	0.500	11.400
B5	6.8	-1.406	0.889	0.013	4.810	167.000	16.900	3.100	18.500
B6	6.791	-1.406	0.856	0.011	2.103	58.200	11.800	1.100	13.600
B8	6.773	-1.406	1.169	0.025	6.191	142.000	26.700	7.100	25.800
B9	6.763	-1.406	0.418	0.021	1.460	51.000	5.600	< 1.4	13.900
B10	6.754	-1.406	0.273	0.014	1.942	21.000	7.600	< 1.6	29.400
C1	6.837	-1.397	0.543	0.034	2.824	165.000	12.100	4.600	18.800
C2	6.828	-1.397	0.261	0.004	0.283	316.000	2.800	< 1.3	3.600
C3	6.818	-1.397	0.680	0.019	4.186	211.000	16.800	2.400	22.800
C4	6.809	-1.397	1.112	0.016	2.988	79.300	20.500	5.200	15.900
C5	6.8	-1.397	0.293	0.003	0.327	300.000	3.400	< 1.4	4.000
C6	6.791	-1.397	0.808	0.045	3.774	136.000	18.400	6.000	28.200
C7	6.782	-1.397	0.661	0.027	3.769	58.300	14.500	2.300	28.700
C8	6.773	-1.397	0.400	0.030	1.915	236.000	9.100	0.800	20.600
C9	6.763	-1.397	0.365	0.077	2.414	292.000	11.200	< 1.4	35.100
C10	6.754	-1.397	0.350	0.008	0.760	25.700	3.800	< 1.3	18.500
D1	6.837	-1.387	1.043	0.009	2.367	155.000	12.600	< 1.5	15.000
D2	6.828	-1.387	1.146	0.026	6.967	165.000	26.300	7.700	23.800
D3	6.818	-1.387	0.797	0.019	3.578	152.000	16.300	2.700	19.100
D4	6.809	-1.387	0.590	0.011	3.152	146.000	12.700	1.000	15.700

Appendix C: Raw data for test samples (continued)

SAMPLE POINT	LATITUDE(N)	LONGITUDE (W)	TiO2	MnO	Fe2O3	Cr	Ni	Cu	Zn
D6	6.791	-1.387	0.674	0.008	0.926	181.800	7.800	< 1.3	18.300
D7	6.782	-1.387	0.682	0.013	2.215	331.000	11.700	0.700	21.800
D8	6.773	-1.387	0.564	0.016	1.967	304.000	8.800	< 1.3	25.700
D9	6.763	-1.387	0.710	0.045	4.856	545.000	21.400	11.100	35.000
D10	6.754	-1.387	0.920	0.027	7.489	102.000	21.000	18.200	36.700
E1	6.837	-1.378	0.957	0.015	6.094	114.000	16.100	< 1.5	19.600
E2	6.828	-1.378	0.480	0.005	0.218	13.400	2.200	< 1.4	2.300
E3	6.818	-1.378	0.637	0.009	2.140	116.300	9.500	< 1.4	16.800
E4	6.809	-1.378	1.039	0.069	3.510	70.700	20.400	10.000	22.200
E6	6.791	-1.378	1.020	0.167	8.743	561.000	135.700	40.500	67.900
E7	6.782	-1.378	1.044	0.138	9.689	238.000	49.900	26.500	55.500
E8	6.773	-1.378	0.738	0.108	5.966	536.000	56.900	18.100	40.100
E9	6.763	-1.378	0.833	0.025	5.056	323.000	14.800	8.400	13.900
E10	6.754	-1.378	0.930	0.038	4.879	109.000	15.300	9.100	23.100
F1	6.837	-1.369	1.267	0.035	6.244	132.000	25.800	12.700	24.900
F2	6.828	-1.369	0.613	0.031	3.861	334.000	13.800	5.000	18.200
F4	6.809	-1.369	0.478	0.008	0.970	203.000	4.500	< 1.3	12.800
F5	6.8	-1.369	0.505	0.038	2.213	47.300	11.700	< 1.4	32.500
F6	6.791	-1.369	0.190	0.043	1.232	13.100	8.000	9.900	41.100
F8	6.773	-1.369	0.859	0.029	10.720	189.000	38.900	21.400	20.900
F9	6.763	-1.369	1.007	0.029	3.235	421.000	34.700	12.400	50.700
G1	6.837	-1.36	0.738	0.037	4.009	206.000	15.300	3.500	17.400
G2	6.828	-1.36	0.746	0.078	6.398	206.000	32.500	11.900	41.700
G3	6.818	-1.36	0.592	0.080	3.763	305.000	21.800	6.700	21.200
G4	6.809	-1.36	0.844	0.055	6.144	121.000	21.300	8.400	26.800
G5	6.8	-1.36	1.151	0.041	4.356	99.000	22.800	17.400	21.400
G6	6.791	-1.36	0.383	0.018	2.481	45.000	7.000	< 1.3	28.700
G7	6.782	-1.36	0.605	0.040	3.482	418.000	16.600	11.700	30.300
G8	6.773	-1.36	0.668	0.023	4.233	584.000	14.500	8.500	37.600

Appendix C: Raw data for test samples (continued)

SAMPLE POINT	LATITUDE(N)	LONGITUDE (W)	TiO2	MnO	Fe2O3	Cr	Ni	Cu	Zn
G9	6.763	-1.36	0.929	0.064	4.801	441.000	17.600	8.900	31.400
G10	6.754	-1.36	0.650	0.013	1.231	111.100	4.800	< 1.3	15.400
H2	6.828	-1.351	0.634	0.025	1.624	47.700	10.200	3.500	15.700
H3	6.818	-1.351	0.584	0.010	2.429	44.200	11.000	3.000	16.500
H4	6.809	-1.351	0.813	0.045	3.900	54.900	18.900	7.800	28.000
H5	6.8	-1.351	0.323	0.016	0.671	44.400	5.700	< 1.3	20.200
H6	6.791	-1.351	0.793	0.012	3.210	239.000	15.300	< 1.4	34.100
H7	6.782	-1.351	0.742	0.022	4.314	102.000	12.100	3.300	29.100
H8	6.773	-1.351	0.867	0.031	6.207	306.000	20.700	11.600	29.800
H9	6.763	-1.351	1.090	0.069	2.788	394.000	17.300	4.200	24.300
H10	6.754	-1.351	0.881	0.012	0.799	106.200	8.100	< 1.3	21.100
I1	6.837	-1.342	0.419	0.005	0.609	341.000	4.700	< 1.3	6.700
I2	6.828	-1.342	0.883	0.033	3.980	179.000	22.800	7.100	28.900
I3	6.818	-1.342	1.088	0.013	2.965	61.600	16.000	1.900	19.000
I4	6.809	-1.342	0.500	0.012	2.767	50.700	11.500	< 1.4	26.500
I5	6.8	-1.342	1.078	0.022	4.622	155.000	22.200	8.900	30.800
I6	6.791	-1.342	0.522	0.049	3.315	262.000	10.900	< 1.4	34.200
I7	6.782	-1.342	0.788	0.014	3.116	46.500	12.400	< 1.4	27.500
I8	6.773	-1.342	0.612	0.040	2.117	30.700	9.800	2.700	39.200
I9	6.763	-1.342	1.071	0.077	5.436	169.000	18.500	17.300	28.700
I10	6.754	-1.342	0.494	0.006	0.544	#VALUE!	4.500	< 1.3	6.700
J1	6.837	-1.333	0.595	0.027	2.357	524.000	12.700	5.600	17.300
J2	6.828	-1.333	0.983	0.052	2.270	127.200	12.300	9.700	18.400
J3	6.818	-1.333	0.308	0.004	0.320	11.500	2.400	< 1.4	7.300
J4	6.809	-1.333	0.505	0.008	1.329	34.400	6.800	< 1.3	9.500
J5	6.8	-1.333	0.449	0.020	1.193	108.000	5.800	< 1.3	19.700
J6	6.791	-1.333	0.720	0.024	7.299	121.000	16.300	9.000	26.200
J7	6.782	-1.333	0.462	0.011	1.886	29.500	5.100	< 1.4	25.400
J8	6.773	-1.333	0.908	0.013	5.065	123.000	22.300	13.600	32.600
J10	6.754	-1.333	431.000	8.000	2.600	22.400	20.500	1.100	4.300

Appendix C: Raw data for test samples (continued)

SAMPLE POINT	LATITUDE(N)	LONGITUDE (W)	Ga	Ge	As	Br	Rb	Sr	Zr
A1	6.837	-1.415	15.700	2.000	11.500	6.500	24.200	33.200	1131.000
A2	6.828	-1.415	20.700	1.500	10.400	6.800	70.700	41.900	755.000
A3	6.818	-1.415	13.400	1.400	5.600	1.200	42.000	23.800	927.000
A5	6.8	-1.415	24.500	1.800	10.400	1.700	241.700	96.100	296.000
A6	6.791	-1.415	18.400	1.100	8.700	2.400	35.300	17.000	474.000
A7	6.782	-1.415	13.000	1.100	5.700	3.100	26.500	17.100	582.000
A8	6.773	-1.415	19.300	0.700	7.300	3.400	30.800	11.300	478.000
A9	6.763	-1.415	20.000	0.800	2.600	4.600	108.300	27.900	668.000
A10	6.754	-1.415	9.800	1.700	2.000	< 0.3	43.600	8.600	510.000
B2	6.828	-1.406	10.900	0.800	3.400	< 0.3	22.200	13.500	663.000
B3	6.818	-1.406	10.900	1.200	3.100	< 0.3	58.800	39.300	621.000
B4	6.809	-1.406	18.600	1.500	6.400	3.200	34.300	12.400	501.000
B5	6.8	-1.406	23.600	1.700	4.300	3.700	26.600	13.000	487.000
B6	6.791	-1.406	18.000	1.400	7.500	3.900	28.400	13.700	642.000
B8	6.773	-1.406	28.200	1.600	6.500	7.400	21.600	25.500	607.000
B9	6.763	-1.406	15.200	1.500	1.800	< 0.3	196.600	47.400	371.000
B10	6.754	-1.406	26.900	1.000	3.600	2.900	174.200	19.800	352.000
C1	6.837	-1.397	24.200	2.400	6.100	4.500	62.300	19.200	449.000
C2	6.828	-1.397	6.400	1.100	0.700	< 0.3	60.700	34.300	563.000
C3	6.818	-1.397	25.500	2.100	5.800	4.300	43.100	16.300	437.000
C4	6.809	-1.397	22.400	1.400	5.800	4.100	22.800	14.300	722.000
C5	6.8	-1.397	3.800	1.000	0.400	< 0.4	28.500	11.100	579.000
C6	6.791	-1.397	25.800	1.900	5.900	3.800	40.300	17.400	563.000
C7	6.782	-1.397	26.300	2.600	4.200	5.100	64.300	25.500	481.000
C8	6.773	-1.397	19.700	1.400	5.600	1.900	58.500	19.000	389.000
C9	6.763	-1.397	27.800	1.800	3.800	2.700	242.000	42.500	325.000
C10	6.754	-1.397	11.900	2.200	0.900	< 0.3	126.800	55.500	623.000
D1	6.837	-1.387	21.400	1.800	2.900	2.700	44.200	19.000	809.000
D2	6.828	-1.387	29.500	2.000	8.400	3.300	14.700	18.400	516.000
D3	6.818	-1.387	21.600	1.800	5.800	3.900	20.700	14.500	482.000
D4	6.809	-1.387	15.800	< 0.7	4.800	3.100	41.500	13.300	497.000

Appendix C: Raw data for test samples (continued)

SAMPLE POINT	LATITUDE(N)	LONGITUDE (W)	Ga	Ge	As	Br	Rb	Sr	Zr
D6	6.791	-1.387	8.600	1.300	4.000	< 0.3	32.700	10.900	658.000
D7	6.782	-1.387	15.200	1.700	4.000	0.800	46.100	13.200	642.000
D8	6.773	-1.387	13.000	1.800	1.700	< 0.3	49.400	19.600	525.000
D9	6.763	-1.387	16.600	1.600	6.900	4.700	38.100	27.800	390.000
D10	6.754	-1.387	24.000	1.800	6.500	4.500	44.800	28.300	505.000
E1	6.837	-1.378	26.400	2.200	4.200	5.000	55.200	22.600	554.000
E2	6.828	-1.378	4.300	1.100	1.700	< 0.3	33.000	23.600	776.000
E3	6.818	-1.378	15.100	< 0.8	3.500	3.600	61.800	17.700	463.000
E4	6.809	-1.378	21.300	1.300	6.700	5.200	27.400	25.900	669.000
E6	6.791	-1.378	20.000	1.800	6.900	4.400	121.100	75.800	278.000
E7	6.782	-1.378	27.200	2.400	4.000	7.000	92.300	40.000	279.000
E8	6.773	-1.378	20.100	1.800	4.300	4.900	83.100	41.100	308.000
E9	6.763	-1.378	17.700	1.200	5.500	3.500	20.900	22.300	839.000
E10	6.754	-1.378	14.900	1.100	5.400	2.400	23.400	24.500	552.000
F1	6.837	-1.369	26.700	2.000	7.100	7.300	22.500	22.900	586.000
F2	6.828	-1.369	15.200	1.400	10.700	1.500	27.000	18.500	421.000
F4	6.809	-1.369	12.400	2.000	4.400	< 0.3	51.500	15.100	467.000
F5	6.8	-1.369	28.700	1.500	5.200	3.900	135.000	21.500	444.000
F6	6.791	-1.369	19.500	< 0.8	10.900	2.300	300.800	111.800	189.800
F8	6.773	-1.369	26.200	2.200	4.000	< 0.3	25.500	19.500	284.000
F9	6.763	-1.369	15.700	1.900	6.000	< 0.3	52.500	76.200	767.000
G1	6.837	-1.36	20.500	2.500	4.900	4.700	42.600	19.200	588.000
G2	6.828	-1.36	24.400	1.600	3.700	4.500	127.200	31.300	391.000
G3	6.818	-1.36	18.400	1.400	5.400	3.000	79.200	21.300	572.000
G4	6.809	-1.36	23.300	2.100	6.800	7.200	47.700	25.400	617.000
G5	6.8	-1.36	17.700	1.100	4.400	5.300	21.000	24.000	627.000
G6	6.791	-1.36	27.400	1.000	7.000	2.300	165.200	36.200	382.000
G7	6.782	-1.36	14.400	1.700	3.000	4.200	37.200	21.900	401.000
G8	6.773	-1.36	13.600	1.100	4.100	0.900	24.400	22.500	405.000

Appendix C: Raw data for test samples (continued)

SAMPLE POINT	LATITUDE(N)	LONGITUDE (W)	Ga	Ge	As	Br	Rb	Sr	Zr
G9	6.763	-1.36	13.400	1.700	7.500	2.600	15.600	22.700	483.000
G10	6.754	-1.36	4.800	1.200	2.100	< 0.3	10.300	44.000	773.000
H2	6.828	-1.351	12.800	1.200	4.200	< 0.3	47.400	16.700	618.000
H3	6.818	-1.351	20.600	1.800	5.000	3.700	62.800	14.000	494.000
H4	6.809	-1.351	23.200	2.200	7.600	4.000	22.800	22.400	565.000
H5	6.8	-1.351	7.200	1.300	3.200	< 0.3	69.900	41.800	391.000
H6	6.791	-1.351	26.800	1.700	4.300	4.000	125.200	33.400	583.000
H7	6.782	-1.351	16.300	1.500	3.700	0.400	57.400	22.700	514.000
H8	6.773	-1.351	18.000	2.100	4.600	2.300	31.500	27.500	562.000
H9	6.763	-1.351	9.700	1.400	4.200	< 0.3	12.900	17.300	1181.000
H10	6.754	-1.351	6.700	1.200	4.400	< 0.3	10.900	20.300	766.000
I1	6.837	-1.342	10.600	1.300	2.000	< 0.3	69.600	31.900	531.000
I2	6.828	-1.342	29.400	1.700	5.000	3.300	44.100	22.500	595.000
I3	6.818	-1.342	21.300	2.100	6.000	2.200	37.000	17.500	786.000
I4	6.809	-1.342	28.500	1.000	2.700	3.100	73.800	19.600	419.000
I5	6.8	-1.342	22.400	1.800	4.100	1.900	32.600	19.200	646.000
I6	6.791	-1.342	29.200	2.200	9.100	5.400	129.500	33.800	471.000
I7	6.782	-1.342	26.800	1.500	3.800	1.800	76.300	17.400	545.000
I8	6.773	-1.342	17.700	2.500	2.100	< 0.3	99.600	41.500	617.000
I9	6.763	-1.342	15.200	1.100	7.100	4.000	25.500	30.500	647.000
I10	6.754	-1.342	3.200	2.000	2.600	< 0.3	6.100	8.100	423.000
J1	6.837	-1.333	15.900	1.000	4.900	< 0.3	45.900	20.900	611.000
J2	6.828	-1.333	15.900	1.100	4.200	1.900	42.700	22.800	795.000
J3	6.818	-1.333	8.700	1.200	0.900	< 0.4	98.500	50.700	404.000
J4	6.809	-1.333	11.700	1.600	3.400	0.900	50.100	19.100	523.000
J5	6.8	-1.333	10.400	1.500	3.000	< 0.3	89.000	34.500	406.000
J6	6.791	-1.333	28.700	1.300	5.600	4.800	33.900	17.300	405.000
J7	6.782	-1.333	26.600	2.000	3.500	2.800	159.400	44.500	466.000
J8	6.773	-1.333	16.500	1.400	4.600	3.700	17.800	20.900	477.000
J10	6.754	-1.333	1.400	52.400	20.700	268.400	10.500	7.300	15.400

Appendix C: Raw data for test samples (continued)

SAMPLE POINT	LATITUDE(N)	LONGITUDE (W)	Nb	Sn	I	Ba	Ce
A1	6.837	-1.415	45.400	1.700	6.000	109.300	92.000
A2	6.828	-1.415	22.900	5.000	14.800	192.500	82.000
A3	6.818	-1.415	34.300	3.600	7.800	111.800	33.000
A5	6.8	-1.415	16.800	4.800	< 5.9	769.000	54.000
A6	6.791	-1.415	24.400	3.100	9.700	91.100	< 23
A7	6.782	-1.415	21.800	4.200	13.400	86.300	94.000
A8	6.773	-1.415	23.000	4.800	12.300	58.300	42.000
A9	6.763	-1.415	32.800	6.200	17.900	164.600	87.000
A10	6.754	-1.415	13.300	2.600	< 5.4	104.300	65.000
B2	6.828	-1.406	14.400	< 1.9	6.000	91.500	60.000
B3	6.818	-1.406	19.200	< 2.1	< 5.0	318.000	58.000
B4	6.809	-1.406	22.000	2.800	15.200	62.000	59.000
B5	6.8	-1.406	34.000	10.100	39.400	79.700	48.000
B6	6.791	-1.406	28.200	2.600	14.600	55.300	55.000
B8	6.773	-1.406	40.600	7.300	35.600	68.100	53.000
B9	6.763	-1.406	15.600	4.800	< 5.4	344.900	43.000
B10	6.754	-1.406	17.700	12.500	11.700	87.300	40.000
C1	6.837	-1.397	19.100	5.000	11.700	110.700	< 23
C2	6.828	-1.397	9.600	< 1.6	< 5.2	235.700	33.000
C3	6.818	-1.397	30.200	4.800	27.500	62.500	< 23
C4	6.809	-1.397	41.400	< 2.3	29.300	49.500	< 24
C5	6.8	-1.397	13.300	< 1.5	< 5.0	90.000	35.000
C6	6.791	-1.397	31.300	11.800	27.600	70.700	84.000
C7	6.782	-1.397	22.800	12.300	19.300	134.100	74.000
C8	6.773	-1.397	21.700	7.100	11.500	60.800	43.000
C9	6.763	-1.397	12.800	7.900	21.000	324.700	70.000
C10	6.754	-1.397	12.700	< 1.6	< 5.4	459.000	76.000
D1	6.837	-1.387	35.600	3.900	13.700	104.500	< 23
D2	6.828	-1.387	48.700	6.400	39.200	53.800	84.000
D3	6.818	-1.387	28.200	4.800	19.000	54.400	41.000
D4	6.809	-1.387	13.300	6.200	12.600	143.300	< 23

Appendix C: Raw data for test samples (continued)

SAMPLE POINT	LATITUDE(N)	LONGITUDE (W)	Nb	Sn	I	Ba	Ce
D6	6.791	-1.387	8.800	1.800	< 5.0	100.100	< 22
D7	6.782	-1.387	15.700	6.900	5.500	107.000	< 23
D8	6.773	-1.387	14.300	3.700	< 5.2	173.700	42.000
D9	6.763	-1.387	17.500	7.600	16.200	193.800	52.000
D10	6.754	-1.387	15.600	8.700	28.600	258.400	< 24
E1	6.837	-1.378	33.200	8.400	15.100	106.100	< 23
E2	6.828	-1.378	13.400	< 1.5	< 5.1	202.100	64.000
E3	6.818	-1.378	21.500	6.900	< 5.7	118.200	59.000
E4	6.809	-1.378	30.200	5.800	29.400	69.700	< 24
E6	6.791	-1.378	8.400	12.400	26.200	392.000	64.000
E7	6.782	-1.378	17.000	13.600	34.500	270.100	118.000
E8	6.773	-1.378	< 5.3	11.800	18.500	280.600	< 24
E9	6.763	-1.378	14.600	< 1.8	7.700	149.000	73.000
E10	6.754	-1.378	17.900	3.200	18.900	198.800	< 24
F1	6.837	-1.369	54.900	4.700	44.000	76.400	101.000
F2	6.828	-1.369	14.500	< 2.4	12.000	66.900	39.000
F4	6.809	-1.369	21.200	6.500	< 5.5	109.000	47.000
F5	6.8	-1.369	23.200	11.600	< 5.9	136.100	68.000
F6	6.791	-1.369	9.400	8.700	< 5.8	734.000	< 24
F8	6.773	-1.369	13.500	4.100	23.800	199.300	142.000
F9	6.763	-1.369	< 5.5	4.700	< 5.5	334.400	50.000
G1	6.837	-1.36	18.500	9.300	19.900	79.500	61.000
G2	6.828	-1.36	13.600	13.800	16.900	272.100	< 24
G3	6.818	-1.36	16.000	7.200	26.300	174.600	87.000
G4	6.809	-1.36	30.100	4.300	25.700	176.800	< 24
G5	6.8	-1.36	22.200	< 1.5	26.600	169.900	73.000
G6	6.791	-1.36	7.800	9.200	14.400	273.500	71.000
G7	6.782	-1.36	8.800	4.000	9.800	282.400	72.000
G8	6.773	-1.36	12.300	2.100	< 5.5	275.600	47.000

Appendix C: Raw data for test samples (continued)

SAMPLE POINT	LATITUDE(N)	LONGITUDE (W)	Nb	Sn	I	Ba	Ce
G9	6.763	-1.36	13.800	1.900	17.300	193.800	58.000
G10	6.754	-1.36	9.100	< 1.8	< 5.2	108.700	< 24
H2	6.828	-1.351	18.800	2.900	8.400	91.300	35.000
H3	6.818	-1.351	25.000	5.100	9.000	106.000	< 23
H4	6.809	-1.351	31.800	4.500	25.100	78.300	65.000
H5	6.8	-1.351	< 4.0	< 1.5	< 5.0	299.000	27.000
H6	6.791	-1.351	26.800	9.100	14.000	282.000	82.000
H7	6.782	-1.351	21.600	2.200	11.900	208.800	48.000
H8	6.773	-1.351	19.600	2.600	23.800	230.000	42.000
H9	6.763	-1.351	23.600	< 2.2	9.100	113.000	84.000
H10	6.754	-1.351	10.800	1.500	< 5.1	211.600	70.000
I1	6.837	-1.342	10.600	3.000	< 5.1	282.500	< 22
I2	6.828	-1.342	30.200	8.800	31.100	99.300	62.000
I3	6.818	-1.342	46.300	6.300	17.100	90.800	< 22
I4	6.809	-1.342	15.300	6.300	21.300	122.100	< 22
I5	6.8	-1.342	31.000	7.000	27.200	138.700	< 24
I6	6.791	-1.342	20.500	10.300	11.000	220.200	< 24
I7	6.782	-1.342	33.400	5.300	18.000	102.600	47.000
I8	6.773	-1.342	22.100	6.900	7.900	393.700	57.000
I9	6.763	-1.342	27.500	< 2.1	14.300	263.000	63.000
I10	6.754	-1.342	5.600	< 1.5	< 4.8	87.800	36.000
J1	6.837	-1.333	9.700	3.800	12.200	135.500	39.000
J2	6.828	-1.333	33.100	2.900	16.600	107.100	61.000
J3	6.818	-1.333	6.900	0.700	< 5.1	323.800	< 23
J4	6.809	-1.333	9.600	2.400	< 5.5	138.000	58.000
J5	6.8	-1.333	8.300	4.700	< 5.2	317.500	49.000
J6	6.791	-1.333	27.200	5.300	28.000	97.000	56.000
J7	6.782	-1.333	16.200	10.400	< 5.6	354.100	53.000
J8	6.773	-1.333	20.400	< 1.7	25.300	216.700	32.000
J10	6.754	-1.333	202.500	43.000			